NOTICE

The quality of this microform is heavily dependent upon the quality of the original thesis submitted for microfilming. Every effort has been made to ensure the highest quality of reproduction possible.

If pages are missing, contact the university which granted the degree.

Some pages may have indistinct print especially if the original pages were typed with a poor typewriter ribbon or if the university sent us an inferior photocopy.

Reproduction in full or in part of this microform is governed by the Canadian Copyright Act, R.S.C. 1970, c. C-30, and subsequent amendments.

AVIS

La qualité de cette microforme dépend grandement de la qualité de la thèse soumise au microfilmage. Nous avons tout fait pour assurer une qualité supérieure de reproduction.

S'il manque des pages, veuillez communiquer avec l'université qui a conféré le grade.

La qualité d'impression de certaines pages peut laisser à désirer, surtout si les pages originales ont été dactylographiées à l'aide d'un ruban usé ou si l'université nous a fait parvenir une photocopie de qualité inférieure.

La reproduction, même partielle, de cette microforme est soumise à la Loi canadienne sur le droit d'auteur, SRC 1970, c. C-30, et ses amendements subséquents.

Catalytic Hydrodenitrogenation of Pyridine and Quinoline

by

Camille Daher Ajaka

A thesis submitted to
the school of Graduate Studies and Research
in partial fulfillment of the requirements for the
degree of
DOCTOR OF PHILOSOPHY
in the Department of Chemical Engineering
at the University of Ottawa
Ottawa, Canada

ISBN 0-315-75079-0

UNIVERSITÉ D'OTTAWA
UNIVERSITY OF OTTAWA

Dedication

TO MY FAMILY AND FRIENDS

Abstract

The reaction networks and the kinetics of the vapor phase catalytic hydrodenitrogenation (HDN) of two model nitrogen-containing heterocyclic compounds, pyridine, quinoline and their mixture, were studied in a bench scale continuous flow, fixed-bed catalytic reactor. The catalyst used in this study was presulfided commercial Ni-Mo/Al_2O_3 (Shell Catalyst 424).

The results indicate that the impact of the process variables on the conversion, yield, and selectivity of the HDN reactions is in the following decreasing order: $T > W/F > \overline{R}$.

The initial aromatic ring saturation reactions of pyridine and quinoline were all reversible at the conditions studied. The removal of nitrogen in pyridine HDN occurred primarily through the pentylamine intermediate, and pentane was the major hydrocarbon produced. The removal of nitrogen in quinoline HDN occurred through the decahydroquinoline intermediate, and propylcyclohexane was the major hydrocarbon produced. The Ni-Mo/Al_2O_3 catalyst exhibited higher selectivity for the reaction pathway of pyridine HDN than that of quinoline HDN. Cracking and hydrocracking took place at temperatures above 648 K.

The presence of pyridine in the HDN of a pyridine-quinoline mixture resulted in an increase in the rate of conversion of quinoline and a decrease in that of pyridine.

On the other hand, the rate of formation of propylcyclohexane (PCH) had increased while the amount of decahydroquinoline (DHQ) produced had decreased, which indicates that the presence of pyridine had enhanced the transformation of DHQ to PCH.

Mixing the two heterocycles had enhanced the conversion and the selectivity of the quinoline HDN at high and low temperature, while the conversion of pyridine had been retarded by the presence of quinoline. The selectivity of the mixture was more than that for either of the components.

Several rate equations were considered to fit the kinetic data. A Langmuir-Hinshelwood reaction mechanism fitted the data best. Arrhenius plots of the pseudo rate constants for the HDN reactions of pyridine, quinoline, and their mixture gave activation energies (E) of 19.84, 26.52 and 13.17 kcal/g-mol, respectively.

Acknowledgments

First, I want to express my sincere gratitude to my thesis advisor, Prof. R. S. Mann, for his invaluable support, guidance, and encouragement during the course of this investigation. I wish to thank the present chairman, Prof. Z. Duvnjak and the former chairman, Prof. G. Neale for the departmental financial support and for the facilities used for this work. Special thanks to Prof. W. Hayduk as Graduate Students Coordinator for his help in starting this work. I am also thankful to Prof. D. D. McLean and Prof. B. C.-Y. Lu for the invaluable discussions and suggestions.

I would like to express my appreciation to Dr. K. C. Khulbe, Mr. S. Boudriga, and Mr. Y. Touhami for the time and help in discussing the results. Sincere thanks to Messrs. A. Bonaldo, L. Tremblay and G. Gasperetti for the technical assistance and the help in maintaining the experimental setup. I thank Mr. P. Lafontain from the Plant Research Centre for the GC/MS analysis. The assistance and friendliness of fellow graduate students are greatly appreciated.

Finally, I thank my family for their love, patience, and encouragement that made this work possible.

Notation

Various symbols, superscripts, subscripts, and abbreviations used frequently in this work are summarized below. All notation is fully defined where it first arises in the text.

Symbols

a	activity
a_m	area of the particle per unit mass
a, b	parameters, Equation D.1
A	defined as per Equation D.8
B	defined as per Equation D.9
C_p	constant pressure heat capacity per unit mass of fluid
d	interplaner spacing of the planes, Equation 3.11
D	molecular diffusivity of the species being transferred into the system of interest
D_{AB}	bulk diffusivity
D_c	combined diffusivity (Knudsen and molecular diffusion)

D_e effective diffusivity

D_K Knudsen diffusivity

D_p catalyst particle diameter

$E(Y)$ expected value of the random variable Y,

F_i molar flow rate of component i, g-mol/hr

$\hat{f}_i$ fugacity of compound i

$f_m(\underline{\xi}_n, \underline{\theta})$ response function defining the expected value of the m^{th} response for the n^{th} run

G mass velocity based on the total cross-sectional area of the reactor

G_m mass velocity based on the total (superficial) cross-sectional area of the reactor

h heat transfer coefficient between the catalyst particle and the bulk fluid

h_T Thiele modulus, given by Equation 2.65

$\underline{H}$ the N×M matrix of m predicted responses for n runs

j_D mass transfer factor

j_H heat transfer factor

J_i molar flux of species i towards the surface relative to molar average velocity, Equation 2.38

k thermal conductivity of the fluid

k reaction rate constant, Equation 2.3

k_i reaction rate constant, Equation 2.5

k_i adsorption constant of compound i

k_{ov} observed rate constant, Equation 2.4

K_{eq} thermodynamic reaction equilibrium constant

K_{eq} overall equilibrium constant, Equation 2.15

K_i adsorption equilibrium constant of component i, Equation 2.6

K_{sr} surface reaction equilibrium constant

k'_1 reaction rate constant of forward reaction

k'_{-1} reaction rate constant of reverse reaction

k'_i desorption constant of compound i

$\overline{L}$ parameter as per Equation 2.66

m number of active sites, Equation 2.14

M molecular weight of the gas mixture, Equation 2.60

N_{Pr} Prandtl number $= \frac{D_p G C_p}{k}$

N_{Re} Reynolds number $= \frac{D_p G}{\mu}$

N_{Sc} Schmidt number $= \frac{\mu}{\rho D}$

N'_{Re} modified Reynolds number $= \frac{D_p G}{\mu(1-\epsilon_B)}$

P_c critical pressure

$P_{f,i}$ film pressure factor of species i

P_i partial pressure of species i

$P_{i,b}$ partial pressure of species i in the bulk

$P_{i,s}$ partial pressure of species i at the surface

P_r reduced pressure

P_s saturation pressure

P_u^t total type-u active sites expressed in pressure

P_v^t total type-v active sites expressed in pressure

r reaction rate

r_{mA} molal reaction rate of component A

$\overline{r}$ pore radius

$\overline{r}$ parameter as per Equation 2.67

R_g gas constant

$\overline{R}$ molar ratio of reactants, g-mol H_2/g-mol nitro-compound

S_g catalyst specific surface area

S_x gross exterior surface area of the particle

S_v	volumetric liquid hourly space velocity
t	time of reaction, Equation 2.3
T	temperature, K
T_b	temperature in the bulk fluid
T_c	critical temperature
T_r	reduced temperature
T_s	temperature at the catalyst surface
u	u-type active sites
u, w	constant parameters Equation D.1
v	specific volume, Equation D.1
v	v-type active sites
V_a	volume of gas adsorbed
V_g	void volume per gram of catalyst
V_m	volume adsorbed equivalent to a monolayer of gas
V_p	gross volume of the catalyst particle
W	weight of catalyst, g
W/F	space time, hr g-cat/g-mol nitro-compound

X_1, X_2, X_3 temperature, space time, and reactants' molar ratio respectively, Equation 3.6

X_i fractional conversion of component i

XS random variable, product of conversion and selectivity

y_{nm} observed value of the m^{th} response variable for the n^{th} run

$\underline{Y}$ the N×M matrix of the measured responses for n runs

Z compressibility factor

superscripts

^{n} order of the reaction

^{T} transpose of a matrix, Equation 3.9

$^\alpha$ order of reaction with respect to A, Equation 2.19

$^\beta$ order of reaction with respect to B, Equation 2.19

subscripts

$_0$ condition at reactor inlet

Greek Symbols

α defined as per Equation D.7

β_i parameter associated with the independent variable x_i, Equation 3.1

δ_A ratio of stoichiometric coefficients, Equation 2.44

ΔH_A molal heat of reaction of A

ΔY pressure gradient, Equation 2.46

ϵ_{nm} value of the random error associated with the

ε catalyst porosity

ε_p porosity of the pellet

η effectiveness factor

θ the angle between the planes in the crystal and the incident beam, Equation 3.11

θ_j fraction of available sites occupied by j

$\underline{\theta}$ P×1 vector of values of parameters

λ mean free path, Equation 2.58

λ wavelength of the x-ray, Equation 3.11

μ fluid viscosity

$\underline{\xi}_n$ vector of values of the operating (independent) variables for the n^{th} run

Π Total pressure

ρ fluid density

ρ_p apparent density of catalyst particle (mass per total particle volume).

τ	pressure dependent residence time, hr g-cat atm/g-mol
τ	tortuosity factor (takes care of length and shape factors)
τ_d	specified relative tolerance, Equation 3.10
ϕ	shape factor, assumed 0.9 for irregular granules
Φ	Thiele-type modulus given by equation 2.70
$\hat{\phi}_i$	fugacity coefficient of compound i
ω	accentric factor

Abbreviations

AA	aromatic amines
AES	Auger Electron Spectroscopy
AN	aniline
APIP	alkyl-piperidines
BzTHQ	5,6,7,8-tetrahydroquinoline
DEC	decane
DHQ	decahydroquinoline
DPEAM	dipentylamine
EAN	ethylaniline
EB	ethylbenzene

ECH	ethylcyclohexane
EPR	Electron Paramagnetic Resonance
ESR	Electron Spin Resonance
ETPIP	ethylpiperidine
HDM	hydrodematalation
HDN	hydrodenitrogenation
HDO	hydrodeoxidation
HDS	hydrodesulfurization
HC	hydrocarbon
IDAN	indan
IR	Infrared Spectroscopy
ISS	Ion Scattering Spectroscopy
MEB	methylethylbenzene
MCH	methylcyclohexane
MNPIP	methylenepiperidine
NC	nitrogen-containing compound
OPA	o-propylaniline
PB	propylbenzene

PCH	propylcyclohexane
PCHAM	propylcyclohexylamine
PCHE	propylcyclohexene
PEAM	pentylamine
PEN	pentane
PEPIP	pentylpiperidine
PIP	piperidine
PNPIP	pentenylpiperidine
PRPIP	propylpiperidine
PYR	pyridine
PyTHQ	1,2,3,4-tetrahydroquinoline
Q	quinoline
SA	secondary amines
SMIS	Secondary Ion Mass Spectroscopy
UPS	Photoelectron Spectroscopy
XPS	X-Ray Photoelectron Spectroscopy
XRD	X-Ray Diffraction

Contents

List of Tables

List of Figures

Chapter 1

Introduction

Catalysis plays a very important role in today's industry. About 90% of all chemical manufacturing processes are catalytic. The first catalytic reaction known is the biocatalytic fermentation in wine manufacturing which goes back to the neolithic age (about 5,000 B.C.). In the 1500's, alchemists formed sulfuric acid by a mysterious catalytic process. In 1831, Pelegrin Phillips obtained the first known patent in catalysis for the reaction

$$SO_2 + \text{air} \xrightarrow[sponge]{Pt} SO_3$$

In 1836, J. J. Berzelius had coined the word 'catalysis' as follows: "It has then proved that several simple and composite soluble and insoluble substances possess the property of exercising upon other substances an effect quite different from chemical affinity. By means of this affinity they produce decomposition into the elements of these substances and different recombinations of the same elements, from which they remain separate. This new force which was unknown until now, is common to both organic and inorganic nature". He called this force the "catalytic force" and the decomposition of substances resulting from this force "catalysis". In 1915, Fritz Haber developed the ammonia synthesis over reduced iron. The year 1936 was the

beginning of the 'modern era' in catalysis due to the catalytic cracking developed by Eugene J. Houdry which revolutionized petroleum refining.

Heterogeneous catalytic reactions are very important to the chemical industry since they provide new and efficient pathways for chemical synthesis which are economically attractive. About 15–20% of all manufactured goods produced in the USA involve heterogeneous catalytic processes. Because of the ability of catalysts to significantly modify the economics of chemical synthesis, a considerable amount of research activity has been directed towards discovering new catalysts or improving the existing ones.

As energy demand increases and the availability of petroleum decreases, it will become necessary to process residual petroleum fractions and liquids derived from coal, oil shale, and tar sand, which contain much higher concentrations of organic nitrogen and sulfur compounds. The removal of these heteroatoms (N,S) is necessary for environmental reasons as well as to increase the quality of the product by increasing the hydrogen/carbon ratio.

Nitrogen compounds lower the grade of fuels due to the following reasons:

1. Fuel bound nitrogen contributes directly to the formation of NO_x in combustion process.

2. The activity of catalysts used in cracking and other processes [69,49,57] such as reforming, isomerization, and polymerization is reduced because these catalysts are acidic whereas nitrogen compounds are basic.

3. High nitrogen concentrations are detrimental to both product quality and product stability. In fact, gums, precipitates, and lacquers formed during the

storage or use of oils and fuels are directly related to the presence of nitrogen compounds [87,68]. In addition, the presence of these compounds, even in trace amounts, leads to poor color and color stability of oils [70,51].

4. Most aromatic nitrogen compounds are biologically harmful and often carcinogenic.

Catalytic hydrodenitrogenation (HDN) is a common process to up-grade these fuels. HDN is a process in which organonitrogen compounds are removed from hydrocarbon feedstocks to produce processible, stable, and environmentally acceptable liquid fuels. When coupled with hydrodesulfurization (HDS), the removal of organic sulfur, the process is commonly referred to as "hydrotreating", which is an integral part of oil refining. On the other hand, hydrocracking is the process in which large organic molecules are converted into smaller ones such as saturated olefins and aromatics.

The function of the hydrocracking catalyst includes hydrogenation, isomerization, and cracking. By controlling and optimizing these functions, improvements in hydrocracking processes and their commercialization have been possible. The principal role of a metal in a hydrotreating catalyst is to keep the acidic sites active throughout hydrogenation [14].

Nitrogen concentrations in synthetic liquids are typically two to five times higher than those in petroleum stocks. The major portion of the nitrogen present in these fuels is found as heterocyclic compounds, which are usually resistant to hydrodenitrogenation. Some characteristic nitrogen compounds found normally in petroleum and coal-derived liquids are shown in Figure 1.1. Studies on the nature of the

PYRIDINE

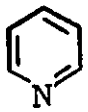

INDOLE

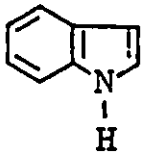

CARBAZOLE

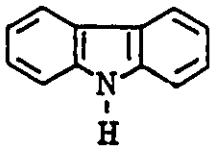

QUINOLINE

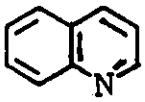

ACRIDINE

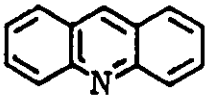

BENZ(C)ACRIDINE

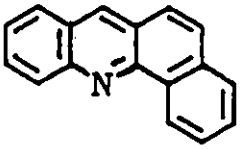

BENZ(A)ACRIDINE

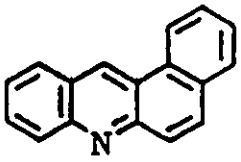

DIBENZACRIDINE

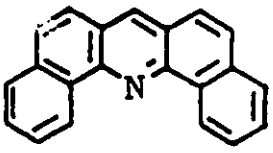

Figure 1.1: Typical nitrogen-containing compounds found in petroleum and coal-derived liquids

nitrogen containing compounds in petroleum have shown that nitrogen concentration increases with increasing boiling point of the petroleum fractions [91]. One or two ring heterocyclic nitrogen compounds are concentrated in the lighter fractions, whereas multiring nitrogen-containing compounds predominate the heavier fractions.

While it has long been recognized that HDN is more difficult than HDS, the former has historically been of little concern to the refiners because of the comparatively small quantities of nitrogen compounds present in conventional petroleum stocks. However, this situation will certainly change in processing high-nitrogen synthetic liquids.

Most of the previous HDN kinetic studies have considered either single model nitrogen compounds or a whole coal derived liquid. This present study is focused on the hydrodenitrogenation of two pure heterocyclic nitrogen compounds, pyridine and quinoline, and their binary mixture. A large percentage of the nitrogen-bearing compounds present in crude oil are derivatives of pyridine. On the other hand, quinoline contains an aromatic ring as well as a heterocyclic one. This makes these two compounds good models for HDN studies.

The present work is undertaken to study the kinetics of the HDN of two pure nitrogen compounds and their mixture. More specifically the objectives of this work are:

- to study the effect of process variables, i.e. temperature (T), space time (W/F), and hydrogen to nitrogen compound molar ratio ($\overline{R}$) on the conversion, selectivity, and yield of the HDN reaction.

- to establish reaction networks for the HDN of single compounds, pyridine and quinoline.
- to develop kinetic models for each HDN reaction.
- to study the interactions between these two model compounds and the effects of mixing on mechanisms and HDN kinetics under industrially relevant reaction conditions.

Chapter 2

Theoretical Aspects

This chapter gives a general outlook about the work done on the HDN of heterocycles, mainly pyridine and quinoline. It also deals with the types of mechanisms that are used for kinetic analysis and the types of reactors and their characteristics. In addition, it sheds some light on the theory of heat and mass transfer on the catalyst surface.

2.1 Literature Review

Hydrodenitrogenation is an integral part of the hydrotreating process in which nitrogen is removed from the oil residuals while hydrogen is being added so as to increase the hydrogen to carbon ratio in the organics produced.

2.1.1 Heteroatoms in Heavy Fuels

The heteroatoms present in fuel feedstocks include sulfur, nitrogen, oxygen, and metal. Crude petroleum contains 0.1–3% wt. sulfur, 0.01–0.3% wt. nitrogen, less than 0.5% wt. oxygen, and 20–100 ppm by wt. metals. In petroleum residuals the percentage of nitrogen is more than 0.3% wt. since nitrogen-containing compounds are concentrated in higher boiling petroleum fractions [97]. Fuels derived from coal,

shales, and tar sands have even higher nitrogen contents [97,9].

Heterocyclic nitrogen compounds are usefully divided into two groups: those which have a six-membered pyridinic ring and those which have a five-membered pyrrolic ring [52]. In the five-membered nitrogen heteroaromatics the extra pair of electrons in nitrogen, which accounts for the usual basicity of nitrogen compounds, is involved in the π-cloud of the ring and is therefore not readily available for interacting with acids. In this sense, this type of compound is regarded as non-basic and has a $pK_a < 2.0$, such as pyrroles, indoles, and carbazoles. In contrast, the nitrogen's unshared pair of electrons in six-membered ring compounds is not tied up in the π-cloud and is therefore available for sharing with acids. Thus these compounds are strong bases and have a $pK_a > 2.0$, such as pyridines, quinolines, and acridines. Table 2.1 shows some of the nitrogen compounds found in fuels with their basicities [103,47]. The ratio of basic to non-basic nitrogen-containing compounds in petroleum is roughly 1:2, while that in synfuels is closer to 2:1. Therefore, synfuels have higher nitrogen concentration and are more basic than light petroleum.

2.1.2 Hydrotreating Reactions

Hydrotreatment is a mild hydrogenation process where the primary objective is the removal of heteroatoms. In addition, hydrotreatment causes some hydrogenation of unsaturated bonds with minimal cracking of large molecules. Hydrotreatment process includes hydrodesulfurization (HDS), hydrodenitorgenation (HDN), hydrodeoxygenation (HDO), and hydrodemetalation (HDM). The main reactions are represented as follows:

Sulfur-containing compound + $H_2 \xrightarrow{catalyst}$ Hydrocarbon + H_2S

Nitrogen-containing compound + $H_2 \xrightarrow{catalyst}$ Hydrocarbon + NH_3

Oxygen-containing compound + $H_2 \xrightarrow{catalyst}$ Hydrocarbon + H_2O

Table 2.1: Nitrogen compounds in fuels and their basisities

Compound	pK_a
Piperidine	11.12
Cyclohexylamine	10.66
Ethylpiperidine	10.45
Ammonia	9.27
2-Methylquinoline	5.83
Acridine	5.58
Pyridine	5.25
Quinoline	4.90
N-Methylaniline	4.85
Aniline	4.63
Pyrrole	0.40
Indole	-3.50[a]
Carbazole	-1.00

a: See Ref. [47]

2.1.3 Hydrotreating Processes

Hydrotreatment is achieved in the presence of hydrogen at pressures of 35-270 atm, temperatures of 300–460 °C, and a catalyst [37]. This process needs a significant amount of hydrogen, mainly because HDN of nitrogen compounds is believed to proceed via saturation of the heterocyclic ring followed by ring fracture and subsequent removal of nitrogen as ammonia. In coal hydrotreating, Fu and Batchelder [32] have shown that the hydrogen consumption increases with increasing reaction temperature and time. On the commercial scale, hydrogen is recovered and recycled to the process with make-up hydrogen.

It is well known that the presence of nitrogen and sulfur compounds in the feed stock are the major cause of catalyst poisoning. Hence, the most important hydrotreating processes are the ones that are concerned with the reduction of the level of sulfur and nitrogen compounds in syncrudes to allow further catalytic processing without the danger of poisoning. Removal of oxygenated compounds occurs usually in the desulfurization or denitrogenation step [26].

2.1.4 Hydrotreating Catalysts

Most hydrotreating catalysts consist of a major metal component such as molybdenum or tungsten (10–20% wt.) and a promoter usually cobalt or nickel (2–5% wt.) supported on γ- alumina. Cobalt and molybdenum (cobalt molybdate) is the most widely used desulfurization catalyst whereas nickel and molybdenum (nickel molybdate), or nickel and tungsten, are commonly used for hydrodenitrogenation.

The metals in a fresh catalyst are generally present as oxides, but are converted to sulfides either in a pretreatment step or in actual operation where organic sulfur compounds and hydrogen sulfide are present. In using oxide and sulfide catalysts, the conditions for presulfidation could have a significant effect on the optimum hydrodenitrogenation activity. Goudriaan and co-workers [40], studying pyridine hydrodenitrogenation over cobalt molybdate catalysts, found that presulfided catalyst was substantially more active than the oxide and that the continuous addition of hydrogen sulfide further increased activity. They concluded that the hydrogenation activity of the sulfided catalyst is substantially greater than that of the oxide and that the presence of hydrogen sulfide had a beneficial effect on the hydrocracking activity of the catalyst. Similar effects were also reported by Mayer [64].

2.1.5 Catalytic Chemistry

Hydrodenitrogenation involves hydrogenolysis of the carbon-nitrogen bonds in nitrogen-containing compounds to give a denitrogenated product and ammonia. Hydrodenitrogenation is more difficult than hydrodesulfurization; hence, it requires more severe conditions and consumes more hydrogen [77,82]. This large hydrogen consumption is attributed to the initial hydrogenation of the ring or complete saturation of the carbon atoms before the hydrogenolysis of the carbon-nitrogen bonds.

In contrast to hydrodenitrogenation, hydrodesulfurization occurs by the direct removal of the sulfur that is the C–S bond breaking is the initial step, and the aromatic saturation is not a prerequisite for C–S bond breaking when the carbon atom is aromatic. This suggests that the appropriate selective catalyst should be able to remove sulfur without doing unnecessary hydrogenation and thus, save hydrogen costs.

2.1.6 HDN of Model Nitrogen Compounds

In this section a literature review of the hydrodenitrogenation kinetics of pyridine, quinoline and oil shale is presented.

Pyridine

Pyridine was first isolated and characterized by Anderson in 1846. The cyclic nature of pyridine was recognized by Korner, and by Dewar, in 1869 [11].

McIlvried [66] studied the HDN of pyridine and found that the reaction involves

successive steps starting with a rapid hydrogenation of pyridine to piperidine followed by slow-ring rupture to form n-pentylamine and rapid denitrification of n-pentylamine to ammonia. The reaction would be in the following manner:

pyridine → piperidine → n-pentylamine → n-pentane + ammonia

The catalyst was a presulfided Ni-Co-Mo/Al_2O_3. The data obtained from piperidine denitrification fit a Langmuir-Hinshelwood type kinetic model. This model is expressed in the following manner

$$\frac{dP_{PIP}}{d(1/S_v)} = -\frac{0.71\Pi P_{H_2} P_{PIP}}{(1+\overline{R})(1+1.57P_{PYR_0})} \times 10^{-4} \tag{2.1}$$

This rate expression was then used to develop the following kinetic model for pyridine

$$\frac{dP_{PYR}}{d(1/S_v)} = -\frac{4.55\Pi P_{H_2} P_{PYR}}{(1+\overline{R})(1+10.5P_{NH_3})} \times 10^{-4} \tag{2.2}$$

where:

P_i partial pressure of component i, psia

$\overline{R}$ molar ratio, g-mole H_2/g-mole nitro-compound

S_v volumetric liquid hourly space velocity, hr^{-1}

Π total pressure, psia

subscripts:

PIP piperidine

PYR pyridine

0 conditions at reactor inlet.

Aboul-Gheit et al. [2] using a batch autoclave and Co-Mo/Al_2O_3 catalyst have studied the hydrodenitrogenation of pyridine in paraffin oil at temperature range 350–400°C and initial hydrogen pressure of 25–100 atm. They concluded that under hydrotreating conditions pyridine is saturated to piperidine then the ring is cracked at different positions to produce a mixture of primary and secondary amines. At low temperature conditions, the production of alkylpiperidines is a side reaction of great significance. The initial hydrogen pressure has a decisive influence upon the rate of pyridine hydrodenitrogenation.

Sonnemans et al. [92] studied the kinetics of pyridine hydrogenation at high hydrogen pressures (1.5–7.5 MPa) on a Mo-Al oxide and Co-Mo-Al oxide catalyst. The data obtained fit a Langmuir type kinetic model with the assumption that the reaction is a first-order in pyridine i.e. pyridine and piperidine have equal and strong adsorption. The rate equation was found to be

$$r = -\frac{dP_{\mathrm{PYR}}}{dt} = k\frac{P_{\mathrm{PYR}}P_{\mathrm{H_2}}^{n}}{P_{\mathrm{PYR_0}}} \tag{2.3}$$

where:

P_{PYR} partial pressure of pyridine, psia

t time of reaction, min.

r reaction rate

k reaction rate constant

n order of the reaction

ir which n, the order of reaction with respect to hydrogen, is 1.5 at 300–375°C and 1.0 at 250°C.

Sonnemans and Mars [94], considering pentylamine as one of the intermediates formed in the hydrogenolysis of pyridine, have studied the kinetics of the conversion of this compound on MoO_3/Al_2O_3 and between 250 to 350°C. Several reactions were observed: cracking to pentene and ammonia, hydrocracking to pentane and ammonia, dehydrogenation to pentanimine and butylcarbonitrile and disproportionation to ammonia and dipentylamine. Both cracking and hydrocracking took place, mainly above 300°C. They concluded that at low conversions the rate of ammonia formation is mainly influenced by the disproportionation reaction, while at conversions above 60% cracking or hydrocracking of pentylamine or dipentylamine is rate-determining in the ammonia formation. But, according to other investigators, the rate determining step in the denitrogenation of heterocyclic bases is the hydrogenation of the aromatic ring [39] or the rupture of this ring [66] and not the deamination of the primary amines.

In another investigation, Sonnemans et al. [95] studied the conversion of piperidine on a $CoO\text{-}MoO_3\text{-}Al_2O_3$ catalysts as a function of temperature, reaction time, initial piperidine partial pressure and the hydrogen pressure. The reaction scheme concluded was as follows:

- Piperidine is converted into ammonia, pentane, and pyridine; pentylpiperidine is an intermediate in the ammonia formation.
- Pentylpiperidine is converted into ammonia and pentane; piperidine, dipentylamine, and pentylamine are intermediate products.

Satterfield and Cocchetto [78] studied pyridine HDN in a continuous flow, fixed bed, catalytic micro reactor using commercial $Ni\text{-}Mo/Al_2O_3$ and stated that the

equilibration between pyridine and piperidine can be a rate-limiting factor under some conditions. At nearly 300°C, equilibrium shifts from piperidine to pyridine. Above 400°C and at a pressure of 11 bars, a maximum in pyridine HDN rate occurs and an equilibrium is established.

Satterfield et al. [82] studied the interaction between catalytic HDN of pyridine and HDS of thiophene and found that sulfur compounds have a dual effect on HDN. First, at low temperatures, thiophene inhibits the reaction by competing with pyridine for hydrogenation sites which retards the conversion of pyridine to piperidine and hence, reduces the overall rate reaction. Second, at high temperatures, hydrogen sulfide, produced from HDS, interacts with the catalyst to improve its hydrogenolysis activity and hence increases the rate of piperidine hydrogenolysis, which is rate-controlling under these conditions, leading to an increase in the overall HDN rate. The above result was confirmed in a later study by Satterfield et al. [83].

Gupta [42] studied the vapour-phase hydrogenation of pyridine over Co-Mo/Al_2O_3 catalyst and concluded that the HDN of pyridine takes place in two steps, hydrogenation of pyridine to piperidine and subsequent conversion of piperidine to pentane and ammonia via pentylamine, pentylpiperidine, and dipentylamine.

Anabtawi et al. [5] studied the vapor-phase hydrogenation of pyridine in an integral flow reactor over Ni-W/Al_2O_3 catalyst. They concluded that the hydrogenation of pyridine proceeds through the following steps:

- Saturation of the double bonds of pyridine to form piperidine
- Disproportionation of piperidine to form ammonia and n-pentylpiperidine

- Formation of n-pentane from n-pentylpiperidine.

The data obtained from the above study fit the following rate equation

$$r = -\frac{dP_{\mathrm{PYR}}}{dt} = k_{ov} P_{\mathrm{PYR}} P_{\mathrm{H_2}} \tag{2.4}$$

It was observed that k_{ov} is dependent on the initial pressure of pyridine, and could be represented as

$$k_{ov} = \frac{k_s}{P_{PYR_0}} + k_i \tag{2.5}$$

where:

k_i reaction rate constant (intercept in a plot of k_{ov} *vs* $1/P_{PYR_0}$, mol/g-cat-hr (N/m^2)

k_{ov} observed rate constant for hydrogenation of pyridine, mol/g-cat-hr

k_s reaction rate constant (slope in a plot of k_{ov} *vs* $1/P_{PYR_0}$, mol/g-cat-hr(N/m^2)

P_i partial pressure of species i, N/m^2

r reaction rate, mol/g-cat-hr(N/m^2)

In a recent work, Vit and Zdrazil [98] studied the activity and selectivity of carbon-supported sulfides of Ru, Pd, Ir, and Pt using simultaneous reaction of pyridine and thiophene. They found that the sulfides of platinum metals were better HDS catalysts and much better HDN catalysts than the commercial Co-Mo/Al_2O_3 or Ni-Mo/Al_2O_3.

Quinoline

Impure quinoline was first obtained from coal tar by Runge in 1834, and in 1842 Gerhardt obtained it as a degradation product from quinine [11].

Doelman and Vlugter [28] studied the HDN of quinoline using prereduced Co-Mo/alumina catalyst and concluded that nitrogen removal from quinoline (Q) proceeded primarily through *py*-tetrahydroquinoline (PyTHQ) and various aniline intermediates, with breakdown of the aniline as the rate-determining step. With the same catalyst, Madkour et al. [63] observed a significant increase in the quinoline HDN rate when large excesses of hydrogen chloride were present, due to the acceleration of the hydrogenolysis reaction.

Flinn et al. [34], studying the HDN of quinoline over presulfided Ni-W/Al_2O_3 in a high purity paraffin oil, found that the reaction is first-order with respect to quinoline. However, it was reported that the reaction involves ring hydrogenation which is the rate-controlling step preceding any nitrogen removal.

Shih et al. [88] studied quinoline HDN using a 1-liter autoclave and presulfided Ni-Mo/γ-alumina (American Cyanamid HDS–9A) catalyst under a pressure of 3.4 MPa and temperature 342°C. An amount of CS_2 (0.05% wt. of carrier oil) was added to maintain the catalyst in the sulfided form. They reported that the hydrogenation reactions are first-order with respect to nitrogen content, whereas they are second-order in hydrogen.

Aboul-Gheit et al. [1], using a batch autoclave and Co-Mo/Al_2O_3 catalyst, studied the HDN of quinoline and found that the first step was the hydrogenation of quinoline to PyTHQ. which is converted to o-propylaniline. The latter compound is then mainly converted to propylbenzene and ammonia. From the above study

they concluded that the first step was very fast whereas the second step was very slow.

Cocchetto and Satterfield [25] studied the chemical equilibria in the HDN of quinoline in a continuous flow, vapor-phase, fixed-bed catalytic micro reactor employing a presulfided commercial Ni-Mo/Al_2O_3. The equilibrium constants were calculated for significant reaction paths. It was concluded that there was a good agreement between the experimental equilibrium constants and the theoretical ones, the largest discrepancy was in that of the hydrogenation of quinoline to PyTHQ.

In another study, Satterfield and Cocchetto [79] have modeled the kinetics of the irreversible intermediate steps i.e. denitrogenation of o-propylaniline (OPA), and hydrogenolysis of *py*-tetrahydroquinoline and decahydroquinoline (DHQ). They also proposed the following Langmuir-Hinshelwood rate expression for o-propylaniline denitrogenation

$$r_{OPA} = -\frac{kK_{OPA}P_{OPA}}{1 + K_{OPA}P_{OPA} + K_{NH_3}P_{NH_3}} \tag{2.6}$$

where:

k pseudo-rate constant for OPA denitrogenation

K adsorption equilibrium constant

P partial pressure

r net rate of formation

subscripts:

OPA o-propylaniline

Satterfield and Gultekin [81], studied the effect of hydrogen sulfide on the HDN of quinoline and found that H_2S had a slight inhibiting effect on the intermediate hydrogenation steps but a marked accelerating effect on the hydrogenolysis steps and hence, an increase in the overall HDN rate, whereas the presence of H_2S had no effect in the case of nitrogen removal which has the following order:

OPA > DHQ > BzTHQ > Q = PyTHQ.

This same result was reported later on by Yang and Satterfield [107] when the HDN reaction were studied in a trickle-bed reactor. On the other hand, Satterfield et al. [84], studied the effect of water and hydrogen sulfide on the HDN of quinoline and deduced that the presence of water can enhance the activity of a Ni-Mo/Al_2O_3 catalyst, but the effect is less pronounced than the enhancing effect of H_2S, while the enhancing effect of H_2S and H_2O together is greater than either one alone.

Miller and Hineman [67] studied the HDN of quinoline over sulfided cobalt-molybdate and deduced that the rate of nitrogen removal is less than one. A Langmuir-Hinshelwood expression was used to interpret the data.

In a recent study done by Yu et al. [110] on the HDN of quinoline over a presulfided Ni-W/Y82 zeolite it has been suggested that the rate-limiting step in denitrogenation is the irreversible reaction from PyTHQ to OPA and that the hydrogenolysis data can be well regressed with a Langmuir-Hinshelwood model.

A more recent work done by Eijsbouts et al. [30] on the HDN of quinoline over carbon-supported transition metal sulfides, at 653 K and 5.5 MPa had shown that the sulfides of the second and the third row gave higher conversion and selectivity than the first row. Furthermore, the maximum conversion was for Rh/C and Ir/C while the lowest one was for Mo/C and W/C. They also concluded that Rh/C and

Ir/C have high selectivity for propylcyclohexane while Ru/C and Re/C have high selectivity to propylbenzene.

Almost all of the above studies concluded that denitrogenation is first order with respect to the concentration of nitrogen species. A discussion of the kinetics of denitrogenation becomes much more complicated when one considers industrially important feeds such as petroleum stocks, shale oil, and coal-derived liquids. These feedstocks contain a large number of unspecified organonitrogen compounds.

Petroleum Feedstocks and Oil Shale

Flinn et al. [34] found that the ease of denitrogenation tends to decrease with the increasing of the boiling point of the petroleum feed. Very high hydrogen pressures are required for complete removal of nitrogen from petroleum feeds. The difficulty in complete denitrogenation is due to the fact that the secondary nitrogen compounds produced from hydrodenitrogenation are more resistant to denitrogenation than the precursors.

McCandless and Berg [65] studied the hydrodenitrogenation of petroleum using a supported nickelous chloride-gaseous chloride catalyst system. It was found that the system was more active for nitrogen removal than commercially available nickel tungsten sulfide and cobalt molybdenum. However, the sulfur removal was at relatively low level. This high hydrodenitrogenation activity may have resulted from the interaction between the acid catalyst system and the basic nitrogen compounds.

Koros et al. [55] studied the hydrodenitrogenation of shale oil over a cobalt

molybdate on alumina catalyst and a pressure of 800 psig and deduced that quinoline-type compounds denitrogenate more readily than indole-type compounds. This result is a direct contrast to that reported by Flinn [34]. However, Silver et al. [89] studied the hydrodenitrogenation of shale oil on Co-Mo/Al_2O_3 at 5000 psig and 750 F and reported that the denitrogenation rate constants for indole-type compounds were greater than that for quinoline-type compounds.

2.2 Kinetic Analysis

Kinetic studies are hampered by empiricism. Only simple homogeneous gas reactions can be treated by the activated-complex theory, collision theory, or more general reaction-rate theories [50]. Most heterogeneous catalytic reactions are too complex to be treated satisfactorily by such theories, and it is therefore necessary to rely on classical, empirical methods. Heterogeneous catalytic reactions consist of at least three single steps: adsorption, surface reaction, and desorption. Considerable simplification results when there is a single rate-determining step. However, only when surface reaction is the rate-limiting step are overall kinetics governed by the kinetics of the reaction step. On the other hand if desorption of product is the rate-limiting step then overall kinetics measured in the gas phase do not reflect the kinetics of the surface-reaction rate [23]. In heterogeneous catalysis it is desired to derive the rate expressions based on the Langmuir-Hinshelwood theory [56].

2.2.1 Mechanistic Steps in Heterogeneous Catalytic Reactions

The sequence of steps for a heterogeneous catalytic reaction is as follows [20]:

1. Mass transfer of reactants from the main body of the fluid to the gross exterior surface of the catalyst particle.

2. Molecular diffusion and/or Knudsen flow of reactants from the exterior surface of the catalyst particle into the interior pore structure.

3. Chemisorption of at least one of the reactants on the catalyst surface.

4. Reaction on the surface. (this may involve several steps.)

5. Desorption of (chemically) adsorbed species from the surface of the catalyst.

6. Transfer of the products from the interior catalyst pores to the gross external surface of the catalyst by ordinary molecular diffusion and/or Knudsen diffusion.

7. Mass transfer of products from the exterior surface of the particle into the bulk of the fluid.

Steps 1 and 7 are highly dependent on the fluid flow characteristics of the system. Hence, the rate of these steps depends on the mass velocity of the fluid stream, the particle size, and the diffusional characteristics of various molecular species. These steps limit the observed rate only when the catalytic reaction is very rapid and the mass transfer is slow. Steps 2 and 6 depend on the degree of porosity of the catalyst, the dimensions of the pores, the degree to which the pores are interconnected, the gross dimensions of the catalyst particle itself, the rate at which the reaction occurs at the catalyst surface, and the diffusional characteristics of the reaction mixture. In most cases a heterogeneous catalytic reaction involves three mechanistic steps, adsorption, surface reaction, and desorption. It is convenient to employ the concept

of a rate limiting step in the treatment of these processes so that the reaction rate becomes equal to that of the slowest step.

2.2.2 Kinetic Models

When the reaction involves two molecules, A and B, then two general mechanisms can be visualized [16]:

Langmuir-Hinshelwood Mechanism

This type of mechanism assumes that both A and B are reacting in the adsorbed state. Consider the general reaction

$$A + B = R + S$$

The rate of the irreversible reaction is given by

$$r = k_1' \theta_A \theta_B \tag{2.7}$$

or

$$r = \frac{k_1' K_A K_B P_A P_B}{(1 + K_A P_A + K_B P_B)^2} \tag{2.8}$$

The rate expression for a reversible reaction is given by

$$r = k_1' \theta_A \theta_B - k_{-1}' \theta_R \theta_S \tag{2.9}$$

or

$$r = \frac{k_1' K_A K_B P_A P_B - k_{-1}' K_R K_S P_R P_S}{(1 + K_A P_A + K_B P_B + K_R P_R + K_S P_S)^2} \tag{2.10}$$

where:

r reaction rate

k'_1 reaction rate constant of forward reaction

k'_{-1} reaction rate constant of reverse reaction

P_i partial pressure of component i

K adsorption equilibrium constant

θ fraction of occupied catalytic sites

subscripts:

$_A$ reactant A

$_B$ reactant B

$_R$ product R

$_S$ product S

Rideal Mechanism

For this type of mechanism it is assumed that one of the reactants, say A, is in the adsorbed phase reacting with the other, say B, in the gaseous phase. The rate of the reaction can be expressed as

$$r = k'_1 \theta_A P_B \tag{2.11}$$

or

$$r = \frac{k'_1 K_A P_A P_B}{1 + K_A P_A + K_B P_B} \tag{2.12}$$

Yang and Hougen [106] have considered several additional surface reaction mechanisms and have developed tables from which rate expressions for these mechanisms may be determined. They have expressed the rate in the following form

$$rate = \frac{(kinetics\ term) \times (potential\ term)}{(adsorption\ term)^n} \tag{2.13}$$

If the hydrogenation reaction is of the form

$$A + H_2 = R$$

then the kinetics term is expressed as

$$kinetics\ term = \eta m K_A \tag{2.14}$$

the potential term is

$$potential\ term \quad _A - \frac{a_R}{K_{eq} a_R} \tag{2.15}$$

and the adsorption term is

$$adsorption\ term = 1 + \frac{K_A a_R}{K_{eq} a_{H_2}} \tag{2.16}$$

where:

η	effectiveness factor
m	number of active sites
K	adsorption equilibrium constant
K_{eq}	overall equilibrium constant
a	activity

subscripts:

$_A$ reactant A

$_R$ product R

In the case of pyridine hydrodenitrogenation, for example, and according to Satterfield and Cocchetto[80], the equilibrium constant between pyridine and piperidine is very large. Then the overall equilibrium constant (K_{eq}) is large. At excess hydrogen the activity (a_{H_2}) is very high also, hence the adsorption term will be equal to unity. The rate expression can be written as

$$rate = (\eta m K_{\mathrm{PYR}})(a_{\mathrm{PYR}}) \tag{2.17}$$

or

$$rate = k(C_{\mathrm{PYR}})^n \tag{2.18}$$

where:

k reaction rate constant

C concentration

superscripts:

^{n} order of the reaction

Power-Law

The nonuniformity of catalyst surfaces and lack of accurate knowledge of the structure of the chemisorbed species and their concentrations have been of great

concern to many investigators. The assumptions of a homogeneous surface is not always true [23] and hence it is suggested to use the power law instead of Langmuir form. According to Smith [90], when the objective is reactor design, where calculations of engineering accuracy are going to be made with the rate equation, the simplicity of the power-law form is advantageous. The general power-law rate expression is

$$r = k_1' P_A^{\alpha} P_B^{\beta} \tag{2.19}$$

where:

r reaction rate

k_1' reaction rate constant

P_i partial pressure of component i

subscripts:

$_A$ reactant A

$_B$ reactant B

superscripts:

$^{\alpha}$ order of reaction with respect to A

$^{\beta}$ order of reaction with respect to B

2.3 Test Reactors

In general, any type of reactor with known contacting pattern may be used to explore the kinetics of catalytic reactions. The operation of catalytic reactors is defined by a number of parameters. For instance, a change in mass defines whether the reactor is a batch or a flow reactor. Exchange of temperature defines whether the reactor is adiabatic or isothermal. There are other parameters such as reactor volume, residence time, and space time which are also important in defining the operation of the catalytic reaction.

The experimental strategy in studying catalytic kinetics usually involves measuring the extent of conversion of gas passing in steady flow through a batch of solids [58]. The following sections give the properties and limitations of two plug flow reactors; the integral and the differential reactors.

2.3.1 Integral Plug Flow Reactors

These reactors are operated at high conversions with reactant composition changing along the catalyst bed. The rate of the reaction changes significantly along the reactor. The reactor can be operated either adiabatically or isothermally. The main reason for errors in the integral data is the lack of isothermicity. The catalyst bed temperature can be maintained constant by two ways; inserting the reactor in a fluidized sand bed and/or catalyst dilution i.e. adding inert solids to the catalyst bed. The reaction rate can be obtained by either integral or differential analysis.

The steps in the integral analysis are:

1. Make a series of runs with fixed feed initial concentration, C_{A_0}, while varying

W/F_{A_0}.

2. Select the rate equation to be tested and with it integrate the plug flow performance equation

$$W/F_{A_0} = \int_0^{X_A} \frac{dX_A}{-r_A} \tag{2.20}$$

where:

W	weight of the catalyst
F_{A_0}	initial flow rate of reactant A
X_A	fractional conversion of component A
r_A	rate of the reaction

3. Evaluate numerically the left-and the right-hand side of the integrated form of the above equation.

4. Plot one against the other and test for linearity.

The rate in an integral reactor is given by

$$-r_A = \frac{dX_A}{dW/F_{A_0}} = \frac{dX_A}{d(W/F_{A_0})} \tag{2.21}$$

The rate can be evaluated by the following procedure

1. Make a series of runs with fixed feed initial concentration, C_{A_0}, while varying W/F_{A_0}.

2. plot X_A versus W/F_{A_0} for all runs.

3. Fit the best curve to the above data making it pass through the origin. The rate at any X_A is the slope at that point.

4. Evaluate C_A and plot C_A versus -r_A. Test for linearity and find the rate constant.

The main advantages of the integral reactor are: (i) Integral reactor data are intrinsically more accurate and (ii) Data at high conversion are preferred for model discrimination.

2.3.2 Differential Plug Flow Reactors

In differential reactors the conversion is small so it is usually reasonable to use a shallow small reactor. The rate is considered to be constant throughout the reactor. The performance equation for a plug flow differential reactor is

$$W/F_{A_0} = \int_{X_{A,in}}^{X_{A,out}} \frac{dX_A}{-r_A} = \frac{X_{A,out} - X_{A,in}}{(-r_A)_{av}} \tag{2.22}$$

where $(r_A)_{av}$ is given by

$$(-r_A)_{av} = \frac{F_{A_0}(X_{A,out} - X_{A,in})}{W} \tag{2.23}$$

The procedure to find the rate expression is as follows

1. Make a series of runs using different $C_{A,in}$.
2. Select the highest value of $C_{A,in}$ and call it C_{A_0}. Make this concentration the basis for calculating F_{A_0}, $X_{A,in}$ and $X_{A,out}$.
3. For each run determine F_{A_0}, W, $X_{A,in}$, $X_{A,out}$, and $C_{A,av}$.
4. Calculate the rate for each run using the above equation.
5. Plot $C_{A,av}$ versus -$(r_A)_{av}$, test for linearity and evaluate the rate constant.

Differential reactors give the rate directly, hence they are more useful in analyzing complex systems.

2.4 Plug-Flow Reactor Equations

All the results of this study were derived from a steady-state, plug-flow, integral reactor. A derivation and understanding of the equations of the plug-flow reactor will help in the kinetic interpretation of the results.

The reaction rate as well as the concentrations vary significantly in the axial direction of a plug-flow reactor. There are several assumptions that are made before deriving the corresponding rate equation:

1. The velocity profile in the reactor is flat, i.e. plug-flow exists. This can be verified by the small size of the catalyst particles, and due to the presence of the fine porous plate at the inlet of the reactor.

2. The reactor operates isothermally, i.e. there are no thermal gradients in the reactor. Theoretically, this assumption can never be valid if heat effects accompany the reaction. However, this ideal state was approximated by putting the reactor in a fluidized bed and fluidizing it properly.

3. No change in the total molar flow rate during the course of the reaction. This assumption can be verified by the large excess of hydrogen.

4. There is no pressure drop across the reactor.

5. There is no axial or radial dispersion in the reactor.

For a heterogeneous catalytic reaction, the rate must be expressed per unit weight or per unit area of the catalyst. Since the two concepts are related through the specific surface area of the material, relations are developed in terms of the former.

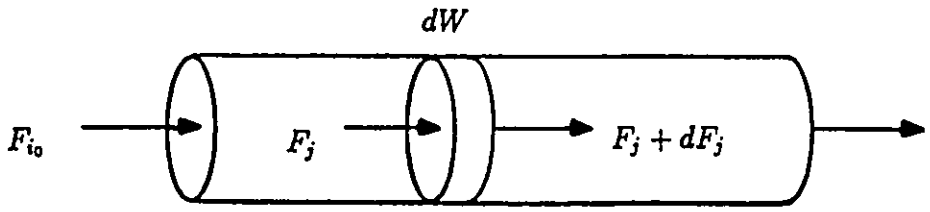

Figure 2.1: Notation for plug flow reactor

A material balance for any non-hydrogen species, j, over a differential element of the reactor (Figure 2.1) gives the following:

input + generation by reaction = output + accumulation

At steady state the accumulation is equal to zero, hence

$$(F_j) + (r_j dW) = (F_j + dF_j) \tag{2.24}$$

The rate of formation of species j in terms of the catalyst weight, W, is given by

$$r_j = \frac{dF_j}{dW} \tag{2.25}$$

where:

F_j molar flow rate of j, g-mol j/hr

W mass of the catalyst, g

r_j net rate of formation of j, g-mol j/hr g-catalyst

Defining the fractional conversion of reactant nitrogen compound, i, into species j as

$$X_j = \frac{F_j}{F_{i_0}} = \frac{(\frac{F_j}{F})\Pi}{(\frac{F_{i_0}}{F})\Pi} = \frac{P_j}{P_{i_0}} \tag{2.26}$$

therefore

$$F_j = F_{i_0} X_j = F_{i_0}\left(\frac{P_j}{P_{i_0}}\right) \tag{2.27}$$

and

$$dF_j = F_{i_0} dX_j = \left(\frac{F_{i_0}}{P_{i_0}}\right) dP_j \tag{2.28}$$

where:

F_{i_0} molar flow rate of reactant nitrogen compound i, g-mol i/hr

P_{i_0} initial partial pressure of reactant nitrogen compound, atm

Π total pressure, atm

P_j partial pressure of species j, atm

Substituting into Equation 2.25

$$r_j = \frac{F_{i_0} dX_j}{dW} = \frac{dX_j}{d\left(\frac{W}{F_{i_0}}\right)} \tag{2.29}$$

or

$$r_j = \frac{F_{i_0} dP_i}{P_{i_0} dW} = \frac{dP_j}{d\left(\frac{P_{i_0} W}{F_{i_0}}\right)} = \frac{dP_j}{d\tau} \tag{2.30}$$

Integrating the above differential rate expressions over the entire plug-flow reactor gives:

$$\frac{W}{F_{i_0}} = \int_{X_{j_0}}^{X_j} \frac{dX_j}{r_j} \tag{2.31}$$

or

$$\tau = \frac{P_{i_0} W}{F_{i_0}} = \int_{P_{i_0}}^{P_j} \frac{dP_j}{r_j} \tag{2.32}$$

In this expression the rate constant depends on the initial partial pressure of the nitrogen compound reactant. During this study, only one variable (W/F) was varied while keeping the initial pressure of the reactants constant, hence, W/F was used instead of τ.

The integrated form of the plug-flow reactor is useful for testing simple kinetic rate expressions against the experimental data. For example, if the hydrocarbon formation of the pyridine HDN reaction is zero order with respect to nitrogen compound i.e. K_{HC}= K_{NH_3}=0, then

$$r_{HC} = k' \tag{2.33}$$

From the design equation

$$\frac{W}{F_{PYR_0}} = \int_0^{X_{HC}} \frac{dX_{HC}}{k'} = \frac{X_{HC}}{k'} \tag{2.34}$$

or

$$X_{HC} = k' \frac{W}{F_{PYR_0}} \tag{2.35}$$

Hence a plot of X_{HC} versus W/F_{PYR_0} should be a straight line passing through the origin.

If τ is used instead of W/F_{PYR_0} then the equation can be written as

$$X_{HC} = \frac{k'}{P_{PYR_0}} \tau \tag{2.36}$$

If hydrocarbon formation is first-order i.e. K_{HC}=K_{NH_3} = K_{PYR}, then

$$r_{HC} = \frac{k' P_{PYR}}{P_{PYR_0}} \tag{2.37}$$

2.5 Mass and Heat Transfer

This section sheds some light on the theory associated with the mass and heat transfer that might occur in a catalytic reactor and shows how to estimate their effects.

2.5.1 External Mass Transfer in Fixed Bed Reactors

There are two general diffusional processes of importance in catalysis: (*i*) mass transfer to and from the external surface of the catalyst and (*ii*) mass transfer in and out the catalyst pores. Mass transfer to the external surface is controlled in a thin boundary layer, usually less than a millimeter in thickness, next to the catalyst surface. The velocity of a fluid passing over the surface of a particle varies rapidly normal to the flow across this boundary layer. At the catalyst surface, the fluid velocity is zero, and rapidly approaches the bulk-stream velocity a short distance from the surface. Near the surface, where fluid velocity is low, little mixing of reactants and products occurs; mass transfer normal to the surface is by molecular diffusion, and may be taken as proportional to the molecular diffusion coefficient *D*.

In some cases, the external surface concentrations do not differ appreciably from those prevailing in the bulk fluid. In other cases, a significant concentration difference arises as a consequence of physical limitations on the rate at which reactant molecules can be transported from the bulk fluid to the exterior surface of the catalyst.

In the gas phase system, it is convenient to define a mass transfer coefficient

based on a partial pressure driving force ($k_{P,i}$) as

$$k_{P,i} = \frac{J_i}{P_{i,b} - P_{i,s}} \tag{2.38}$$

then the mass transfer coefficient based on a concentration driving force ($k_{C,i}$) is

$$k_{C,i} = k_{P,i} R_g T \tag{2.39}$$

The most convenient mathematical form for correlating mass transfer data is in terms of the well known Chilton-Colburn j_D factor [21]

$$j_D = \frac{k_{C,i}\rho}{G_m} N_{Sc}^{2/3} \tag{2.40}$$

where N_{Sc} is Schmidt number and it is given by

$$N_{Sc} = \frac{\mu}{\rho D} \tag{2.41}$$

where:

J_i molar flux of species i towards the surface relative to molar average velocity

$P_{i,b}$ partial pressure of species i in the bulk

$P_{i,s}$ partial pressure of species i at the surface

R_g gas constant

ρ fluid density

μ fluid viscosity

D molecular diffusivity of the species being transferred into the system of interest

G_m mass velocity based on the total (superficial) cross-sectional area of the reactor

The j_D factor can be expressed in terms of the film pressure factor for species A, $P_{f,A}$, as

$$P_{f,A} = \frac{(\Pi + \delta_A P_A) - (\Pi + \delta_A P_{A,s})}{ln\left(\frac{\Pi+\delta_A P_A}{\Pi+\delta_i P_{A,s}}\right)} \tag{2.42}$$

then j_D can be expressed as

$$j_D = \frac{k_{P,A} P_{f,A}}{G_m} N_{Sc}^{2/3} \tag{2.43}$$

where:

Π total pressure

P_A partial pressure of species A

$P_{A,s}$ pressure of species A at the catalyst surface

and δ_A is given by

$$\delta_A = \frac{r + s + ... - a - b...}{a} \tag{2.44}$$

where $a, b, r, s, ...$ are the stoichiometric coefficients of the reaction

$$aA + bB + ... \rightleftharpoons rR + sS + ...$$

The effect of mass transfer can be determined from the following relation

$$r_{mA} = k_{G,A} a_m \phi (P_A P_{A,s}) \tag{2.45}$$

where:

r_{mA} molal reaction rate of component A

a_m area of the particle per unit mass

ϕ shape factor, assumed 0.9 for irregular granules

The pressure gradient, ΔY, can be determined from the equations and charts proposed by Yoshida et. al [109]. The pressure gradient is given by the equation

$$\Delta Y_A = \frac{\Delta P_A}{P_A} = \frac{r_{mA}}{a_m \phi G_m} (j_D)^{-1} \frac{P_{A,s}}{\Pi} (N_{Sc})^{2/3} \tag{2.46}$$

Correlations for mass transfer factors (j_D) in packed beds are given by Petrovic and Thodos [73], Chu et al. [22], and Riccetti and Thodos [76] at different ranges of Reynolds number (N_{Re}) or modified Reynolds number (N'_{Re}).

$$N_{Re} = \frac{D_p G}{\mu} \tag{2.47}$$

$$N'_{Re} = \frac{D_p G}{\mu(1-\varepsilon_B)} \tag{2.48}$$

where D_p is the particle diameter.

According to Petrovic and Thodos, for $3 < N_{Re} < 2000$

$$j_D = \frac{0.357}{\varepsilon_B N_{Re}^{0.359}} \tag{2.49}$$

According to Chu et al., for $1 < N'_{Re} < 30$

$$j_D = 5.7(N'_{Re})^{-0.78} \tag{2.50}$$

and for $30 < N'_{Re} < 10^4$

$$j_D = 1.77(N'_{Re})^{-0.44} \tag{2.51}$$

Riccetti and Thodos had suggested that, for $100 < N'_{Re} < 7000$

$$j_D = \frac{1}{(N'_{Re})^{-0.40} - 1.5} \tag{2.52}$$

where ε_B is the void fraction of bed arising from spaces between particles.

Calculations and estimations for the external and internal mass transfer effects are shown in Appendix J.

2.5.2 Heat Transfer

Heat transfer to or from a large fixed bed of catalyst often represents a significant problem. However there are a variety of operating techniques that can be used to facilitate control over the bed temperature. These include the use of inert diluents in the bed stream to moderate the temperature changes, and the use of "cold shot" or gas bypass technique in which a fresh cold reactant stream is mixed with a hot stream that has undergone partial reaction. Recycle of a product stream and partial temporary poisoning of the catalyst are two other expedients that can be used to help regulate the temperature in fixed bed reactors. In laboratory studies aimed at a determination of the rate expression for the intrinsic chemical reaction, external gradients in temperature and concentration can be made negligible by operating under the following constraints [20].

1. Using a reactant stream that is diluted with inerts to reduce the reaction rate so that the energy evolved per unit volume is greatly reduced below that encountered in the absence of inerts.

2. Employ high mass velocities to minimize resistance to heat and mass transfer.

Heat transfer between a fluid and a catalyst particle occurs primarily through the same combination of molecular and convective processes that are responsible for mass transfer in such systems. At sufficiently high temperatures, one must also allow for radiation contributions to the energy transfer processes within the reactor. Radiation effects are not significant at temperatures below 400°C for packed bed reactors comprised of pellets with characteristic dimensions of less than 1/4 in.

Experimental data on heat transfer in fixed and fluidized bed reactors are correlated in terms of a j factor for heat transfer, j_H

$$j_H = \left(\frac{h}{C_p G}\right)\left(\frac{C_p \mu}{k}\right)^{2/3} = \frac{h}{C_p G} N_{Pr}^{2/3} \tag{2.53}$$

where:

μ fluid viscosity

C_p constant pressure heat capacity per unit mass of fluid

k thermal conductivity of the fluid

G mass velocity based on the total cross-sectional area of the reactor

h heat transfer coefficient between the catalyst particle and the bulk fluid

N_{Pr} Prandtl number given by

$$N_{Pr} = \frac{D_p G C_p}{k} \tag{2.54}$$

The effect of heat can be verified from the difference between the temperatures of the bulk fluid and that of the catalyst surface given by the following relation.

$$T_s - T_b = \frac{r_{mA}(-\Delta H_A)}{\phi h a_m} \tag{2.55}$$

where:

T_s temperature at the catalyst surface

T_b temperature in the bulk fluid

ΔH_A molal heat of reaction of A

Correlations for the j factor for heat transfer can be estimated from expressions developed by Gamson et al. [36] for $N_{Re} > 350$ as

$$j_H = 1.06 N_{Re}^{-0.41} \tag{2.56}$$

The j factor for heat transfer at $N_{Re} \leq 350$, was correlated by Wike and Hougen [105]

$$j_H = 1.95 N_{Re}^{-0.51} \tag{2.57}$$

Calculations for the heat transfer effects are shown in Appendix J.

2.6 Diffusion

The geometry of the pore structure makes it impossible to determine accurately the effective length of the diffusion path. Interconnections within the pore structure, the tortuous character of individual pores, and variations in cross-sectional area along the pore length all contribute to the difficulty of the task.

One or more of several different mechanisms may be responsible for the mass transfer process. These include ordinary bulk diffusion, Knudsen diffusion, surface diffusion, and bulk flow. For the majority of the catalysts and conditions used in industrial practice, the only significant mechanisms are bulk diffusion and Knudsen

diffusion. The relative importance of these two processes depends on the relative values of the mean free path and the pore dimensions.

Ordinary or Bulk Diffusion

Ordinary or bulk diffusion is primarily responsible for molecular transport when the mean free path of a molecule is small compared with the diameter of the pore. The mean free path (λ) is the average distance a molecule travels between intermolecular collisions. A rough equation for λ is given by Wheeler [104].

$$\lambda = \frac{10^{-5}}{\Pi} \tag{2.58}$$

where Π is the pressure in atm. and λ is in cm.

At 1 atm. the mean free path (λ) of typical gaseous species is of the order of 10^{-5} cm or 10^{3} Å. In pores larger than 10^{-4} cm the mean free path is much smaller than the pore dimension, and collisions with other gas phase molecules will occur much more often than collisions with the pore walls. Under these circumstances the effective diffusivity will be independent of the pore diameter and, within a given catalyst pore, ordinary bulk diffusion coefficients may be used in Fick's first law to evaluate the rate of mass transfer and the concentration profile in the pore.

Knudsen Diffusion

Knudsen diffusion will be the dominant mechanism of mass transfer whenever the mean free path between collisions is large compared with the pore diameter. This situation prevails when the gas density is low or when the pore dimensions are very small. The molecules hitting the walls are momentarily adsorbed and then are given off in random directions (diffusely reflected). After a collision with the

pore wall, the molecule will usually fly to another spot on the wall before having a collision with a second gas phase molecule. Many collisions with the walls will take place for each collision between gas phase molecules.

Assuming that the pores are straight cylinders of radius $\bar{r}$, then according to the kinetic theory of gases and making use of Fick's law, the effective Knudsen diffusivity is given as

$$D_K = 9.7 \times 10^3 \bar{r} \sqrt{\frac{T}{M}} \tag{2.59}$$

where:

D_K Knudsen diffusivity, cm^2/s

T temperature, K

$\bar{r}$ pore radius, cm

or

$$D_K = 19400 \frac{\varepsilon^2}{\tau S_g \rho_p} \sqrt{\frac{T}{M}} \tag{2.60}$$

where:

ε catalyst porosity

τ catalyst tortuosity

S_g catalyst specific surface area

ρ_p catalyst particle density

T absolute temperature

M molecular weight of the gas mixture

The relation between the bulk diffusivity (D_{AB}) and Knudsen diffusivity is given by

$$\frac{\lambda}{2\overline{r}} = \frac{D_{AB}}{D_K} \tag{2.61}$$

Effectiveness Factor

When diffusion and reaction occur simultaneously within a porous solid structure, concentration gradients of reactant and product species are established. If the diffusional processes are rapid compared to the rate of the chemical reaction, then reaction takes place inside the pores of the catalyst. In this case only a small concentration gradient will exist between the exterior and the interior of the particle. On the other hand, if the catalyst is very active, many reactant molecules will have been converted to products before they have had time to diffuse into the pores. In this case there will be steep concentration gradients of both reactant and product species near the periphery of the particle.

Quantitative analytical treatments of the effects of mass transfer and reaction within the porous structure were first carried out by Thiele [96], Wheeler [104], Aris [6], and many other investigators. Emphasis was on the development of a technique that can be used to analyze quantitatively the factors that determine the effectiveness with which the surface area of a porous catalyst is used. Hence, the effectiveness factor, η, for a catalyst particle is defined as

$$\eta = \frac{actual\ rate\ for\ the\ entire\ catalyst\ particle}{rate\ evaluated\ at\ exterior\ surface\ conditions} \tag{2.62}$$

The intrinsic chemical reaction rate expression can be determined by the proper choice of experimental conditions that eliminate both external and intraparticle

mass transfer resistances. By evaluating the effectiveness factor, η, the true reaction rate can be calculated.

With the assumptions that the reaction is first-order, the catalyst pore has a cylindrical shape, and under isothermal conditions, the effectiveness factor was found to be

$$\eta = \frac{r_{pore}}{r_{ideal}} = \frac{\pi \overline{r}^2 \left(\frac{D_c h_T C_0}{\overline{L}}\right) tanh(h_T)}{2\pi \overline{r} \overline{L} k_1' C_0} \tag{2.63}$$

or

$$\eta = \frac{tanh(h_T)}{h_T} \tag{2.64}$$

Where h_T is the Thiele modulus which is defined as

$$h_T = \left(\frac{2k_1' \overline{L}^2}{\overline{r} D_c}\right)^{1/2} \tag{2.65}$$

The parameters $\overline{L}$ and $\overline{r}$ are given by

$$\overline{L} = \frac{V_p}{S_x} \tag{2.66}$$

$$\overline{r} = \frac{2V_g}{S_g} \tag{2.67}$$

where:

k_1' reaction rate constant per unit surface area

V_p gross volume of the catalyst particle

S_x gross exterior surface area of the particle

V_g void volume per gram of catalyst

S_g surface area per gram of catalyst

D_c combined diffusivity (Knudsen and molecular diffusion)

At equimolal counter diffusion, D_c is given by the equation

$$\frac{1}{D_c} = \frac{1}{D_{AB}} + \frac{1}{D_K} \tag{2.68}$$

D_{AB} can be found using the methods suggested by Reid and Sherwood [75], while D_K is directly proportional to the pore radius ($\overline{r}$)

$$D_K = 9.7 \times 10^{-3} \overline{r} \sqrt{\frac{T}{M}} \tag{2.69}$$

where:

T temperature in K

M molecular weight

From all of the above, we conclude that for low values of h_T (slow reaction, rapid diffusion) the effectiveness factor approaches unity. For h_T above 2.0, $tanh(4h_T)$=1 and the effectiveness factor may be approximated by $1/h_T$.

In terms of effective diffusivity, D_e, a new Thiele-type modulus is defined as

$$\Phi_S = \overline{r} \sqrt{\frac{k_1' \rho_p S_g}{D_e}} \tag{2.70}$$

where:

$\overline{r}$ radius of catalyst particle

k_1' rate constant for first-order reaction

ρ_p apparent density of catalyst particle (mass per total particle volume).

S_g surface area per gram of catalyst

D_e effective diffusivity given by

$$D_e = \frac{D_c \varepsilon_p}{\tau} \tag{2.71}$$

where:

D_c combined diffusivity

ε_p porosity of the pellet

τ tortuosity factor (takes care of length and shape factors)

then the effectiveness factor is

$$\eta = \frac{3}{\Phi_s}\left[\frac{1}{tanh(\Phi_s)} - \frac{1}{\Phi_s}\right] \tag{2.72}$$

For large values of Φ_s (>30), $tanh(\Phi_s)$ approaches unity and the effectiveness factor approaches $3/\Phi_s$, hence the reaction is diffusion limited within the pellet. At low values of Φ_s, the effectiveness factor approaches unity and hence the reaction is surface reaction limited.

2.7 Catalyst

A catalyst is a substance that affects the rate or the direction of a chemical reaction, but is not appreciably consumed in the process [20].

The chemical composition is the major factor that determines the catalyst activity. However, with a constant chemical composition, the catalytic characteristics

may vary over a wide range depending on the conditions and methods of catalyst preparation.

The catalytic properties of a catalyst can be determined by the following characteristics:

1. Catalytic activity which is the ratio of the rate of reaction at any time to the rate of reaction with a fresh catalyst.

2. Selectivity which is the rate of formation of desired product to the rate of formation of undesired products.

3. Stability which includes thermal stability, resistance to poisoning, and reproducible in its behavior.

4. Mechanical strength to resist attrition or crushing.

5. Hydrodynamic characteristics which is determined by the size, shape, and density of catalyst pellet.

Apart from the above listed characteristics, a hydrodenitrogenation catalyst must (1) effectively remove nitrogen from the organonitrogen molecule mostly through the C–N fission, (2) be able to operate in the presence of organosulfur compounds and H_2S, (3) not be easily poisoned by other petroleum impurities such as sulfur compounds or organometallic compounds and finally (4) they must not cause too much dehydrogenation and polymerization that leads to coking.

2.7.1 Hydrotreating Catalyst Models

Three models had been proposed by De Beer and Schuit for the structure of hydrotreating catalysts with the general composition Co(Ni)- Mo(W)/γ-Al_2O_3 [27].

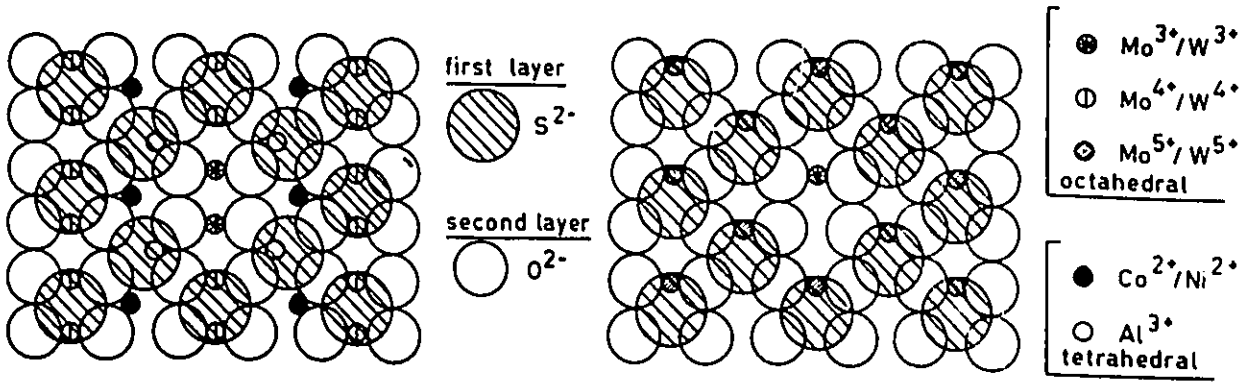

Figure 2.2: Monolayer sites

The Monolayer Model

An epitaxial monolayer of MoO_3 is supposed to be formed on γ-Al_2O_3 surface during catalyst preparation. This monolayer model was first introduced by Lipsch and Schuit [59] and later on, Sonnemans and Mars proved that experimentally [93]. They also found that commercial catalysts contain appreciably less MoO_3 than necessary for one monolayer coverage.

The structural aspects of promoter (Co or Ni) introduction in oxide catalyst systems have been widely investigated [60,7,8,74]. It was established that a certain portion of the promoter cations penetrates some distance into the support, with Co^{2+} preferring tetrahedral sites and Ni^{2+} preferring the octahedral ones.

After reduction and partial sulfiding, the ideal monolayer catalyst might present a picture as shown in Figure 2.2 [86]. The tetrahedral sites would be occupied by Co^{2+}, the octahedral sites by Mo^{6+}. The oxygen ions on top of Mo sites can be replaced by sulfur, resulting in the formation of Mo^{5+} and Mo^{4+}sites. The S/Mo

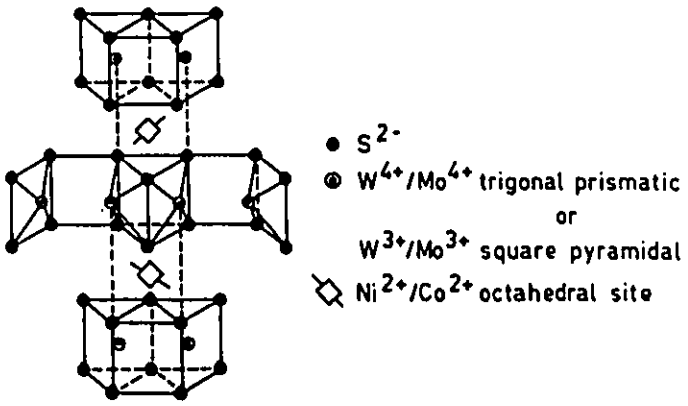

Figure 2.3: Farragher-Coosse model for Ni-WS_2 edges

ratio remains ≤ 1. Sulfur vacancies correspond with single or dual Mo^{3+} sites.

The (pseudo) intercalation model

This model starts from the layer structure of disulfides such as MoS_2 and WS_2, where the cations occur in trigonal prismatic surrounding the cationic sites between successive sulfur-layers being alternatively completely empty or all filled.

According to Voorhoeve et al. [100,99] and Farragher and Cossee[33] intercalation of Ni(Co) may occur at the layer edges between $MoS_2(WS_2)$ layers in octahedral holes situated adjacent to Mo(W) ions. This leads to the formation of single and dual sites of exposed $Mo^{3+}(W^{3+})$ ions seated above a square planar array of sulfur ions at the edges of the layers. Figure 2.3 gives the Farragher-Cossee model for Ni-"intercalated" WS_2 edges.

The synergetic model

This model was first proposed by Hagenbach et al. [43,44]. They showed that mixtures of MoS_2 and Co_9S_8 demonstrate a considerable "synergetic" effect i.e. the addition of Co_9S_8 to MoS_2 enhanced the activity of MoS_2 for hydrodesulfurization, hydrogenation, and isomerization. It has been also shown that the highest activity was obtained at a Co/(Mo+Co) ratio of 0.2.

Chapter 3

Methodology

This chapter includes the strategies followed in designing the experiments, the methods used to select the rate equation, and the procedure to evaluate the parameter estimates of the kinetic models.

3.1 Design of Experiments

An important part of this work was to design the experiments in such a way as to achieve the objectives of this research project, that is verifying the effect of process variables (T, W/F, $\overline{R}$) on the hydrodenitrogenation reactions, establishing reaction networks, and finding the kinetic model or models that fit the experimental data adequately.

Since hydrodenitrogenation is an integral part of the hydrotreating operations, the operating conditions considered in this study were chosen in ranges close to the typical ones for the industrial hydrotreating processes suggested by Hengstebeck [46]. These ranges are: temperature between 588 and 698 K, total pressure between 7.8 and 205 atm, and liquid hourly space velocity (LHSV) between 1.5 and 8.0 hr^{-1}.

In this study the total pressure was kept constant at 69 atm except for Runs

Q3505 and Q3505R where the total pressure was 34.5 atm. The temperature was varied between 498 and 673 K. The space time was varied between 42 and 210 hr g-cat/g-mol nitro-compound. The hydrogen to nitrogen feed molar ratio was kept constant at 13 g-mol H_2/g-mol nitro-compound except for Run PR13 where it was varied between 7 and 19.

3.1.1 Process Variables Effect

A set of experiments was designed especially for the determination of the impact of the operating variables (T, W/F, $\overline{R}$) on the HDN reaction. A two-level factorial design is an acceptable screening tool for such purpose. This design helps detect the influence of the operating variables on the response variable. This influence can be described by a first degree polynomial of the form

$$E(Y) = \beta_0 + \beta_1 x_1 + \beta_2 x_2 + ... \tag{3.1}$$

where $E(Y)$ is the expected value of the random variable Y, β_i is the parameter associated with the independent variable x_i.

In addition to its use as a screening tool, the fractional factorial design provides valuable information about the possible interaction between various operating variables.

According to Bacon [10], three-level factorial designs are efficient in situations involving two or three operating variables. The influence of k operating variables can be described by a second degree polynomial model having the form

$$\begin{aligned} E(Y) = \beta_0 + \beta_1 x_1 + \beta_2 x_2 + ... + \beta_k x_k \\ + \beta_{11} x_1^2 + \beta_{22} x_2^2 + ... + \beta_{kk} x_k^2 \\ + \beta_{12} x_1 x_2 + \beta_{13} x_1 x_3 + ... + \beta_{k-1,k} x_{k-1} x_k \end{aligned} \tag{3.2}$$

In order to estimate the squared terms, at least three values of each operating variable must be tested. Box and Behnken [17] have proposed a useful class of three-level fractional factorial designs. Construction of a three-level fractional factorial design for the case of three operating variables is illustrated in Table 3.1. Values of the operating variables are quoted in coded form, where -1, 1, and 0 are the lower value, the upper value, and the centre point of the operating variables respectively.

Table 3.1: design for three operating variables.

x_1	x_2	x_3
-1	1	0
1	-1	0
-1	-1	0
1	1	0
-1	0	-1
1	0	1
-1	0	1
1	0	-1
0	1	1
0	-1	-1
0	1	-1
0	-1	1
0	0	0
0	0	0
0	0	0

Model Building

In model building, the most independent variable is not measured directly but is calculated from other quantities. As in the case here, the yield can be expressed as the product of selectivity and fractional conversion and is denoted by Y. The

temperature is defined as:

$$X_1 = \frac{T - 623}{50} \tag{3.3}$$

The space time is defined as:

$$X_2 = \frac{W/F - 126}{84} \tag{3.4}$$

The reactants' molar ratio is defined as:

$$X_3 = \frac{\overline{R} - 13}{6} \tag{3.5}$$

Then the model can be expressed as

$$\begin{aligned} Y = a_0 + a_1 X_1 + a_2 X_2 + a_3 X_3 \\ + a_{12} X_1 X_2 + a_{13} X_1 X_3 + a_{23} X_2 X_3 \\ + a_{11} X_1^2 + a_{22} X_2^2 + a_{33} X_3^2 \end{aligned} \tag{3.6}$$

3.1.2 Kinetic Experiments

After verifying the effect of process variables, a full scale design was considered for the kinetic study. The reactants molar ratio was kept constant at 13 g-mol H_2/g-mol nitro-compound. Each set of experiments consisted of seven runs. In each set the temperature was kept constant while varying the space time at seven different values starting with the highest flow rate for faster breakthrough. The samples considered for analysis were collected at steady state. A steady state was declared after getting three identical chromatograms from the on-line analysis. The tar trap were emptied after each run and the flow rates of hydrogen and nitrogen-compound were decreased in the same ratio.

3.1.3 Selection of Rate Equation

There are several approaches to find the rate expression that fits the data best. The integrated form of the design equation of the plug-flow reactor is

$$\frac{W}{F} = \int_0^X \frac{dX}{r} \tag{3.7}$$

This general rate equation of a catalytic flow system is based on unit mass of the catalyst. The rate equation that can accurately predict the reaction behavior is obtained after obtaining the mechanism of that reaction. The mechanism of a reaction can be detected by the initial rate method described by Yang and Hougen [106]. The initial rate is obtained by plotting the fractional conversion versus the space time and determining the slope of the curve as the space time approaches zero. By plotting the initial rates versus the partial pressure or the reactants' molar ratio, one can predict the mechanism from the shape of that curve.

Besides the initial rate procedure, there are other methods that use the finite values of conversion in order to establish the true rate equation that represents the data. Some of these methods are: linearizing the rate equation and solving for the rate constants, and using the method of least squares to solve the integrated form of the design equation.

Another efficient way to determine whether the reaction is adsorption controlling, surface reaction controlling, or desorption controlling is by model discrimination from the regression of the experimental data and then determine as to which step is the rate-controlling.

3.1.4 Mathematical Modeling

Quantitative interpretation and analysis of the experimental results can only be accomplished through mathematical modeling of the kinetics. Two types of models were considered, a lumped compound model in which it is assumed that nitrogen-containing compounds react with hydrogen to give hydrocarbons and ammonia, and a mechanistic model that considers the reactions of each compound separately. Each model resulted in a set of differential equations. These equations are solved by a differential equation solver. The parameters of these equations are estimated by a nonlinear least square regression technique. A parameter estimation in differential equations program was used to estimate parameters from observations of multi response variables. The 'best' estimates of these parameters are taken as those that minimize the sum of squares of deviations between observed and predicted values of all the response variables rather than only one response variable. By doing so one can expect more precise estimates of the model parameters. This multi response parameter estimator developed by Lozej, McLean, and lately by Guay [61] makes use of Box and Draper criterion [18].

After the conversion of the estimation algorithm the model adequacy is confirmed by several checks

- Step 1: Determine whether the estimated parameters are reasonable.
- Step 2: Check for the discrepancies between observed and predicted values of the responses.
- Step 3: Plot the residuals versus the predicted values of the responses. In general, trends in plots of residuals indicate lack of fit.

- Step 4: Plot the observed values of the responses versus the predicted values. These kinds of plots offer easy ways to detect inadequacies.

3.1.5 Integral Analysis

Regression analysis was carried out on the models to be tested. For the non-linear models a non-linear iterative method (Levenberg-Marquardt) that produces least squares estimates of the parameters was applied. For this algorithm one must input the data, the regression expression, declare the parameters, provide a range of possible values of these parameters, and specify the derivatives of the model with respect to each of the parameters. The procedure first evaluates the residual sum of squares at each combination of starting values. The starting values with the lowest sum of squares then serves as the initial estimates of the parameters and as such a starting point for the iterative procedure. The iterative method regresses the residuals onto the partial derivatives of the model with respect to the parameters until the iterations converge. The model forms and the parameter estimates obtained may be used as a basis for the differential analysis.

3.1.6 Differential Analysis

Making use of the reaction network of the HDN reaction, mechanistic models can be developed. Information of all the measured responses were combined to provide more precise parameter estimates [12]. An estimation criterion was developed by Box and Draper [18] for this situation since the least squares criterion cannot be used. This is due to the fact that the variance of the observed responses at any point in time are not independent [61]. This analysis is referred to as Parameter Estimation In Differential Equations, a software developed by members of the

Chemical Engineering Department at the University of Ottawa [61].

In multi response cases the observed and predicted values of the response variables are related by the expression

$$y_{nm} = f_m(\underline{\xi}_n, \underline{\theta}) + \epsilon_{nm} \tag{3.8}$$

where:

y_{nm} observed value of the m^{th} response variable for the n^{th} run

$f_m(\underline{\xi}_n, \underline{\theta})$ response function defining the expected value of the m^{th} response for the n^{th} run

$\underline{\xi}_n$ vector of values of the operating (independent) variables for the n^{th} run

$\underline{\theta}$ P×1 vector of values of parameters

ϵ_{nm} value of the random error associated with the measurement of the m^{th} response variable for the n^{th} run

The program provides estimates of parameters which minimize the quantity

$$d(\underline{\theta}) = det \underline{Z}^T \underline{Z} \tag{3.9}$$

where

$$\underline{Z} = \underline{Y} - \underline{H}$$

$\underline{Y}$ the N×M matrix of the measured responses for n runs

$\underline{H}$ the N×M matrix of m predicted responses for n runs

Convergence of the estimation algorithm is determined using one of the two criteria. The first criterion is based upon the value of the determinant, $d(\underline{\theta})$. Iterations are terminated when

$$\frac{d(\underline{\theta}_i) - d(\underline{\theta}_{i+1})}{d(\underline{\theta}_i)} < \tau_d \tag{3.10}$$

where τ_d is a specified relative tolerance. The second convergence criterion used in this program is one proposed by Bates and Watts [13,12] in which the size of the proposed increment in the parameter vector is compared to the estimated size of the confidence region of the parameters. If the size of the increment is small relative to the precision of the estimates then convergence is declared.

The program requires as input the experimental data, the rate equations, the derivatives with respect to each of the responses and with respect to each of the parameters.

3.2 Surface Studies Experiments

Spectroscopy is the study of the interactions of electromagnetic radiations with matter. It provides a record of the amount of electromagnetic energy absorbed by a material as a function of the energy of the radiation employed. This record (spectrum) is unique to the sample and can be utilized to identify or quantify constituents, establish or follow changes in structure, or perhaps provide insight into mechanistic and kinetic details of a chemical reaction [71].

Three types of studies were carried out on the catalysis to shed some light on the structure and the properties of that catalyst. The techniques used in these studies are; electron spin resonance, x-ray diffraction, and adsorption.

3.2.1 Electron Spin Resonance

Electron Spin Resonance (ESR) is a useful technique to measure the concentration of the species with only unpaired electrons and to identify electron acceptors or donors in semiconductors. A catalyst which is made from two different metal oxides, as in this present case, yields a signal with a given intensity. The intensity of this signal varies with the composition of these oxides. In general, the activity of the catalyst is related to the intensity of the signal.

The ESR technique employs both external magnetic field and radiofrequency photons. The substance to be tested is placed in the magnetic field and adsorption of electromagnetic energy i.e. the radiofrequency photons, is observed. ESR spectra were taken at different conditions and the relative intensities were measured. More detail about the ESR studies are found in Appendix F.

3.2.2 X-Ray Diffraction

X-Ray Diffraction (XRD) techniques can furnish a variety of information not obtainable by other instrumental methods. The most distinctive and ultimate application of x-ray diffraction is determination of crystal structure. It can also give a detailed picture of the dispersion of metal particles on the catalyst support.

When a beam of x-rays impinges on a sample placed in its path, three main processes occur [15].

1. Some x-rays are scattered with no change in wave length.

2. Some x-rays are scattered with a change in wave length, which depends on the angle at which they are scattered.

3. Some x-rays are adsorbed, with the subsequent production of fluorescent x-rays.

Coherent scattering of x-rays is necessary for diffraction to occur. There are three main techniques by which the geometry of x-ray diffraction has been handled. The Bragg method (used in this investigation) had simplified the calculation by considering the diffraction to occur from planes to atoms. The Bragg's law for diffraction can be written as

$$\lambda = 2d\ sin\theta \tag{3.11}$$

where d is the interplaner spacing of the planes, λ is the wavelength of the x-ray, and θ is the angle of incidence, i.e. the angle between the planes in the crystal and the incident beam. The Debeye-Scherrer powder camera is the mostly common used for x-ray diffraction. The camera used in this investigation is the Debeye-Scherrer with the Straumanis modification.

In the powder method the catalyst sample is ground to fine powder (about 50 μm), and mounted on a glass filament in such a way that it can be bathed in a monochromatic x-ray beam. A narrow strip of film is pressed inside a cylindrical holder the axis of which coincides with that of the sample. The x-ray reflections are detected as lines on the film. Each of these lines corresponds to the reflections from all the planes of one form. The rays diffracted by these planes lie along the surface of a cone of half-angle 2θ whose axis is the incident beam.

3.2.3 Adsorption

These studies were carried out using *AccuSorb* 2100*E* in order to determine the specific area, pore volume, and pore size distribution. Physical measurements of

the volume of gas adsorbed as a function of pressure at a fixed temperature permit calculation of the volume of gas required to form a layer of one-molecule thickness. The main equation used for calculation is

$$\frac{P}{V_a(P_s - P)} = \frac{1}{V_m C} + \left[\frac{C-1}{V_m C}\right]\frac{P}{P_s} \tag{3.12}$$

A plot of $\frac{P}{V_a(P_s-P)}$ versus $\frac{P}{P_s}$ gives a straight line, the intercept and slope of which are $\frac{1}{V_m C}$ and $\frac{C-1}{V_m C}$ respectively. Using this information with the knowledge of the physical dimensions of single adsorbed molecule, the surface area of the adsorbing solid can be computed.

Chapter 4

Properties of Materials

This chapter deals with the properties of the various materials used in this research, mainly the reactants and the major products. A general outlook at the physical and chemical properties is given. The health and safety factors are addressed as well.

4.1 Pyridine

All six-membered fully unsaturated heterocycles are formally related to benzene in that one or more of the CH groups of benzene is replaced by a heteroatom. Pyridine is the simplest of such compounds. It is a planar molecule, the ring system being a slightly distorted hexagon because the C–N bond (1.45 Å) are shorter than the C–C bond (1.48 Å) [38]. The pyridine molecule has a complete cycle of p-orbitals containing six π-electrons. Pyridine can thus be classed as aromatic because it obeys the Hückel rule (it has $4n + 2$ π-electrons). Pyridine is a water-miscible liquid, boiling point 115°C, with an unpleasant odor. It is also an excellent polar solvent.

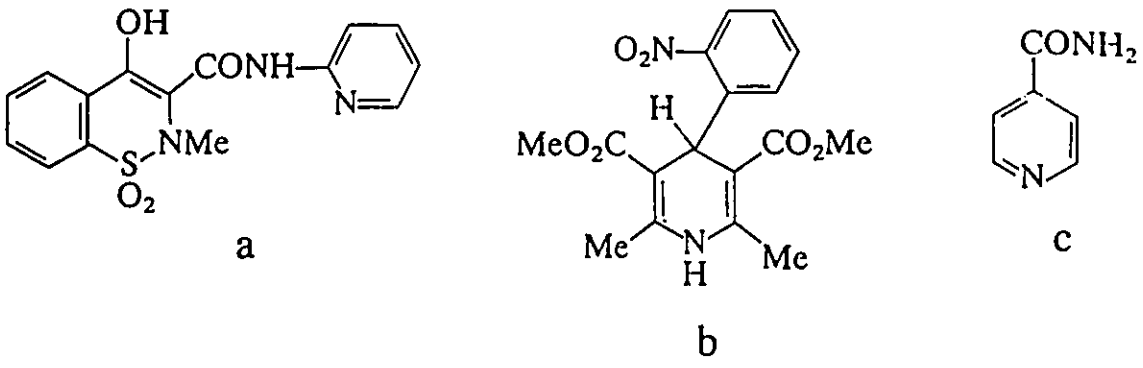

Figure 4.1: Pyridine-base pharmaceuticals

4.1.1 Source, Synthesis, and Uses

Pyridine and several methyl- and ethylpyridines are available on a large scale from the carbonization of coal. Coal tar contains about 0.2% of a mixture of pyridine bases. Pyridine and methylpyridines can be synthesized by different routs. For example, the vapor-phase reactions of acetaldehyde, formaldehyde and ammonia over silica-alumina catalyst give pyridine and a mixture of methylpyridines. There are many other naturally occurring pyridines such alkaloid nicotine found in tobacco.

The pyridine molecule is widely used as a basis for many pharmaceutical products. Among these products are piroxicam, Figure 4.1-a, an inflammatory, nifedipine, Figure 4.1-b, which is effective for the treatment of angima, and isoniazid, Figure 4.1-c, used in tuberculosis therapy. 3-Methylpyridine is a commercially important precursor to pyridine-3-carboxylic acid (nicotinic acid), one of the B group of vitamins.

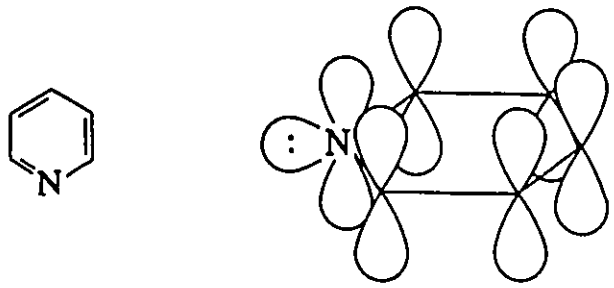

Figure 4.2: Representation of the structure of pyridine

4.1.2 Chemistry of Pyridines

Pyridine is the most 'benzene-like' of the heterocyclic compounds. The presence of the nitrogen atom in the ring does, of course, represent a major perturbation of the benzene structure. The lone pair of electrons in the plane of the ring, Figure 4.2, provides a cite for protonation and alkylation. This structure allows pyridines to have reactions which show analogies to those of three types of model systems [38]:

1. Tertiary amines: Reactions at the nitrogen lone pair, including protonation, alkylation, and coordination to Lewis acids.

2. Benzene: Substitution reactions and resistance to addition and ring opening.

3. Conjugated imines or carbonyl compounds: susceptibility to attack by nucleophiles at the α- and γ-carbon atoms.

Pyridine and alkylpyridines are weak bases which form salts with strong acids.

4.2 Quinoline

Quinoline is a heterocycle in which a benzene ring and a pyridine ring are fused through carbon. Both ring systems occur naturally and both were originally isolated from coal tar. Quinoline has a boiling point of 237°C, which is often used in the laboratory as a high boiling basic solvent [38]. The solubility of quinoline in water varies from 8.4 g/l at 10.0°C to 12.0 g/l at 73.0°C [35].

4.2.1 Source, Synthesis, and Uses

Like pyridine, quinolines and isoquinolines are available from the carbonization of coal and from oil residuals. There are many methods of synthesis of this ring system. One of these methods is the *Skraup* synthesis which consists of heating an aniline with glycerol and sulfuric acid, which acts as an acid catalyst and a dehydrating agent. This reaction is violently exothermic, hence a moderator such as iron(II) sulfate is usually added.

The quinoline skeleton is used as the bases of many pharmaceutical products. Alkaloid quinine, Figure 4.3-a, is a traditional antimalarial drug. Oxamniquine, a derivative of tetrahydroquinoline, Figure 4.3-b, is used to eradicate blood flukes (*Schisotosma mansoni*), which are a major cause of disease in tropical regions. Papaverine, Figure 4.3-c, is an opium alkaloid which is a nonspecific smooth muscle relaxant and a vasodilator.

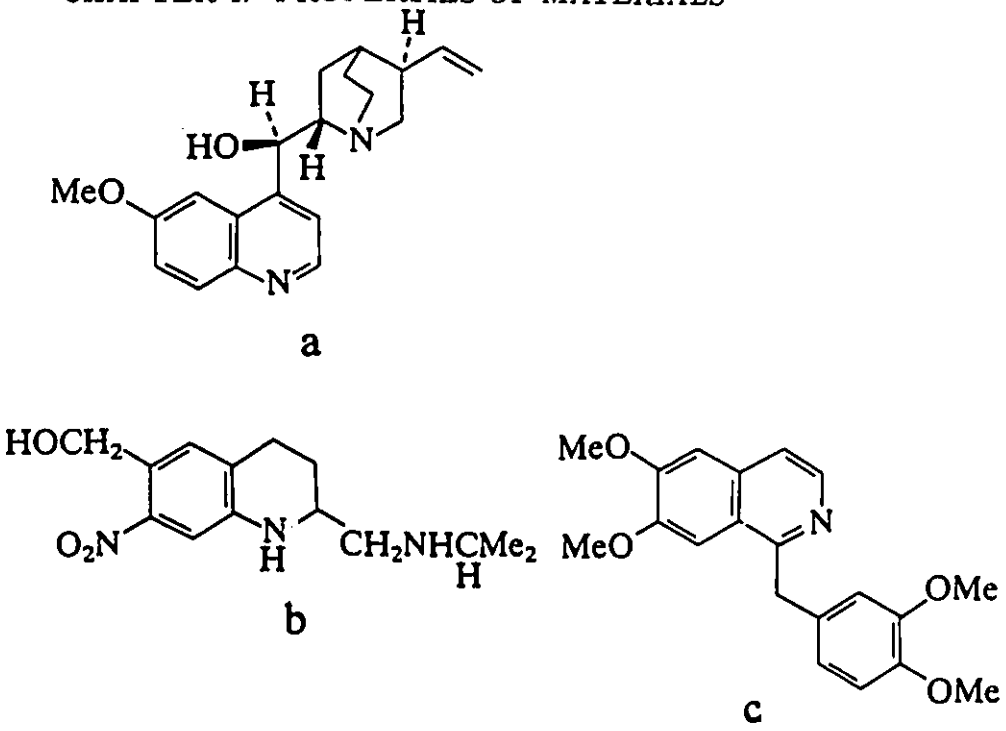

Figure 4.3: Quinoline-base pharmaceuticals

4.2.2 Chemistry of Quinolines

Many of the reactions of quinolines and isoquinolines are analogous to those of pyridine. Protonation and reaction with other electrofiles at nitrogen are much the same as with pyridine. The nitrogen atoms are also selectively active positions in the heterocyclic rings to nucleophilic attack, as in pyridine. On the other hand, electrophilic substitution which is difficult in pyridine is much easier in quinoline and isoquinoline [38]. One significant difference between pyridine and its benzo analogs is that quinoline and isoquinoline undergo addition reactions much more readily in the nitrogen containing ring.

4.3 Possible HDN Products

Hydrodenitrogenation reactions resulted in a great number of organic products especially at high temperatures and high space time. Most of these compounds are

not significant, (present in small amounts) hence they were not considered in the calculations. The major products were isolated and identified. Their properties were taken either from the manufacturer or from literature. Some of the properties of the major products are listed in Table 4.1.

Table 4.1: Major HDN products of pyridine and Quinoline

Compound	Manufacturer	Density g/ml	Boiling Point K	Purity %
Pentane	BDH Inc.	0.6262	36.1	99
Decane	Fisher Scientific	0.7300	174.1	–
Pentylamine	Eastman	0.7547	104.4	–
Ethylpiperidine	Aldrich	0.8237	130.8	99
Piperidine	Fisher Scientific	0.8606	106.0	99
Propylpiperidine	Prepared in Lab.	0.8231	151.2	–
Pyridine	Fisher Scientific	0.9819	115.1	99
Pentylpiperidine	Prepared in Lab.	0.8282	198.2	–
Dipentylamine	Aldrich	0.7771	202.0	99
Methylcyclohexane	Aldrich	0.7694	100.9	99
Ethylcyclohexane	Aldrich	0.7880	131.8	99
Propylcyclohexane	Aldrich	0.7936	156.7	99
Propylcyclohexene	Aldrich	0.8240	155.0	75
Propylcyclohexylamine	Aldrich	0.8590	60.0	98
Propylbenzene	Eastman	0.8620	159.2	–
Methylethylbenzene	Aldrich	0.8807	165.2	99
Indan	Aldrich	0.9639	178.0	97
Decahydroquinoline	Aldrich	0.9610	203.0	97
Ethylbenzene	Fisher Scientific	0.8670	136.2	–
Aniline	Fisher Scientific	1.0217	184.0	100
Bz-Tetrahydroquinoline	Aldrich	1.0304	222.0	–
Ethylaniline	Aldrich	0.3962	204.7	98
Propylaniline	Aldrich	0.9602	226.0	97
Quinoline	Aldrich	1.0929	237.0	96
Py-Tetrahydroquinoline	Aldrich	1.0588	251.0	98

4.4 Toxicity and Safety regulations

According to the Material Safety Data Sheets provided by the manufacturer, pyridine, quinoline, as well as all other nitrogen-containing products are harmful if swallowed, inhaled, or absorbed through the skin. They are irritating to mucous membranes and upper respiratory tract. They cause skin and severe eye irritation. Most of these substances are central nervous system depressant. Poisoning may affect the liver, kidneys, and heart.

Prolonged or repeated exposure to nitrogen-containing compounds may cause one or more the following symptoms depending on the substance, the concentration of that substance and the exposure period: dizziness, drowsiness, transient headache, vertigo, nervousness, insomnia, nausea, vomiting, abdominal discomfort, back pain and urinary frequency.

Extreme caution must be taken while working with the above substances. A Gas Mask equipped with an organic vapor cartridge is to protect the worker from inhaling the organic fumes. For eye protection one should wear splash-proof safety goggles. Appropriate hand gloves must be worn to avoid contact with the skin. These chemicals must be used only in a chemical fume hood.

Chapter 5

Experimental

The experimental apparatus used in this study was similar to the ones used by Cocchetto [24], Gupta [42], and Anabtawi [4].

5.1 Kinetic Studies

The kinetic data were collected from an integral flow, fixed bed catalytic reactor under steady state at a pressure of 69 atm, a temperature range between 495 and 673 K, a space time (W/F) between 42 and 210 hr g-cat/g-mol nitro-compound and a molar ratio ($\overline{R}$) of 13 g-mol H_2/g-mol nitro-compound. Heat and mass transfer were negligible under the operating conditions (see Appendix J).

5.1.1 Experimental Apparatus

The hydrodenitrogenation experiments were carried out in a continuous flow, fixed-bed catalytic reactor. The reactor was operated isothermally in the integral mode. A schematic of the experimental apparatus is shown in Figure 5.1. The experimental setup consisted essentially of a packed bed reactor, a furnace (fluidized sand bath), a tar trap, a feed pump and facilities for controlling, sampling, metering and analysis of the product. The reactor was made of 316 stainless steel tubing. The

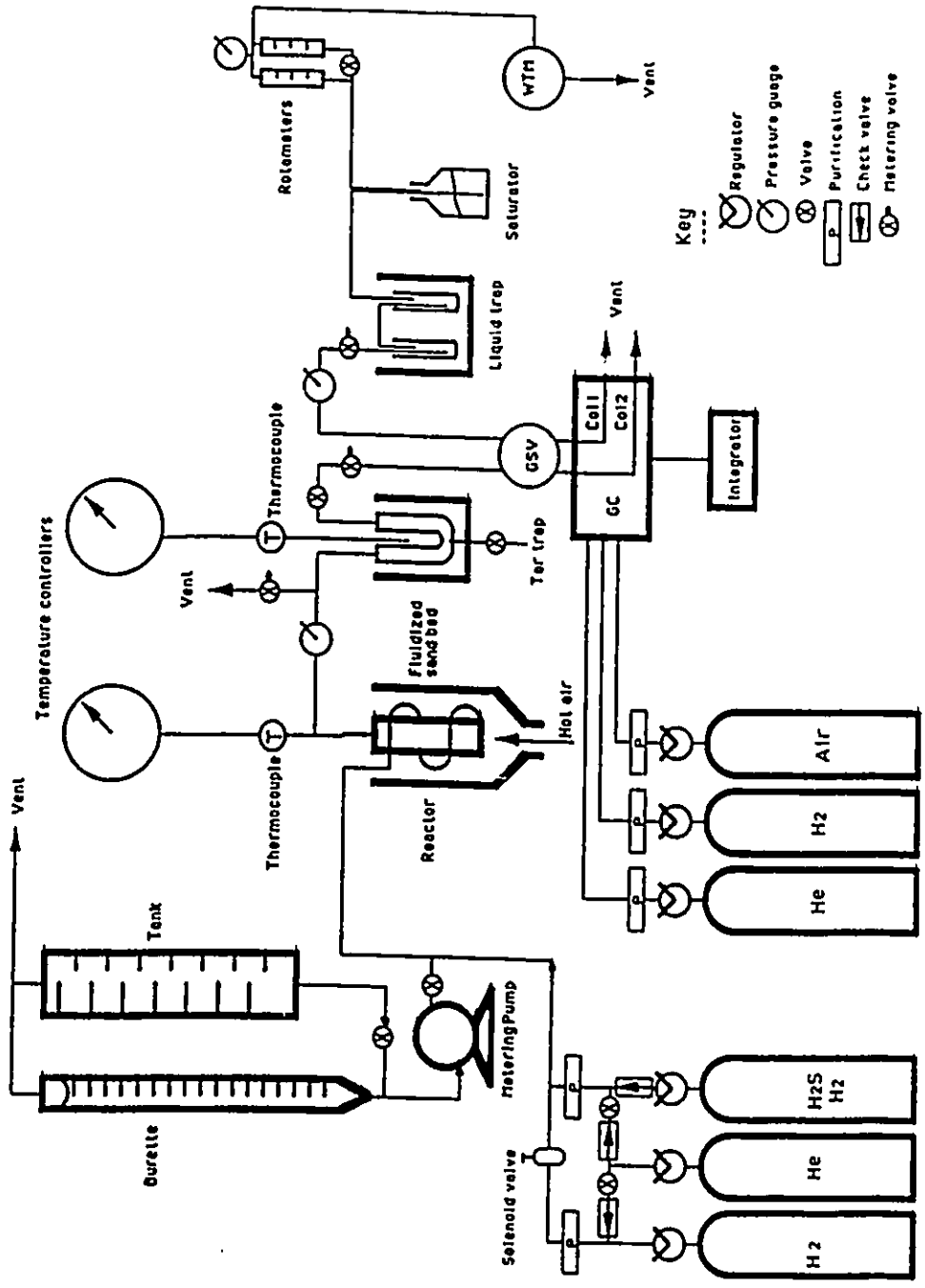

Figure 5.1: Schematic diagram of the experimental apparatus

reactor and preheater coil were immersed in a fluidized sand bath. The tar trap, installed after the reactor was maintained at 250°C. The flow rate was controlled manually with a fine metering valve maintained at about 260°C to prevent any condensation of the products. The main sections of this apparatus are described in detail in the following sections.

5.1.2 Reactant Feed Section

Reactant hydrogen was supplied from a high-pressure (2500 psig) cylinder equipped with a single-stage regulator (*Matheson Gas Products, No. 4T*) which was used to control the reactor pressure to the desired level. Hydrogen stream was passed through three stages of purification: (*i*) an oxygen trap that contains a highly active metal that converts oxygen to water, (*ii*) a moisture trap that contains molecular sieve 13X, and (*iii*) a hydrocarbon trap that contains activated carbon. Hydrogen was then passed through a solenoid valve (*ASCO*, 2200 *psi*, *Ascolectric Ltd. Canada*), then through a check valve (*Nupro*, 10 *psi*) to prevent any back-mixing, and finally through a preheater before entering the reactor.

A high-pressure metering pump (*Milton Roy Company, FL. USA*) was used to feed liquid reactant to the system. The metering pump was calibrated for different pressures and different liquid feeds. The instantaneous flow rate shown by the pump setting was checked frequently with the cumulative flow rate shown by the difference in the burette reading per time. Liquid feed was pumped through a mixing tee where it was flash vaporized into the preheated hydrogen stream which was maintained at about 230°C by wrapping the tubings with a heating tape (*GLAS – COL USA*). The temperature of the heating tape was controlled by a variable autotransformer

(*Fisher Scientific Co. USA*) and a temperature controller (*Honeywell*). Then the reactants enter the preheating coil immersed in the fluidized sand bed surrounding the reactor.

An auxiliary feed system allows a mixture of 10% H_2S in H_2 to be fed through a low pressure regulator (*KIM Products Inc.*) to the reactor to sulfide the catalyst periodically. The H_2S stream was made in such a way so that it did not pass through the gas sampling valve and the gas chromatograph to avoid corrosion and any side reactions that might cause blocking of the 1/16 in. tubes of that valve.

Another auxiliary feed system, helium, which was used to purge the H_2S/H_2 as well as the H_2 feed systems. Purification units similar to the ones used for the hydrogen feed were installed to the H_2S/H_2 and the He streams. Proper check valves and shutoff valves were also located in the setup so as to prevent any back-mixing of the products and these gases.

5.1.3 Reactor Section

The reactants stream was connected to a three-way valve (*Autoclave Engineers* $10V - 2005$), while one branch led to the reactor the other bypassed the reactor to meet again through a similar valve and form one stream before entering the tar trap.

The reactor was a 316 stainless steel tubing of length 7.25 in. (18.415 cm) and an i.d. of 0.42 in. (1.067 cm). The catalyst bed was secured from both ends by porous stainless steel plates (40 microns). The catalyst extrudates were crushed to 20/24 mesh size (0.03 in. or 0.774 mm average diameter). The radial aspect ratio was about 13.8, sufficiently large to avoid channelling and wall heat transfer limitations

(low limit is 4) [29]. The axial aspect ratio was 237.9 which is much greater than the minimum value of 30 to insure plug flow operation [29]. Hence, axial dispersion and conduction were not significant.

Reactor and final preheating coil (1/8 in. o.d. stainless steel tubing) were immersed in a fluidized sand bed heater. Reaction temperature was measured with a 1/8 in. type-K thermocouple placed in the catalyst bed and connected to a temperature controller (*Honeywell*). The sand bed was fluidized by hot air. It was controlled by two temperature controllers; one was a *Thermotrol Precision* (*GCA Corp. USA*) controller and the other was a *Honeywell* controller. Reactants reach the desired temperature while in the preheater before entering through the lower inlet of the reactor which was mounted vertically in the sand bed. At steady state the temperature of the sand bed and that of the reaction were within 2 to 3°C, thus insuring isothermal operation.

A tar trap made of a U-shape, 316 stainless steel tubing of 1.067 cm i.d. was installed at the exit line of the reactor. It was packed with spherical pyrex glass beads (3 mm diameter) supported on two stainless steel screens. The bottom part of the trap was free so that tar can be collected and then removed after each run The tar trap was maintained at 250°C, a temperature low enough to condense the tar (high boiling point products) and high enough not to condense any of the major products.

The total pressure of the reactor was measured by a 3500 psig test gauge (*Matheson, Part No.*63-5633) located after the tar trap and protected by a porous stainless steel plate (20 microns) installed just after the tar trap. The flow rate was controlled manually with a very fine metering valve (*Nupro SS − 4MG2*) after replacing its

packing by Virgin Teflon so that it can operate at high temperature. This valve was protected by a 15-micron filter (*Nupro, Co.*) to avoid the blocking of its orifice by any kind of particles. The temperature of this valve as well as the tubings from the reactor to the liquid trap were maintained at 260°C to prevent any condensation of the products. Another metering valve ($Whitey\ 316 - SS\ 31RF2$) located between the filter and the fine metering valve was used for the initial adjustment of flow rate at the beginning of each run and for shutoff purpose in some cases.

5.1.4 Sampling and Analysis Section

Reactor effluents were passed through an eight port gas sampling valve (GSV) with two matched 1.20 cc loops for the on-line analysis of the products. The GSV was mounted in a special isothermal oven maintained at 200°C and located in the gas chromatograph. The pressure inside the GSV was 5 psig and it was controlled by a very fine metering valve similar to the one that controls the flow rate of the product stream. and it was located downstream the GSV. Pressure in the gas sampling valve was measured by 100 psig test guage (*Matheson Part No.* $63-5612$) located between the two fine metering valves. A 15-micron filter (*Nupro Co.*) was located just before the gas sampling valve to protect and prevent any potential blocking of the GSV loops.

After leaving the GSV, the product stream was passed through a liquid trap to condense the organics of the reactor effluent. The liquid trap was made of two test tubes connected in series and immersed in a water bath. In the case of pyridine hydrodenitrogenation reaction, ice-water was used to trap the organic liquids, while in the case of the hydrodenitrogenation of quinoline or pyridine-quinoline mixture,

the liquid trap was operated at room temperature due to the high melting point of some products. For safety measures a three-way valve was installed just upstream the liquid trap. One line led to the trap while the other led to the vent. This allowed the removal of the products without the risk of the exposure to their fumes.

The effluent stream leaving the liquid trap was passed through a saturator to remove all the remaining organics and some of the ammonia gas which dissolves in water. The remaining stream which is mainly hydrogen and some ammonia was passed through either one of two rotameters; a $601 - Matheson$ rotameter to monitor low flow rates, or a $602 - Matheson$ rotameter for higher flow rates.

Before entering the rotameters, the effluent stream was passed through an empty flask that acts as a buffer port and through a moisture trap that acts also as a filter to guard against erroneous rotameters readings because of the fouling of the tubes or the floats. The gas stream was then led to a wet test meter (WTM) ($GCA/Precision\ Scientific$) before it is vented out. The instantaneous flow rate shown by the rotameter was checked periodically with the cumulative flow rate shown by the wet test meter. A very close agreement between the two readings and that of the calibration curve was observed.

Product analysis was done by a gas chromatograph (GC) ($HP-5730A$) equipped with a thermal conductivity detector (TCD), a flame ionization detector (FID), dual columns, and temperature programming capability. Chromatograms, retention times, and peak areas were produced by an integrator ($HP - 3380A$).

Quantitative analysis was done by injecting liquid samples through the flame ionization detector (FID). Some samples from the liquid product were also subjected to gas chromatography/mass spectroscopy (GC/MS) analysis ($FINNIGAN-MAT$ 4500)

to identify unknowns and to confirm the gas chromatography analysis. The gas chromatography/mass spectroscopy was done at the "Plant Research Centre", Ottawa. Typical GC/MS chromatogram illustrating the separation of pyridine HDN products is shown in Figure 5.2.

5.1.5 Gas Chromatographic Analysis

Considerable time and effort were spent to develop a column capable of separating the major HDN products. Several packed columns were tried at different operating conditions in order to get the best separation by reducing peak tailing, and/or overlapping of peaks. Finally two identical stainless steel columns, 10'x1/8" o.d. were constructed in our laboratory by packing them with 10% Carbowax 20M, 1% KOH on 80–100 mesh Chromosorb P (acid washed) and considered for the HDN product analysis. The following operating conditions were found suitable for the separation: Injector temperature 200°C, detector temperature 250°C, initial column temperature 70°C, initial time 0 min., program rate 8°C/min., final column temperature 200°C, final time 45 min., and carrier gas (helium) flow rate 20 cc/min.

For quantitative analysis several standard solutions with varying concentrations were prepared for calibration. The relative response factor for each of the available compounds was measured. Some of these compounds were prepared in our laboratory, such as n-pentylpiperidine and piperidine,1-ethyl. A plot of the peak area versus the concentration of the corresponding compound was found to be linear in the range of interest. The major products of pyridine and quinoline HDN with their retention times are listed in Table E.1.

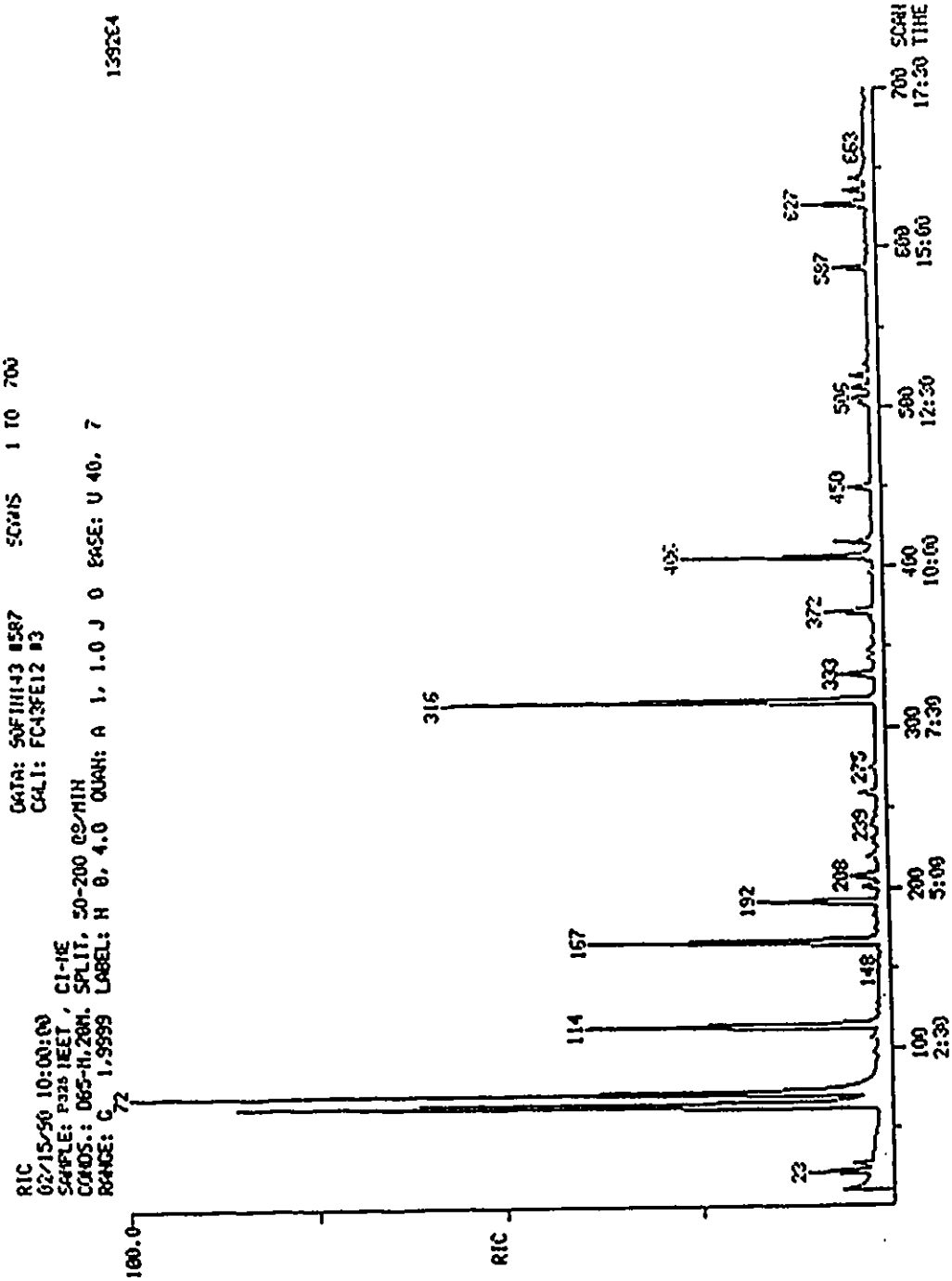

Figure 5.2: A typical GC/MS chromatogram for pyridine HDN products, column: Megabore DB5-M, 20 m.

5.1.6 Catalyst Preparation

To demonstrate the effect of the catalyst support on its activity, a catalyst having the same oxide composition as the commercial one but supported on pumice was prepared in our laboratory. Pumice stone is relatively inert in comparison with alumina. The catalyst was prepared by the impregnation method. Pumice stone, a porous igneous rock, usually containing 67 to 75% silica and 10 to 20% alumina of glassy texture [45], was crushed and sieved to 20/24 mesh, washed with water and calcined at 500°C for 12 hours. 2.38 g of ammonium molybdate and 1.77 g of nickel nitrate were dissolved in 20 ml of water and added to 12.60 g of pumice at room temperature. The mixture was dried at room temperature for 12 hours, stirring it from time to time. After that the catalyst was calcined by heating in air for 12 hours at 500°C. The nominal composition of the catalyst was about 3.03% NiO and 12.94% MoO_3.

5.1.7 Column preparation

The column packing was prepared as follows: 0.25 g of KOH was dissolved in methanol and added to 22.25 g of Chromosob P (acid washed, 80–100 mesh) placed in a shallow dish. The mixture was dried at room temperature with frequent stirring. 2.50 g of Carbowax 20M were dissolved in methylene chloride and added to the above mixture. The resulting slurry was dried as before till it regained its powdery form. Two identical 10'x1/8" o.d. stainless steel pipes were packed and the packing was secured by glass wool. The columns were coiled to the proper size to fit in the GC oven, then conditioned and used for the separation of the HDN products.

Before packing the columns, the stainless steel tubes were cleaned and flushed with the following liquids [102]

1. Methylene Chloride
2. Acetone
3. Concentrated Hydrochloric acid
4. water
5. Ammonium Hydroxide
6. N-Methyl Pyrrolidine
7. Acetone
8. Methylene Chloride

The tubing was then dried for 20 min. with inert carrier (Helium) and packed immediately after that.

Conditioning of the columns was done according to the following steps:

1. Columns were connected to the injection port only (not to the detector)
2. Carrier gas (He) flow rate was set at 20 ml/min.
3. System was checked for leaks
4. Initial oven temperature was 50°C
5. Initial time was 30 min.
6. Rate of temperature increase was 2°C/min.

7. Final temperature was 210°C

8. Final time was about 16 hours.

5.2 Surface Characterization studies

There are several techniques which have been developed in surface science that have a potential application in the study of catalysts and catalytic reactions. The techniques which have the most significant impact in catalysis fall in two categories, electron and ion spectroscopies [26].

The important electron spectroscopies used for solving catalysts' problems are: (1) X-Ray Photoelectron Spectroscopy (XPS) which measures the distribution of the valence electrons in a solid; (2) Ultraviolet Photoelectron Spectroscopy (UPS) which gives a higher resolution and greater signal intensity than the XPS for valence electron studies; (3) Auger Electron Spectroscopy (AES) which is used primarily for atomic identification and surface analysis [19]. The most important ion spectroscopies which received attention in connection with catalyst problems are the Secondary Ion Mass Spectroscopy (SMIS) and the Ion Scattering Spectroscopy (ISS). These techniques have some application in catalyst characterization and composition.

In addition to the above mentioned techniques, there are many others such as the Electron Spin Resonance (ESR), the Infrared Spectroscopy (IR), and the X-Ray Diffraction (XRD) which are used to shed lights on the catalyst problems. In this study, two different techniques have been used: the first is the ESR or sometimes called Electron Paramagnetic Resonance (EPR), and the second is the XRD.

For the ESR studies two sets of experiments were performed, the first set consisted of twelve different steps; the second set consisted of fifteen steps with the extra steps to cover the sulfiding process. The spectra were taken after each step and then analyzed. (see Appendix F, Tables F.1 and F.2.) The equipment used is $B-ER$ 414/418 *spectrometer* from $Bruker-Physik\ AG$.

For the XRD studies the catalyst was crushed and sieved to 250–270 mesh size, then mounted on a glass filament and exposed to x-rays for about four hours. The lines produced after the development of the film were studied to identify the number of phases and the structure of the crystals. The equipment used is *Philips* $PW1009$ x-ray diffractometer that uses *Debye Scherrer* photographic technique.

Chapter 6

Results and Discussion

The effect of reaction variables on pyridine HDN were investigated using a three-level factorial design as discussed in Chapter 3. For this investigation the temperatures were 573, 623, and 673 K. The space times were 42, 126, and 210 hr g-cat/g-mol nitro-compound, and the reactants' molar ratios were 7, 13, and 19 g-mol H_2/g-mol nitro-compound. The nitro-compound was either pyridine, quinoline, or pyridine-quinoline mixture.

For the kinetic studies the reactants' molar ratio was kept constant at 13 g-mol H_2/g-mol nitro-compound. The space times were 42, 70, 98, 126, 154, 182, and 210 hr g-cat/g-mol nitro-compound. The temperatures were 498, 523, 548, 573, 598, 623, 648, and 673 K. In the case of pyridine-quinoline mixture, the levels of temperature were 498, 573, 623, and 673 K.

At 498 K the nitrogen removal for any of the three systems was negligible. Runs at this temperature were made in order to get information about the reaction at low conversion and hence have better understanding of the reaction mechanism and network.

The effect of the above mentioned process variables on conversion (X), selectivity

(S), and yield (Y) was studied at constant total pressure (P). Conversion is defined as the moles of nitrogen compound consumed per moles of nitrogen compound fed. Selectivity is defined as the ratio of pure hydrocarbons to nitrogen compounds produced. Yield is defined as the ratio of moles of hydrocarbons produced to the moles of nitrogen compound fed. Nitrogen removal or denitrogenation is defined as the mole percentage of the reactant nitrogen compound converted into hydrocarbons. In this study, product distribution was calculated on the basis of organic products only (i.e. ammonia free basis), because the quantitative analysis of the products was made by using the flame ionization detector. The on-line analysis, using a thermal conductivity detector with a gas sampling valve having two matching loops, was considered for the qualitative analysis and for determining the steady state of each experimental settings. The on-line analysis was not considered for the quantitative analysis because of the possible deposits inside the sampling loops or due to fluctuation of the pressure or temperature in these loops which affects their volume. Due to limitations in the quantity of data that can be represented clearly in a single graph, only organic products that are significant are presented.

Preliminary experimental data obtained have indicated that the experimental apparatus is operating properly; this was verified by comparing the present results with that cited in literature [78,66,2,92,5]. In addition, the analysis of these results had shown that the results are reproducible. Reproducibility was confirmed by running the experiment at standard conditions (T=623 K, W/F=126 hr g-cat/g-mol nitro-compound, $\overline{R}$=13 g-mol H_2/g-mol nitro-compound), or by repeating some of the experimental runs (see Runs P250, P250R, P275, and P275R: Appendix B).

6.1 Catalyst Activity

Deactivation of the presulfided Ni-Mo/Al_2O_3 was made by running the experiment at the standard conditions for several days. Samples of the organic liquid products were taken at different times and analyzed to determine the change in the activity of the catalyst with respect to the time in stream. Selectivity was used as a simple measure of catalyst activity. As shown in Figure 6.1, the catalyst activity decreased rapidly with time of catalyst in stream from 0.831 at 12 hours to 0.318 after 96 hours. After about 170 hours the catalyst reached a constant activity. This Figure also indicates that as the catalyst time in the stream increases, the extent of denitrogenation decreases. The extent of denitrogenation observed at the standard conditions remained essentially constant after about 170 hours, and so all the data were collected after the catalyst had been in the stream for over 200 hours. The catalyst activity was checked periodically by replicating some of the runs (see data for Runs P250, P250R, P275, P275R in Appendix B) or by reproducing the data taken at the beginning of the run and at the end of that run. No significant change in catalyst activity was detected after 200 hours or after each run.

The virgin catalyst was sulfided at a temperature of 623 K, a pressure of 15 psig, and a flow rate of 40 ml/min. using a mixture of 9.8% H_2S in H_2 for 12 hours. The catalyst was resulfided at the same conditions after each run. From the product distribution of the replicates it was shown that sulfiding the used catalyst after the end of each run did not increase the activity of that catalyst but it helped maintaining it at a constant level. The effect of sulfiding was investigated by analyzing the ESR spectra for the unsulfided and the sulfided catalyst. More detail about the ESR studies are found in Section 3.2.1 and in Appendix F.

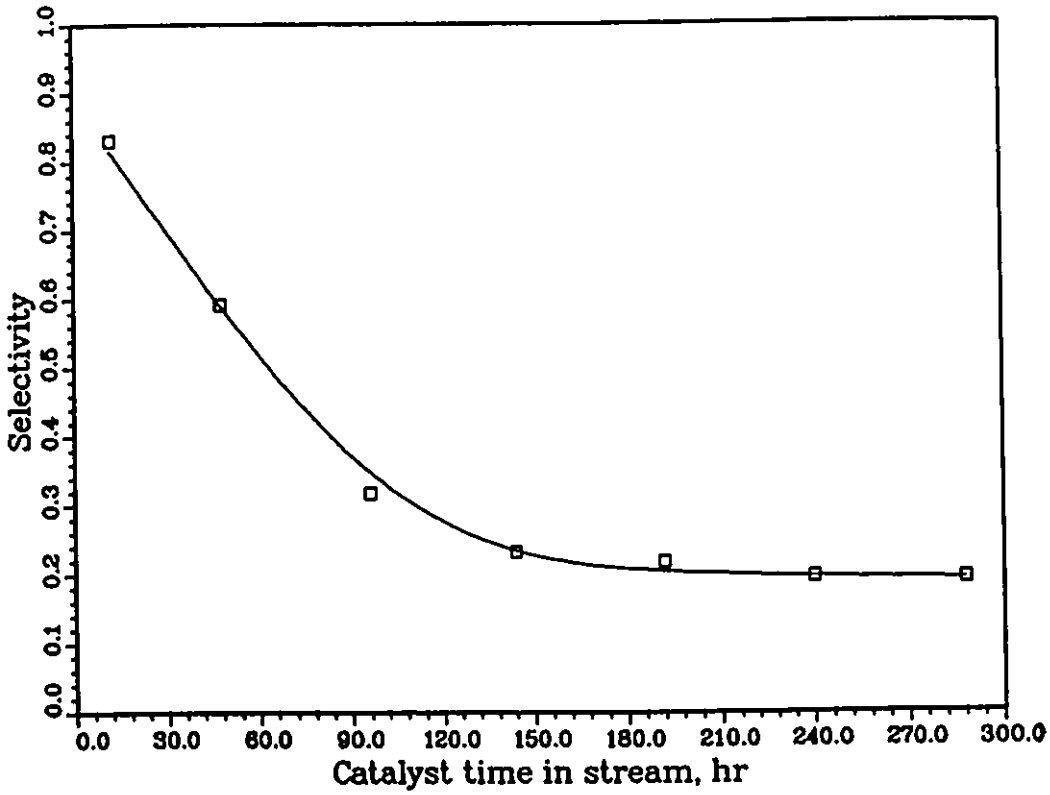

Figure 6.1: Catalyst deactivation during Pyridine HDN; standard conditions.

6.2 Effect of Process Variables

A statistical model was built in order to determine the effect of the process variables (T, W/F, $\overline{R}$), on the pyridine HDN. Information about possible interaction between these operating variables as well as their squared terms were also detected. In this model the random variable, XS, is the product of conversion times selectivity. The independent variables X_1, X_2, and X_3 represent the temperature, the space time, and the reactants' molar ratio respectively. The data used for model building are presented in Table 6.1. In this Table the first letter in the run number represents the first letter of the nitrogen compound feed, the first three digits represent the temperature in degree Celsius, the fourth digit represents the level of the space time, the fifth digit represents the reactants' molar ratio level of the experimental design described above, and the letter R was introduced when there is a replicate. The complete form of the model that represents the above data is

$$\begin{aligned} E(Y) = \beta_0 + \beta_1 x_1 + \beta_2 x_2 + \beta_3 x_3 \\ +\beta_{11} x_1^2 + \beta_{22} x_2^2 + \beta_{33} x_3^2 \\ +\beta_{12} x_1 x_2 + \beta_{13} x_1 x_3 + \beta_{23} x_2 x_3 \end{aligned} \tag{6.1}$$

The linear regression of the data gave the following model

$$\begin{aligned} E(XS) = 16.44 + 28.79 X_1 + 8.80 X_2 + 1.49 X_3 \\ +9.01 X_1 X_2 + 0.6425 X_1 X_3 + 0.1650 X_2 X_3 \\ +15.73125 X_1^2 - 1.4812 X_2^2 + 0.3062 X_3^2 \end{aligned} \tag{6.2}$$

This result indicates that the higher the temperature, the larger the catalyst to feed flow rate, and the lower the nitrogen compound feed to hydrogen ratio gave

Table 6.1: design for three operating variables.

Run number	Temperature (K)	W/F hr g-cat/g-mol	R g-mol H_2/g-mol feed	XS %
P30073	573	210	13	4.96
P40013	673	42	13	42.07
P30013	573	42	13	.79
P40073	673	210	13	106.04
P30041	573	126	7	2.11
P40047	673	126	19	74.13
P30041	573	126	19	3.15
P40041	673	126	7	60.52
P35077	623	210	19	23.65
P35011	623	42	7	7.21
P35071	623	210	7	19.67
P35017	623	42	19	10.53
P35043	623	126	13	17.87
P35043R	623	126	13	16.06
P35043RR	623	126	13	17.05

higher yields. Another information that can be deduced from the above model is that temperature has the greatest impact on the HDN reaction then the space time and finally the hydrogen to feed molar ratio. The impact of temperature on the HDN reaction was more than three times that of the space time, on the other hand, the impact of space time was about six times that of the hydrogen to nitrogen compound molar ratio. As a result the interaction between the temperature and the space time was significant, and so was the squared term of temperature, while the other interaction and squared terms were not significant. Since the impact of the reactants' molar ratio was much lower than the temperature and the space time, the value of the former was kept constant during the kinetic experiments.

Table 6.2 shows the effect of temperature on conversion, selectivity, and yield

Table 6.2: Effect of temperature (T) on conversion, selectivity, and yield of the HDN reaction of pyridine on Ni-Mo/Al_2O_3.

run number	temperature (K)	W/F	$\overline{R}$	conversion (%)	selectivity $\times 10^{-2}$	yield $\times 10^{-2}$
.P2254	498	126.0	13	10.25	1.17	.10
P2504	523	126.0	13	45.02	.66	.25
P2754	548	126.0	13	73.29	1.24	.75
P3004	573	126.0	13	84.07	3.22	2.14
P3254	598	126.0	13	92.89	9.66	6.58
P3504	623	126.0	13	97.66	18.30	10.71
P3754	648	126.0	13	100.00	56.34	26 82
P4004	673	126.0	13	100.00	80.32	31.32

of the HDN reaction of pyridine at W/F=126 hr g-cat/g-mol pyridine and $\overline{R}$=13 g-mol H_2/g-mol pyridine. The fact that the selectivity at 498 K was higher than that at 523 K is because Run P225 was made before the catalyst had reached its constant activity. This effect is represented graphically in Figure 6.2.

The effect of space time on the conversion, selectivity, and yield of pyridine HDN reaction was verified by varying it between 42 and 210 hr g-cat/g-mol pyridine, while keeping the values of T and $\overline{R}$ at 623 K and 13 g-mol H_2/g-mol pyridine respectively. Results of Run P350 are represented graphically in Figure 6.3.

The effect of reactants' molar ratio on the conversion, selectivity, and yield of the pyridine HDN rection was verified by varying it between 7 and 19 g-mol H_2/g-mol pyridine, while keeping the values of T and W/F at 623 K and 126 hr g-cat./g-mol pyridine respectively. Results of Run PR13 are represented graphically in Figure 6.4.

Figures 6.2, 6.3, and 6.4 confirms the results of the statistical model (Section 6.2).

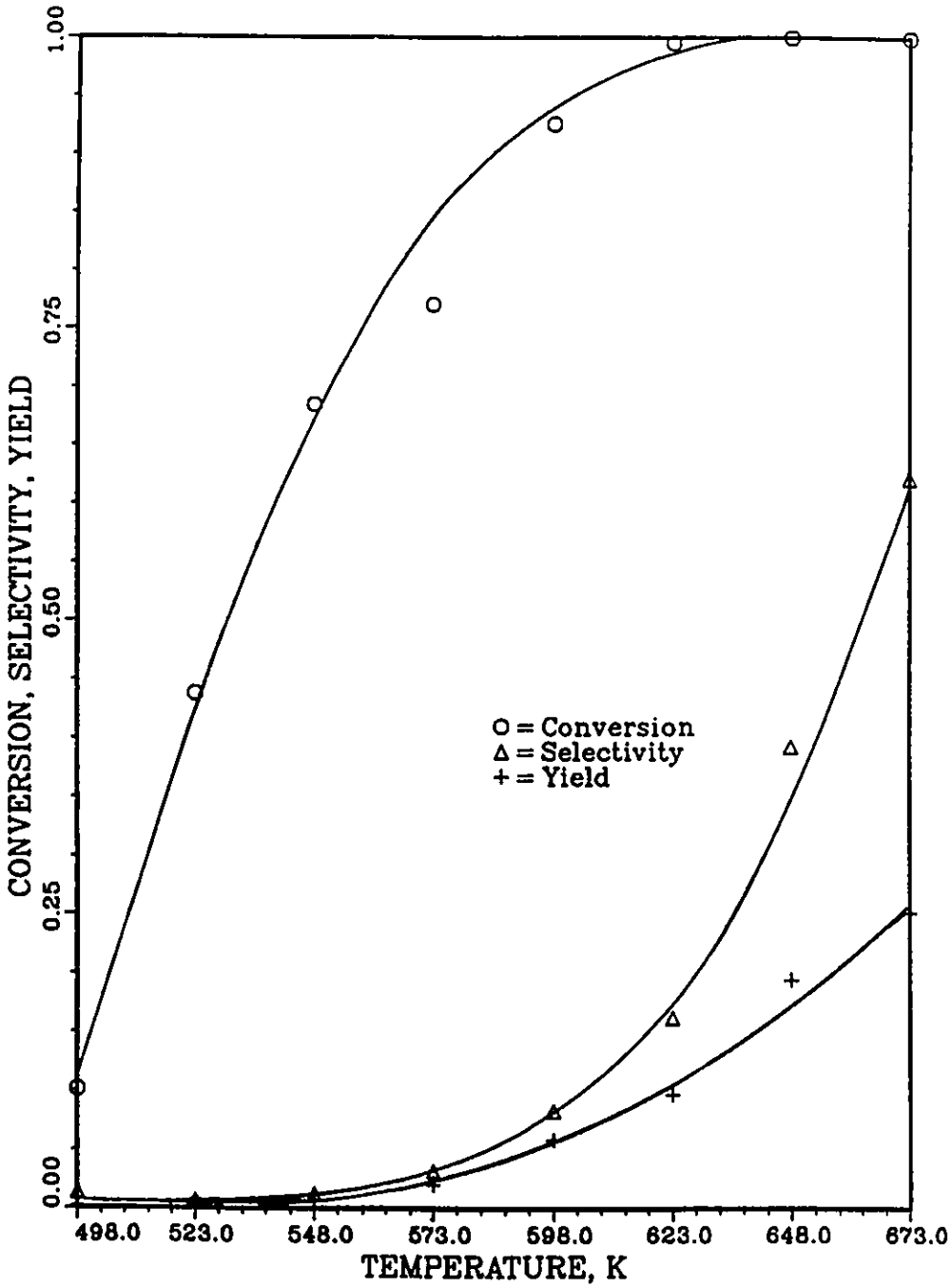

Figure 6.2: Effect of temperature (T) on conversion, selectivity, and yield of pyridine HDN over Ni-Mo/Al_2O_3 at W/F=126 and $\overline{R}$=13.

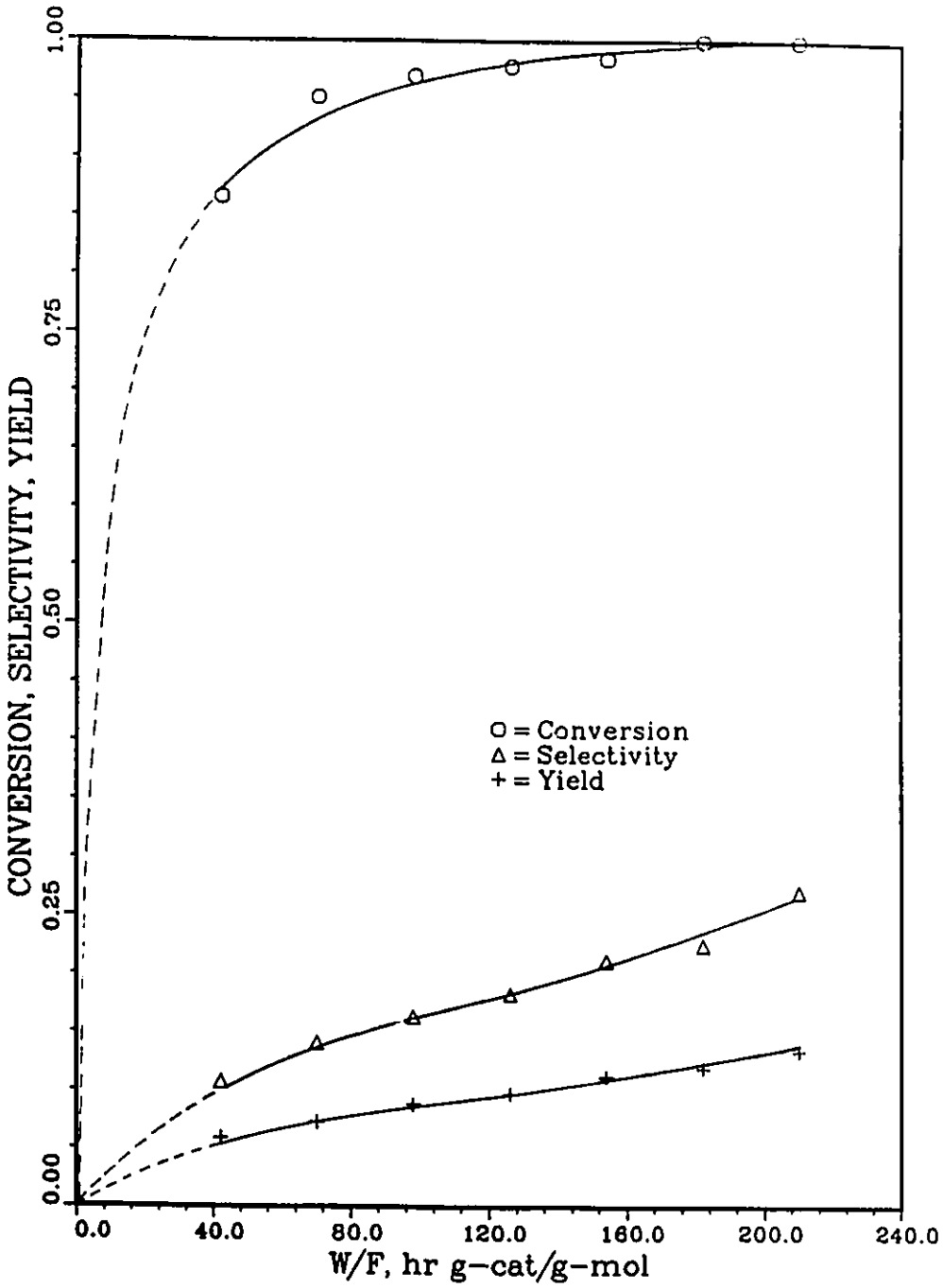

Figure 6.3: Effect of space time (W/F) on conversion, selectivity, and yield of pyridine HDN over Ni-Mo/Al_2O_3 at T=623 K and $\overline{R}$=13.

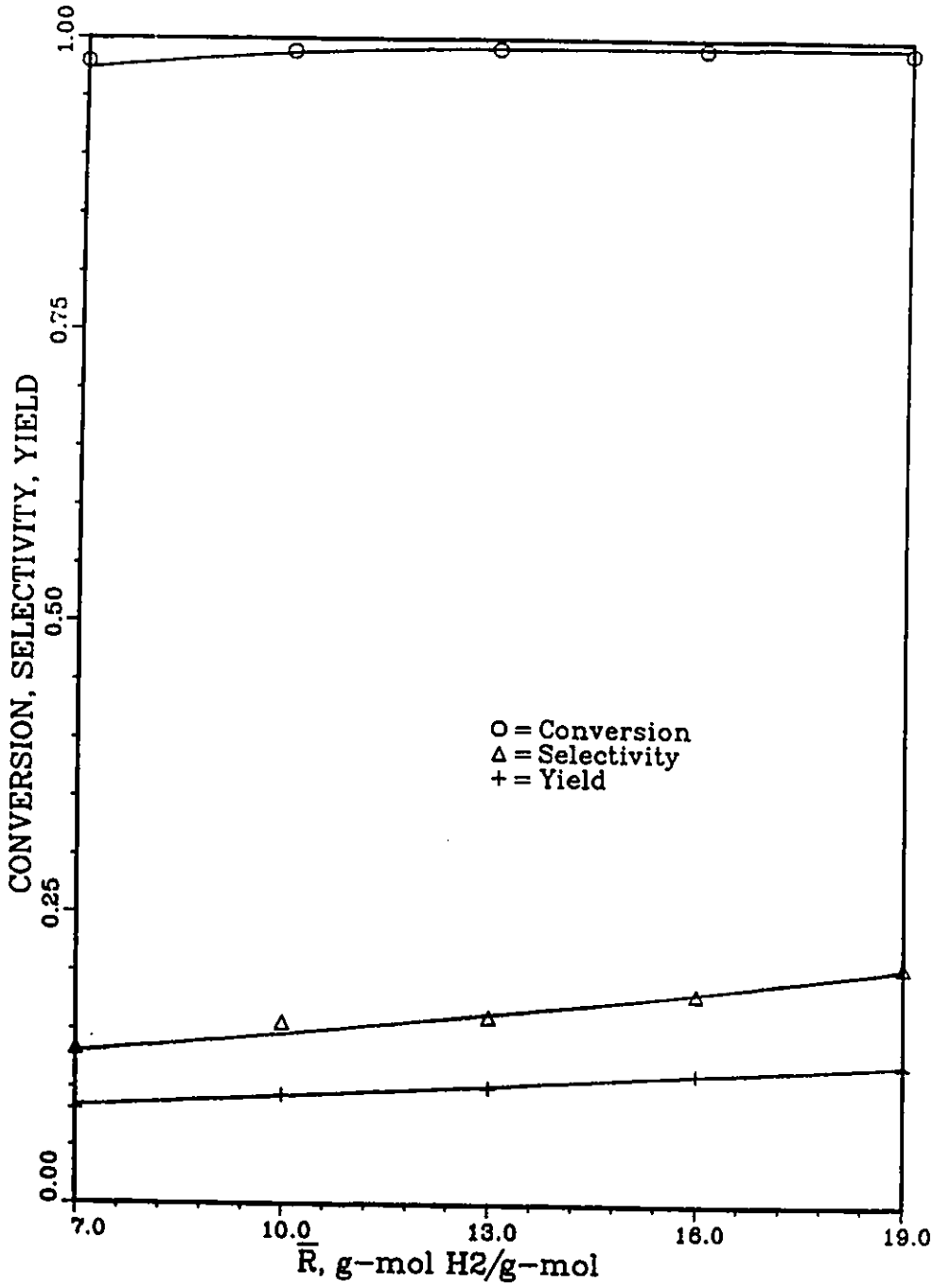

Figure 6.4: Effect of molar ratio ($\overline{R}$) on conversion, selectivity, and yield of pyridine HDN over Ni-Mo/Al_2O_3 at T=623 and W/F=126.

6.3 Effect of Total Pressure

The effect of the reactor total pressure on the HDN reaction of quinoline was verified by running the experiment at a pressure of 34.5 atm, a temperature of 623 K, and reactants' molar ratio of 13 g-mol H_2/g-mol quinoline (Run Q3505). The results of this run and Run Q350 (P=69 atm) are listed in Table 6.3. From this

Table 6.3: Effect of total pressure on the HDN reaction of quinoline over Ni-Mo/Al_2O_3 at T=623 K and $\overline{R}$=13.

W/F	pressure = 34.5 atm			pressure = 69 atm		
	conversion (%)	selectivity $\times 10^{-2}$	yield $\times 10^{-2}$	conversion (%)	selectivity $\times 10^{-2}$	yield $\times 10^{-2}$
42.0	59.99	0.13	0.07	88.21	1.53	1.30
70.0	74.23	0.33	0.24	91.47	3.47	2.99
98.0	75.00	1.20	0.87	92.97	5.97	5.09
126.0	82.68	1.28	1.05	93.95	7.35	6.21
153.0	84.05	2.35	1.94	94.21	9.47	7.85
182.0	85.63	4.66	3.92	94.29	16.08	12.74
210.0	90.88	5.09	4.61	94.30	27.33	20.03

Table it was shown that when the reactor pressure was doubled, the conversion, selectivity, and yield of the reaction had increased. The rate of increase in the selectivity and yield was more than the rate of increase in conversion. At high space time, 210 hr g-cat/g-mol quinoline, a conversion over 90% was achieved at both pressures, but the selectivity as well as the yield at the higher pressure was about five folds of that at the low pressure. As the space time increases the reactants will have more access to the catalytic sites in order to form products, and hence the conversion was high even at low pressure. On the other hand, the production of hydrocarbons requires large amount of hydrogen, and so at high pressure more

hydrogen is present for the HDN reaction which explains the higher selectivity at high space time. These results are represented graphically in Figures 6.5 to 6.7.

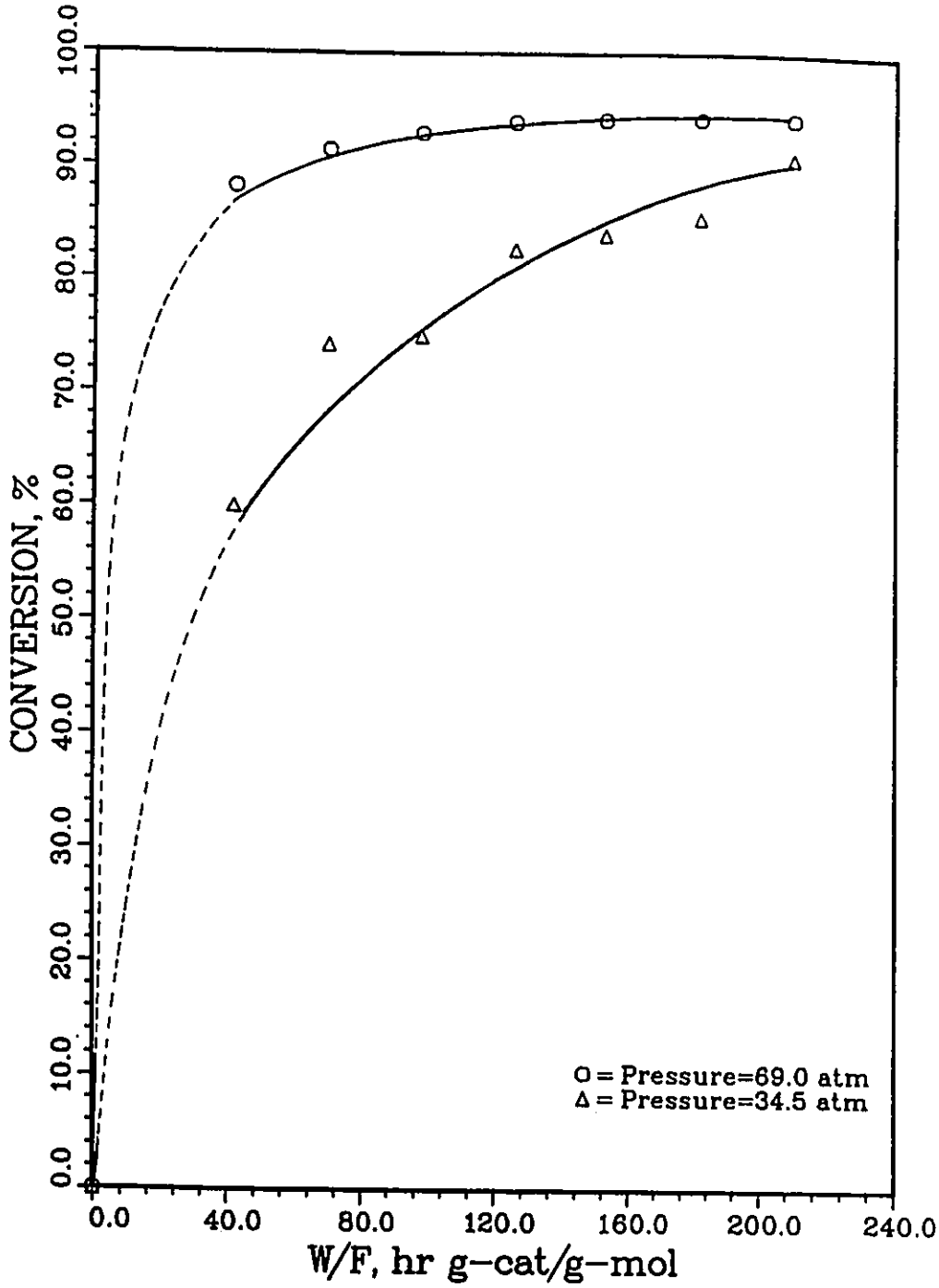

Figure 6.5: Effect of pressure and space time on the conversion of quinoline HDN; T=623 K, $\overline{R}$=13

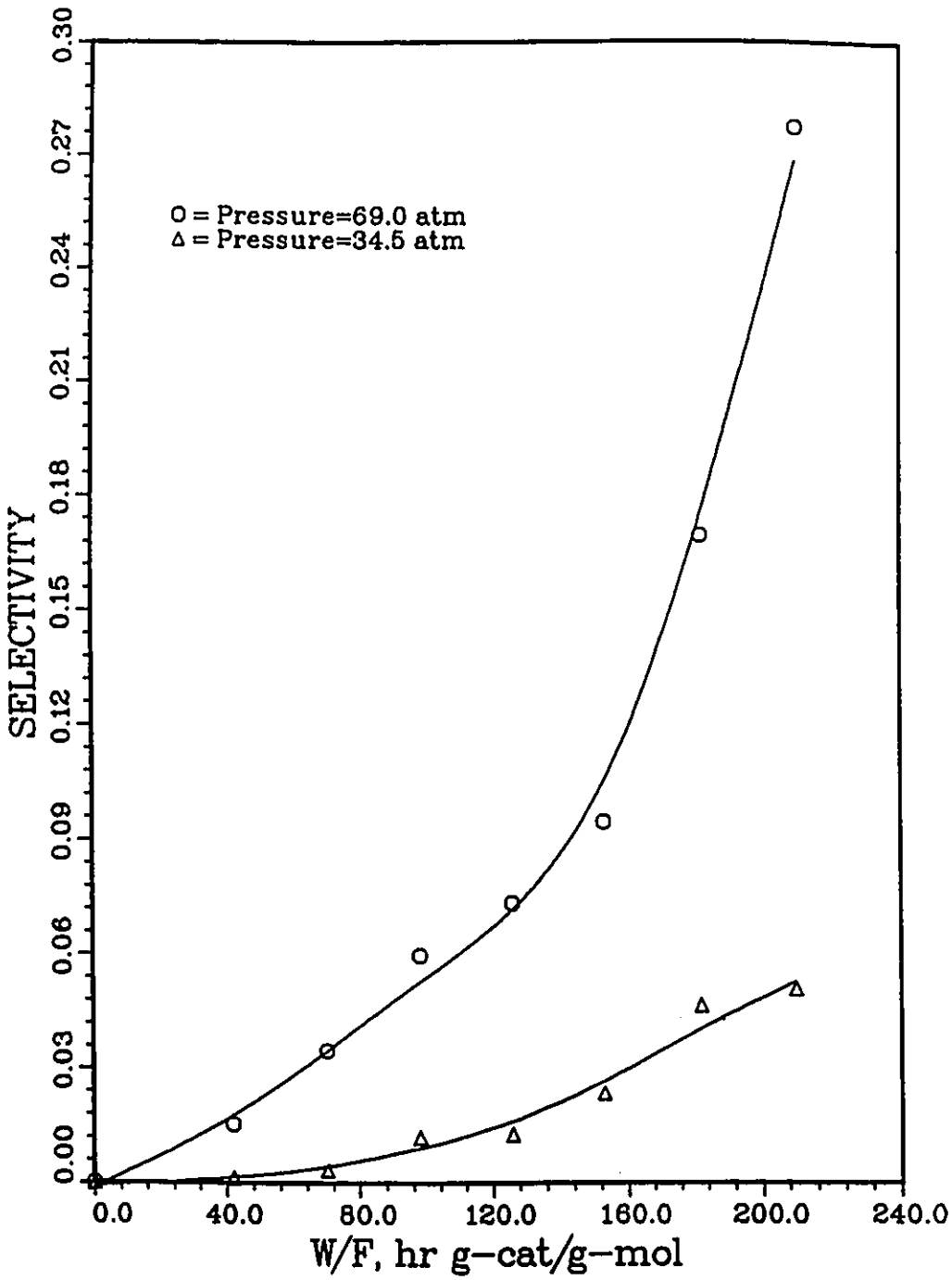

Figure 6.6: Effect of pressure and space time on the selectivity; quinoline HDN; T=623 K, $\overline{R}$=13

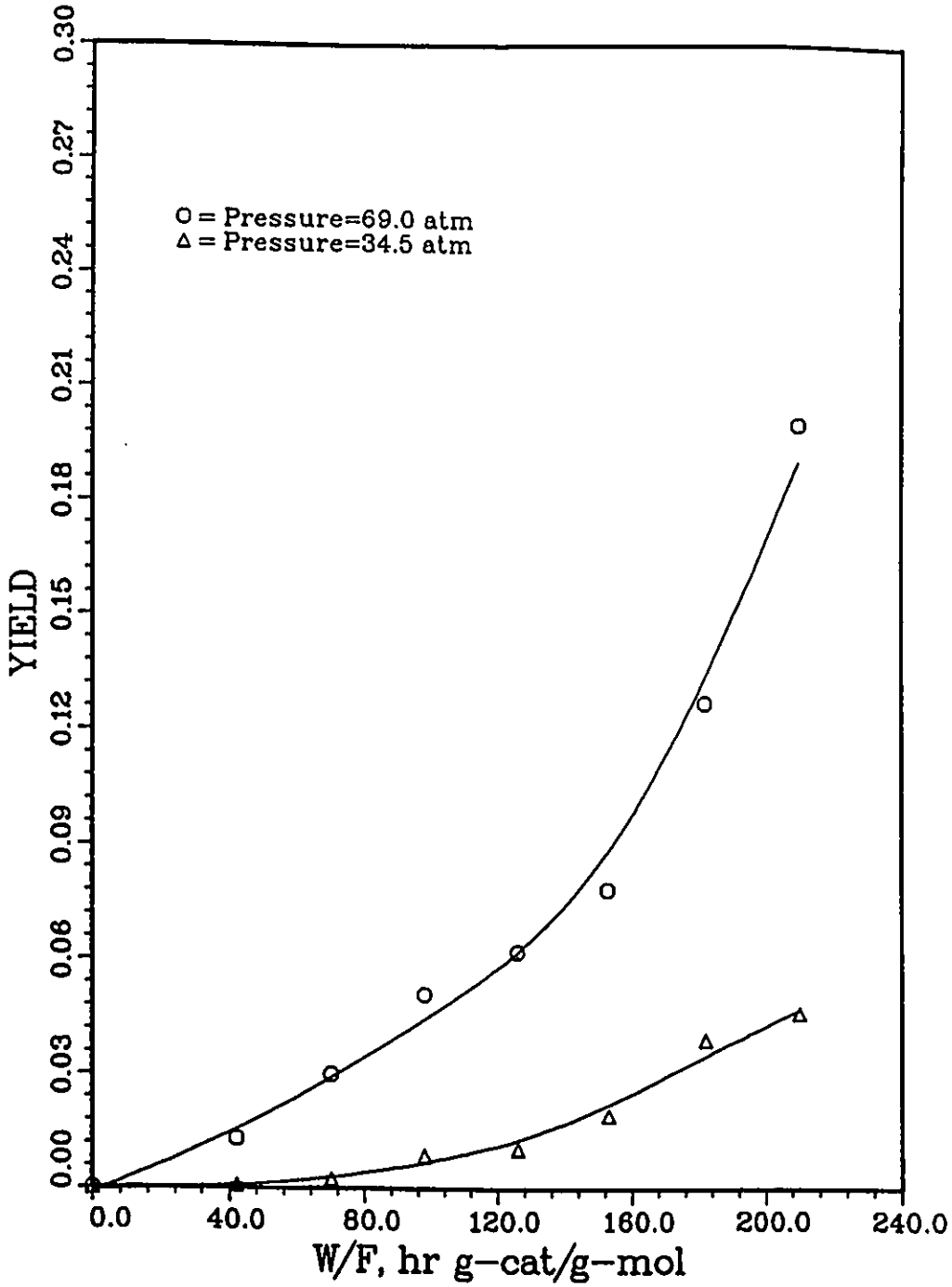

Figure 6.7: Effect of pressure and space time on the yield; quinoline HDN; T=623 K, $\overline{R}$=13

6.4 Effect of Support on Catalyst Activity

The role of the catalyst support on the activity of the catalyst was verified by preparing a catalyst having the same oxide composition as the commercial one (3.03% wt Ni and 12.94% wt Mo) but supported on pumice stone. Results of the experiments conducted with this catalyst indicated that, the commercial catalyst with alumina support had higher activity than the one with pumice support (compare Figure 6.3 and Table 6.4). This result was to be expected due to the small surface area of pumice stone compared to that of alumina, and consequently less number of active sites available for the reaction.

A blank run was made at $\overline{R}$=13, W/F=126, and T at 623, 673 and 773 K, in order to verify if a homogeneous reaction can take place. Only traces of piperidine and ethylpiperidine were detected at temperatures between 623 and 673 K. At higher temperature, 773 K, pentane was also detected but in very minute amounts. This small conversion may be due to the thermal decomposition of pyridine or due to the adsorption of the reactants at the reactor surface or the preheater that might act as a catalyst surface.

Table 6.4: Effect of space time (W/F) on conversion, selectivity, and yield of the HDN reaction of pyridine on Ni-Mo/Pumice.

run number	temperature (K)	W/F	$\overline{R}$	conversion (%)	selectivity $\times 10^{-2}$	yield $\times 10^{-2}$
PS3501	623	42.0	13	7.02	0.66	0.03
PS3502	623	70.0	13	8.10	0.68	0.04
PS3503	623	98.0	13	10.72	0.70	0.09
PS3504	623	126.0	13	21.37	0.73	0.11

6.5 Results of ESR and XRD Studies on Catalyst

Results of the ESR and XRD studies performed on the catalyst are presented in the following sections.

6.5.1 ESR Results

The ESR is a technique that measures the concentration of the species with only unpaired electrons. Molybdenum can exist in any of the four valencies, 6+, 5+, 4+, and 3+ which correspond to d^0, d^1, d^2, and d^3 configuration respectively. Mo^{+6} is diamagnetic and, therefore gives no ESR signal. Mo^{+4} species, even if it was paramagnetic would not be observed except at very low temperatures. The only two possible ions that can be detected are Mo^{+3} and Mo^{+5}.

Figure 6.8 shows the ESR spectra of Ni-Mo/Al_2O_3 catalyst which was used in the present study. The effect of sulfiding the Mo/Al_2O_3 or M-Mo/Al_2O_3 (where M = Ni, Co, or W) catalysts is well described in literature [54,53,108]. When the catalyst was sulfided the major part of molybdenum is converted to MoS_2 and MS_2. Smaller amounts of oxysulfides, polymeric sulfur and different valencies of molybdenum or metals (Ni, Co, W) may be present. Sulfiding the catalyst had resulted in a significant increase in the intensity of Mo^{+5} line. The enhancement of Mo^{+5} ions could be due to the following mechanism.

$$H_2S \longrightarrow H^+ + SH^- \tag{6.3}$$

$$Mo^{+6} + H^+ \longrightarrow Mo^{+5} + \frac{1}{2}H_2 \tag{6.4}$$

On the other hand, the addition of pyridine at high temperature (400°C) resulted in a decrease in the intensity of the Mo^{+5} line. This decrease was more significant when

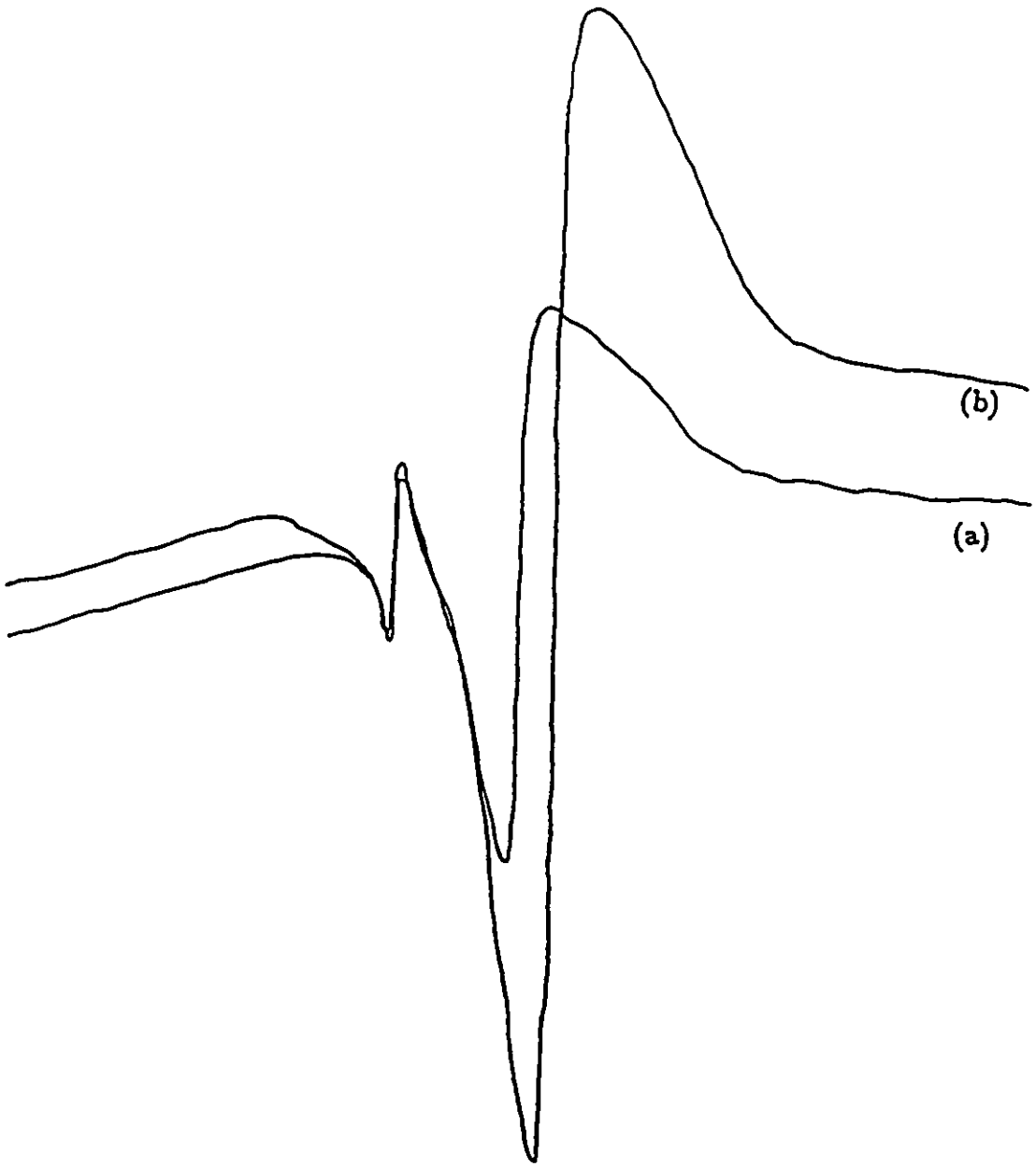

Figure 6.8: ESR spectra of Ni-Mo/Al_2O_3. (a) degassed catalyst, (b) H_2 added at high temperature.

the catalyst was unsulfided. The reactions at the catalyst surface are as follows

$$2Mo^{+6} + H_2 \longrightarrow 2Mo^{+5} + 2H^+ \tag{6.5}$$

$$Mo^{+5} + R \longrightarrow Mo^{+6} + R^- \tag{6.6}$$

where R represents a hydrocarbon.

6.5.2 XRD Results

The oxide catalyst was photographed using the *Debye Scherrer* technique. It is known that MoO_3 and NiO are crystalline while Al_2O_3 is amorphous. The lines produced on the x-ray film correspond to the MoO_3. The lines that correspond to NiO were not present due to the low concentration of this oxide on the catalyst surface. This result is in good agreement with what was reported by Grimblot et al. that if the molar ratio Ni/(Ni+Mo) < 0.5, only the MoO_3 can be detected [41].

The presence of alumina cannot be detected by the X-ray diffraction at low temperatures. Calcining the Ni-Mo/Al_2O_3 at high temperature (above 800 K) will result in observing the presence of alumina in the sample [48]. Studies carried out by Schönberg [85] have revealed the existence of Mo_4O_{11}, Mo_8O_{23}, and Mo_9O_{26} besides MoO_2 and MoO_3.

6.6 Hydrodenitrogenation Results

The HDN experiments were conducted on pyridine, quinoline, and their mixture. Table 6.5 shows the conditions of these experiments.

Heterocyclic nitrogen compounds promote catalyst deactivation by interacting with the acidic sites and due to coke formation especially at high temperatures. Therefore more active catalysts operating at lower temperatures will have a great

Table 6.5: list of experiments

run number	temperature (K)	pressure atm	feed	$\bar{R}$	W/F	number of samples
P225	498	69	pyridine	13	42–210	7
P250	523	69	pyridine	13	42–210	7
P250R	523	69	pyridine	13	42–210	7
P275	548	69	pyridine	13	42–210	7
P275R	548	69	pyridine	13	42–210	7
P300	573	69	pyridine	13	42–210	7
P325	598	69	pyridine	13	42–210	7
P350	623	69	pyridine	13	42–210	7
P375	648	69	pyridine	13	42–210	7
P400	673	69	pyridine	13	42–210	7
PR13	623	69	pyridine	7–19	126	5
PS350[a]	623	69	pyridine	13	42–126	4
Q225	498	69	quinoline	13	42–210	7
Q250	523	69	quinoline	13	42–210	7
Q275	548	69	quinoline	13	42–210	7
Q300	573	69	quinoline	13	42–210	7
Q325	598	69	quinoline	13	42–210	7
Q350	623	69	quinoline	13	42–210	7
Q375	648	69	quinoline	13	42–210	7
Q375R	648	69	quinoline	13	42–210	7
Q400	673	69	quinoline	13	42–210	7
Q3505	623	34.5	quinoline	13	42–210	7
PQ225	498	69	quinoline pyridine	13	42–210	7
PQ300	573	69	quinoline pyridine	13	42–210	7
PQ350	623	69	quinoline pyridine	13	42–210	7
PQ400	673	69	quinoline pyridine	13	42–210	7

a: Catalyst support was pumice stone

effect on maintaining the catalyst activity. Molybdenum had been widely used in the hydrotreating processes mainly because of its resistance to poisoning. Sulfiding the molybdenum catalyst had increased its activity significantly. On the other hand, the activity of this catalyst was maintained at a constant level by sulfiding it frequently. Goudriaan et al. [40], studying the HDN of pyridine over cobalt molybdate catalyst, had reported that at high conversion levels, the temperature required to attain a certain degree of nitrogen removal is about 25°C lower with a sulfided catalyst than with the catalyst in its oxide form. In a recent study of pyridine HDN over Mo/Al_2O_3 at a total pressure of 69 atm, a temperature of 623 K, and a space time between 126 and 210 hr g-cat/g-mol nitro-compound, it was found that sulfiding the catalyst resulted in an increase in the fractional conversion by one fold, whereas the denitrogenation percent had increased by seven folds [3],

6.6.1 Pyridine Hydrodenitrogenation

The product distribution of the organic products indicated that the major reaction intermediates formed during the HDN of pyridine over presulfided $Ni\text{-}Mo/Al_2O_3$ were piperidine (PIP), ethylpiperidine (ETPIP), propylpiperidine (PRPIP), and pentylpiperidine (PEPIP). Other nitrogen-containing compounds such as pentylamine (PEAM) and dipentylamine (DPEAM) were also detected but in small amounts. Two primary hydrocarbon products were identified, pentane (PEN) and decane (DEC). Other nitrogen-containing compounds as well as hydrocarbons were present but in small percentages and were identified by the gas chromatography/mass spectroscopy studies on selected samples of the organic liquid product.

Some of these products were: piperidine,1-1-methylene, piperidine,1-1-pentenyl, cyclopentane, pentane,2-3-3-trimethyl, decane,2-3-5-trimethyl, 2-pentene,2-methyl.

Product Distribution

The main product of pyridine HDN at 498 K was piperidine. Small amount of propylpiperidine was detected at high W/F. The highest conversion obtained in that run was about 16%, while the highest denitrogenation percent was 0.35%. This run, as mentioned before, was made in order to study the behavior of the HDN reaction at low conversion and hence have more information about the reaction network. Increasing the reaction temperature to 523 K and at the same W/F value, had resulted in an increase in the conversion by more than four folds and an increase in the yield of the reaction by more than two folds (see Figures 6.9 to 6.12).

At 548 and 573 K the major products were piperidine and alkyl-piperidines (APIP) i.e. ETPIP, PRPIP, and PEPIP. The conversion at both temperatures and at a space time of 210 hr g-cat/g-mol nitro-compound was about 90%, but the yield of the reaction was more significant at 573 (see Figures 6.13 to 6.16).

At 598 K, piperidine production reached a maximum level at a space time of 168 hr g-cat/g-mol nitro-compound then it started decreasing giving rise to higher concentrations of the alkyl-piperidines especially pentylpiperidine and ethylpiperidine, besides hydrocarbons. As it can be shown from the product distribution (Figure 6.17), the rate of pyridine conversion decreases with space time as well as the rate of formation of piperidine. This behavior is due to the chemical equilibrium. Ethylpiperidine reached its maximum level at 623 K and a space time around 140

hr g-cat/g-mol nitro-compound (Figure 6.18), at the same time piperidine production had decreased in the same rate where it reached a constant level at the same space time. After that the production of ETPIP started decreasing giving rise to more hydrocarbons especially pentane and alkyl-pentanes. At both temperatures the conversion was 100% at space times over 160 hr g-cat/g-mol nitro-compound. More hydrocarbons were produced at 623 than at 598 K (see Figures 6.19 to 6.22).

At 648 and 673 K the production of hydrocarbons increased with the decrease in the production of the nitrogen-containing compounds. This decrease indicates that these compounds are not final products.

The effect of temperature on the product distribution of pyridine HDN reaction showed that the production of hydrocarbons (pentanes and decanes) increased with the increase in temperature (Figure 6.23). The product analysis had shown traces or no pentylamine in the stream. This result lead to the belief that pentylamine is adsorbed at the catalyst surface as soon as it is formed and bond breaking is taking place at either C_5 to form pentylpiperidine or at both C_3 and C_5 giving rise to the formation of ethylpiperidine and propylpiperidine. The presence of ETPIP and PRPIP in the product stream, together with the product distribution of the organic products had suggested a new reaction network as shown in Figure 6.24.

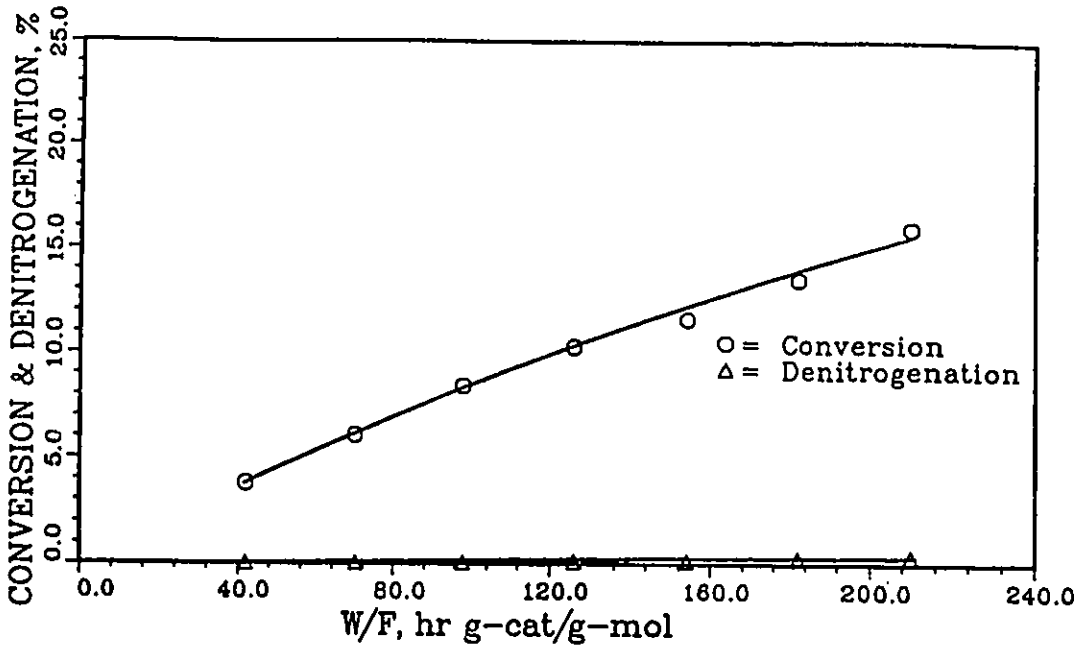

Figure 6.9: Effect of W/F on conversion & denitrogenation of pyridine; T=498 K

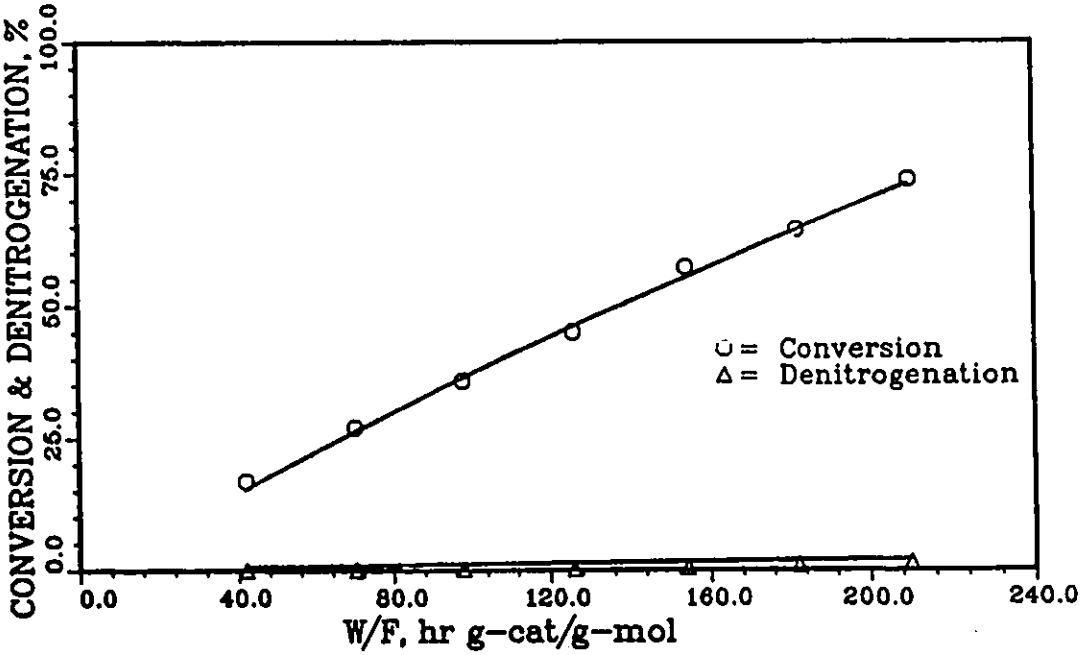

Figure 6.10: Effect of W/F on conversion & denitrogenation of pyridine; T=523 K

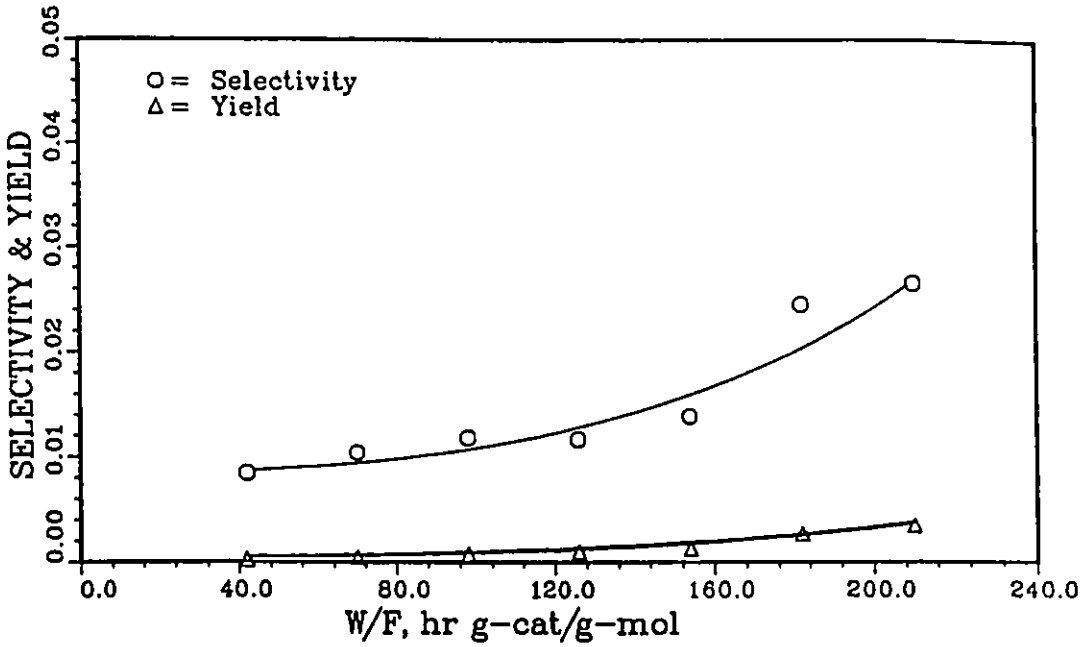

Figure 6.11: Effect of W/F on selectivity & yield; pyridine HDN; T=498 K

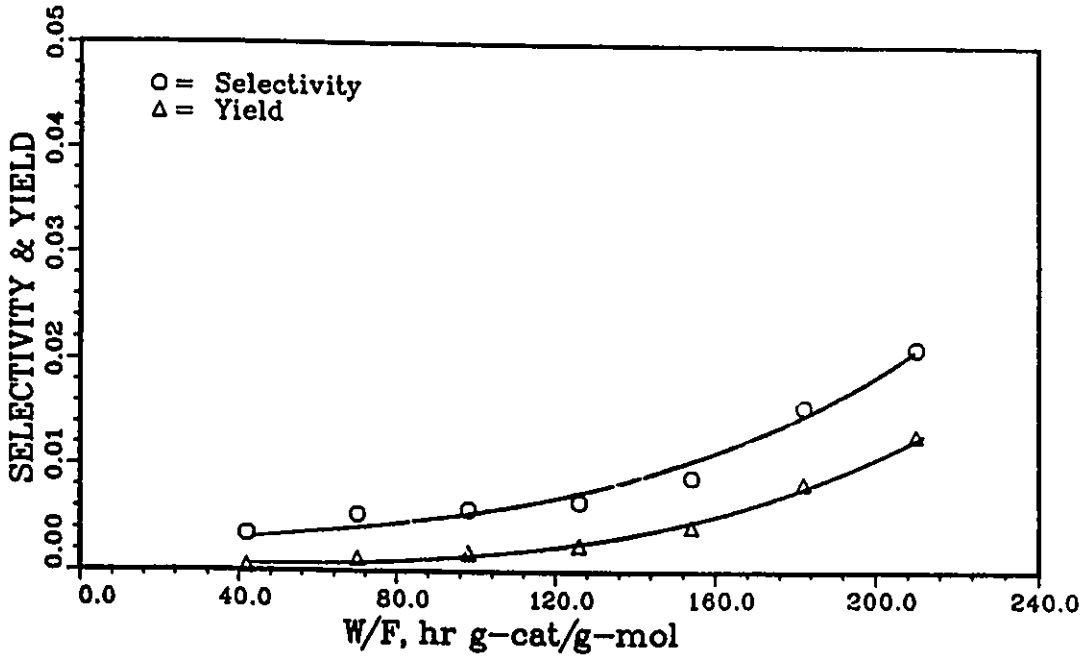

Figure 6.12: Effect of W/F on selectivity & yield; pyridine HDN; T=523 K

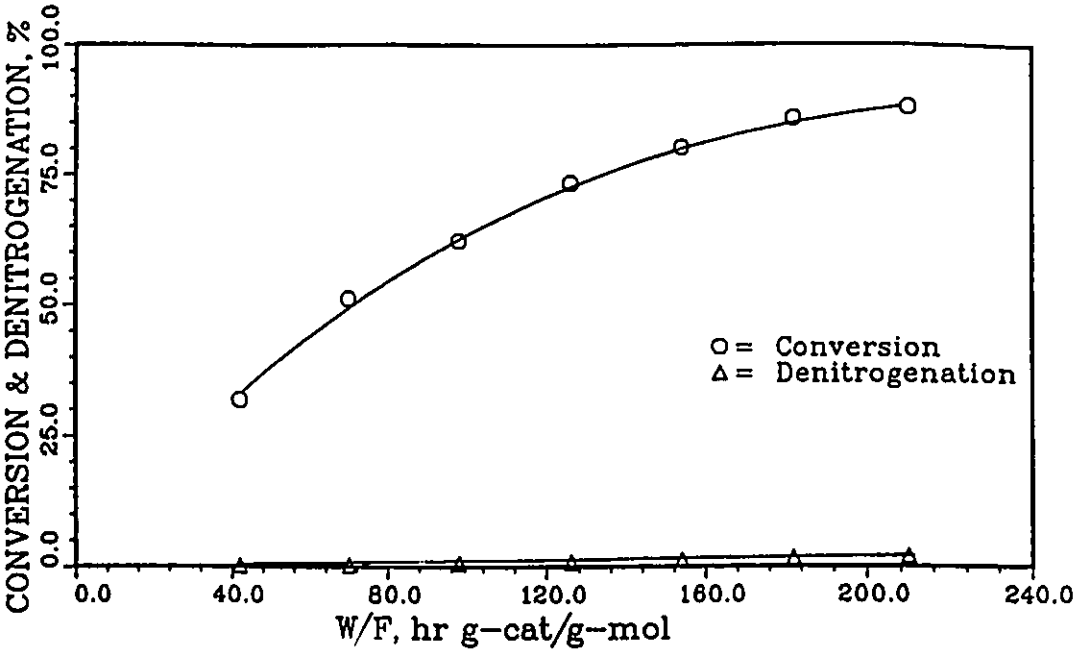

Figure 6.13: Effect of W/F on conversion & denitrogenation of pyridine; T=548 K

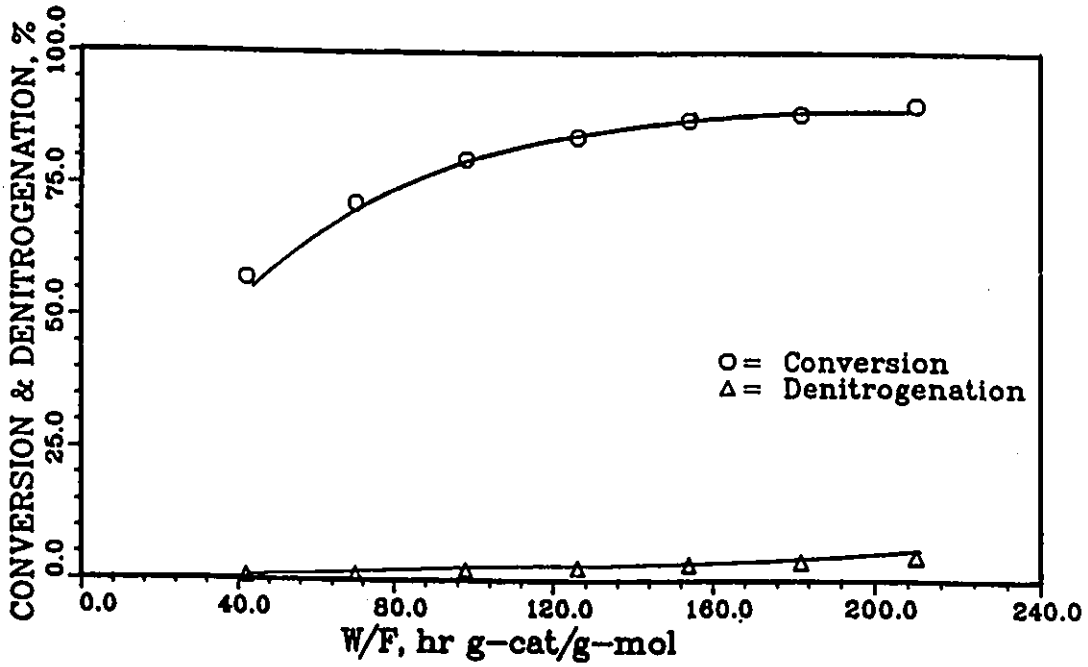

Figure 6.14: Effect of W/F on conversion & denitrogenation of pyridine; T=573 K

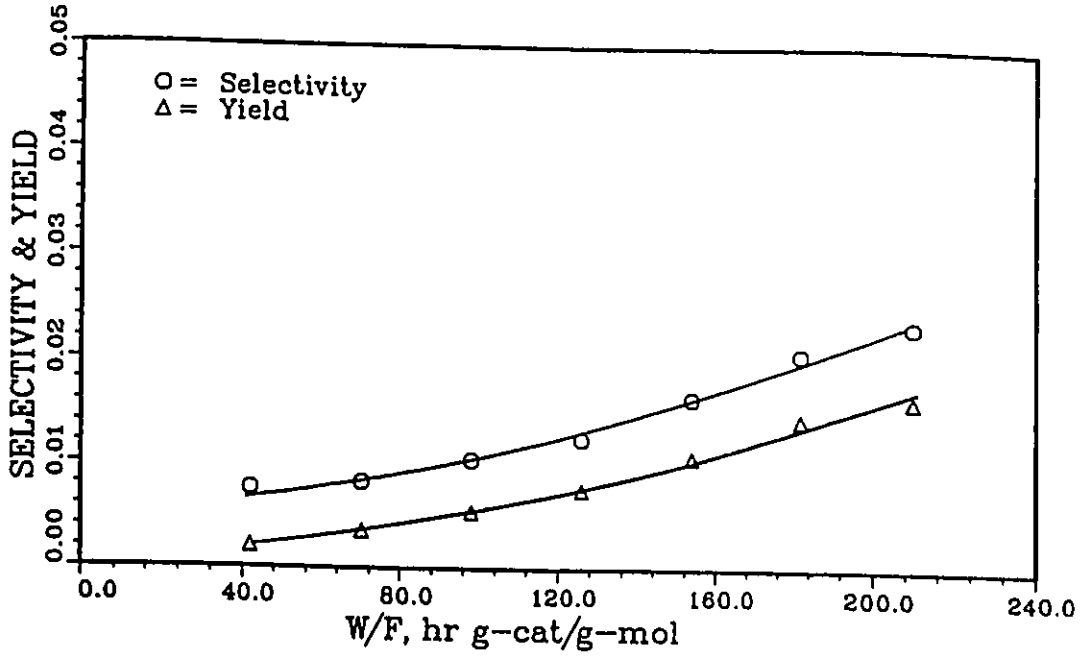

Figure 6.15: Effect of W/F on selectivity & yield; pyridine HDN; T=548 K

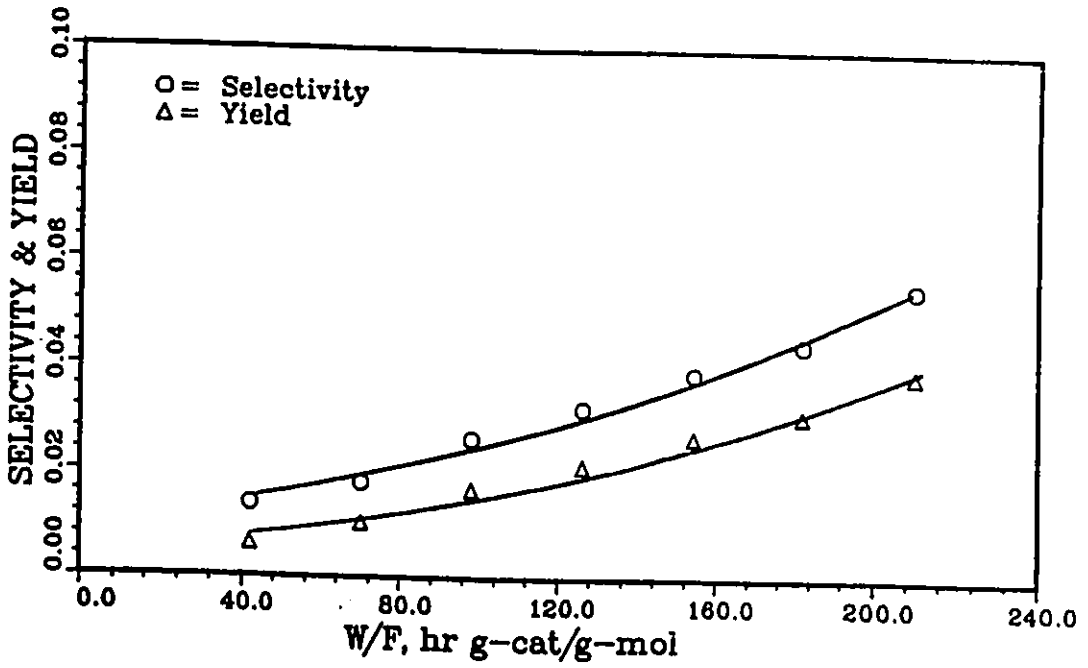

Figure 6.16: Effect of W/F on selectivity & yield; pyridine HDN; T=573 K

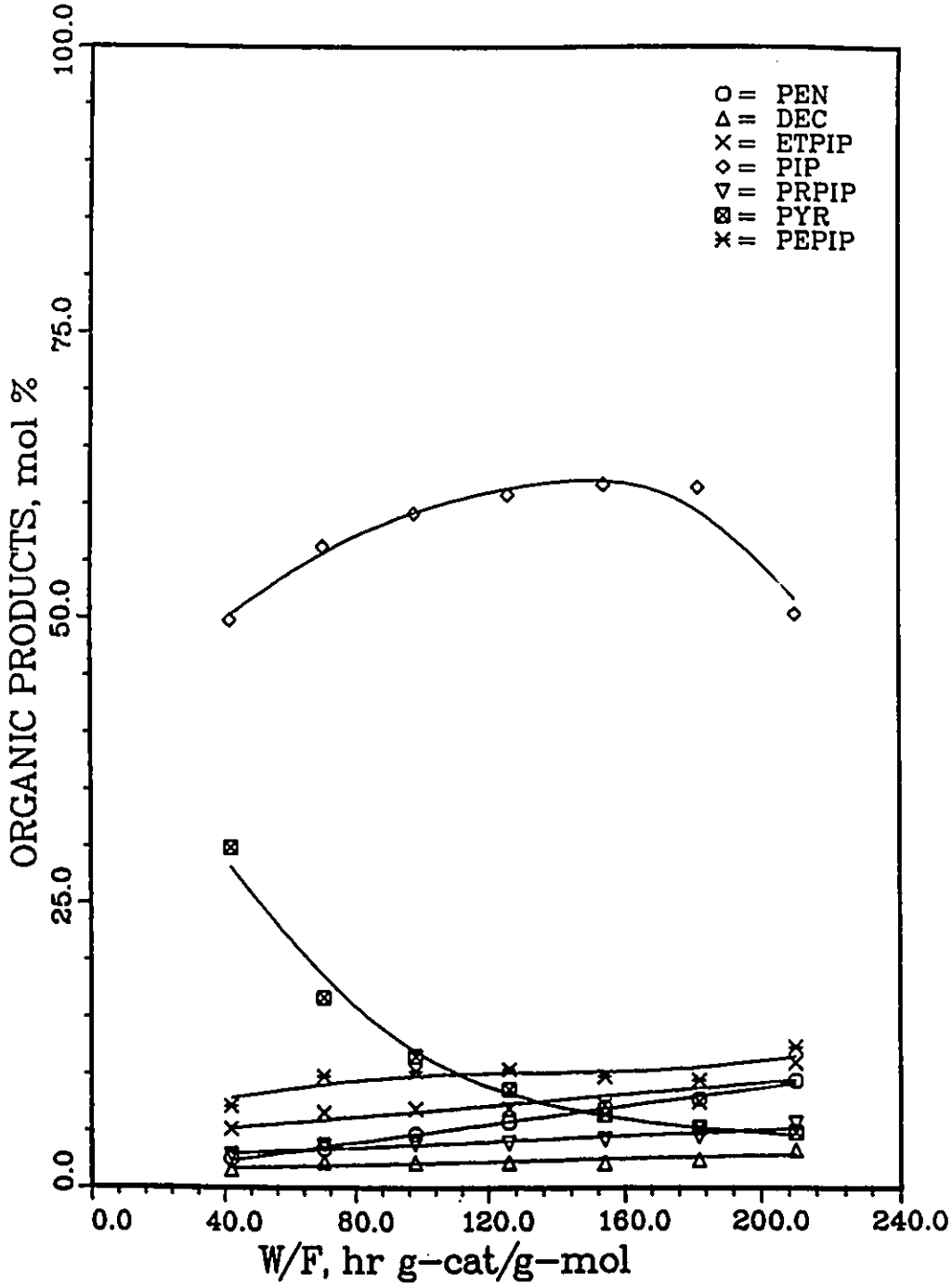

Figure 6.17: Pyridine HDN products; T=598 K, $\overline{R}$=13

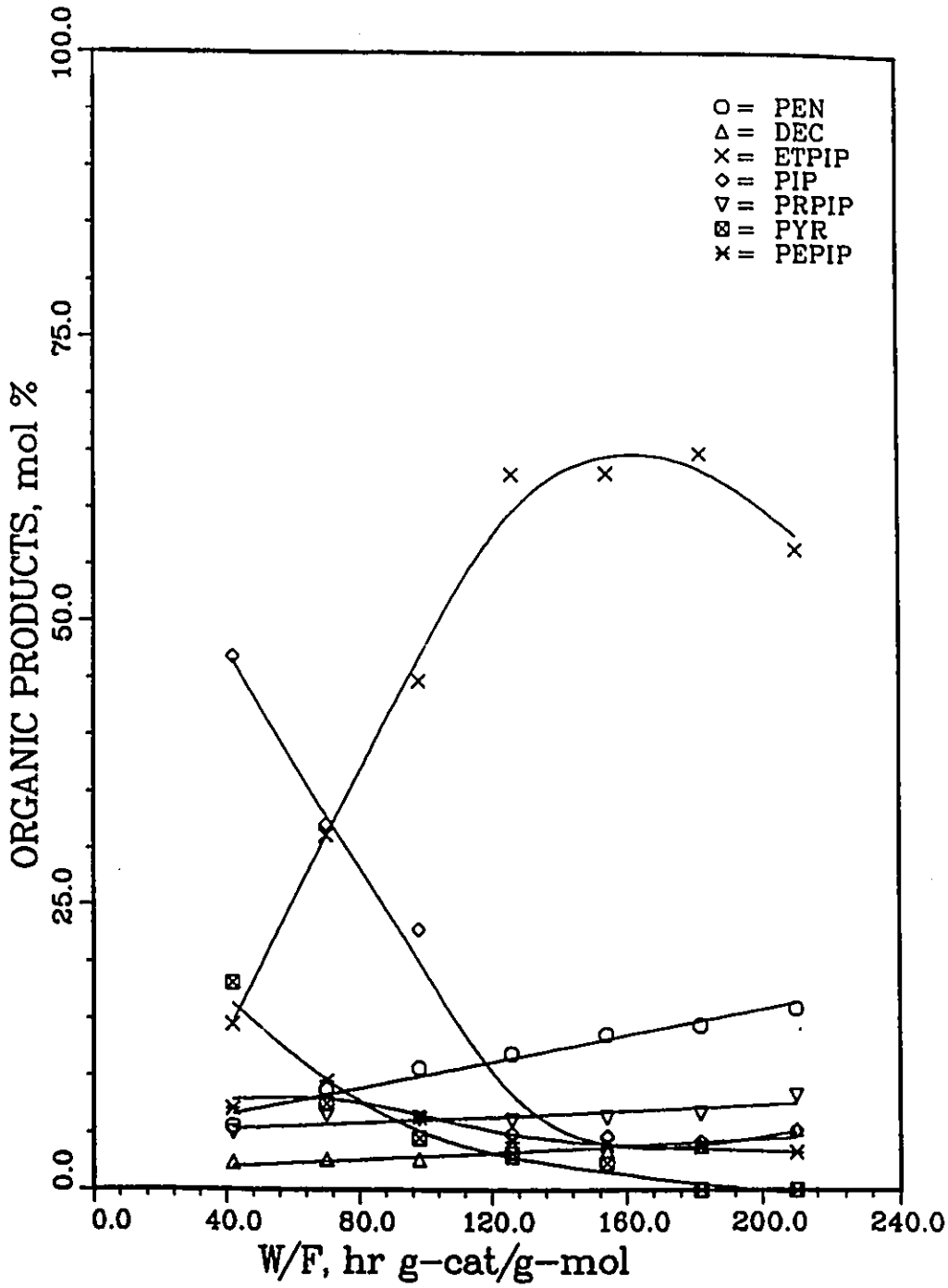

Figure 6.18: Pyridine HDN products; T=623 K, $\overline{R}$=13

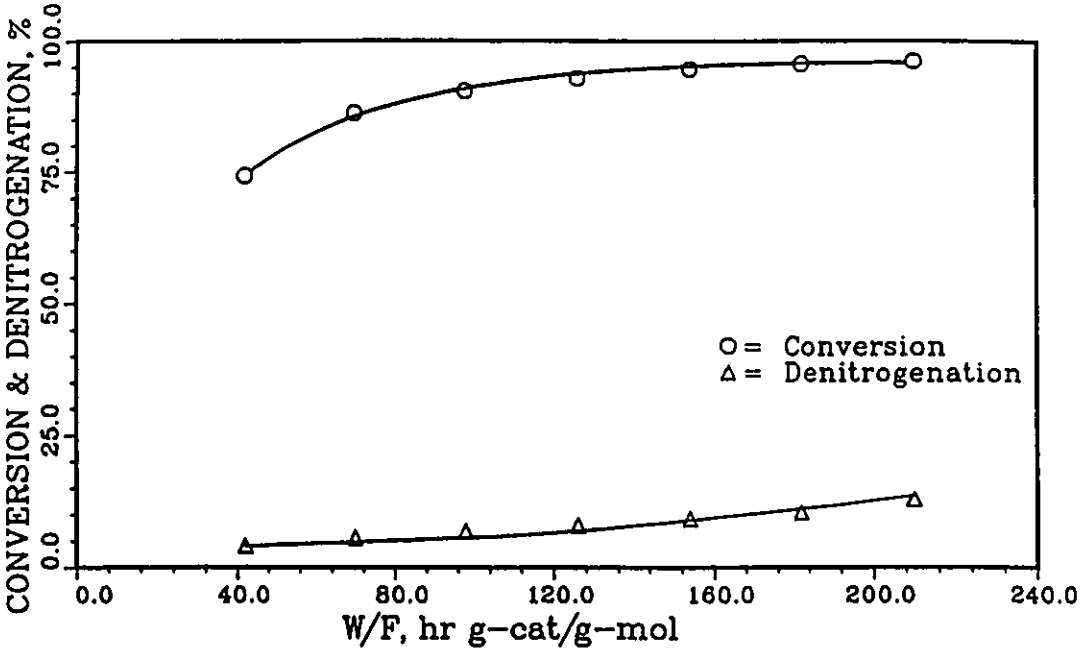

Figure 6.19: Effect of W/F on conversion & denitrogenation of pyridine; T=598 K

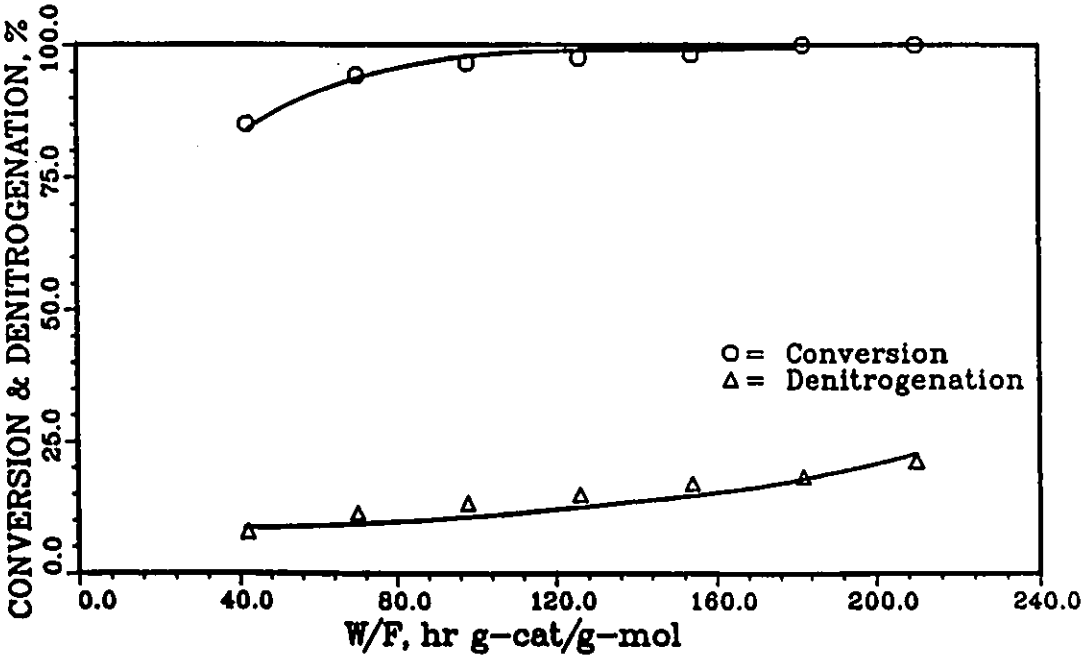

Figure 6.20: Effect of W/F on conversion & denitrogenation of pyridine; T=623 K

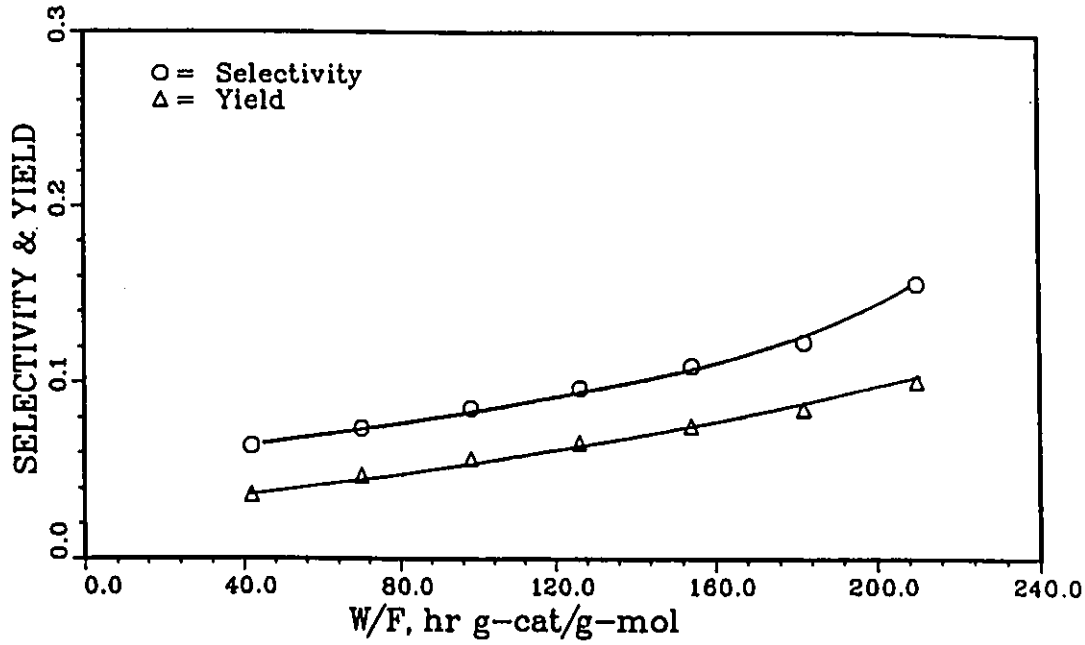

Figure 6.21: Effect of W/F on selectivity & yield; pyridine HDN; T=598 K

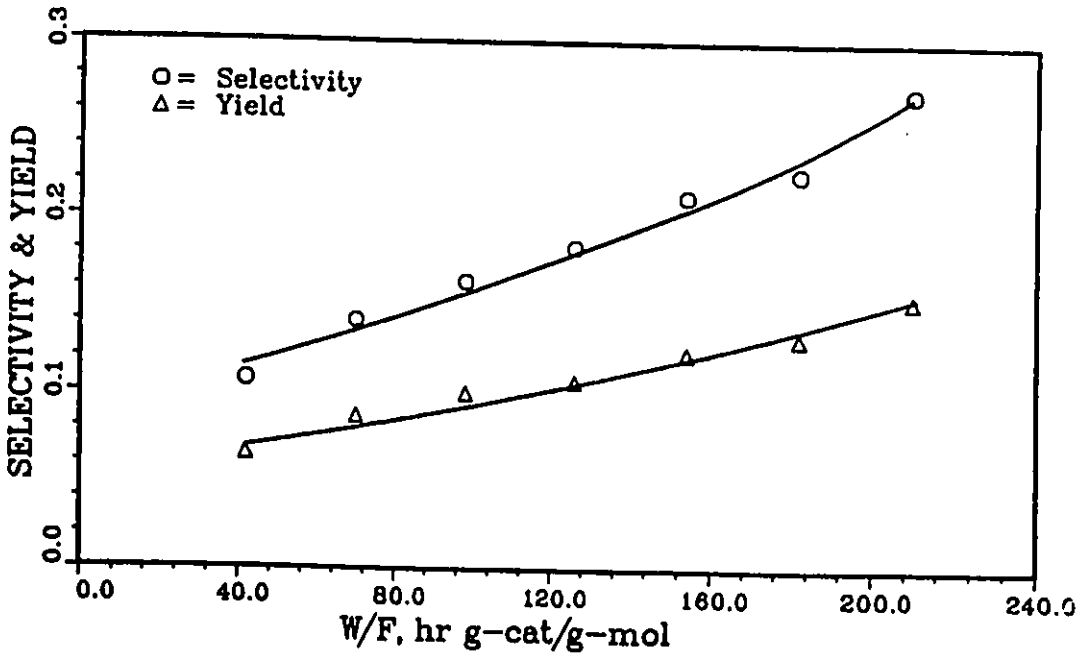

Figure 6.22: Effect of W/F on selectivity & yield; pyridine HDN; T=623 K

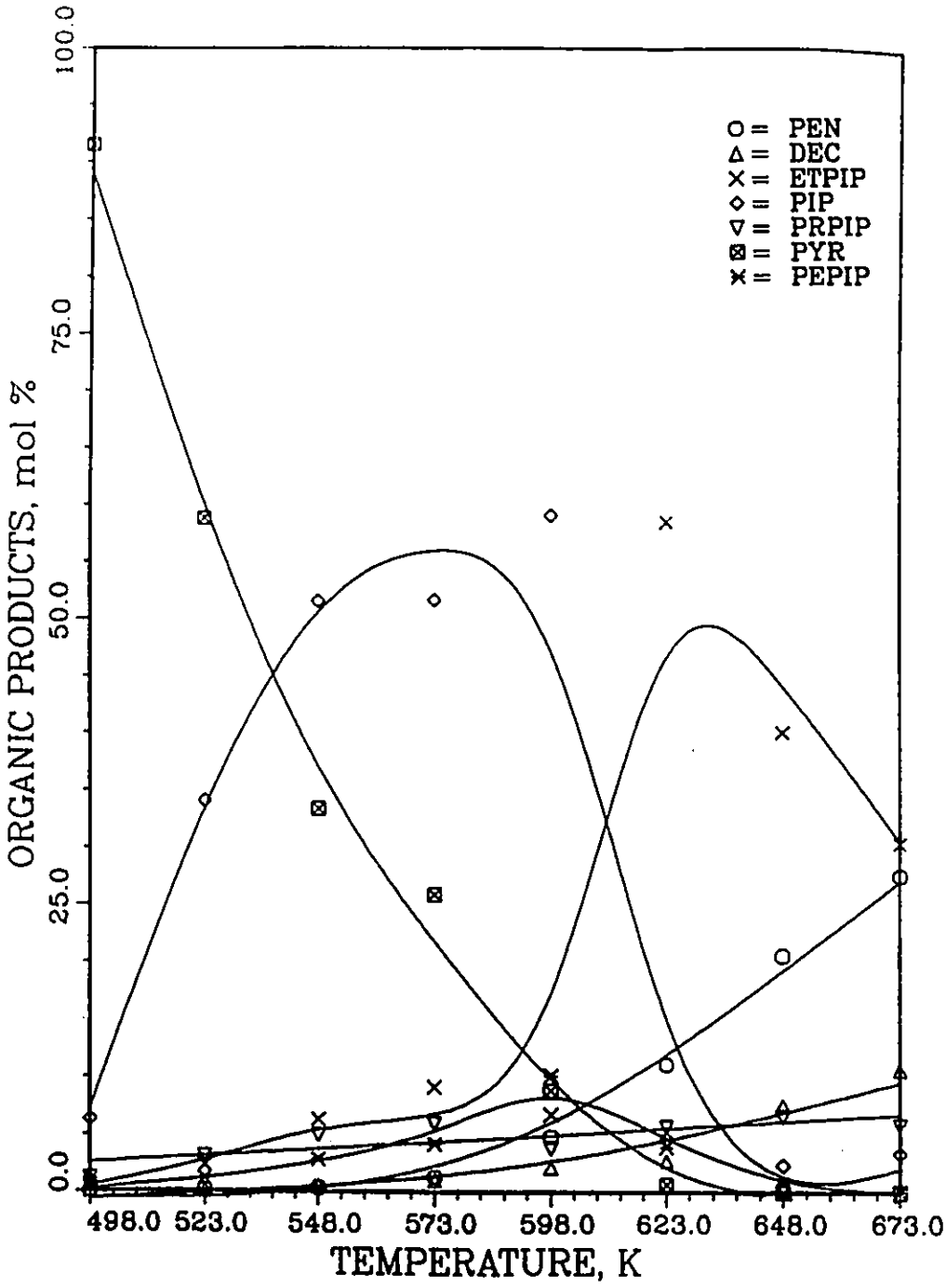

Figure 6.23: Pyridine HDN products; W/F=126, $\overline{R}$=13

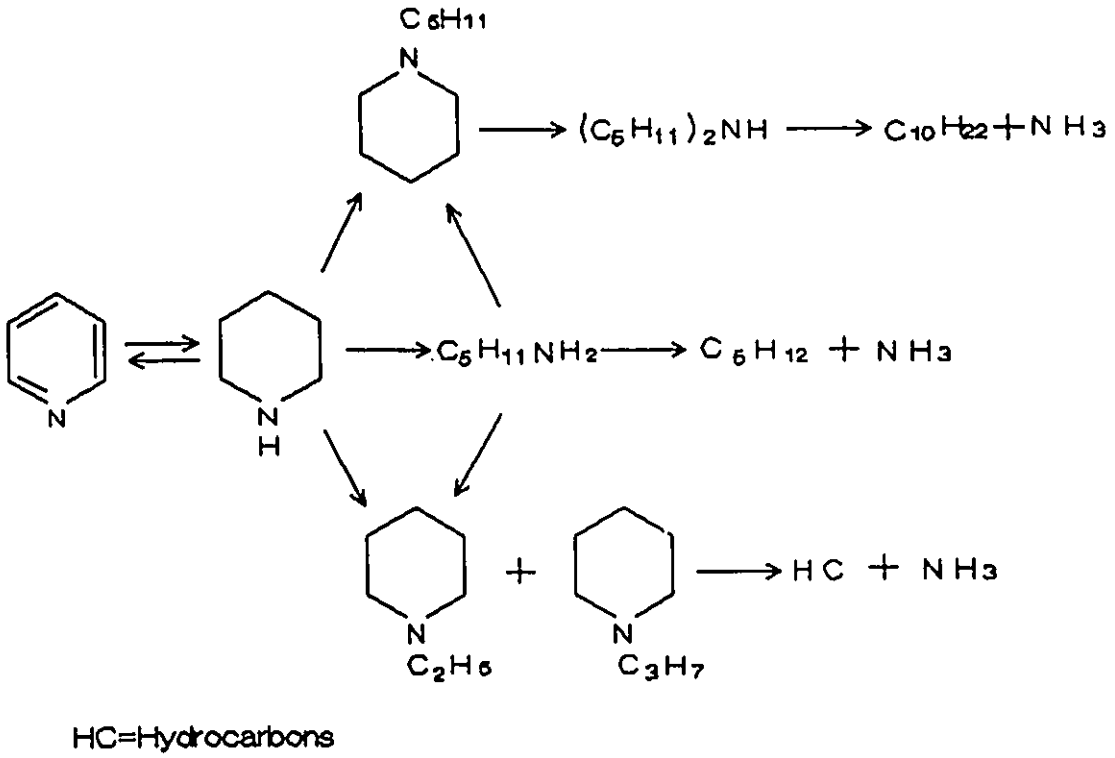

Figure 6.24: Reaction network for the HDN of pyridine over Ni-Mo/Al_2O_3 (Shell Catalyst 424)

6.6.2 Quinoline Hydrodenitrogenation

The product distribution of the organic products indicated that the major reaction intermediates formed during the HDN of quinoline over commercial presulfided Ni-Mo/Al_2O_3 are 1,2,3,4-tetrahydroquinoline (PyTHQ), 5,6,7,8-tetrahydroquinoline (BzTHQ), decahydroquinoline (DHQ), o-propylaniline (OPA), and aniline (AN). Other nitrogen-containing compounds such as ethylaniline (EAN), propylcyclohexylamine (PCHAM) were also detected. In addition, many hydrocarbon products were identified but the most significant ones were propylcyclohexane (PCH) and propylbenzene (PB) in addition to methylethylbenzene (MEB), ethylbenzene (EB), propylcyclohexene (PCHE), and ethylcyclohexane (ECH). Other hydrocarbons were present but in small percentages such as methylcyclohexane (MCH) and indan (IDAN). The gas chromatography/mass spectroscopy studies on selected samples of the organic liquid product helped in confirming the gas chromatography results and in identifying some of the unknown products such as methylbenzenamine, methylaniline, and methylpropylpyridine.

Product Distribution

The main product at 498 K and W/F between 42 and 210 hr g-cat/g-mol nitro-compound was PyTHQ. Small amount of BzTHQ was also detected. At a space time of 210 hr g-cat/g-mol nitro-compound, the conversion was relatively high (80%) compared to the denitrogenation percent (0.38%) or to the yield of the reaction (0.37×10^{-2}). From this run it is deduced that even at low temperature, hydrogenation of quinoline is much easier than its denitrogenation. This result applies also to the HDN of pyridine.

At a temperature of 523 K it is noted that as W/F increases the rate of production of PyTHQ decreases giving rise to the formation of DHQ. Comparing Figures 6.25 to 6.28 one can realize that at a W/F of 210 hr g-cat/g-mol nitro-compound, increasing the temperature by 25 K had resulted in an increase of 14% in conversion while the percent denitrogenation had increased by 140%, and the yield of the reaction and its selectivity had increased by 83% and 108% respectively.

At 548 and 573 K the major products were PyTHQ, DHQ, and BzTHQ. OPA was also found but in small amounts. The conversion at both temperatures and at a space time of 210 hr g-cat/g-mol nitro-compound was about 93%, but the denitrogenation percent and the yield of the reaction at 573 K were almost twice as that at 548 K (see Figures 6.29 to 6.32). At 573 K the rate of conversion of PyTHQ was equal to the rate of production of DHQ, Figure 6.33, this behavior is due to the chemical equilibrium between these two products.

At 598 K, the rate of production of BzTHQ starts increasing with a significant increase in the DHQ production. At 623 K, DHQ reached a maximum of production at a space time of 160 hr g-cat/g-mol nitro-compound, then it starts decreasing with the increase in space time giving rise to the production of PCH, as it can be shown in Figure 6.34. The conversion at both temperatures was 94%, but the yield of the reaction was 160% more at 623 than at 598 K. This result indicates that increasing the temperature did not result in an increase in the rate of hydrogenation whereas the rate of denitrogenation had increased significantly. (see Figures 6.35 to 6.38).

At 648 K the production of PyTHQ continued to decrease while the production of BzTHQ was increasing. This confirms the belief that at high temperatures the quinoline HDN is shifted towards the BzTHQ path [31]. At 673 K the production

of PyTHQ remained constant, with an increase in the OPA production. As it can be shown in Figure 6.39, the production of hydrocarbons was increasing while that of BzTHQ was decreasing with the increase in space time. The decrease in the production of the nitrogen-containing compounds indicates that these compounds are not final products. In general, the product distribution showed that the production of hydrocarbons mainly PCH and PB increased with the increase in temperature (Figure 6.40).

Several reaction networks have been proposed for the quinoline HDN reaction [88,24,31,30]. The reaction path is affected by the reaction conditions, method of analysis, and type of catalyst used. Taking into consideration these reaction networks and the distribution of products obtained in this work, a reaction network was suggested as shown in Figure 6.41.

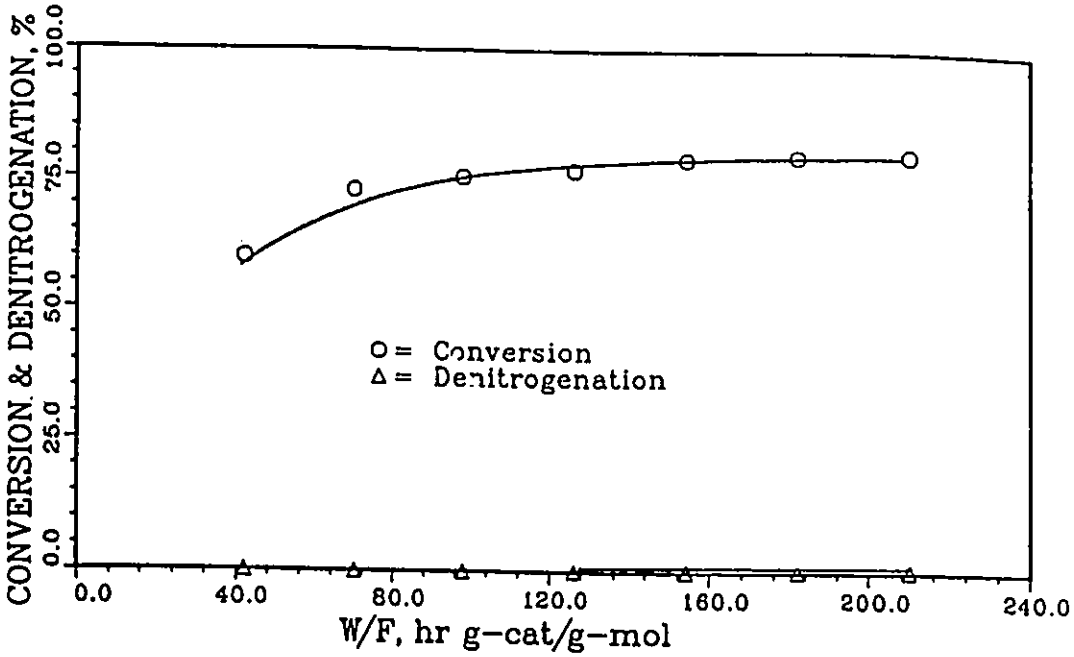

Figure 6.25: Effect of W/F on conversion & denitrogenation of quinoline; T=498 K

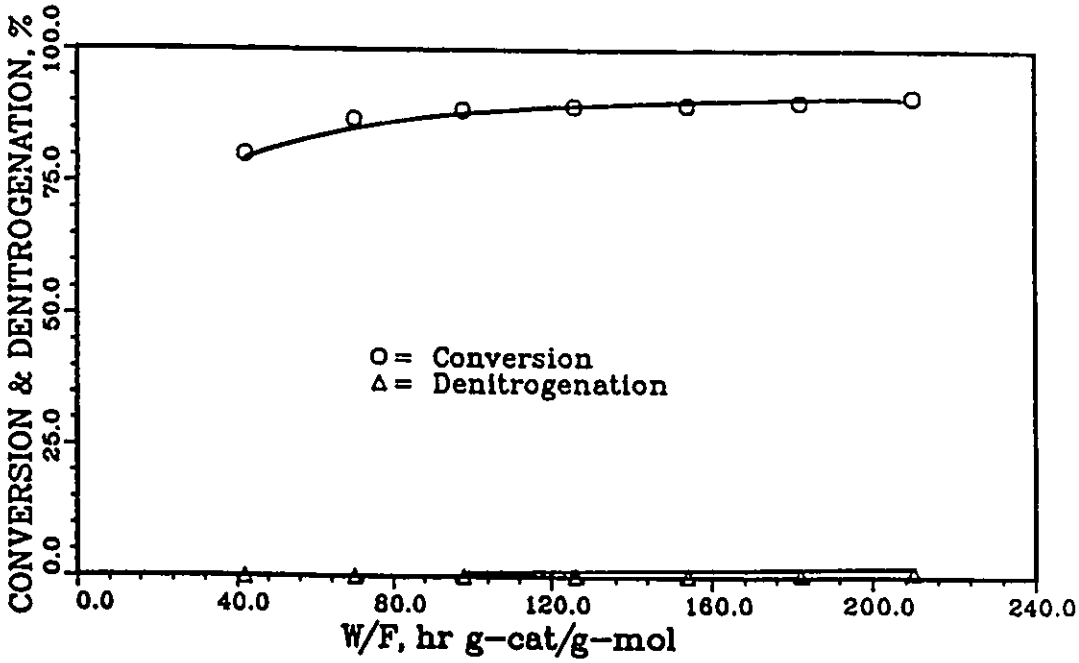

Figure 6.26: Effect of W/F on conversion & denitrogenation of quinoline; T=523 K

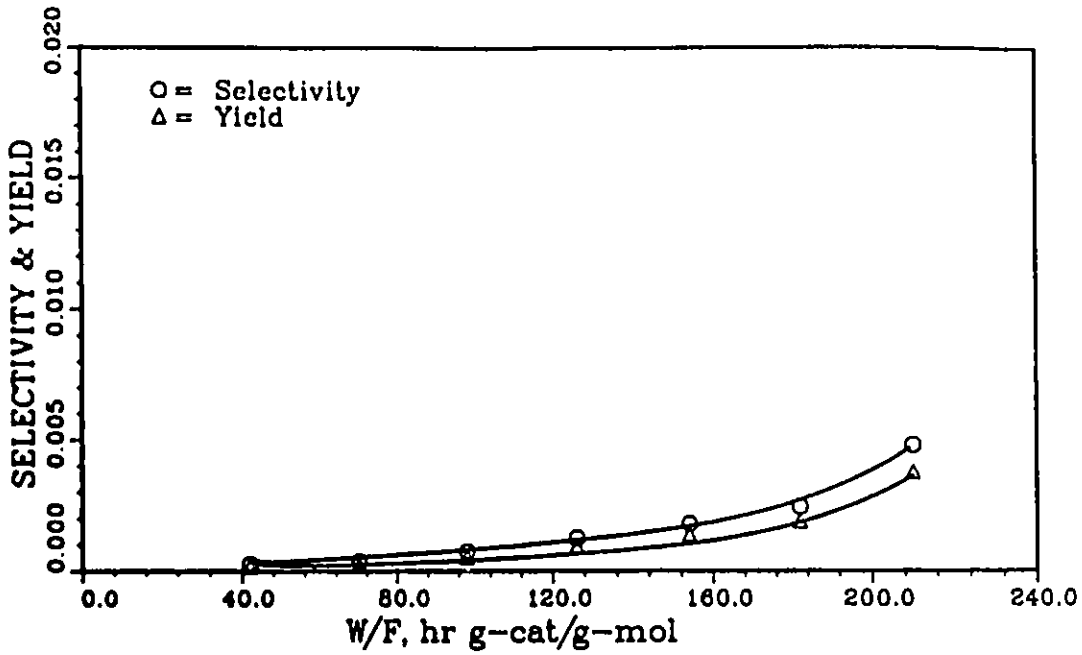

Figure 6.27: Effect of W/F on selectivity & yield; quinoline HDN; T=498 K

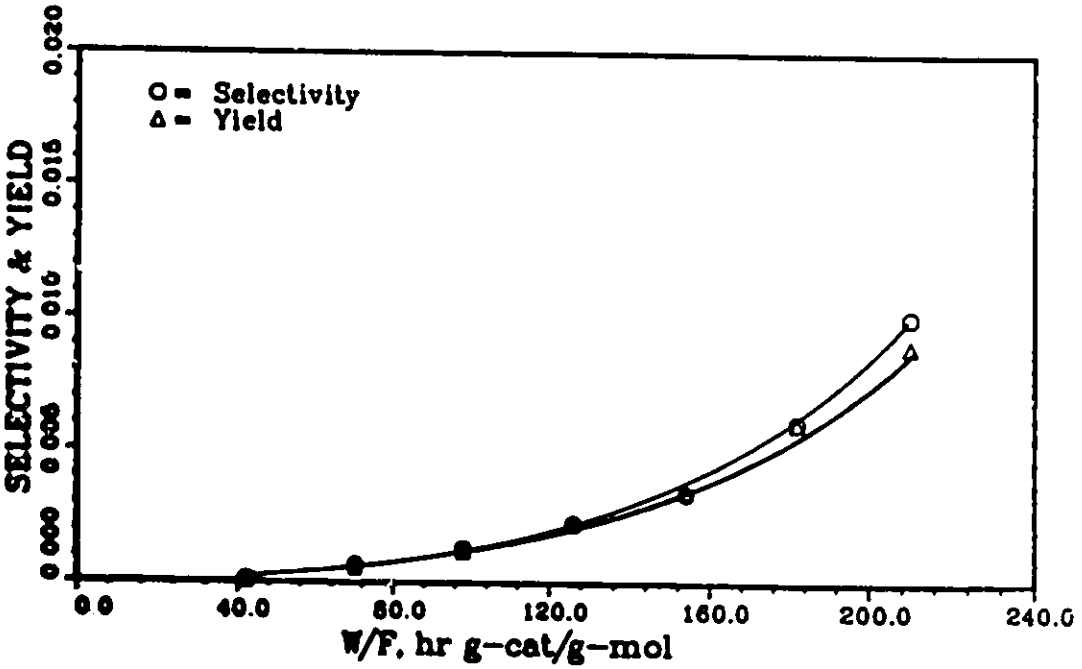

Figure 6.28: Effect of W/F on selectivity & yield; quinoline HDN; T=523 K

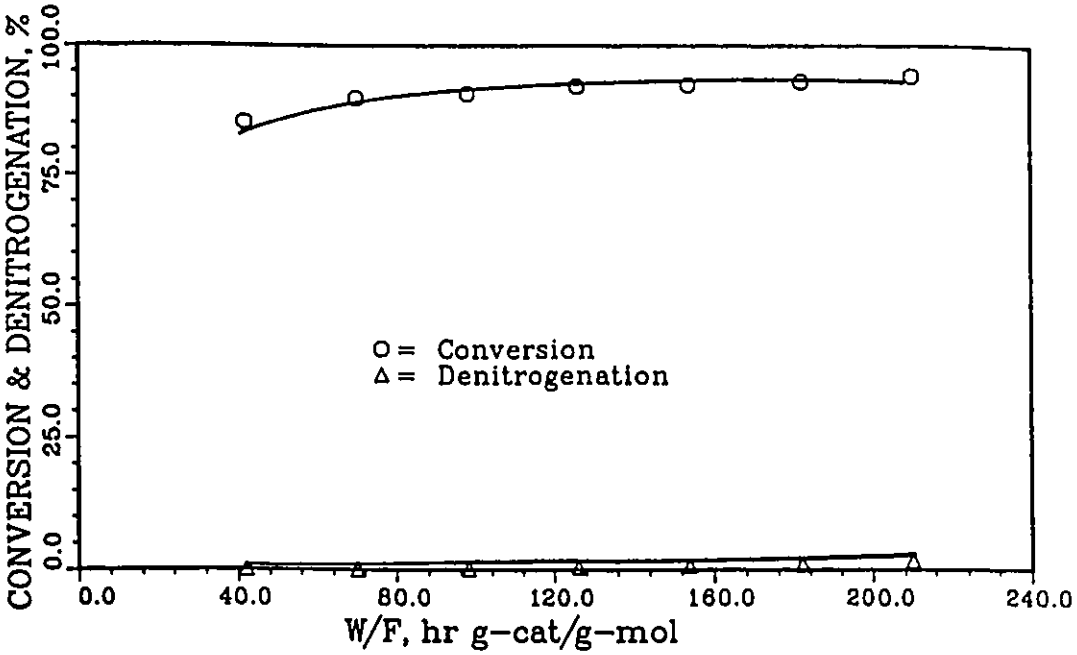

Figure 6.29: Effect of W/F on conversion & denitrogenation of quinoline; T=548 K

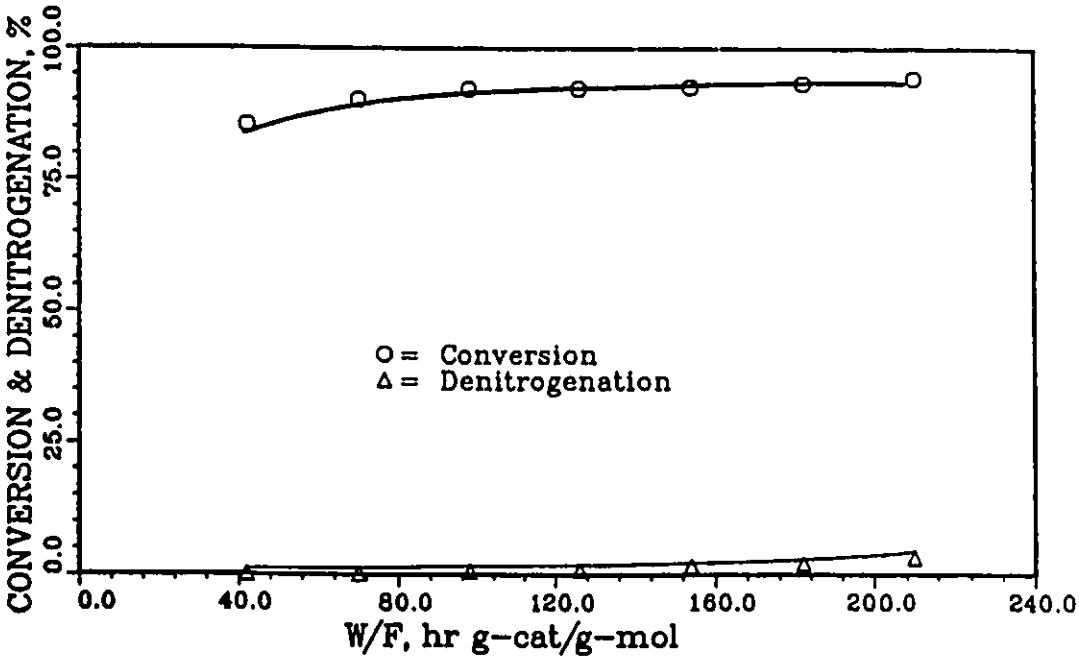

Figure 6.30: Effect of W/F on conversion & denitrogenation of quinoline; T=573 K

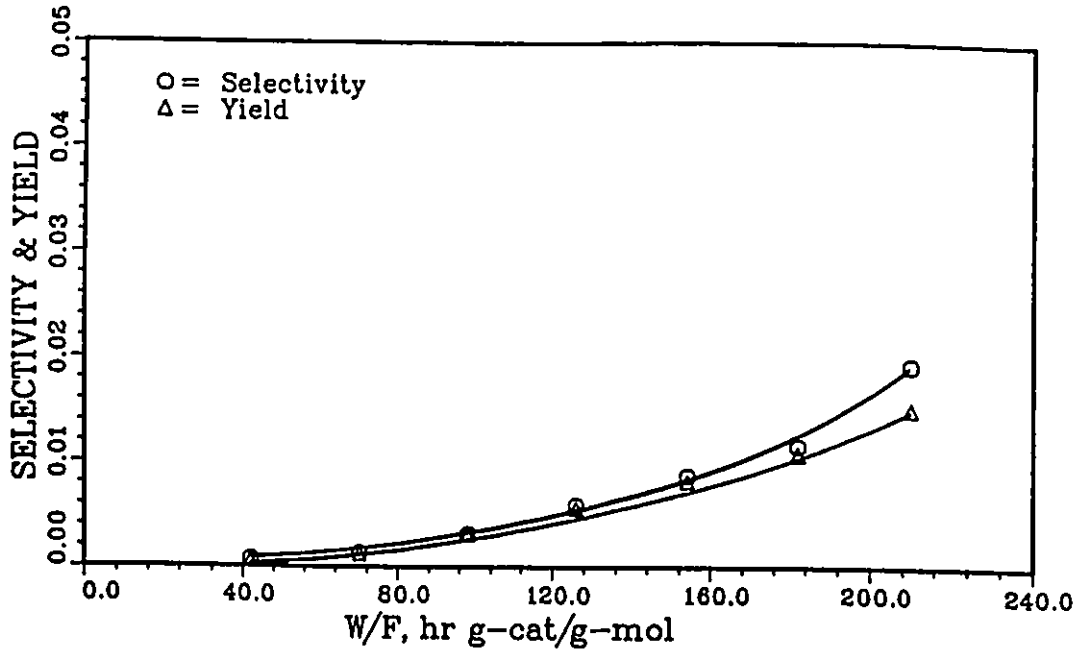

Figure 6.31: Effect of W/F on selectivity & yield; quinoline HDN; T=548 K

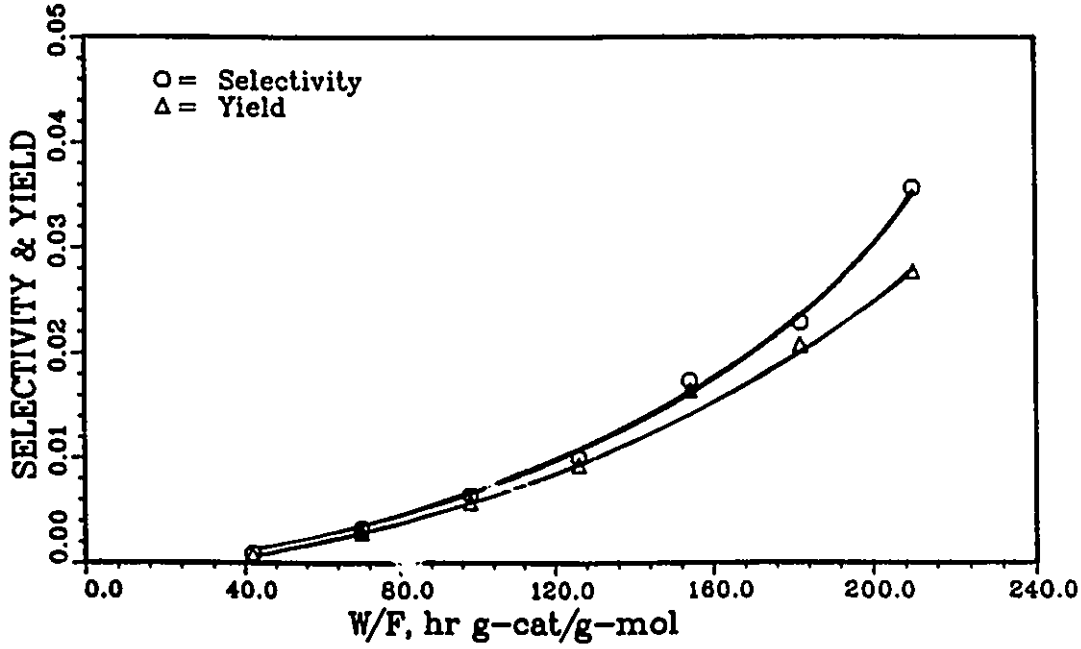

Figure 6.32: Effect of W/F on selectivity & yield; quinoline HDN; T=573 K

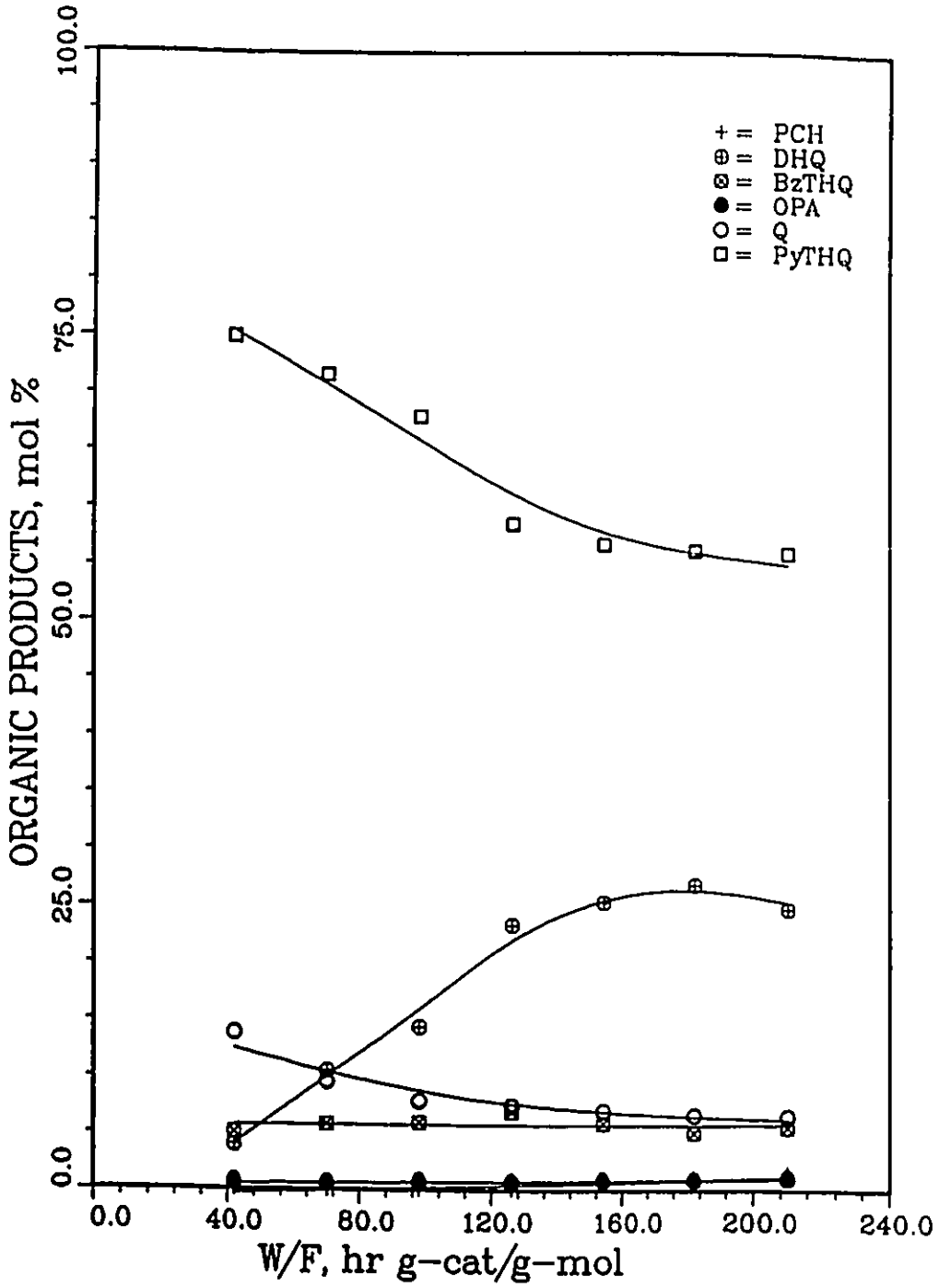

Figure 6.33: Quinoline HDN products; T=573 K, $\overline{R}$=13

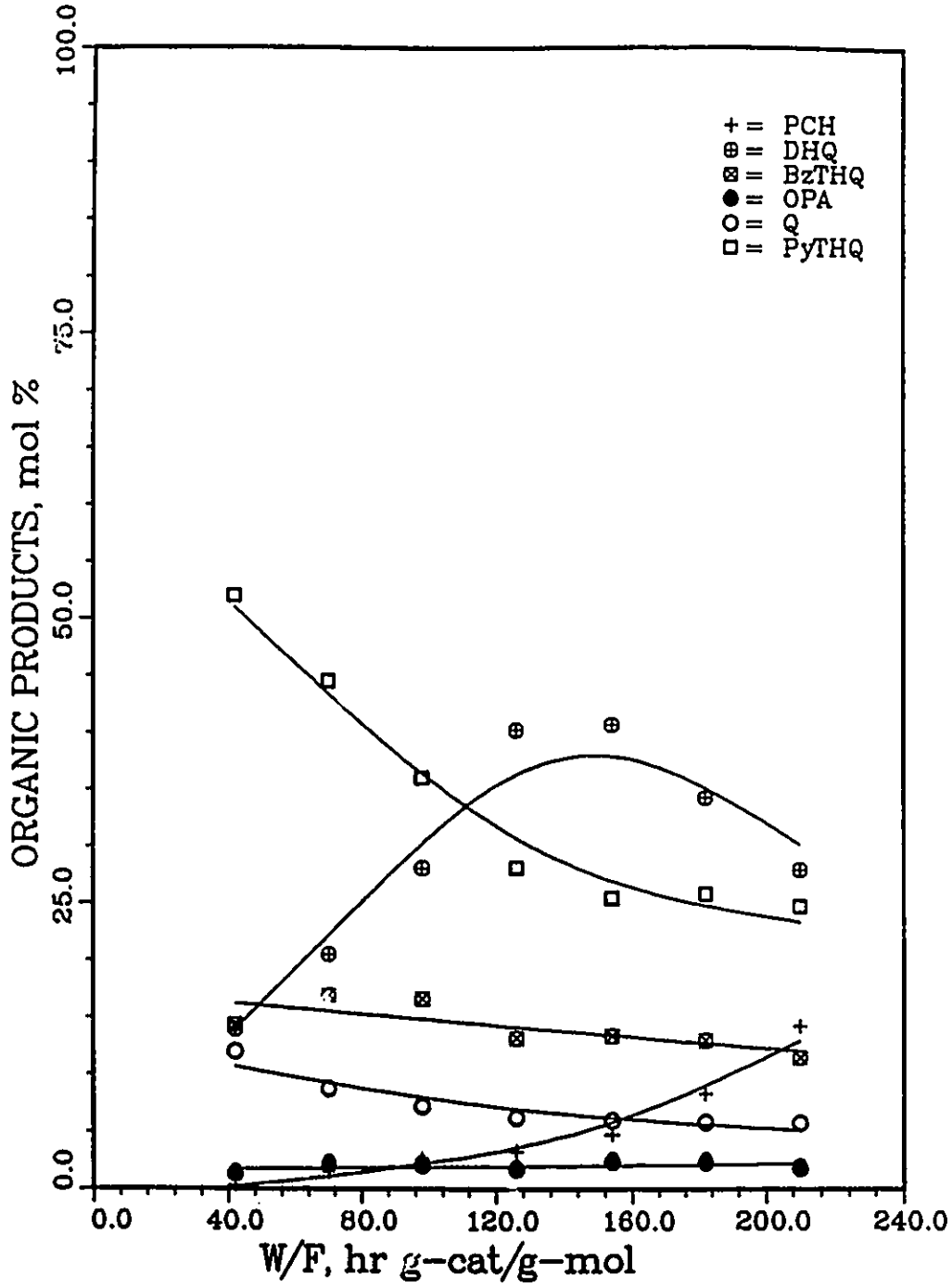

Figure 6.34: Quinoline HDN products; T=623 K, $\overline{R}$=13

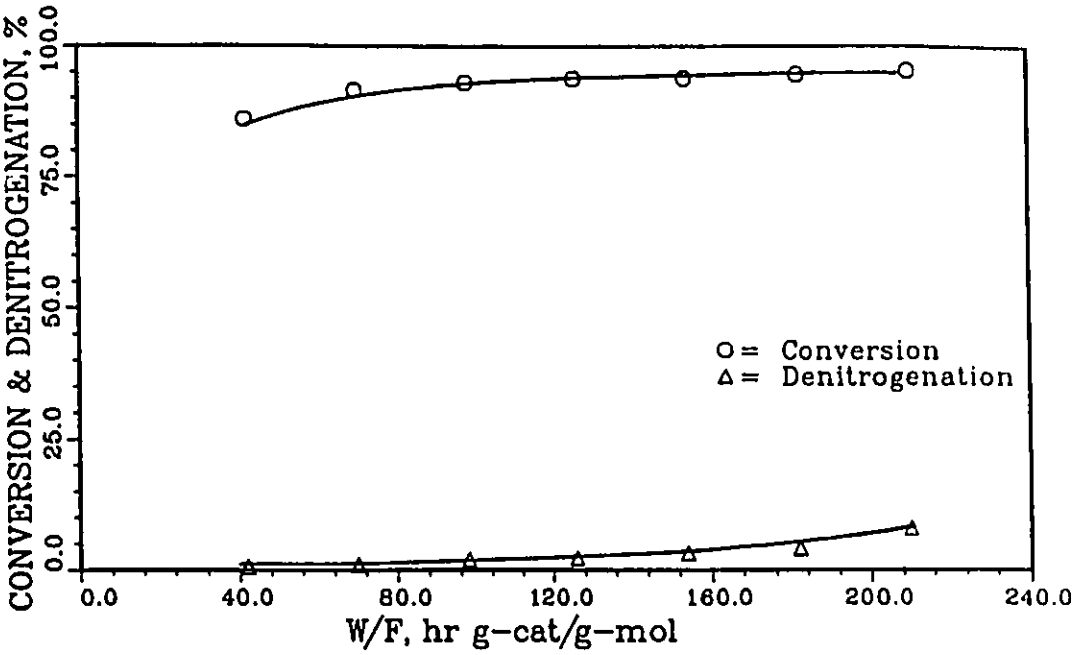

Figure 6.35: Effect of W/F on conversion & denitrogenation of quinoline; T=598 K

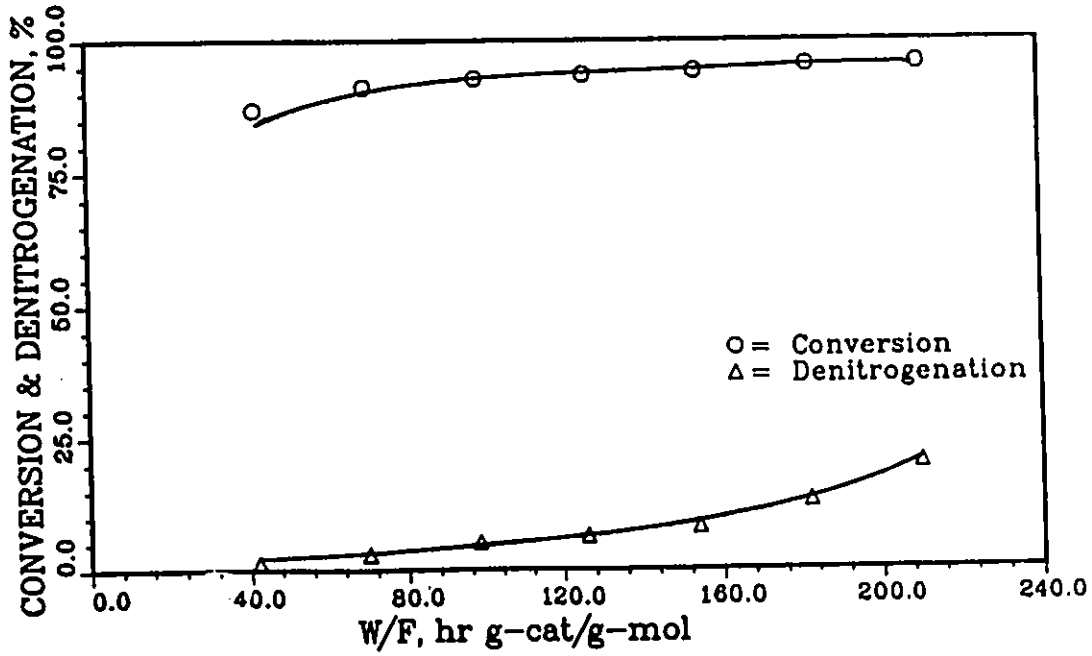

Figure 6.36: Effect of W/F on conversion & denitrogenation of quinoline; T=623 K

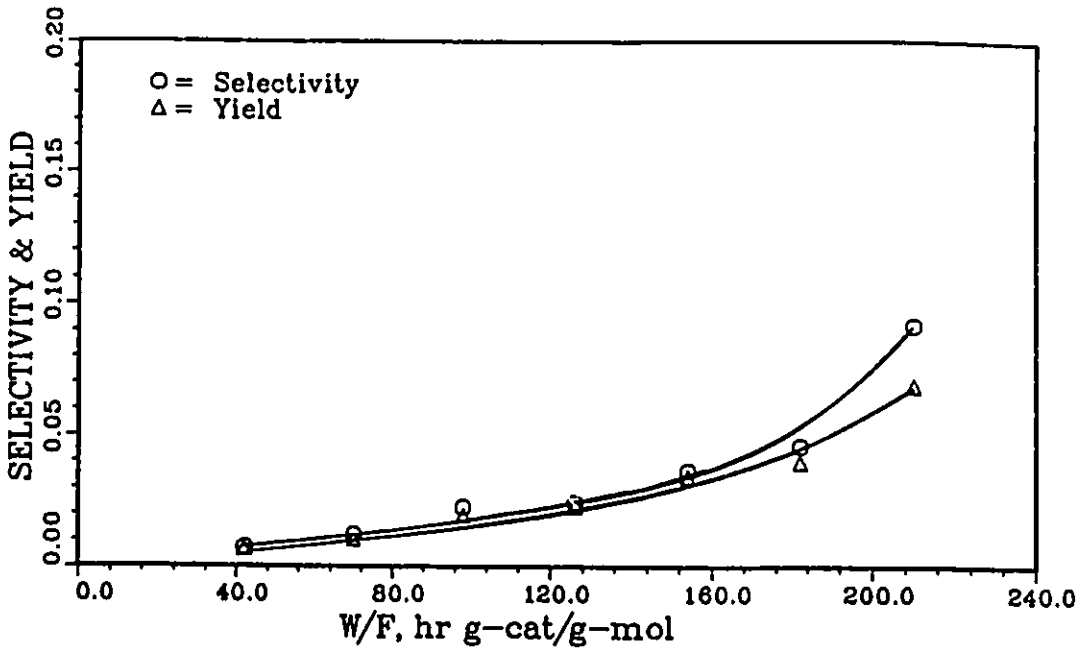

Figure 6.37: Effect of W/F on selectivity & yield; quinoline HDN; T=598 K

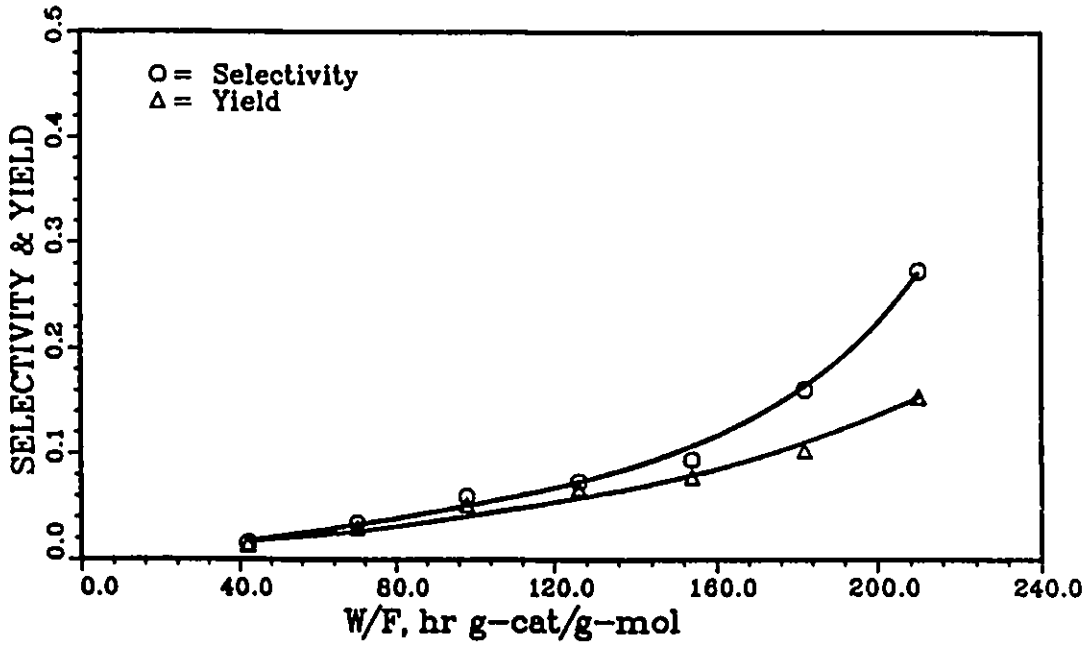

Figure 6.38: Effect of W/F on selectivity & yield; quinoline HDN; T=623 K

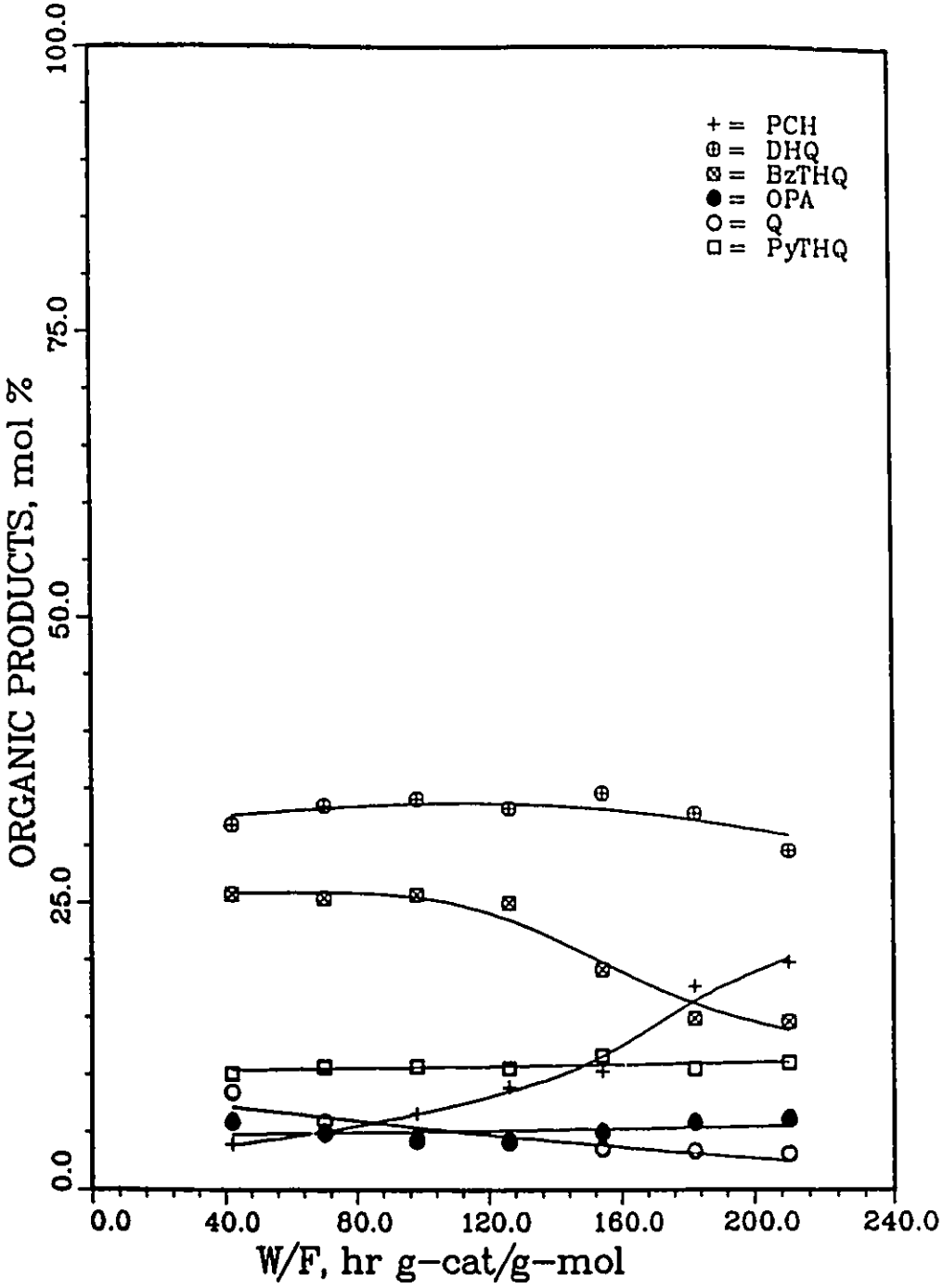

Figure 6.39: Quinoline HDN products; T=673 K, $\overline{R}$=13

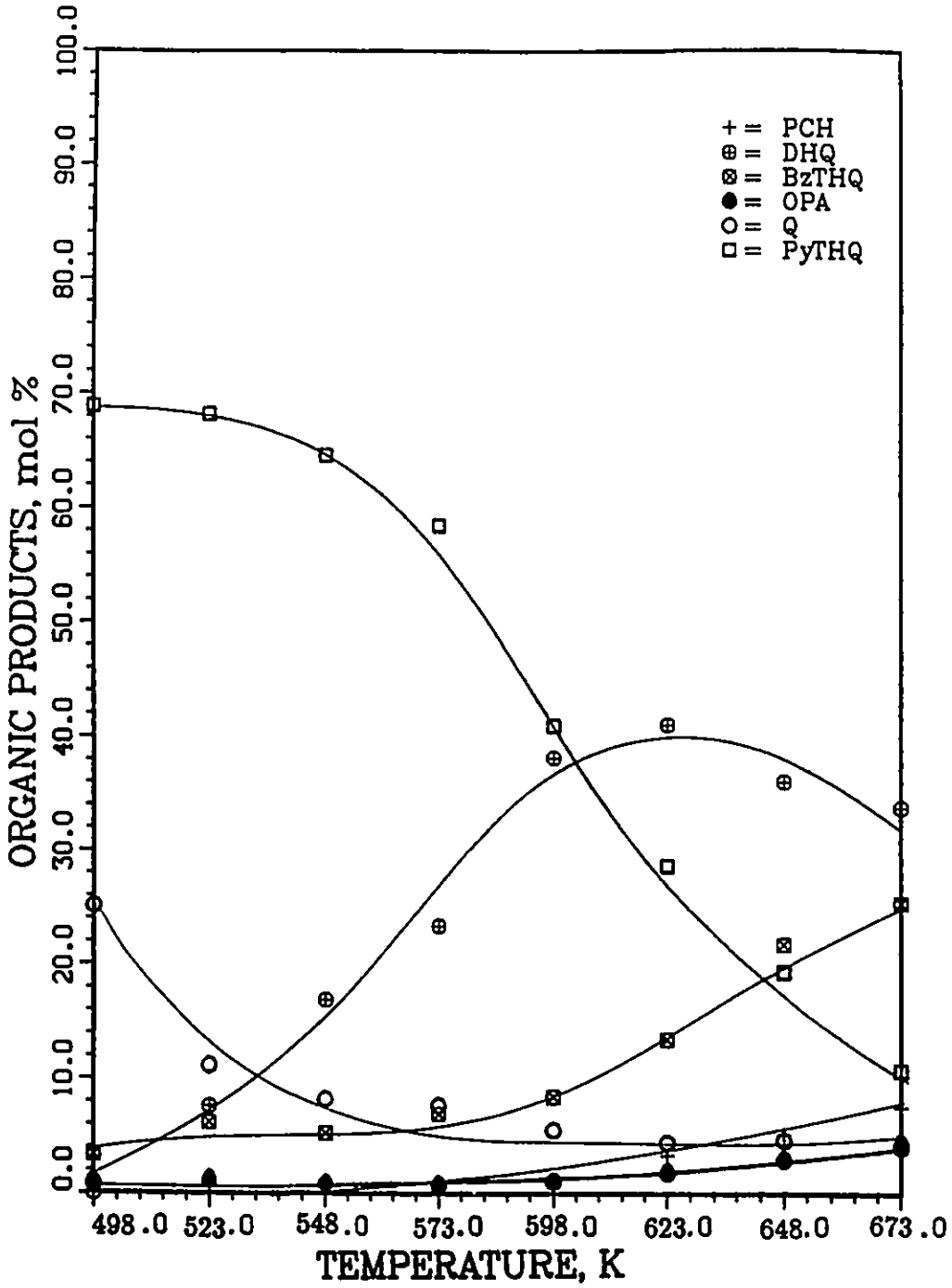

Figure 6.40: Quinoline HDN products; W/F=126, $\overline{R}$=13

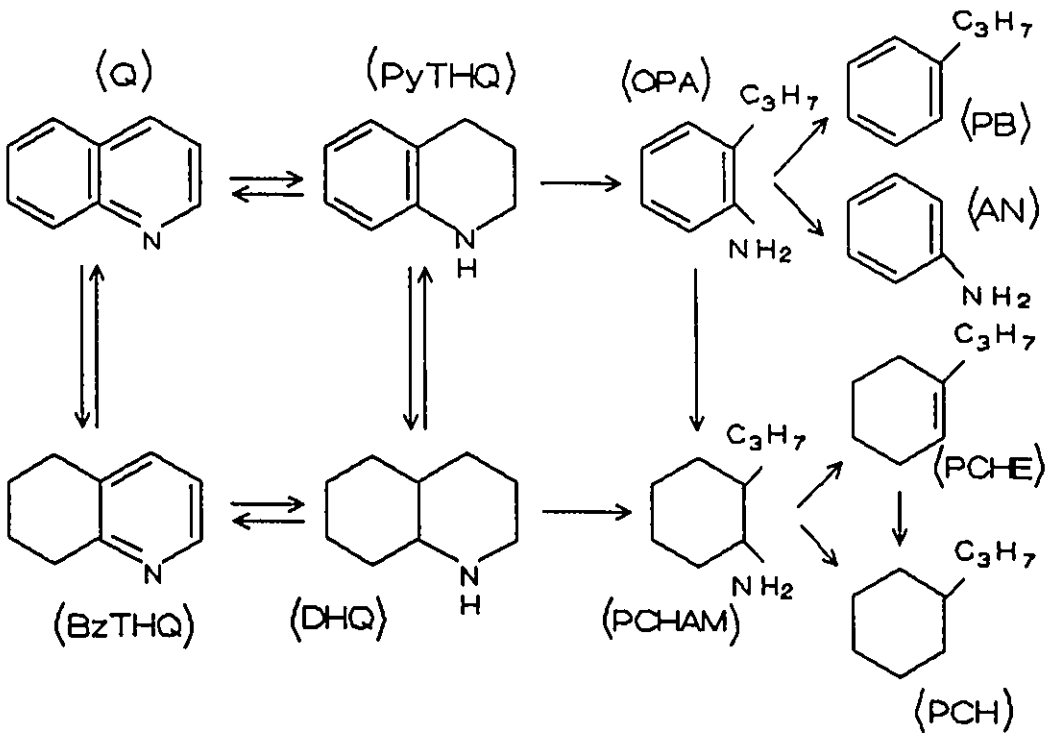

Figure 6.41: Reaction network for the HDN of quinoline over Ni-Mo/Al_2O_3 (Shell Catalyst 424)

6.6.3 Pyridine-Quinoline Mixture Hydrodenitrogenation

An equimolar mixture of pyridine and quinoline was used for the hydrodenitrogenation experiments of this part. The reactants' flow rates and hence the space times for these experiments were identical to those in the pure component runs. The temperatures of these experiments were 498, 573, 623, and 673 K. Most of the products detected in these runs were identical to those identified in the single compound runs of pyridine and quinoline.

At 498 K the only products detected were piperidine, pentylpiperidine, propylcyclohexane, and 1,2,3,4-tetrahydroquinoline. From the product distribution, Figure 6.42, one can realize that the conversion of pyridine was very low while that of quinoline was high. Comparing the present result with that of single components runs conducted under the same conditions, it can be stated that the rate of conversion of pyridine to piperidine was retarded by the presence of quinoline. In the mean time the presence of pyridine had enhanced the conversion of quinoline to PyTHQ.

At 573 K, some of the PyTHQ had converted to DHQ. The highest conversion achieved at that temperature was 83% while the highest denitrogenation percent was only 4%. Again at this temperature, it was found that the conversion of quinoline was higher than that of pyridine. At 623 K more hydrocarbons were detected in addition to nitrogen-compounds. At high space time, quinoline had converted completely. Most of the hydrocarbons produced are from the HDN of quinoline, on the other hand, pyridine had converted to piperidine and alkyl-piperidines. The highest conversion was about 99%, and the highest denitrogenation was about 28%. (See Figures 6.43 to 6.46).

At 673 K, pentanes and decanes were detected, but in small amounts. The major hydrocarbon product was PCH in addition to MCH, ECH, and MEB. The highest denitrogenation achieved was about 75%. At this temperature, quinoline and PyTHQ were converted completely mostly to hydrocarbons. Pyridine was also converted but mostly to nitrogen compounds. The distribution of the HDN products is shown in Figure 6.47. It is to be noted that the amount of PCH detected at this temperature was about 60% by mole, which leads to believe that some of the alkyl-radicals produced from the adsorption of the PEAM (C_2H_5 -, C_3H_7 , or C_5H_9–) on the catalyst surface were reacting to produce the alkyl-cyclohexanes especially PCH. The distribution of the organic products of the HDN reaction of the pyridine-quinoline mixture with respect to temperature is shown in Figure 6.48.

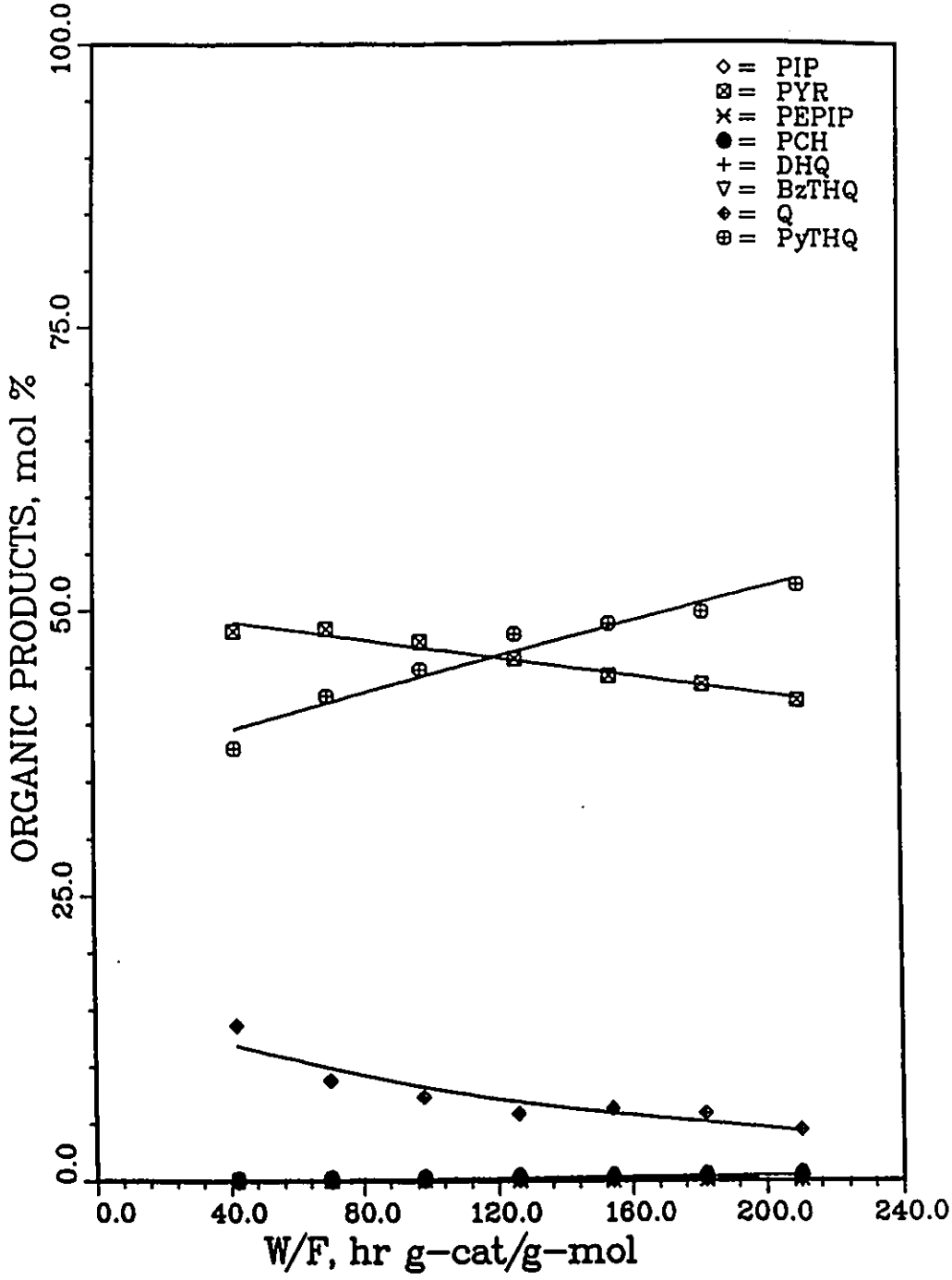

Figure 6.42: Pyridine-quinoline HDN products; T=498 K, $\overline{R}$=13

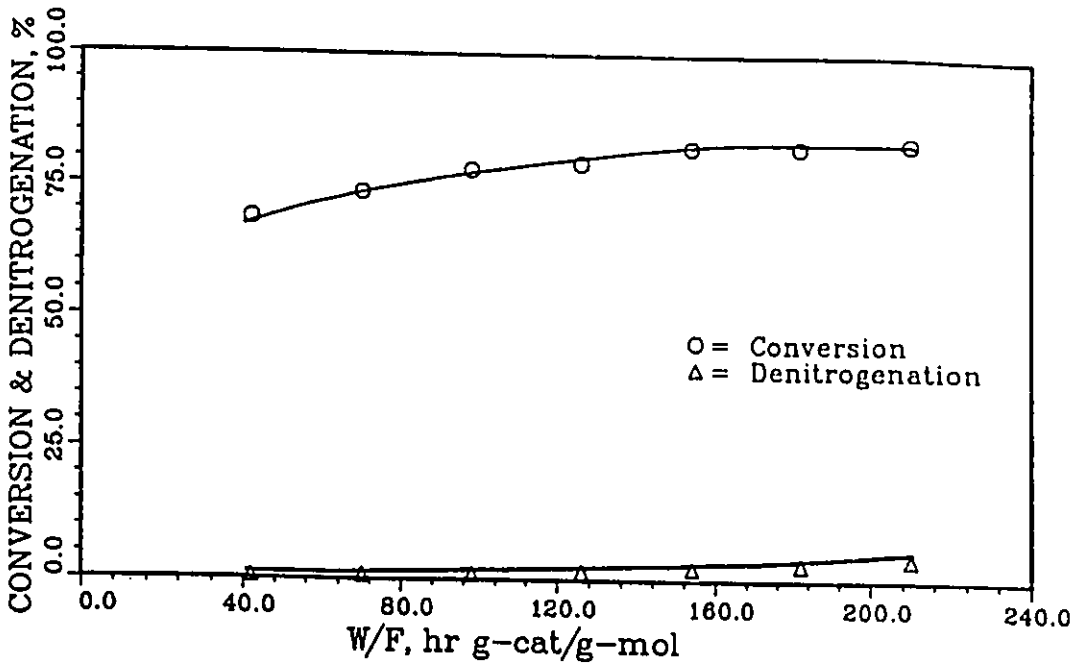

Figure 6.43: Effect of W/F on conversion & denitrogenation of mixture; T=573 K

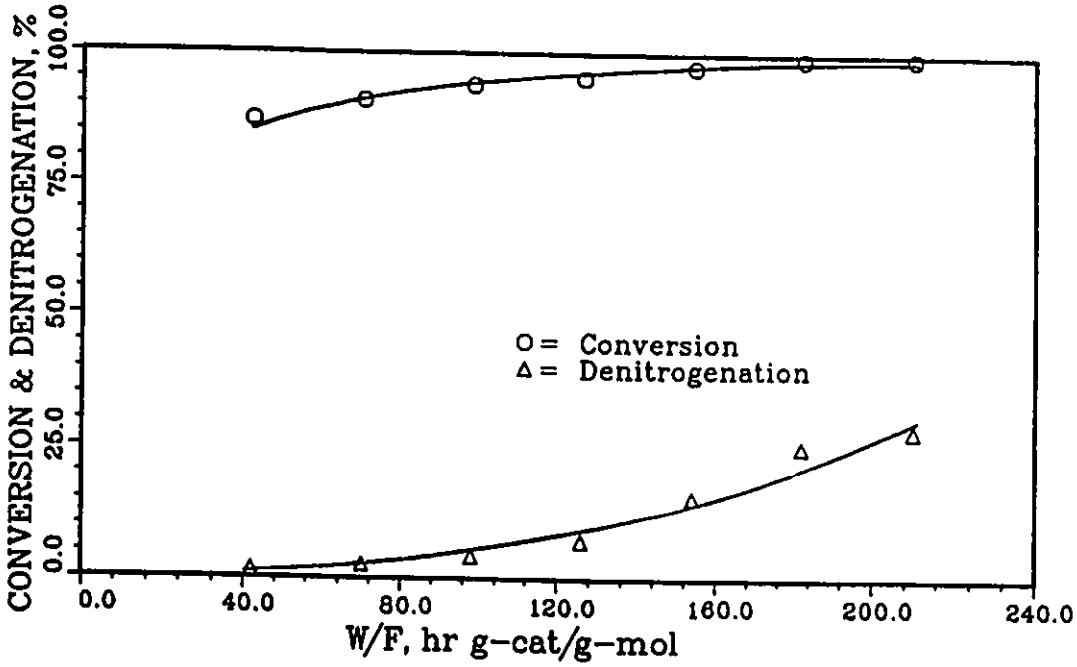

Figure 6.44: Effect of W/F on conversion & denitrogenation of mixture; T=573 K

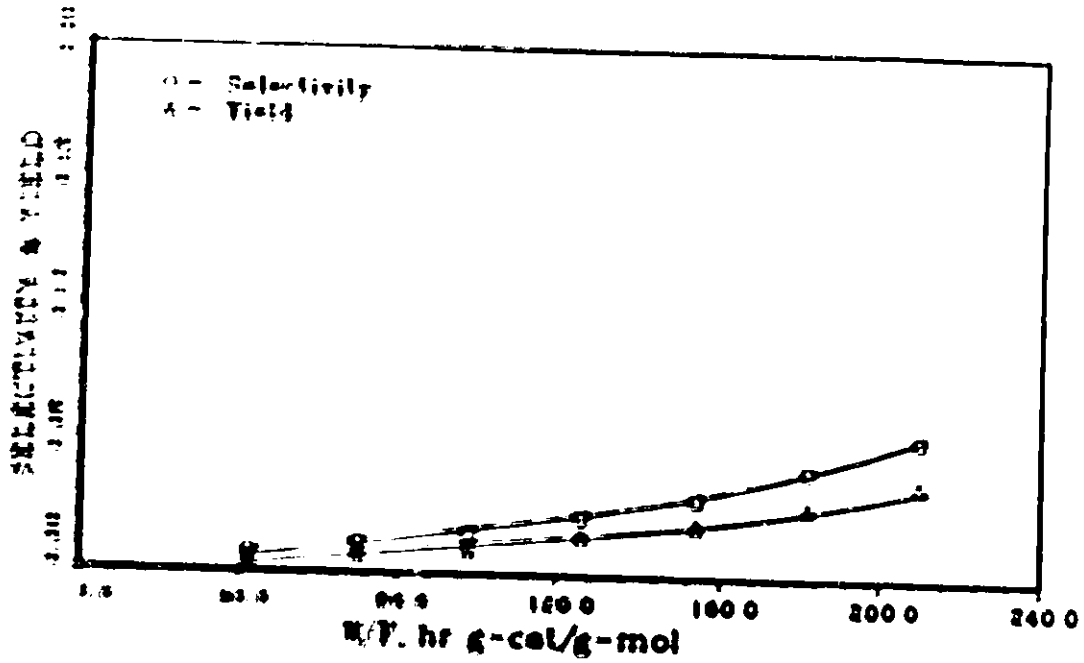

Figure 6.43 Effect of W/F on selectivity & yield mixture HDN, T=623 K

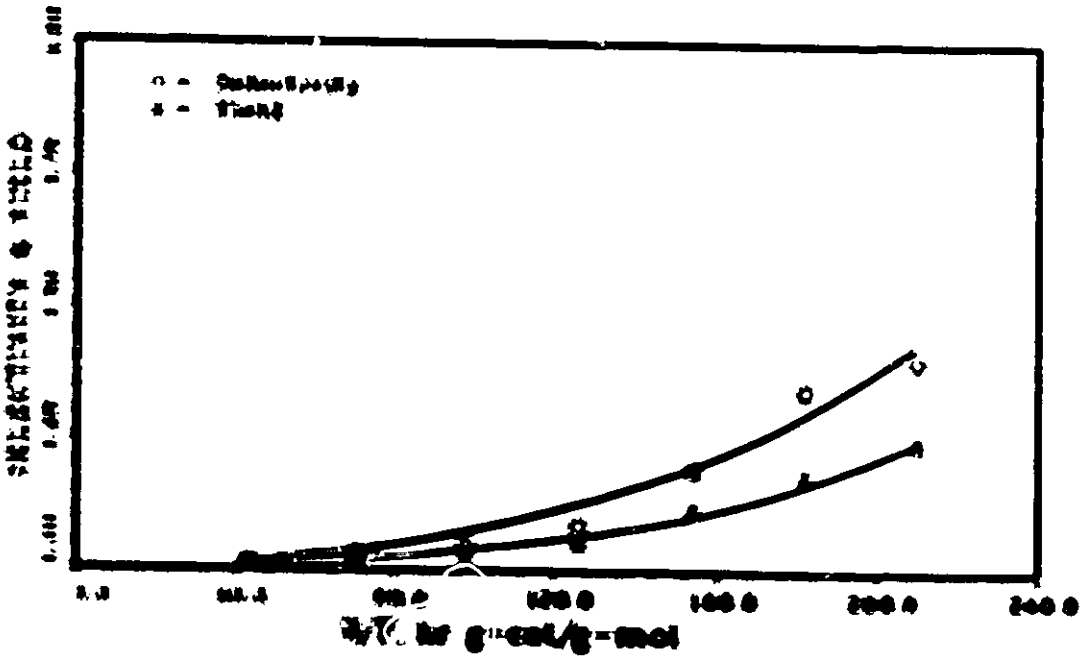

Figure 6.44 Effect of W/F on selectivity & yield mixture HDN, T=623 K

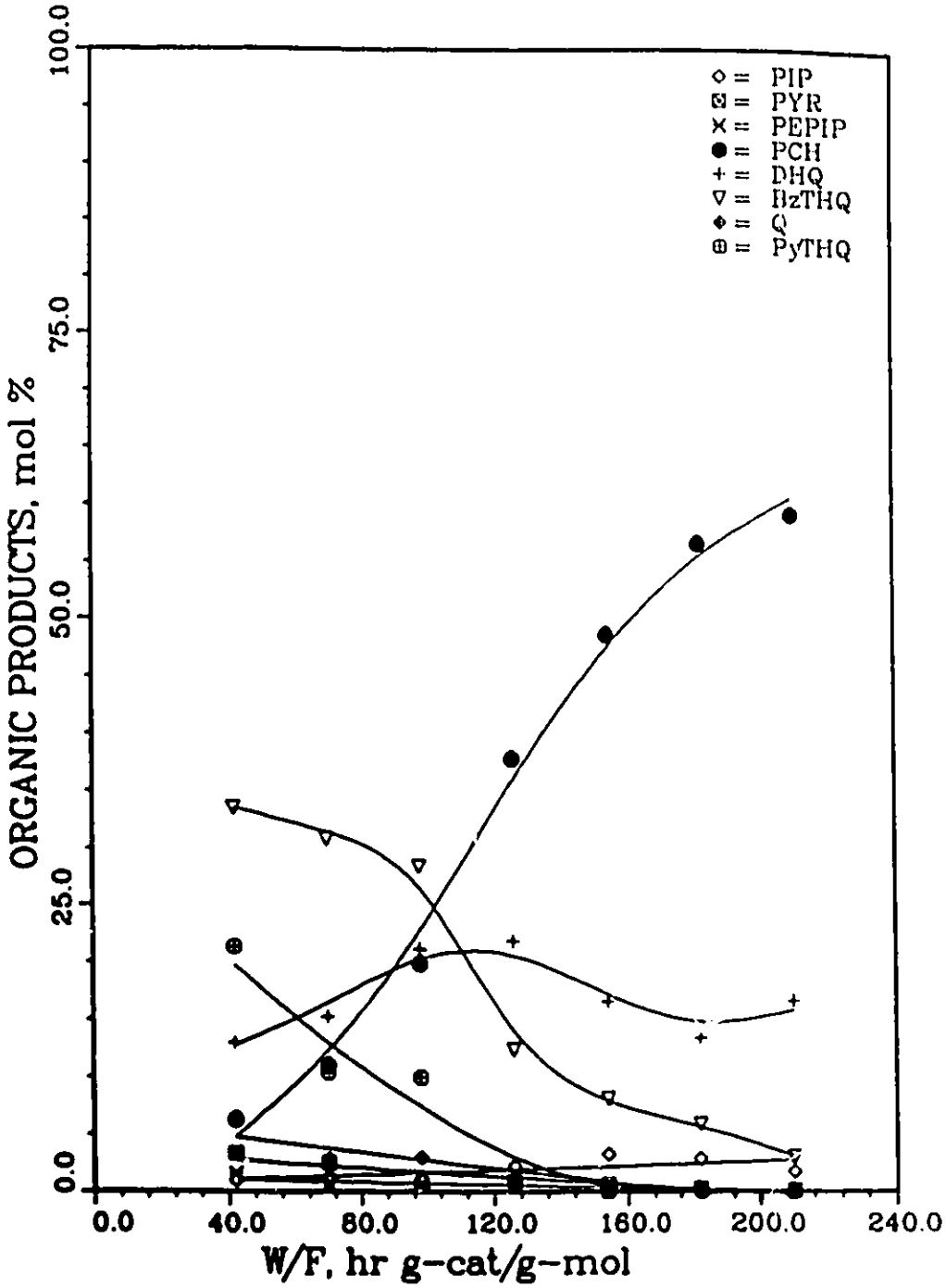

Figure 6.47: Pyridine-quinoline HDN products; T=673 K, $\bar{R}$=13

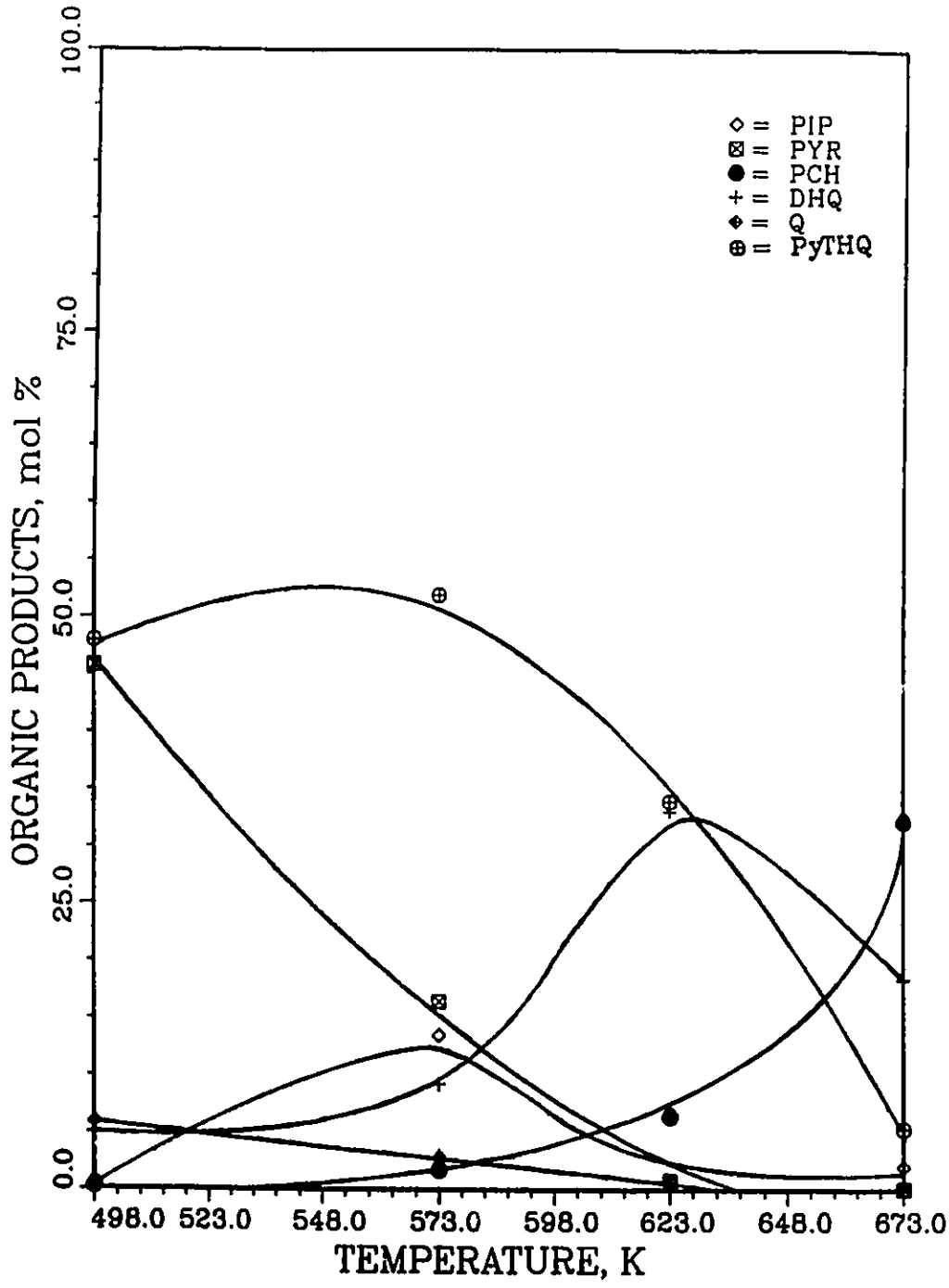

Figure 6.48: Pyridine-quinoline HDN products; W/F=126, $\overline{R}$=13

6.7 Kinetic Modelling

As mentioned in Chapter 3, two types of kinetic models were considered to represent the kinetic data.

1. Lumped compound models

2. Mechanistic models

6.7.1 Lumped Compound Models

Several models were considered depending on the overall HDN reaction assumed.

Model 1

If the overall HDN reaction is lumped as

$$A + H_2 \longrightarrow HC + NH_3$$

where A is the nitrogen compound and HC is the product hydrocarbon, then the appropriate Langmuir-Hinshelwood rate expression for the above reaction is

$$-r_A = r_{HC} = r_{NH_3} = \frac{k_1' K_A P_A}{1 + K_A P_A + K_{NH_3} P_{NH_3}} \tag{6.7}$$

At a 1 kPa partial pressure of nitrogen compounds, and even at high temperature, the catalyst surface will be completely saturated with these compounds, then $K_A P_A + K_{NH_3} P_{NH_3} >> 1$ [92]. At excess hydrogen, $P_{A_0}=P_A + P_{NH_3}$. Then the above equation will be reduced to

$$-r_A = \frac{k_1' P_A}{P_A + (K_{NH_3}/K_A)(P_{A_0} - P_A)} \tag{6.8}$$

Recalling the plug-flow reactor material balance,

$$\frac{W}{F_{A_0}} = \frac{1}{P_{A_0}} \int_{P_{A_0}}^{P_A} \frac{dP_A}{r_A} \tag{6.9}$$

and substituting the value of r_A gives

$$\frac{W}{F_{A_0}} = \frac{1}{P_{A_0}} \int_{P_{A_0}}^{P_A} \frac{P_A + (K_{NH_3}/K_A)(P_{A_0} - P_A)}{k_1' P_A} dP_A \tag{6.10}$$

Integrating the above equation gives

$$k_1' \left(\frac{W}{F_{A_0}}\right) = \left(1 - \frac{K_{NH_3}}{K_A}\right) \left(\frac{P_{A_0} - P_A}{P_{A_0}}\right) - \left(\frac{K_{NH_3}}{K_A}\right) \ln\left(\frac{P_A}{P_{A_0}}\right) \tag{6.11}$$

or

$$k_1' \left(\frac{W}{F_{A_0}}\right) = \left(1 - \frac{K_{NH_3}}{K_A}\right) X_A - \left(\frac{K_{NH_3}}{K_A}\right) \ln(1 - X_A) \tag{6.12}$$

where X_A is the fractional conversion of the reactant nitrogen compound.

The value of the pseudo first-order reaction constants, k_1', can be estimated by either one of the two methods:

1. Graphically, by plotting $\frac{W}{F_{A_0}}$ *vs* $\left(1 - \frac{K_{NH_3}}{K_A}\right) x_A - \left(\frac{K_{NH_3}}{K_A}\right) \ln(1 - x_A)$ and changing the value of the fraction $\left(\frac{K_{NH_3}}{K_A}\right)$ so as to get a linear correlation, with the line passing through the origin, the slope of which is the pseudo rate constant.

2. Non-linear regression analysis of Equation 6.8 using the non-linear iterative method (Levenberg-Marquardt).

Results from the non-linear regression gave better estimation for the model parameters, and hence it was considered in fitting the above model.

Model 2

In this model the overall HDN reaction is represented by the following lumped equation

$$A + H_2 = AA + SA + HC$$

where A is the reacting nitrogen compound, AA, SA, and HC represent the product aromatic amines, secondary amines, and hydrocarbons respectively.

In this model it is assumed that aromtic amines (PYR, Q, BzTHQ, OPA, AN) have equal adsorbtivities which is different from that of the secondary amines (PIP, ETPIP, PRPIP, PEPIP, PyTHQ, DHQ) [24]. Together with the assumption that there is a complete coverage of the catalyst surface by nitrogen compounds, the rate expressions for the HDN reactions will be greatly simplified and become of the form

$$-r_A = \frac{k_1' K_{AA} P_A}{K_{AA} P_{AA} + K_{SA} P_{SA} + K_{NH_3} P_{NH_3}} \tag{6.13}$$

$$-r_A = \frac{k_1' P_A}{P_{AA} + (K_{SA}/K_{AA}) P_{SA} + (K_{NH_3}/K_{AA}) P_{NH_3}} \tag{6.14}$$

The mole fraction of hydrocarbons is equal to that of ammonia then the above equation can be written as

$$-r_A = \frac{k_1' P_A}{P_{AA} + (K_{SA}/K_{AA}) P_{SA} + (K_{NH_3}/K_{AA}) P_{HC}} \tag{6.15}$$

With the assumption that all nitrogen compounds have equal adsobtivities, i.e. $K_{AA} = K_{SA}$, then Equation 6.15 can be written in the following simple form

$$-r_A = \frac{k_1' P_A}{P_{AA} + P_{SA} + (K_{NH_3}/K_A) P_{HC}} \tag{6.16}$$

Model 3

In this model the overall HDN reaction is represented by the following lumped equation

$$A + H_2 = NC + HC$$

where A is the reacting nitrogen compound, NC is the product nitrogen compounds, and HC is the product hydrocarbons. This model is expressed in terms of the fugacities of the compounds instead of their partial pressures. Calculations of the fugacities are shown in Appendix D.

Assuming that hydrogen and nitrogen compounds are adsorbed on two different catalytic sites [31,110], and nitrogen compounds have comparable adsorption equilibrim constants [88], and since hydrogen is in excess and the partial pressure of nitrogen compound is greater than 1 kPa [92], then the surface-controlled reaction can be written as

$$-r_3 = \frac{k\left[\hat{f}_A\hat{f}_{H_2} - \hat{f}_{NC}\hat{f}_{HC}/K_{eq}\right]}{\left[\hat{f}_A + (K_{NC}/K_A)\hat{f}_{NC} + (K_{HC}/K_A)\hat{f}_{HC}\right]^2} \tag{6.17}$$

If the reaction is irreversible then

- The surface-controlled rate expression will be

$$-r_3 = \frac{k_A K_A K_{H_2}\hat{f}_A\hat{f}_{H_2}}{\left[(1 + K_{H_2}\hat{f}_{H_2})(1 + K_A\hat{f}_{A_0} + K_{HC}\hat{f}_{HC})\right]} \tag{6.18}$$

  and with the above mentioned assumptions the rate expression will be reduced to

$$-r_3 = \frac{k_s\hat{f}_A}{\hat{f}_{A_0} + (K_{HC}/K_A)\hat{f}_{HC}} \tag{6.19}$$

- The adsorption-controlled rate expression will be

$$-r_1 = \frac{k_a \left[\hat{f}_A \hat{f}_{H_2} - \hat{f}_{NC}\hat{f}_{HC}/K_{eq}\right]}{\hat{f}_{H_2}\left[1 + K_A \hat{f}_{A_0} + K_{HC}\hat{f}_{HC}\right]} \tag{6.20}$$

or

$$-r_1 = \frac{k_{ad} \left[\hat{f}_A - \hat{f}_{NC}\hat{f}_{HC}/K_{eq}\right]}{\hat{f}_{A_0} + (K_{HC}/K_A)\hat{f}_{HC}} \tag{6.21}$$

- The desorption-controlled rate expression will be

$$-r_4 = \frac{k'_{nc} \left[K_{eq}\hat{f}_A \hat{f}_{H_2} - \hat{f}_{NC}\hat{f}_{HC}\right]}{\hat{f}_{HC}\left[1 + K_A \hat{f}_{A_0} + K_{HC}\hat{f}_{HC}\right]} \tag{6.22}$$

or

$$-r_4 = \frac{k_{da} \left[K_{eq}\hat{f}_A - \hat{f}_{NC}\hat{f}_{HC}\right]}{\hat{f}_{HC}\left[\hat{f}_{A_0} + (K_{HC}/K_A)\hat{f}_{HC})\right]} \tag{6.23}$$

$k_a = k_A P_u^t$

$k'_{nc} = k'_{NC} P_u^t$

A detailed derivation for the above equations is shown in Appendix I.

6.7.2 Mechanistic Models

Due to the complexity of the HDN reaction networks of pyridine as well as of quinoline, and due to the limiting number of data points at each experimental run, simplified reaction networks for both pyridine and quinoline HDN (Figures 6.49 and 6.50) were considered for the quantitative kinetic analysis.

The adsorption phenomena in pyridine and quinoline HDN suggest that the reaction rates are best described by Langmuir-Hinshelwood kinetic expressions. The Langmuir adsorption isotherm is a reasonable approximation of the true adsorption

behavior, then the fraction of the catalytic sites occupied by the nitrogen compounds is given by

$$\theta_j = \frac{K_j P_j}{1 + \sum_j K_j P_j} \tag{6.24}$$

Since hydrogen is assumed to be adsorbed on different sites than that of nitrogen compounds, hence it can be neglected from the above equation. If the partial pressure of nitrogen compound is greater than 1 KPa, as in our case, then $\sum_j \theta_j = 1$ and $\sum_j K_j P_j >> 1$ [92], hence the above equation will be reduced to

$$\theta_j = \frac{K_j P_j}{\sum_j K_j P_j} \tag{6.25}$$

where θ_j is the fraction of available sites occupied by j, K_j is the adsorption equilibrium constant of j, and P is the partial pressure of j.

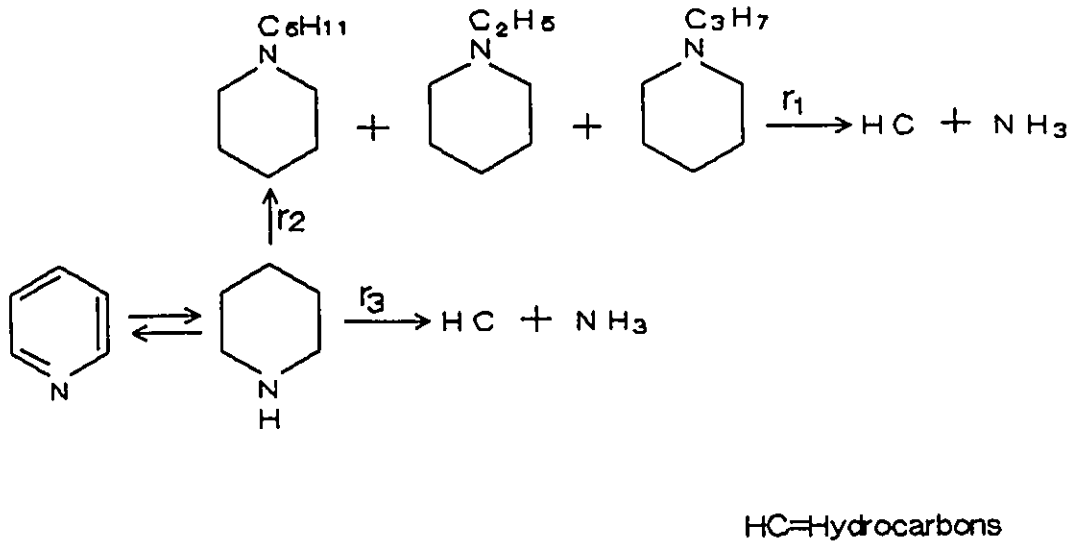

Figure 6.49: Simplified reaction network for the HDN of pyridine over commercial Ni-Mo/Al_2O_3 (Shell Catalyst 424)

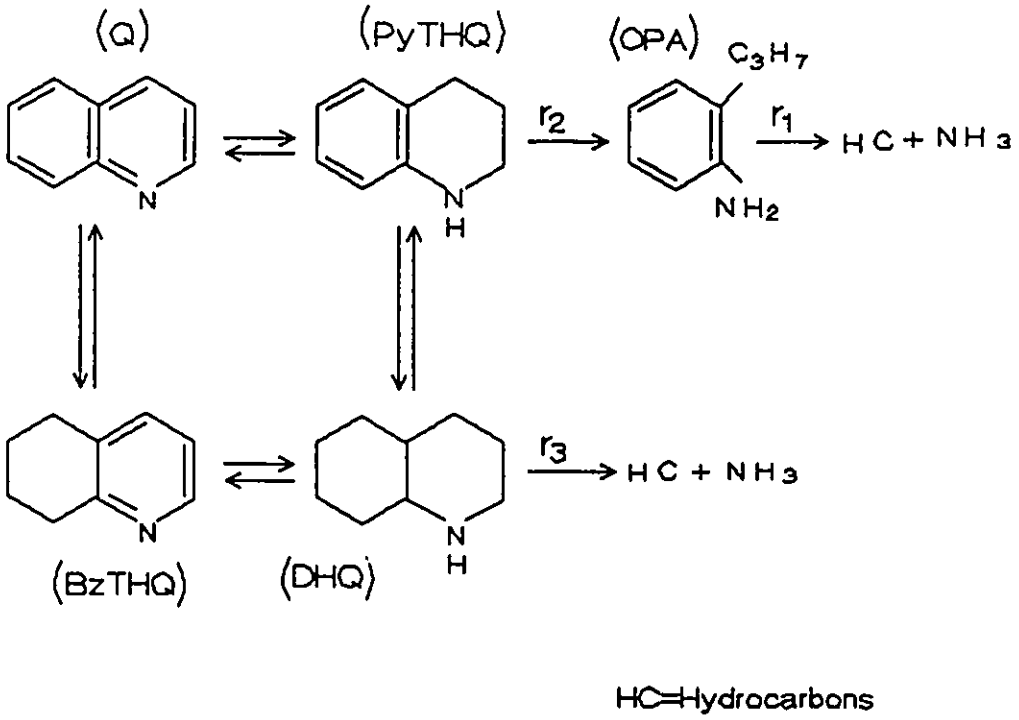

Figure 6.50: Simplified reaction network for the HDN of quinoline over commercial Ni-Mo/Al_2O_3 (Shell Catalyst 424)

Pyridine Kinetic Modelling

From the simplified reaction network of pyridine and from the above justified assumptions, the rate of denitrogenation of alkyl-piperidines (ETPIP, PRPIP, PEPIP) is given by

$$r_1 = \frac{k_1' K_{SA} P_{APIP}}{K_{AA} P_{AA} + K_{SA} P_{SA} + K_{NH_3} P_{NH_3}} \tag{6.26}$$

or

$$r_1 = \frac{k_1' (K_{SA}/K_{AA}) P_{APIP}}{P_{AA} + (K_{SA}/K_{AA}) P_{SA} + (K_{NH_3}/K_{AA}) P_{NH_3}} \tag{6.27}$$

Where:

r_1 rate of hydrogenlysis of alkyl-piperidines to hydrocarbons and ammonia.

P_{AA} partial pressure of aromatic amines (P_{PYR})

P_{SA} partial pressure of secondary amines ($P_{PIP} + P_{ETPIP} + P_{PRPIP} + P_{PEPIP}$)

Since the partial pressure of ammonia is equal to that of hydrocarbons, then r_1 can be written as

$$r_1 = \frac{k_1' (K_{SA}/K_{AA}) P_{APIP}}{P_{AA} + (K_{SA}/K_{AA}) P_{SA} + (K_{NH_3}/K_{AA}) P_{HC}} \tag{6.28}$$

Similarly, the rate of hydrogenolysis of pipreidine to alkyl-piperidines can be expressed as

$$r_2 = \frac{k_2' (K_{SA}/K_{AA}) P_{PIP}}{P_{AA} + (K_{SA}/K_{AA}) P_{SA} + (K_{NH_3}/K_{AA}) P_{HC}} \tag{6.29}$$

and the rate of hydrogenolysis of piperidine to ammonia and hydrocarbons is given by

$$r_3 = \frac{k_3'(K_{SA}/K_{AA})P_{PIP}}{P_{AA} + (K_{SA}/K_{AA})P_{SA} + (K_{NH_3}/K_{AA})P_{HC}} \tag{6.30}$$

From the above expressions the rate of formation of alkyl-piperidines is expressed as

$$r_{APIP} = r_2 - r_1 = \frac{(K_{SA}/K_{AA})[k_2'P_{PIP} - k_1'P_{APIP}]}{P_{AA} + (K_{SA}/K_{AA})P_{SA} + (K_{NH_3}/K_{AA})P_{HC}} \tag{6.31}$$

the rate of hydrogenolysis of piperidine

$$r_{PIP} = -(r_2 + r_3) = -\frac{(K_{SA}/K_{AA})(k_2' + k_3')P_{PIP}}{P_{AA} + (K_{SA}/K_{AA})P_{SA} + (K_{NH_3}/K_{AA})P_{HC}} \tag{6.32}$$

and the rate of hydrogenation

$$r_{HC} = r_1 + r_3 = \frac{(K_{SA}/K_{AA})[k_1'P_{APIP} + k_3'P_{PIP}]}{P_{AA} + (K_{SA}/K_{AA})P_{SA} + (K_{NH_3}/K_{AA})P_{HC}} \tag{6.33}$$

With the assumption that all nitrogen compounds adsorb equally, then the above three equations will be reduced to

$$r_{APIP} = r_2 - r_1 = \frac{k_2'P_{PIP} - k_1'P_{APIP}}{P_{AA} + P_{SA} + (K_{NH_3}/K_{AA})P_{HC}} \tag{6.34}$$

$$r_{PIP} = -(r_2 + r_3) = -\frac{(k_2' + k_3')P_{PIP}}{P_{AA} + P_{SA} + (K_{NH_3}/K_{AA})P_{HC}} \tag{6.35}$$

$$r_{HC} = r_1 + r_3 = \frac{k_1'P_{APIP} + k_3'P_{PIP}}{P_{AA} + P_{SA} + (K_{NH_3}/K_{AA})P_{HC}} \tag{6.36}$$

$$\tag{6.37}$$

Quinoline Kinetic Modelling

The simplified reaction network of quinoline HDN was considered for the quantitative kinetic analysis. Again, it is assumed that the aromatic amines (Q, BzTHQ,

OPA, AN) have equal adsoptivities, and that the secondary amines (PyTHQ, DHQ) have equal adsorptivities too. Following the same argument as that of pyridine kinetic modelling, the rate expression for OPA denitrogenation becomes.

$$r_1 = \frac{k_1' K_{AA} P_{OPA}}{K_{AA} P_{AA} + K_{SA} P_{SA} + K_{NH_3} P_{NH_3}} \tag{6.38}$$

or

$$r_1 = \frac{k_1' P_{OPA}}{P_{AA} + (K_{SA}/K_{AA}) P_{SA} + (K_{NH_3}/K_{AA}) P_{HC}} \tag{6.39}$$

Where:

r_1 rate of hydrogenlysis of OPA to hydrocarbons and ammonia.

P_{AA} partial pressure of aromatic amines ($P_Q + P_{BzTHQ} + P_{OPA}$)

P_{SA} partial pressure of secondary amines ($P_{PyTHQ} + P_{DHQ}$)

Similarly, the rate of hydrogenolysis of PyTHQ to OPA can be expressed as

$$r_2 = \frac{k_2' (K_{SA}/K_{AA}) P_{PyTHQ}}{P_{AA} + (K_{SA}/K_{AA}) P_{SA} + (K_{NH_3}/K_{AA}) P_{HC}} \tag{6.40}$$

and the rate of hydrogenolysis of DHQ to ammonia and hydrocarbons is given by

$$r_{\mathrm{DHQ}} = -r_3 = -\frac{k_3' (K_{SA}/K_{AA}) P_{DHQ}}{P_{AA} + (K_{SA}/K_{AA}) P_{SA} + (K_{NH_3}/K_{AA}) P_{HC}} \tag{6.41}$$

From the above expressions the rate of formation of OPA is expressed as

$$r_{OPA} = r_2 - r_1 = \frac{(K_{SA}/K_{AA})[k_2' P_{PyTHQ} - k_1' P_{OPA}]}{P_{AA} + (K_{SA}/K_{AA}) P_{SA} + (K_{NH_3}/K_{AA}) P_{HC}} \tag{6.42}$$

the rate of hydrogenolysis of PyTHQ

$$r_{PyTHQ} = -r_2 = -\frac{k_2' (K_{SA}/K_{AA}) P_{PyTHQ}}{P_{AA} + (K_{SA}/K_{AA}) P_{SA} + (K_{NH_3}/K_{AA}) P_{HC}} \tag{6.43}$$

[illegible]

$$[illegible] \tag{4.4}$$

[illegible]

$$[illegible] \tag{4.5}$$

$$[illegible] \tag{4.6}$$

$$[illegible] \tag{4.7}$$

$$[illegible] \tag{4.8}$$

$$[illegible] \tag{4.9}$$

4.3 Results of Kinetic Modelling

[illegible]

4.3.1 [illegible]

[illegible]

Table 6.6 Variation of rate constants with respect to temperature at R 13, pyridine

run number	temperature (K)	rate constants g mol/sec g cat
P225	498	$0.1332 \cdot 10^{-5}$
P250	523	$0.5400 \cdot 10^{-5}$
P275	548	$0.1115 \cdot 10^{-4}$
P300	573	$0.2937 \cdot 10^{-4}$
P325	598	$0.3255 \cdot 10^{-4}$
P350	623	$0.9515 \cdot 10^{-4}$

constant over the temperature range. It varied from 1.64 at 498 K to 0.21 at 598 K. The Arrhenius plot of $\ln k_1$ vs $1/T$ gave a straight line. Figure 6.51. The activation energy was found to be 18.64 ± 0.17 kcal/g mol. This value is higher than 13.69 kcal/g mol reported by Anabtawee et al. [5] and close to 22.11 kcal/g mol calculated from the rate constants reported by Somorjai et al. [37].

Quinoline HDN data were fitted to this model. The percentage relative error ranged between 20 and 50 which indicates a poor fit for the data. The previous previous HDN data gave good correlations only at low temperatures (498 and 523 K). The results of the nonlinear regression are presented in Appendix C.

6.9.2 Model 2

The parameters of this model (equations 6.56) were estimated using the same method as in Model 1. The data of the three systems were fitted to this model. The previous HDN data were fitted to this model. The percentage relative error was low at low temperatures but unusually high at higher temperatures above 573 K. From the Arrhenius plot of $\ln k_2$ vs $1/T$ the average activation energy was found to be 15.28 ± 0.09 kcal/g mol (see Figure 6.52). The pyridine HDN

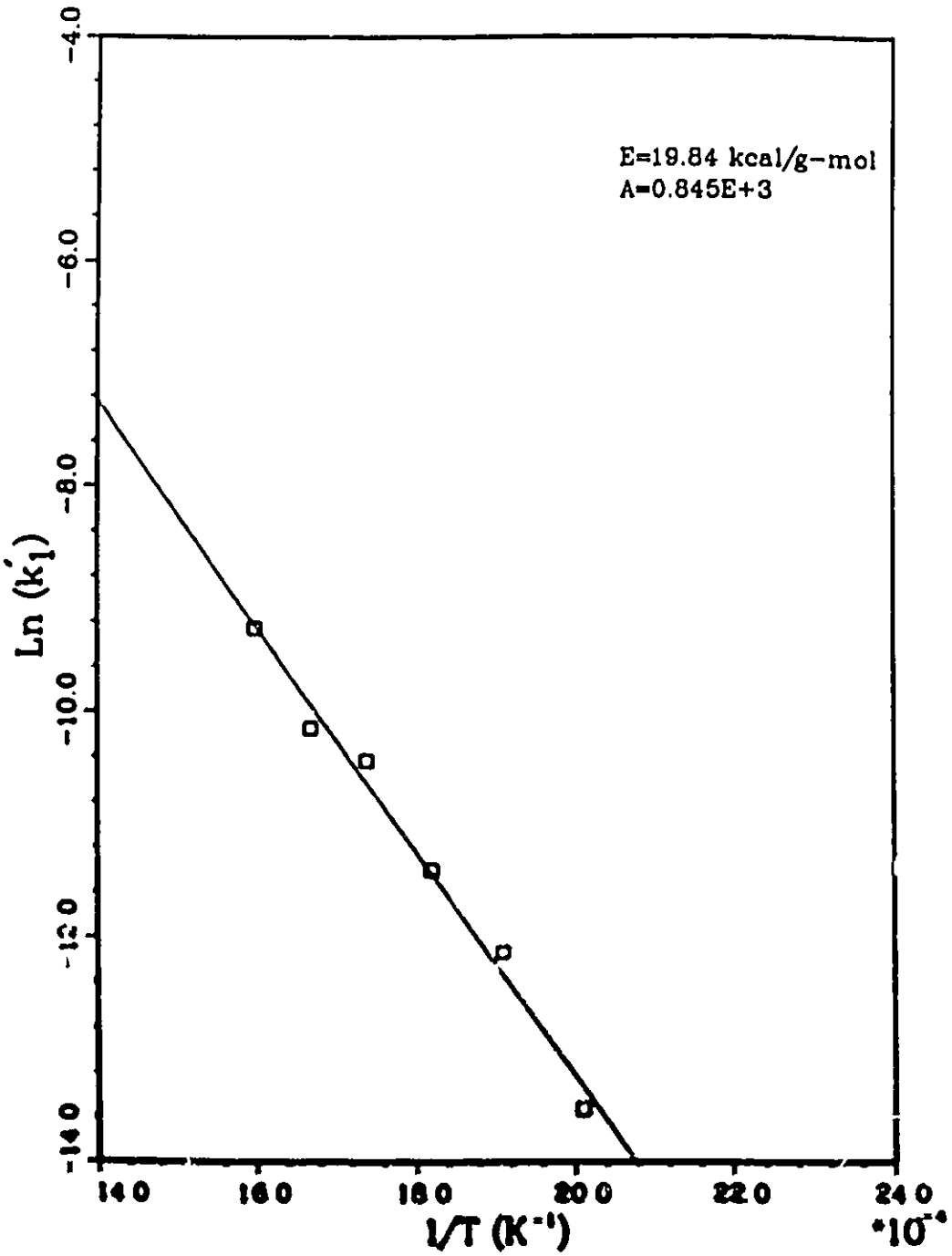

Figure 6.3: Arrhenius plot of ln k'_1 vs 1/T, pyrrolizine, Model 1

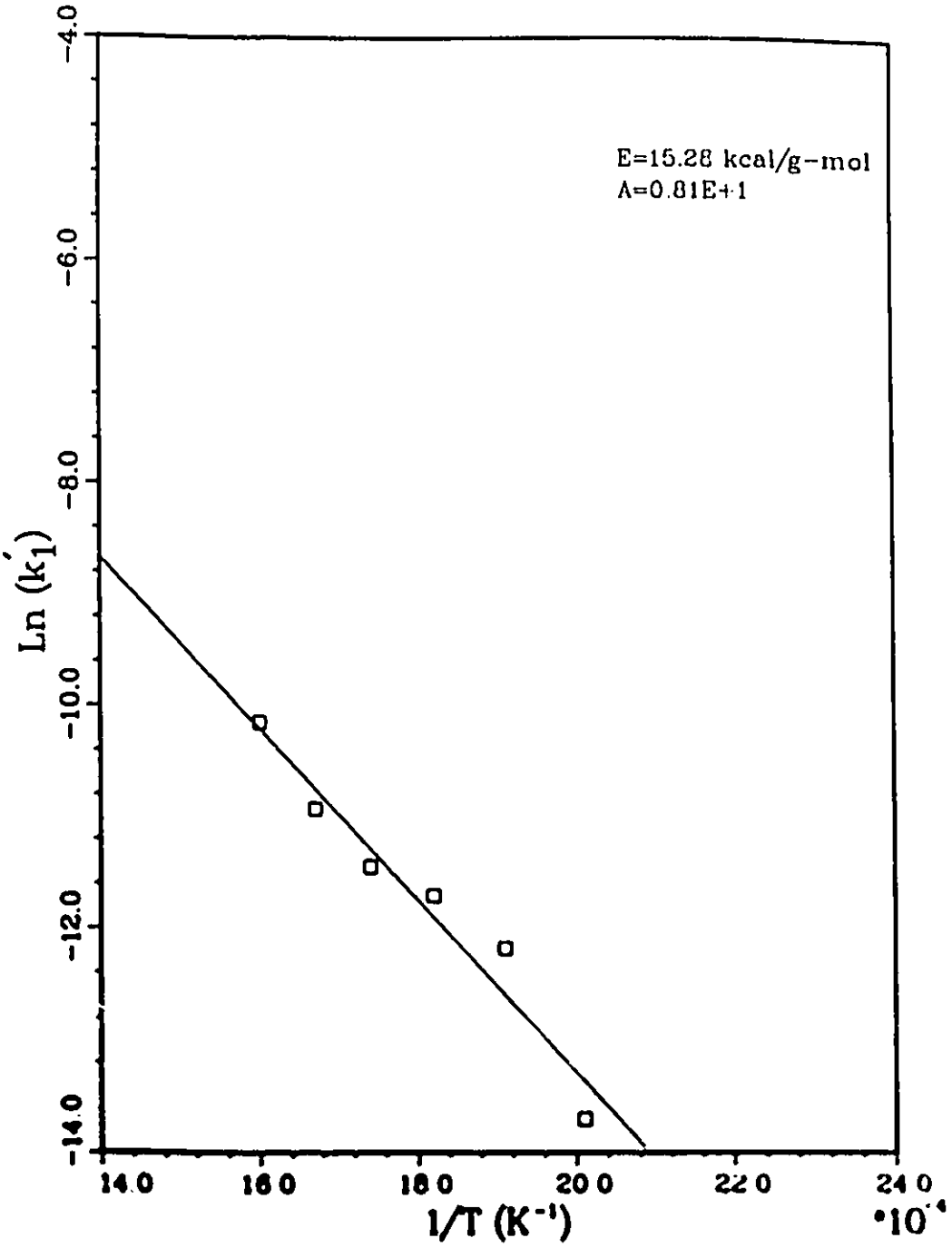

Figure 6.32 Arrhenius plot of ln k'_1 vs 1/T, pyrolysis, Model 3

data gave an absolute percentage relative error less than 10% except at two data points which indicates a satisfactory fit of the experimental data. The values of the rate constants, k_1', predicted by this model (Table 6.7) were used to calculate the average activation energy of the quinoline HDN reaction. As in the case of pyridine HDN, the value of the ratio K_{NH_3}/K_A was not constant at the different temperatures, it decreased with the increase in temperature. From the Arrhenius plot of ln k_1' *vs* 1/T, Figure 6.53, the activation energy was found to be 26.52 ± 0.15 kcal/g-mol. This value is between 20 kcal/g-mol reported by Shih et al. [88], and 30.19 kcal/g-mol predicted by Aboul-Gheit et al. [1] or 30.83 kcal/g-mol reported by El-Bishtawi [31].

The pyridine-quinoline HDN data were fitted to this model. The percentage relative error was between -6.89 and 9.41 which indicates a good fit for the data. The values of the rate constants at the various temperatures (Table 6.8) were used to calculate the the average activation energy of the HDN reaction. From the Arrhenius plot of ln k_1' *vs* 1/T, Figure 6.54, the activation energy was found to be 13.17 ± 0.03 kcal/g-mol.

Fitting the HDN data of the three systems to Model 3 did not give satisfactory results. A fit is considered not adequate if the percentage relative error is high or if the values of the adsorption equilibrium constants came out to be negative.

6.8.3 Mechanistic Model

Due to the limitations in the number of data points, the mechanistic model was based on the simplified reaction networks of pyridine and quinoline. In the case of pyridine HDN reaction a set of three differential equations with three responses

Table 6.7: Variation of rate constants with respect to temperature at $\overline{R}$=13; quinoline

run number	temperature (K)	rate constants g-mol/sec g-cat
Q225	498	0.1696×10^{-5}
Q250	523	0.2135×10^{-5}
Q275	548	0.1584×10^{-4}
Q300	573	0.1699×10^{-4}
Q325	598	0.6925×10^{-4}
Q350	623	0.2855×10^{-3}
Q375	648	0.5092×10^{-3}
Q400	673	0.1301×10^{-2}

Table 6.8: Variation of rate constants with respect to temperature at $\overline{R}$=13; pyridine-quinoline mixture

run number	temperature (K)	rate constants g-mol/sec g-cat
PQ225	498	0.8055×10^{-5}
PQ300	573	0.4472×10^{-4}
PQ350	623	0.1311×10^{-3}
PQ400	673	0.2421×10^{-3}

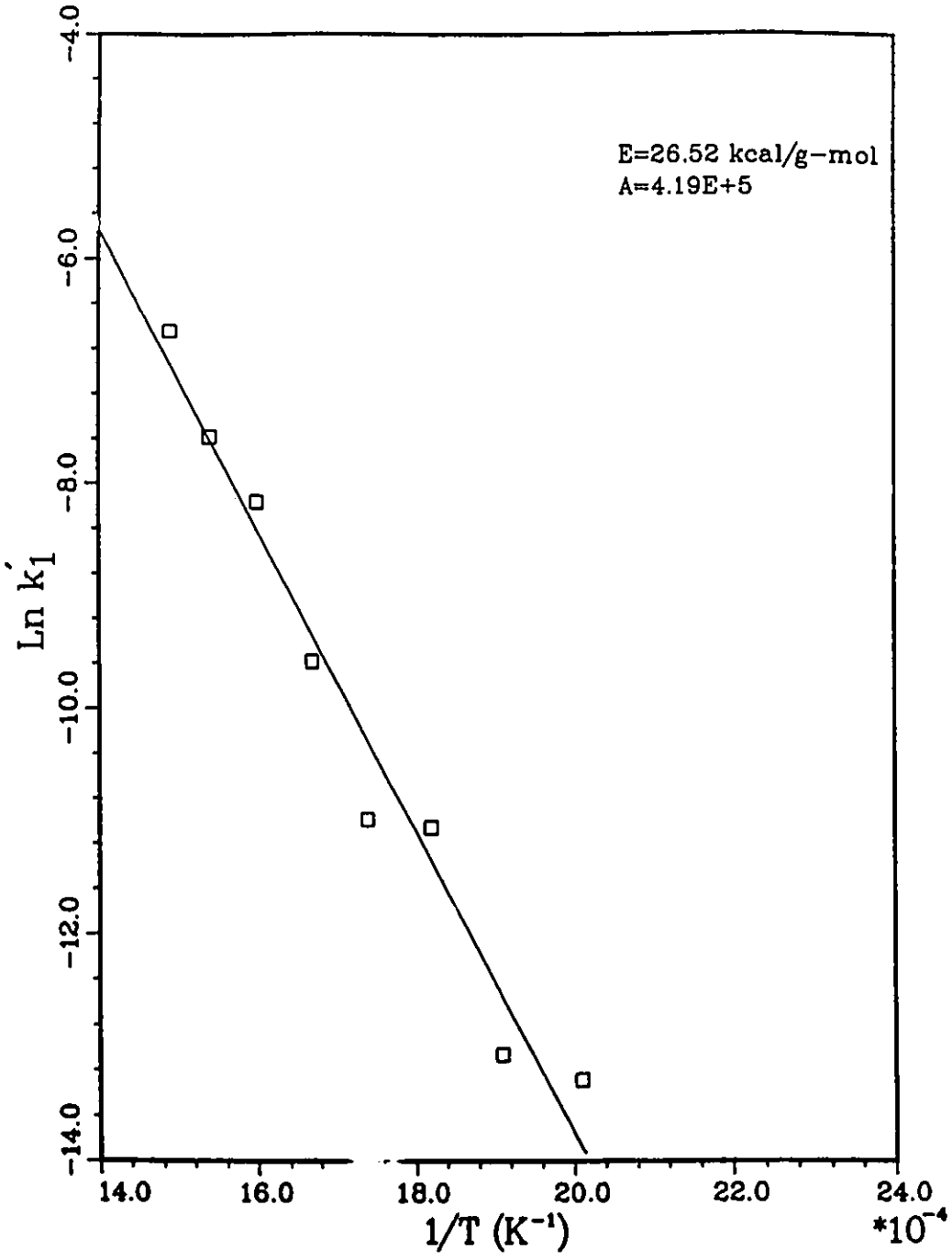

Figure 6.53: Arrhenius plot of ln k'_1 *vs* 1/T; quinoline, Model 2.

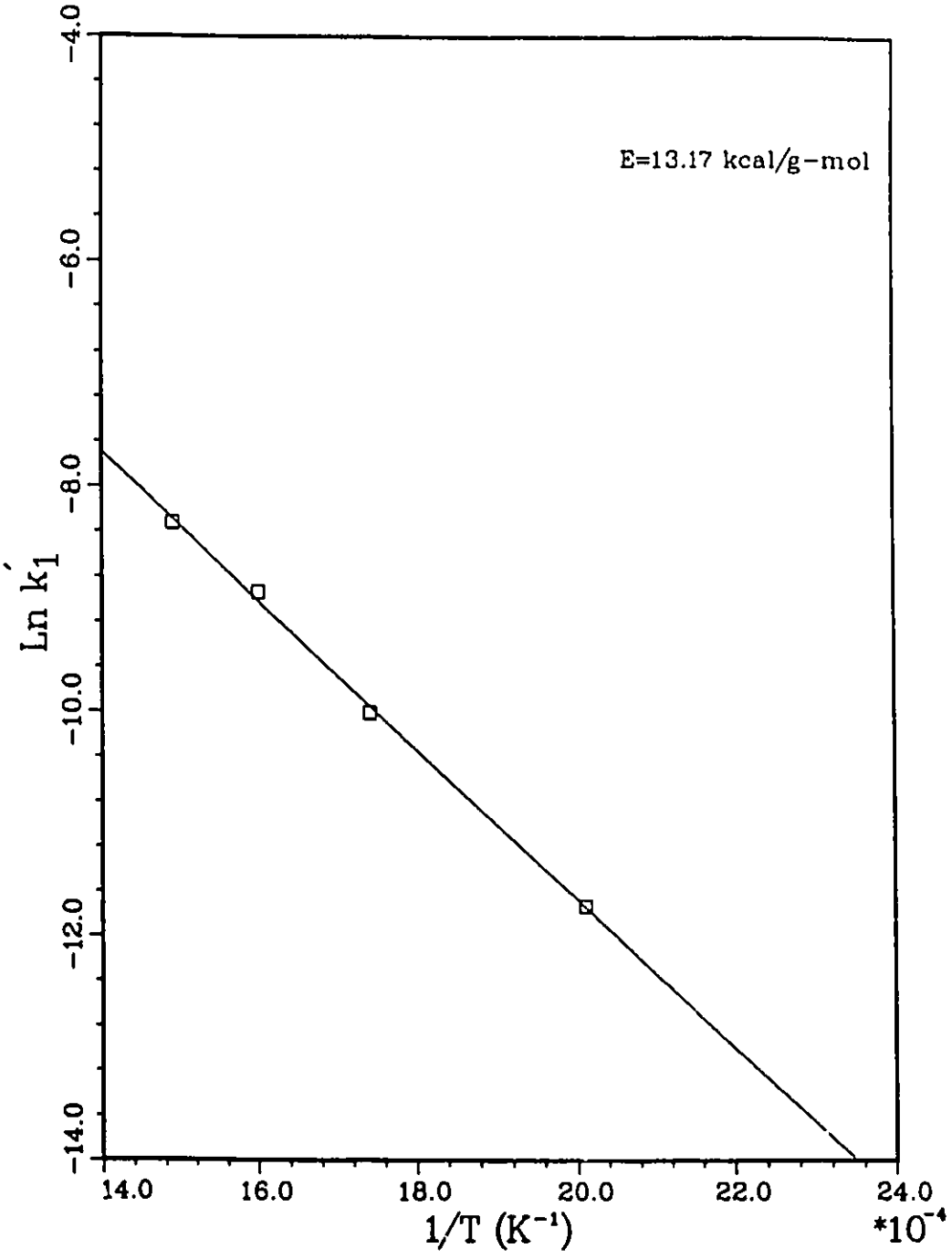

Figure 6.54: Arrhenius plot of ln k_1' *vs* 1/T; mixture, Model 2.

and four parameters were resulted, while in the case of quinoline HDN a set of four differential equations with four responses and four parameters were obtained. These equations were solved by a differential equation solver. The parameters of these equations were determined by a nonlinear regression technique. The computer program that contains the differential equations that represent the reaction network of the quinoline HDN and the derivatives with respect to the responses and the parameters is shown in Appendix H. This program is called by the main program PAREIDE FORTRAN (PARameter Estimation In Differential Equations).

Pyridine

The rate constants for the hydrogenolysis steps of the pyridine HDN reaction, shown in the simplified reaction network (Figure 6.49), were estimated at different temperatures. The Arrhenius plots of the pseudo rate constants for the hydrogenolysis reactions are shown in Figures 6.55 to 6.57. Comparison of these Figures reveals that the pseudo rate constants for the hydrogenolysis of alkyl-piperidines is an order of magnitude larger than that of the hydriogenolysis of piperidine to alkyl-piperidines. The average activation energy for the hydrogenolysis of piperidine to alkyl-piperidine was 19.15 $\pm$ 0.06 kcal/g-mol. The activation energy of the hydrogenolysis of alkyl-piperidines to hydrocarbons was 16.05 $\pm$ 0.07 kcal/g-mol, while that of the hydrogenolysis of piperidine to hydrocarbons was 13.44 $\pm$ 0.02 kcal/mol. This result indicates that rate of pyridine HDN reaction is determined by the rate of hydrogenation of piperidine to alkyl-piperidines.

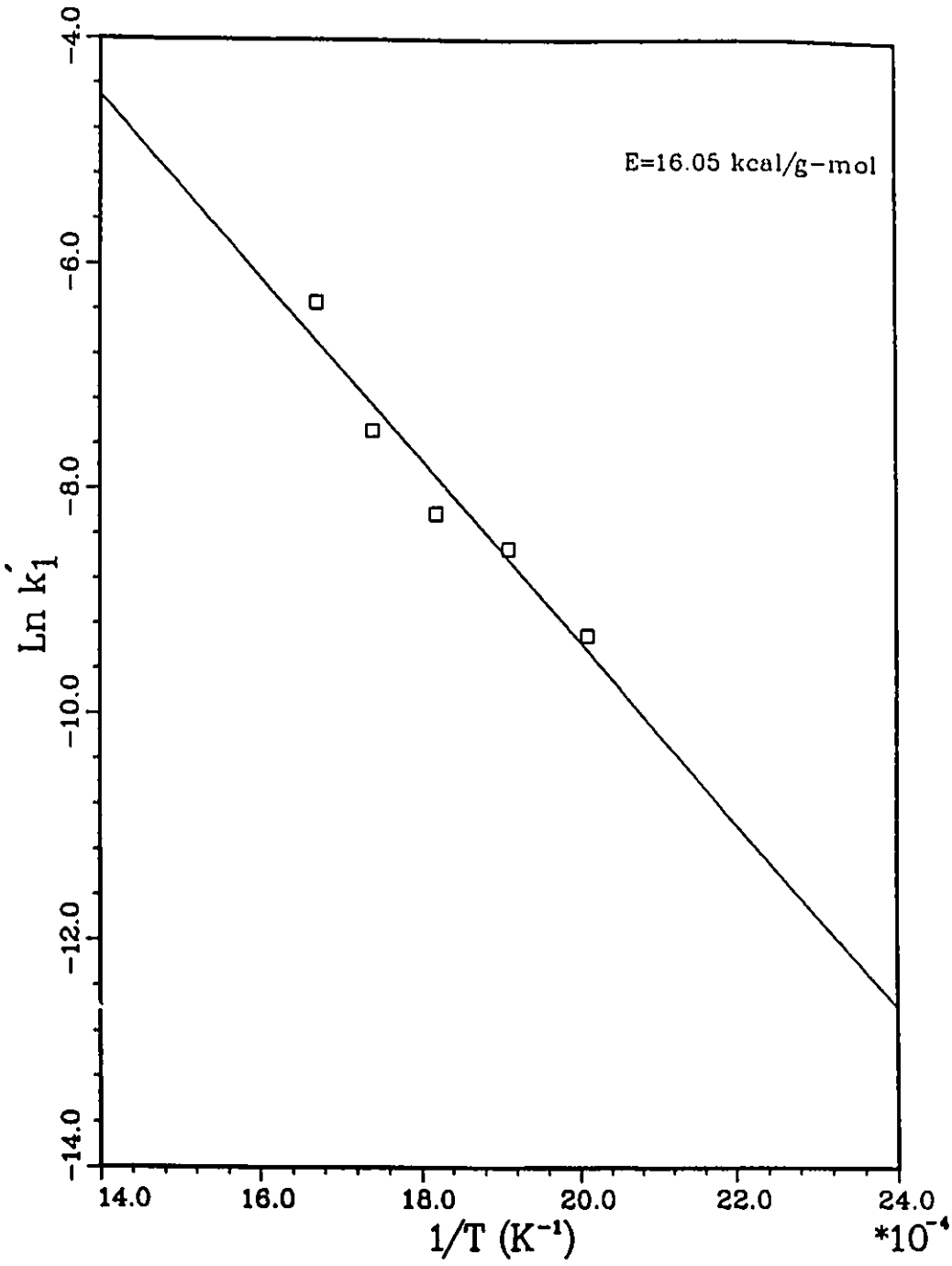

Figure 6.55: Arrhenius plot of ln k_1' *vs* 1/T; APIP to HC.

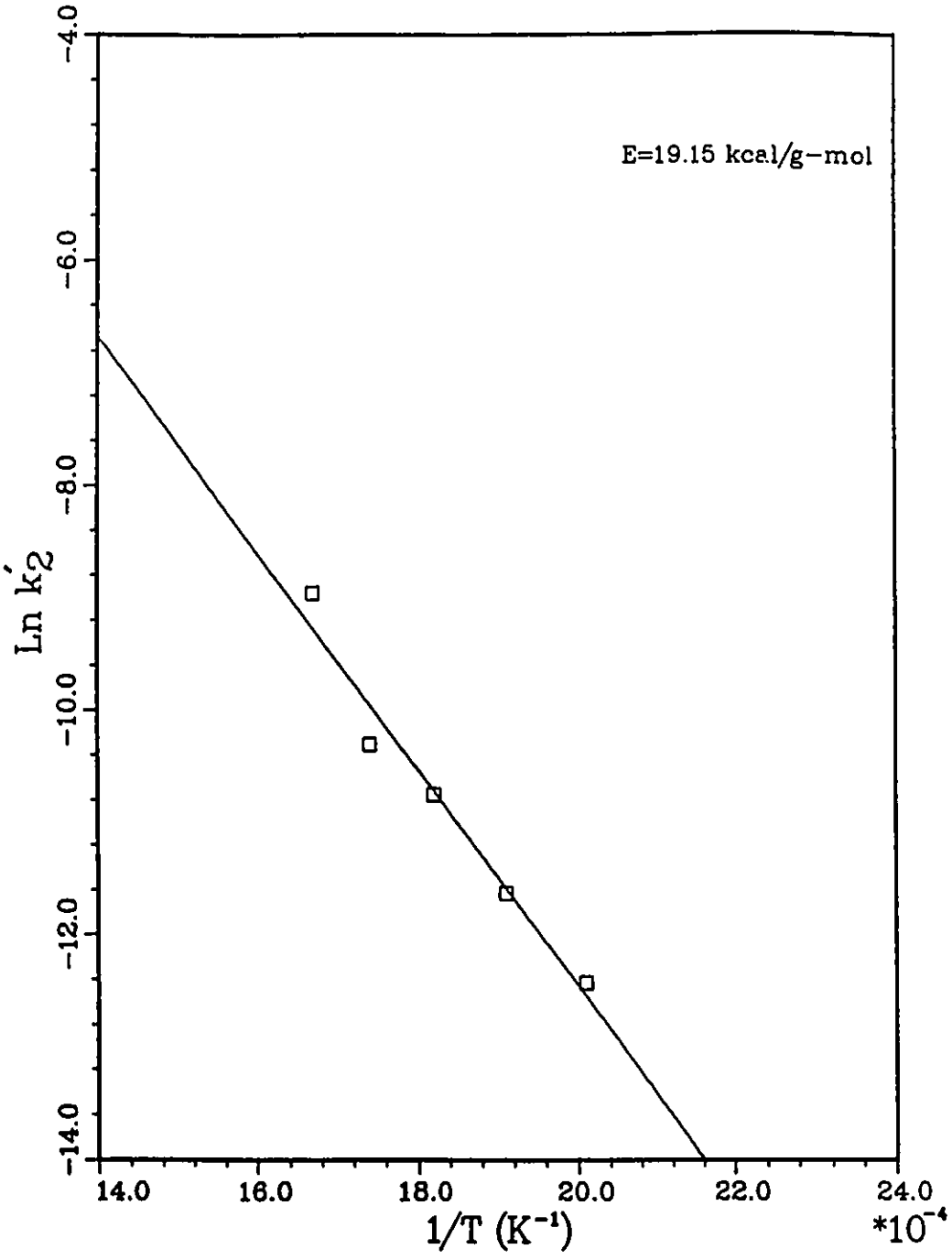

Figure 6.56: Arrhenius plot of ln k_2' *vs* 1/T; PIP to APIP.

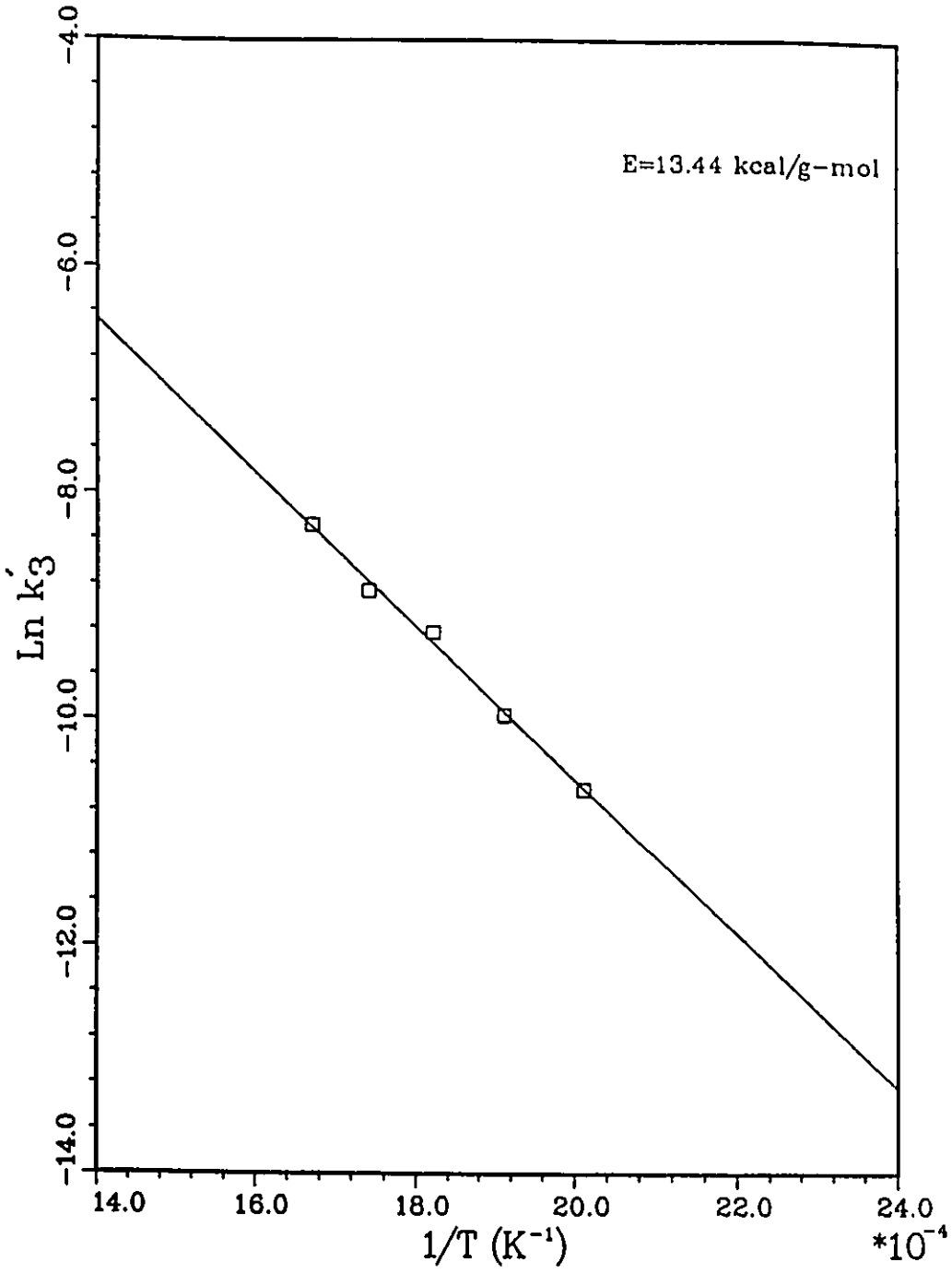

Figure 6.57: Arrhenius plot of ln k_3' *vs* 1/T; PIP to HC

Quinoline

The rate constants for the hydrogenolysis steps of the quinoline HDN reaction, shown in the simplified reaction network (Figure 6.50), are estimated at different temperatures making use of the differential equation solver coupled with the parameter estimator. The Arrhenius plots of the pseudo rate constants for the hydrogenolysis reactions are shown in Figures 6.58 to 6.60. Comparison of these figures reveals that the pseudo rate constants for the hydrogenolysis of decahydroquinoline is an order of magnitude larger than that of the hydriogenolysis of PyTHQ. The same result was reported be Cocchetto [24]. On the other hand the pseudo rate constants of the hydrogenolysis of OPA is about an order of magnitude larger than that of DHQ. The average activation energy for the hydrogenolysis of PyTHQ to OPA was 40.52 $\pm$ 0.13 kcal/g-mol. The activation energy for the hydrogenolysis of DHQ to hydrocarbons was 36.57 $\pm$ 0.11 kcal/g-mol and that for the hydrogenolysis of OPA to hydrocarbons was 23.58 $\pm$ 0.08 kcal/g-mol. These activation energies were a little higher than the ones reported by Cocchetto (37 kcal/g-mol for PyTHQ, 33 kcal/g-mol for DHQ, and 19 kcal/g-mol for OPA) [24], or the values reported by Shih at al. (35 kcal/g-mol for PyTHQ and 31 kcal/g-mol for DHQ) [88].

Recalling that the average activation energy of quinoline HDN is 26.52 kcal/g-mol, one can conclude that the rate of hydrodenitogenation of quinoline is determined by the rate of hydrogenation of PyTHQ.

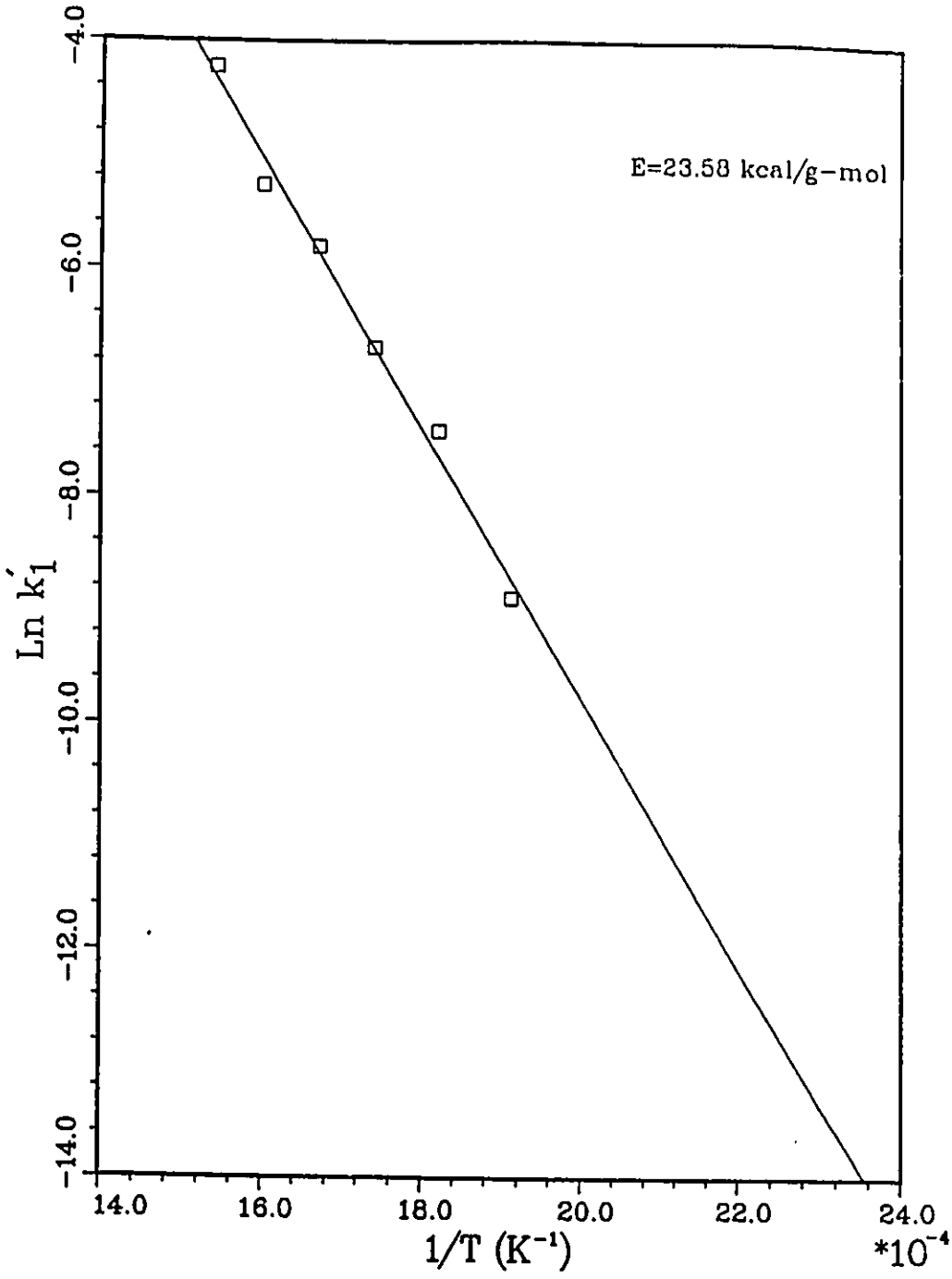

Figure 6.58: Arrhenius plot of ln k_1' *vs* 1/T; OPA to HC.

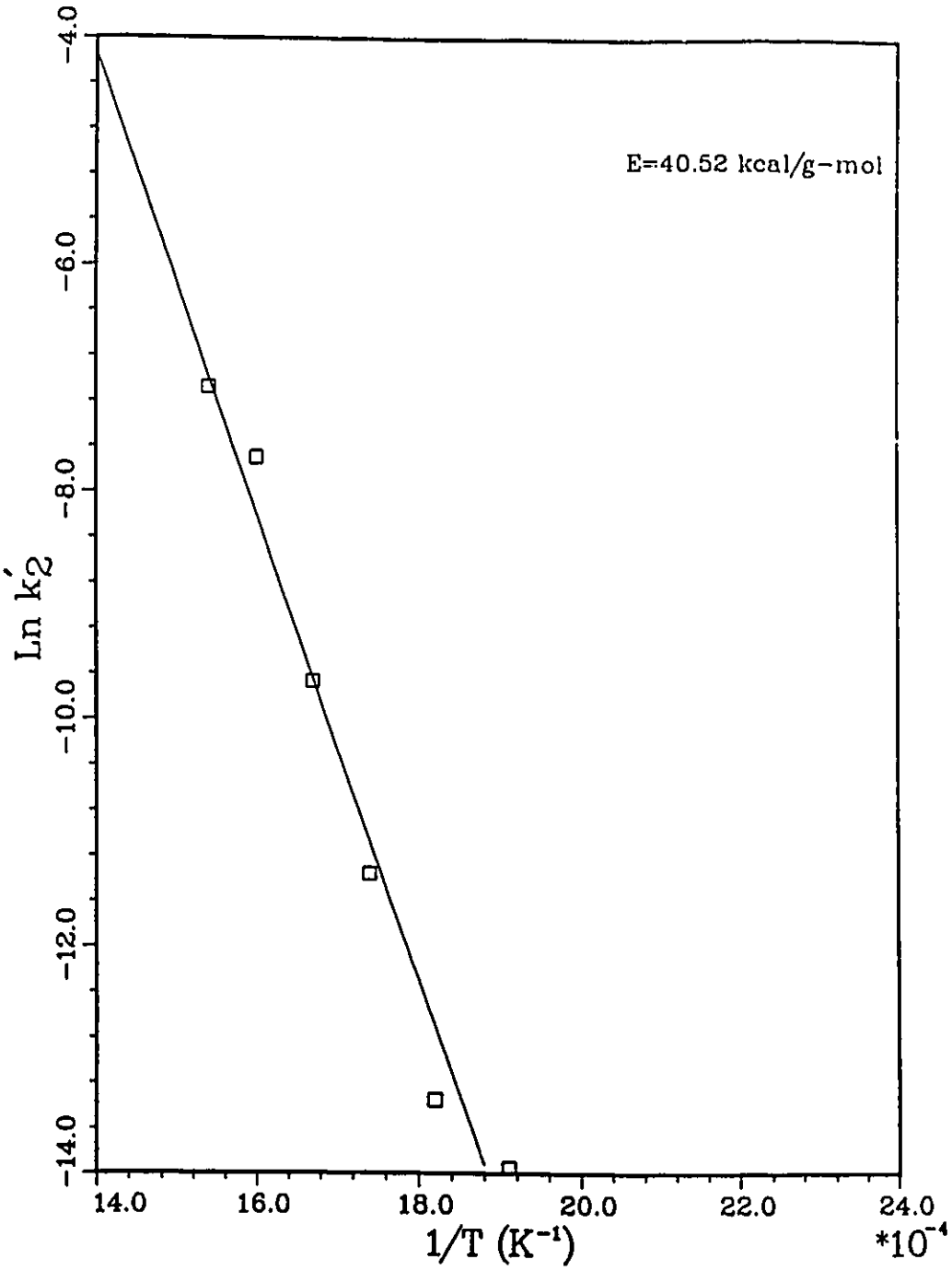

Figure 6.59: Arrhenius plot of ln k_2' *vs* 1/T; PyTHQ to OPA.

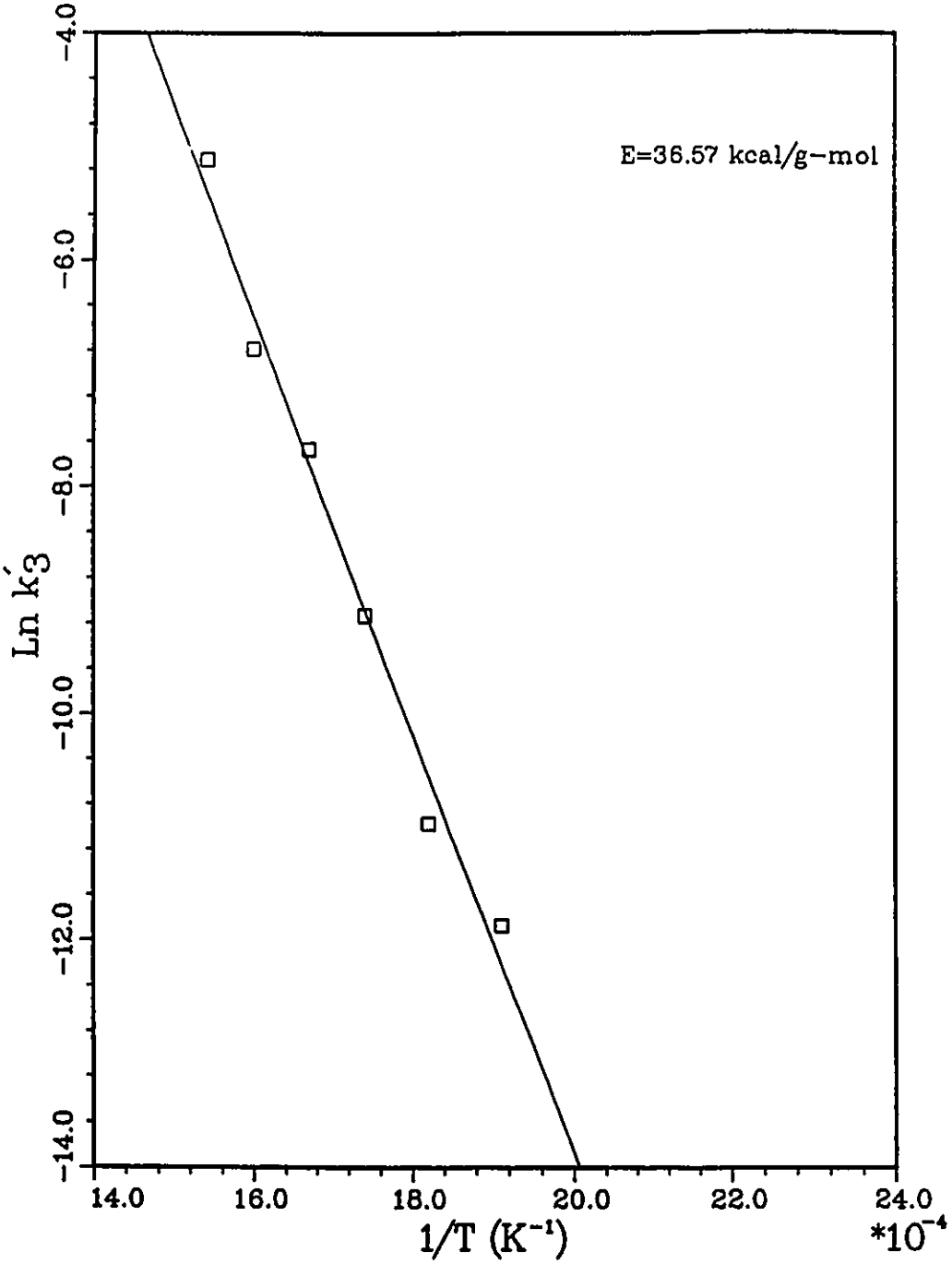

Figure 6.60: Arrhenius plot of ln k_3' *vs* 1/T; DHQ to HC.

Chapter 7

Conclusions and Recommendations

In this study, the HDN reactions of pyridine, quinoline, and pyridine-quinoline mixture were investigated. Reaction networks were developed for both pyridine and quinoline. Several models were examined to fit the data. The parameters of these models were estimated.

7.1 Conclusions

The main conclusions drawn out of this research project are:

- The product distribution of pyridine HDN, and the presence of ETPIP and PRPIP in significant amounts as intermediate products, suggested a new reaction network for pyridine HDN reaction.
- The pseudo first order model fit the data well.
- The adsorption of ammonia with respect to the nitrogen compounds had decreased with the increase in reaction temperature.

- The conversion of pyridine was complete at the reaction conditions and at temperatures above 623 K.
- Quinoline did not achieve complete conversion even at 673 K. This result may be due to the fact that more nitrogen compounds were produced from the HDN of quinoline than that in the case of pyridine HDN, which results in an increase in the competitive adsorption of the product nitrogen compounds on the catalyst active sites.
- At high temperatures the quinoline HDN is shifted towards the BzTHQ path.
- The values of the activation energies of the hydrogenolysis steps of pyridine HDN had shown that the rate determining step for pyridine HDN is the hydrogenation of piperidine to alkyl-piperidines.
- The values of the activation energies of the hydrogenolysis steps of quinoline HDN had shown that the rate determining step for quinoline HDN is the hydrogenolysis of PyTHQ to OPA.
- Mixing pyridine and quinoline resulted in a significant increase in the rate of conversion as well as the selectivity of the quinoline HDN reaction.
- The presence of quinoline had retarded the rate of conversion as well as the selectivity of the pyridine HDN reaction.
- In general, mixing the two nitrogen compounds had increased the selectivity of the HDN reaction via the production of PCH and other alkyl-cyclohexanes.

7.2 Recommendations

The following suggestions are recommended for further research

- Taking more data points at each temperature so as to be able to evaluate all the kinetic constants of the reaction networks.
- Hydrodenitrogenation of different compositions of pyridine-quinoline mixture to see the effect of composition on the selectivity of the reaction.
- Hydrodenitrogenation of each of the major nitrogen products so as to have better understanding of the reaction network.
- Hydrodenitrogenation of mixtures of quinoline and each of the nitrogen compounds resulting from pyridine HDN in order to identify which of these compounds is affecting the conversion and the selectivity of quinoline.

Bibliography

[1] A. K. Aboul-Gheit, I. K. Abdou, and A. Mustafa. Hydrodenitrogenation Studies. Part-II-Quinoline. *Egypt. J. Chem.*, 17(5):631, 1974.

[2] A. K. Aboul-Gheit, I. K. Abdou, and A. Mustafa. Hydrodenitrogenation Studies. Part-I-Pyridine. *Egypt. J. Chem.*, 17(5):617, 1974.

[3] C. D. Ajaka, K. C. Khulbe, and R. S. Mann. Hydrodenitrogenation of Pyridine over MoO-Alumina. 1991. Unpublished Data.

[4] J. A. Anabtawi. *Hydrodenitrogenation of Pyridine on NiO-WO_3-Al_2O_3 Catalyst.* Master's thesis, University of Ottawa, 1978.

[5] J. A. Anabtawi, R. S. Mann, and K. C. Khulbe. Hydrogenation of Pyridine over Ni-W/Alumina Catalyst. *J. Catal.*, 63:459, 1980.

[6] R. Aris. *The Mathematical Theory of Diffusion and Reaction in Permeable Catalysts, Volumes I and II.* Calendon Press, Oxford, 1975.

[7] J. H. Ashley and P. C. H. Mitchell. CoO-MoO_3-Al_2O_3 Catalysts. I. Spectroscopic and Magnetic Study of the Fresh Catalyst and Model Compounds. *J. Chem. Soc. A*, 2821, 1968.

[8] J. H. Ashley and P. C. H. Mitchell. CoO-MoO_3-Al_2O_3 Catalysts. II. Incorporation of Cobalt(II) and Molybdenum(VI) into γ-Alumina. *J. Chem. Soc. A*, 2730, 1969.

[9] M. T. Atwood. Production of Shale Oil. *Chem. Tech.*, 617, 1973.

[10] D. Bacon. *Strategies for Engineering Process Analysis.* Assembled by D. D. McLean, University of Ottawa, 1988.

[11] G. M. Badger. *The Chemistry of Heterocyclic Compounds.* Academic Press, Inc., New York, 1961.

[12] D. M. Bates and D. G. Watts. A Generalized Gauss-Newton Procedure for Multirespons Parameter Estimation. *Journal of Scientific and Statistical Computing*, 7:49, 1987.

[13] D. M. Bates and D. G. Watts. A Multiresponse Gauss-Newton Algorithm. *Commun. Stat. Sim. Comp.*, 13:705, 1984.

[14] H. Beuther and O. A. Larson. Role of Catalytic Metals in Hydrocracking. *Ind. Eng. Chem. Process Des. Dev.*, 4(2):177, 1965.

[15] D. F. Boltz. *Selected Topics in Modern Instrumental Analysis.* Prentice-Hall, Inc., New York, 1952.

[16] G. C. Bond. *Catalysis by Metals.* Academic Press, New York, 1962.

[17] G. E. P. Box and D. W. Behnken. Some New Three Level Designs for the Study of Quantitative Variables. *Thechnometrics*, 2:455, 1960.

[18] G. E. P. Box and N. Draper. The Bayesian Estimation of Common Parameters from Several Response Variables. *Biometrika*, 52:355, 1965.

[19] C. C. Chang. Auger Electron Spectroscopy. *Surface Sci.*, 25:53, 1971.

[20] Hill G. Charles, Jr. *An Introduction to Cemical Engineering Kinetics & Reactor Design.* John Wiley & Sons Inc., New York, 1977.

[21] T. H. Chilton and A. P. Colburn. Mass Transfer (Adsorption) Coefficients. *Ind. Eng. Chem.*, 26(11):1183, 1934.

[22] J. C. Chu, J. Kalil, and W. A. Wetteroth. Mass Transfer in a Fluidized Bed. *Chemical Engineering Progress*, 49:141, 1953.

[23] Alfred Clark. *The Theory of Adsorption and Catalysis.* Academic Press, New York, 1970.

[24] J. F. Cocchetto. *Reaction Network and Kinetics of Vapor-Phase Catalytic Hydrodenitrogenation of Quinoline.* PhD thesis, Massachusetts Institute of Technology, 1979.

[25] J. F. Cocchetto and C. N. Satterfield. Chemical Equilibria among Quinoline and its Reaction Products in Hydrodenitrogenation. *Ind. Eng. Chem. Process Des. Dev.*, 20:49, 1981.

[26] J. A. Cusumano, R.A. Dalla Betta, and R.B. Levy. *Catalysis in Coal Conversion.* Academic Press, Inc., New York, 1978.

[27] B. Delmon, P. A. Jacobs, and G. Poncelet. *Preparation of Catalysts.* Alsevier Scientific Publiushing Company, Amsterdam, 1976.

[28] J. Doelman and J. C. Vlugter. Model Studies on the Catalytic Hydrogenation of Nitrogen Containing Oils. *Proc. Sixth World Pet. Cong.*, III:247, 1963.

[29] L. K. Doraiswamy and D. J. Tajbl. Laboratory Catalytic Reactors. *Cat. Rev.-Sci. Eng.*, 10(2):177, 1974.

[30] S. Eijsbouts, V. H. J. De Beer, and R. Prins. Hydrodenitrogenation of Quinoline over Carbon-Supported Transition Metal Sulfides. *J. Catal.*, 127:619, 1991.

[31] R. F. El-Bishtawi. ***Hydrodenitrogenation of Quinoline, Acridine and their Mixture.*** PhD thesis, Oklahoma State University, 1986.

[32] R. T. Ellington. ***Liquid Fuels from Coal.*** Academic Press, Inc., New York, 1977.

[33] A. L. Farragher and P. Cossee. Catalytic Chemistry of Molybdenum and Tungsten Sulfides and related Ternary Compounds. *Proc. of the 5th Int. Cong. on Catal.*, 1301, 1973. (J. W. Hightower, Ed.).

[34] R. A. Flinn, O. A. Larson, and H. Beuther. How Easy is Hydrodenitrogenation? ***Hydrocarbon Process and Pet. Ref.***, 42(9):129, 1963.

[35] Editor G. Jones. ***Heterocyclic Compounds; Quinolines.*** Volume 32, John Wiley and Sons Inc., New York, USA, 1977.

[36] B. Gamson, G. Thodos, and O. Hougen. Heat, Mass and Momentum Transfer in the Flow of Gases through Granular Solids. ***Transactions of the American Institute of Chemical Engineers***, 39:1, 1943.

[37] B. C. Gates, J. R. Katzer, and G. C. A. Schuit. *Chemistry of Catalytic Processes.* McGraw Hill, New York, 1979.

[38] T. L. Gilchrist. *Heterocyclic Chemistry.* Pitman Publishing Ltd., London, England, 1985.

[39] F. Goudriaan. *Hydrodenitrogenation of Pyridine.* PhD thesis, Twente University of Technology, Enschede, The Netherlands, 1974.

[40] F. Goudriaan, H. Gierman, and J. C. Flugter. Effect of Hydrogen Sulfide on the Hydrodenitrogenation of Pyridine. *J. Inst. Pet. London*, 59:40, 1973.

[41] J. Grimblot, E. Payen, and J. P. Bonnelle. Investigation of Coprecipitated nio-moo_3 Catalysts by X-ray Diffraction,XPS, Laser Raman and IR. *Proc. of the 4th Int. Conf. The Chemistry and Uses of Molybdenum.*, 261, 1982. (Climax Molybdenum Co.).

[42] R. K. Gupta. *Hydrodenitrogenation of Pyridine over Cobalt Molybdate Catalyst.* Master's thesis, University of Ottawa, 1977.

[43] G. Hagenbach, Ph. Courty, and B. Delmon. Catalytic Activity of Cobalt and Molybdenum Sulfides in the Hydrogenolysis of Thiophene, Hydrogenation of Cyclohexene, and Isomerization of Cyclohexane. *J. Catal.*, 23:295, 1971.

[44] G. Hagenbach, Ph. Courty, and B. Delmon. Physicochemical Investigation of Catalytic Activity Measurements on Crystallized Molybdenum Sulfide-Cobalt Sulfide Mixed Catalysts. *J. Catal.*, 31:264, 1973.

[45] G. G. Hawley. *The Condensed Chemical Dictionary.* Litton Educational Publishing, Inc., New York, 1981.

[46] R. J. Hengstebeck. *Petroleum Processing.* McGraw Hill Book Company, New York, 1959.

[47] W. J. Houlihan. *Heterocyclic Compounds.* John Wiley & Sons Inc., New York, 1972.

[48] A. Iannibello, S. Marengo, G. Morelli, and P. Tittarelli. Surface Structure and Phase Transition in the MoO_3/Al_2O_3 and WO_3/Al_2O_3 Systems. Effect of addition of Ni^{2+} and Co^{2+}. *Proc. of the 4th Int. Conf. The Chemistry and Uses of Molybdenum.*, 256, 1982. (Climax Molybdenum Co.).

[49] D. M. Jewell and G. K. Dart. Identification of Nitrogen Bases in Heavy Gas Oil Chromatographic Methods of Separation. *J. Chem. Eng. Data*, 9(2):297, 1964.

[50] H. S. Johnston. *Gas Phase Reaction Theory.* Ronald Press, New York, 1966.

[51] R. Kartzmark and J. B. Gilbert. Hydrotreat Naphthanic Lube Stocks. *Hydrocarbon Process and Pet. Ref.*, 46(9):143, 1967.

[52] A. R. Katritzky. *Handbook of Heterocyclic Chemistry.* Pregao press, 1985.

[53] A. J. A. Konings, W. L. J. Brenntjes, D. C. Koningsberger, and V. H. J. de Beer. ESR Studies on Hydrodesulfurization Catalysts: Nickel- or Cobalt-Promoted Sulfided Tungesten- or Molybdenum-Containing Catalysts. *J. Catal.*, 67:145, 1981.

[54] A. J. A. Konings, A. M. van Dooren, D. C. Koningsberger, V. H. J. de Beer, A. L. Farragher, and G. C. A. Schuit. ESR Studies on Hydrodesulfurization

Catalysts: Supported and Unsupported Sulfided Molybdenum and Tungesten Catalysts. *J. Catal.*, 54:1, 1978.

[55] R. M. Koros, S. Bank, J. E. Hoffman, and M. I. kay. Hydrodenitrogenation of Shale Oil. *Preprints, Div. Pet. Chem. ACS*, 12(4):B165, 1967.

[56] K. Laidler. *Chemical Kinetics.* McGraw Hill Book Co., New York, 1965.

[57] O. A. Larson. Kinetic Effects Due to Poisons in Hydrocarbon Hydrogenation Process. *Preprints, Dvi. Pet. Chem. ACS*, 12(4):3, 1967.

[58] Octave Levenspiel. *Cemical Reaction Engineering.* John Wiley & Sons Inc., New York, 1972.

[59] J. M. J. D. Lipsch and G. C. A. Schuit. The CoO-MoO_3-Al_2O_3 Catalyst. II. The Structure of the Catalyst. *J. Catal.*, 15:179, 1969.

[60] J. M. J. D. Lipsch and G. C. A. Schuit. The CoO-MoO_3-Al_2O_3 Catalyst. III. Catalytic Properties. *J. Catal.*, 15:174, 1969.

[61] N. Lozej and D. D. McLean. *PARE-I-DE: Parameter Estimation in Differential Equations, User's Guide.* Department of Chemical Engineering, University of Ottawa, Ottawa, 1990.

[62] A. L. Lydersen. Estimation of Critical Properties of Organic Compounds. *Univ. Wis. Coll. Eng. No.3*, April 1955. Madison.

[63] M. M. Madkour, B. H. Mahmoud, I. K. Abdou, and J. C. Vlugter. The Effect of Chlorides on the Hydrogenation of Nitrogen-Containing Model Substances. *J. Indian Chem. Soc.*, 46(8):720, 1969.

[64] J. F. Mayer. *Interactions Between Hydrodesulfurization and Hydrodenitrogenation Reactions.* PhD thesis, Massachusetts Institute of Technology, 1974.

[65] F. P. McCandless and L. Berg. Hydrodenitrogenation of Petroleum Using a Supported Nickelous Chloride-Gaseous Chloride Catalyst System. *Ind. Eng. Chem. Process Des. Dev.*, 9:110, 1970.

[66] H. G. McIlvried. Kinetics of the Hydrodenitrification of Pyridine. *Ind. Eng. Chem. Process Des. Dev.*, 10(1):125, 1971.

[67] T. J. Miller and M. F. Hineman. Non-First-Order Hydrodenitrogation Kinetics of Quinoline. *J. Catalysis*, 85:117, 1984.

[68] A. C. Nixon, C. A. Cole, and H. B. Minor. Effect of Composition and Storage on the Properties of Jet Fuels. *J. Chem. Eng. Data*, 4:187, 1959.

[69] A. G. Oblad, T. H. Milliken, Jr., and G. A. Mills. Chemical Characteristics and Structure of Cracking Catalysts. *Advances in Catalysis*, II:199, 1951.

[70] A. A. Oswald and F. Noel. Role of Pyrroles in Fuel Instability. *J. Chem. Eng. Data*, 2(2):294, 1961.

[71] R. Park. *Experimental Methods in Catalytic Research.* Academic Press, New York, 1976. Vol. 3, Physical Chemistry Series.

[72] R. H. Perry, D. W. Green, and J. O. Maloney. *Perry's Chemical Engineering Handbook.* McGraw Hill, New York, 1984. 6TH Ed.

[73] L. J. Petrovic and G. Thodos. Mass Transfer in the Flow of Gases Through Packed Beds. *Ind. Eng. Chem. Fundamentals*, 7:274, 1968.

[74] P. Ratnasamy, R. P. Mehrotra, and A. V. Ramaswamy. Interaction Betwween the Active Components and Support in Co-Mo-Al_2O_3 Systems. *J. Catal.*, 32:63, 1974.

[75] R. C. Reid and T. K. Sherwood. *The Properties of Gases and Liquids.* McGraw Hill, New York, 1966. 2nd Ed.

[76] R. E. Riccetti and G. Thodos. Mass Transfer in the Flow of Gases Through Fluidized Beds. *AICHE J.*, 7:442, 1961.

[77] L. D. Rollman. Catalytic Hydrogenation of Model Nitrogen, Sulfur, and Oxygen Compounds. *J. Catal.*, 46:243, 1977.

[78] C. N. Satterfield and J. F. Cocchetto. Pyridine Hydrodenitrogenation: An Equilibrium Limitation on the Formation of Piperidine Intermediate. *AICHE J.*, 21(6):1107, 1975.

[79] C. N. Satterfield and J. F. Cocchetto. Reaction Network and Kinetics of the Vapor-Phase Catalytic Hydrodenitrogenation of Quinoline. *Ind. Eng. Chem. Process Des. Dev.*, 20:53, 1981.

[80] C. N. Satterfield and J. F. Cocchetto. Thermodynamic Equilibria of Selected Heterocyclic Nitrogen Compounds with Their Hydrogenated Derivatives. *Ind. Eng. Chem. Process Des. Dev.*, 15:272, 1976.

[81] C. N. Satterfield and S. Gultekin. Effect of Hydrogen Sulfide on the Catalytic Hydrodenitrogenation of Quinoline. *Ind. Eng. Chem. Process Des. Dev.*, 20:62, 1981.

[82] C. N. Satterfield, M. Modell, and J. F. Mayer. Interactions Between Catalytic Hydrodesulfurization of Thiophene and Hydrodenitrogenation of Pyridine. *AICHE J.*, 21(6):1100, 1975.

[83] C. N. Satterfield, M. Modell, and J. Wilkens. Simultaneous Catalytic Hydrodenitrogenation of Pyridine and Hydrodesulfurization of Thiophene. *Ind. Eng. Chem. Process Des. Dev.*, 19:154, 1980.

[84] C. N. Satterfield, C. M. Smith, and M. Ingalls. Catalytic Hydrodenitrogenation of Quinoline. Effect of Water and Hydrogen Sulfide. *Ind. Eng. Chem. Process Des. Dev.*, 24:1000, 1985.

[85] N. Schonberg. On the Existence of a Metallic Molybdenum Oxide. *Acta. Chem. Scand.*, 8:617, 1954.

[86] G. C. A. Schuit and B. C. Gates. Chemistry and Engineering of Catalytic Hydrodesulfurization. *AICHE Journal*, 19:417, 1973.

[87] F. G. Schwartz, W. L.Whisman, C. S. Allbright, and C. C. Ward. Storability of Gasoline, Causes a Gum Formation, Description of Investigation with Radioactive Marked Indicators. *U.S. Bur. Mines, Bull.*, 626:1, 1964.

[88] S. S. Shih, J. R. Katzer, H. Kwart, and A. B. Stiles. Quinoline Hydrodenitrogenation: Reaction Network and kinetics. *Am. Chem. Soc. Div. Pet. Chem. Priprints*, 22(9):129, 1977.

[89] H. F. Silver, N. H. Wang, H. B. Jensen, and R. E. Poulson. Comparison of Shale Gas Oil Denitrification Reactions over Cobalt-Molybdenum and Nickel-Tungsten Catalysts. *Preprints, Div. Pet. Chem. ACS*, 17(4):G94, 1967.

[90] J. M. Smith. *Chemical Engineering Kinetics.* McGraw Hill Book Co., New York, 1981. 3rd Ed.

[91] L. R. Snyder. Petroleum Nitrogen Compounds and Oxygen Compounds. *Preprints, Div. Pet. Chem. ACS*, 4(2):C43, 1970.

[92] J. Sonnemans, G. H. Van Den Berg, and P. Mars. The Mechanism of Pyridine Hydrogenolysis on Molybdenum Containing Catalysts, II. Hydrogenation of Pyridine to Piperidine. *J. Catal.*, 31:220, 1973.

[93] J. Sonnemans and P. Mars. The Mechanism of Pyridine Hydrogenolysis on Molybdenum-Containing Catalysts. I. The Monolayer MoO_3-Al_2O_3 Catalyst: Preparation and Catalytic Properties. *J. Catal.*, 31:209, 1973.

[94] J. Sonnemans and P. Mars. The Mechanism of Pyridine Hydrogenolysis on Molybdenum-Containing Catalysts, III. Cracking, Hydrocracking, Dehydrogenation, and Disproportionation of Pentylamine. *J. Catal.*, 34:215, 1974.

[95] J. Sonnemans, W. J. Neyens, and P. Mars. The Mechanism of Pyridine Hydrogenolysis on Molybdenum-Containing Catalysts, IV. The Conversion of Piperidine. *J. Catal.*, 34:230, 1974.

[96] E. W. Thiele. Relation Between Catalytic Activity and Size of Particle. *Ind. Eng. Chem.*, 31:916, 1939.

[97] H. Tschamber and E. DeRuiter. *Coal Science, Advances in Chemistry, Series 55.* Am. Chem. Soc., 1966.

[98] Z. Vit and M. Zdrazil. Simultaneous Hydrodenitrogenation of Pyridine and Hydrodesulfurization of Thiophene over Carbon-Supported Platinum Metal Sulfides. *J. Catal.*, 119:1, 1989.

[99] R. J. H. Voorhoeve. Electron Spin Resonance Study of Active Centers in Nickel-Tungsten Sulfide Hydrogenation Catalyst. *J. Catal.*, 23:236, 1971.

[100] R. J. H. Voorhoeve and J. C. M. Stuiver. Kinetics of Hydrogenation on Supported and Bulk Nickel-Tungsten Sulfide Catalyst. *J. Catal.*, 23:228, 1971.

[101] S. M. Walas. *Phase Equilibria in Chemical Engineering.* Butterworth Publishers, MA, USA, 1979.

[102] J. Q. Walker, M. T. Jackson, Jr., and J. B. Maynard. *Chromatographic Systems.* Academic Press, New York, 1972.

[103] R. C. Weast, M. J. Astle, and W. H. Beyer. *CRC Handbook of Chemistry and Physics.* CRC Press, Inc., Boca Raton, Florida, 1986. 66TH Ed.

[104] A. Wheeler. Reaction Rates and Selectivity in Catalyst Pores. *Advances in Catalysis*, 3:249, 1951.

[105] C. Wike and O. Hougen. Mass Transfer in the Flow of Gases through Granular Solids Extended to Low Modified Reynold Numbers. *Transactions of the American Institute of Chemical Engineers*, 41:445, 1945.

[106] K. H. Yang and O. A. Hougen. Detremination of Mechanism of Catalyzed Gaseous Reactions. *Chemical Engineering Progress*, 46(3):146, 1950.

[107] S. H. Yang and C. N. Satterfield. Catalytic Hydrodenitrogenation of Quinoline in a Trickle-Bed Reactor. Effect of Hydrogen Sulfide. *Ind. Eng. Chem. Process Des. Dev.*, 23:20, 1984.

[108] S. H. Yang and C. N. Satterfield. Some Effects of Sulfiding of a NiMo/Alumina Catalyst on its Activity for Hydrodenitrogenation of Quinoline. *J. Catal.*, 81:168, 1983.

[109] F. Yoshida, D. Ramaswami, and O. Hougan. Temperatures and Partial Pressures at the Surfaces of Catalyst Particles. *AICHE J.*, 8(1):5, 1962.

[110] C. Yu, W. J. Hatcher, and W. Bertch. Hydrodenitrogation of Quinoline with Y-Type Zeolite. *Ind. Eng. Chem. Res.*, 28:13, 1989.

Appendix A

Calibration Curves

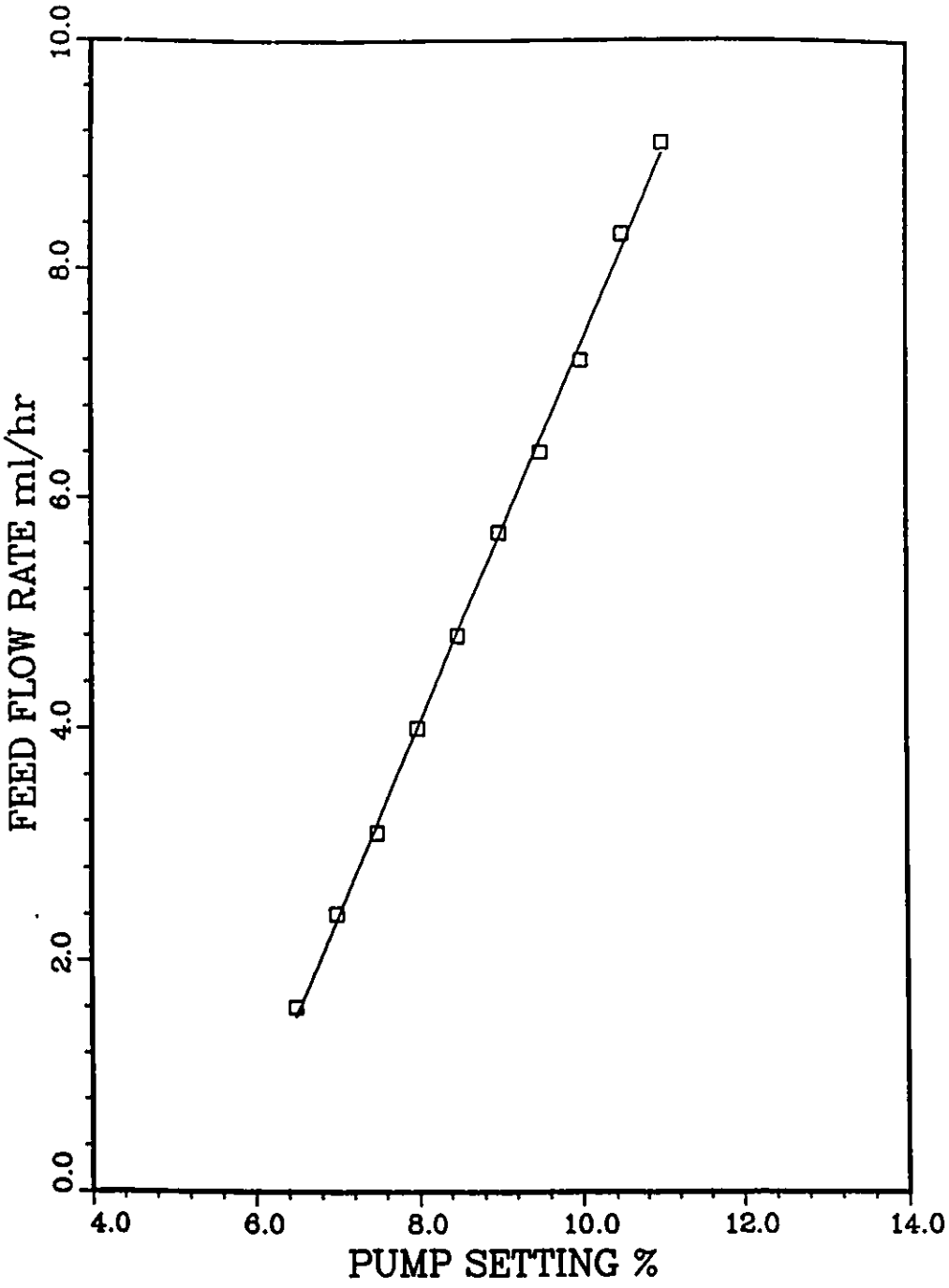

Figure A.1: Metering pump calibration

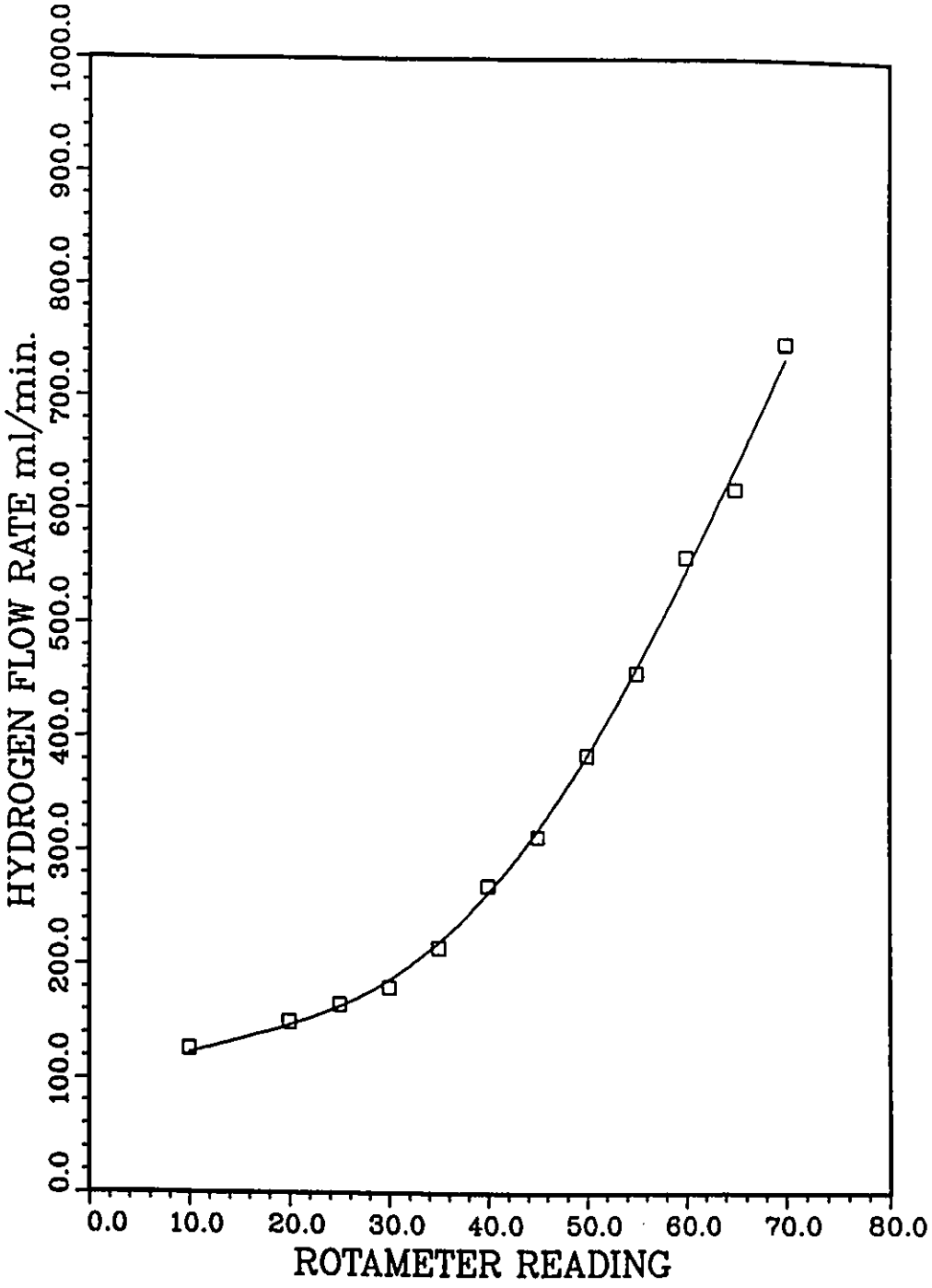

Figure A.2: Rotameter calibration

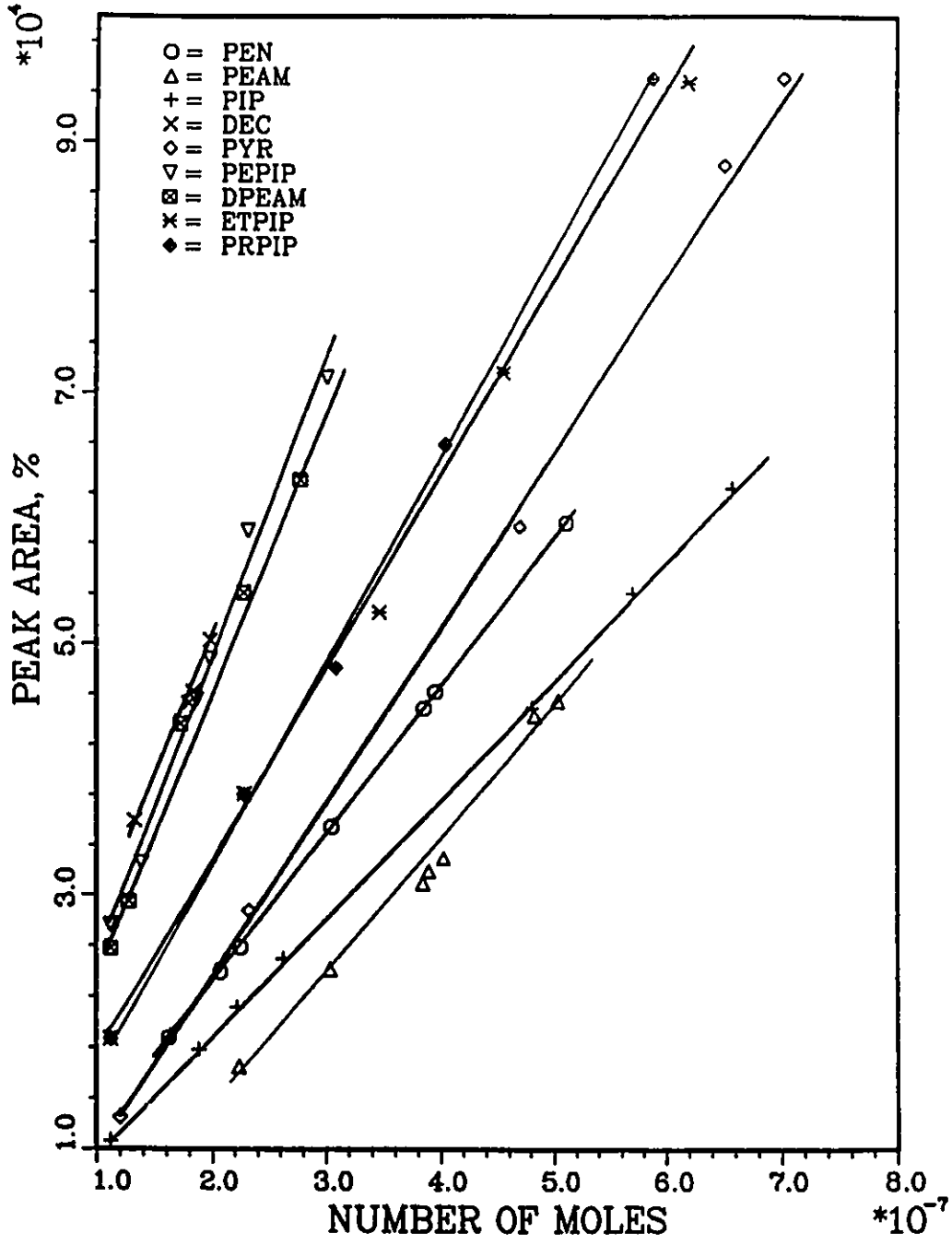

Figure A.3: Gas chromatograph calibration

Appendix B

Experimental Runs

In this Appendix the experimental runs of the kinetic study are presented. The following tables are taken from the output of the computer program that performs the mass balance. Each table shows the run number, the nitro-compound feed, the conditions of the reaction at that run, the mole percent of each organic product, and the percent denitrogenation obtained from each run.

RUN: P225

Feed: Pyridine

Temperature (K)	Pressure (atm)	Molar Ratio (g-mol H2/g-mol feed)
498.00	69.00	13.00

W/F (hr g-cat/g-mol feed)

42.00	70.00	98.00	126.01	153.99	182.02	210.00

Organic Products, mole %							
PEN	0.02	0.03	0.05	0.06	0.08	0.22	0.29
DEC	0.01	0.02	0.03	0.04	0.05	0.05	0.07
PEAM	0.00	0.00	0.00	0.00	0.00	0.00	0.00
ETPIP	0.18	0.50	0.55	0.59	0.66	0.85	1.03
PIP	1.91	2.15	4.56	6.20	7.15	8.78	10.47
PRPIP	0.72	1.38	1.16	1.17	1.31	0.89	0.97
PYR	97.01	95.49	93.20	91.47	90.28	88.48	86.30
PEPIP	0.16	0.27	0.30	0.31	0.30	0.43	0.54
DPEAM	0.00	0.00	0.00	0.00	0.00	0.00	0.00
PNPIP	0.00	0.16	0.15	0.17	0.15	0.29	0.34
MNPIP	0.00	0.00	0.00	0.00	0.00	0.00	0.00
UN.	0.00	0.00	0.00	0.00	0.00	0.00	0.00
Denitrogenation %	0.03	0.05	0.08	0.10	0.13	0.28	0.35

RUN: P250

Feed: Pyridine

Temperature (K)	Pressure (atm)	Molar Ratio (g-mol H2/g-mol feed)
523.00	69.00	13.00

Organic Products, mole %	W/F (hr g-cat/g-mol feed)						
	42.00	70.00	98.00	126.01	153.99	182.02	210.00
PEN	0.03	0.09	11	0.16	0.22	0.64	1.12
DEC	0.02	0.04	0.08	0.11	0.25	0.29	0.34
PEAM	0.00	0.00	0.00	0.00	0.00	0.00	0.00
ETPIP	0.84	1.25	1.57	2.28	3.29	3.96	4.85
PIP	11.95	19.64	26.71	34.04	43.16	48.71	55.95
PRPIP	1.03	1.89	2.51	3.04	3.94	4.37	4.30
PYR	85.30	76.00	67.71	58.82	46.81	39.41	29.51
PEPIP	0.50	0.76	0.94	1.15	1.89	2.12	3.30
DPEAM	0.00	0.00	0.00	0.00	0.00	0.00	0.00
PNPIP	0.32	0.34	0.37	0.40	0.44	0.49	0.63
MNPIP	0.00	0.00	0.00	0.00	0.00	0.00	0.00
UN.	0.00	0.00	0.00	0.00	0.00	0.00	0.00

Denitrogenation %

0.05	0.13	0.19	0.27	0.47	0.93	1.46

RUN: P250R

Feed: Pyridine

Temperature (K)	Pressure (atm)	Molar Ratio (g-mol H2/g-mol feed)
523.00	69.00	13.00

W/F (hr g-cat/g-mol feed)

	42.00	70.00	98.00	126.01	153.99	182.02	210.00
Organic Products, mole %							
PEN	0.02	0.06	0.09	0.10	0.21	0.25	1.21
DEC	0.04	0.07	0.09	0.14	0.25	0.32	0.38
PEAM	0.00	0.00	0.00	0.00	0.00	0.00	0.00
ETPIP	0.60	1.22	1.54	2.12	3.21	3.89	4.76
PIP	10.63	19.82	27.16	31.77	43.45	50.69	58.98
PRPIP	0.67	1.87	2.45	2.71	3.81	3.23	4.30

PYR	87.41	75.81	67.43	60.93	46.77	38.05	25.74
PEPIP	0.51	0.73	0.88	1.45	1.76	2.34	3.31
DPEAM	0.00	0.00	0.00	0.00	0.00	0.00	0.00
PNPIP	0.11	0.41	0.36	0.78	0.53	1.23	1.34
MNPIP	0.00	0.00	0.00	0.00	0.00	0.00	0.00
UN.	0.00	0.00	0.00	0.00	0.00	0.00	0.00

Denitrogenation %

0.07	0.13	0.18	0.24	0.46	0.57	1.58

RUN: P275

Feed: Pyridine

Temperature (K)	Pressure (atm)	Molar Ratio (g-mol H2/g-mol feed)
548.00	69.00	13.00

W/F (hr g-cat/g-mol feed)

42.00	70.00	98.00	126.01	153.99	182.02	210.00

Organic

Products,

mole %							
PEN	0.08	0.11	0.17	0.30	0.62	1.05	1.33
DEC	0.13	0.27	0.42	0.56	0.62	0.63	0.62
PEAM	0.00	0.00	0.00	0.00	0.00	0.00	0.00
ETPIP	1.98	3.44	4.60	6.59	7.73	8.78	8.56
PIP	23.48	37.42	46.36	54.01	58.50	61.98	61.23
PRPIP	2.13	3.93	4.18	5.16	5.62	6.34	5.77
PYR	71.38	52.97	41.89	30.31	22.94	16.69	14.53
PEPIP	0.77	1.82	2.29	2.95	3.73	4.20	7.19
DPEAM	0.00	0.00	0.00	0.00	0.00	0.00	0.00
PNPIP	0.05	0.04	0.08	0.13	0.25	0.33	0.77
MNPIP	0.00	0.00	0.00	0.00	0.00	0.00	0.00
UN.	0.00	0.00	0.00	0.00	0.00	0.00	0.00

Denitrogenation %

0.21	0.38	0.60	0.86	1.24	1.68	1.94

RUN: P275R

Feed: Pyridine

Temperature (K)	Pressure (atm)	Molar Ratio (g-mol H2/g-mol feed)
548.00	69.00	13.00

	W/F (hr g-cat/g-mol feed)						
	42.00	70.00	98.00	126.01	153.99	182.02	210.00
Organic Products, mole %							
PEN	0.08	0.12	0.16	0.45	0.36	0.55	1.35
DEC	0.13	0.24	0.44	0.52	0.55	0.68	0.87
PEAM	0.00	0.00	0.00	0.00	0.00	0.00	0.00
ETPIP	1.94	3.51	4.43	6.66	7.58	8.67	6.55
PIP	24.62	38.97	45.03	47.76	53.76	55.46	65.63
PRPIP	2.30	3.80	4.03	4.97	5.30	6.30	6.38
PYR	70.14	51.77	43.49	36.50	28.67	24.32	10.54
PEPIP	0.78	1.56	2.36	3.04	3.50	3.70	7.99
DPEAM	0.00	0.00	0.00	0.00	0.00	0.00	0.00
PNPIP	0.01	0.02	0.07	0.09	0.27	0.32	0.70
MNPIP	0.00	0.00	0.00	0.00	0.00	0.00	0.00
UN.	0.00	0.00	0.00	0.00	0.00	0.00	0.00
Denitrogenation %	0.22	0.36	0.60	0.97	0.91	1.23	2.21

RUN: P300

Feed: Pyridine

Temperature (K)	Pressure (atm)	Molar Ratio (g-mol H2/g-mol feed)
573.00	69.00	13.00

W/F (hr g-cat/g-mol feed)

Organic Products, mole %	42.00	70.00	98.00	126.01	153.99	182.02	210.00
PEN	0.33	0.62	1.09	1.43	1.93	2.48	3.27
DEC	0.38	0.57	0.88	1.11	1.25	1.19	1.35
PEAM	0.00	0.00	0.00	0.00	0.00	0.00	0.00
ETPIP	4.34	7.64	7.04	10.05	10.77	10.74	11.75
PIP	37.48	48.50	55.92	56.78	60.24	60.72	60.87
PRPIP	3.35	5.02	6.05	6.56	6.36	6.93	7.14
PYR	48.20	32.83	23.61	18.86	14.99	13.63	11.58
PEPIP	5.48	4.60	4.89	4.58	3.89	3.73	3.50
DPEAM	0.00	0.00	0.00	0.00	0.00	0.04	0.01

PNPIP	0.44	0.22	0.53	0.64	0.56	0.53	0.54
MNPIP	0.00	0.00	0.00	0.00	0.00	0.00	0.00
UN.	0.00	0.00	0.00	0.00	0.00	0.00	0.00

Denitrogenation %

0.71	1.19	1.96	2.53	3.18	3.67	4.62

RUN: P325

Feed: Pyridine

Temperature (K)	Pressure (atm)	Molar Ratio (g-mol H2/g-mol feed)
598.00	69.00	13.00

W/F (hr g-cat/g-mol feed)

	42.00	70.00	98.00	126.01	153.99	182.02	210.00
Organic Products, mole %							
PEN	2.60	3.44	4.70	5.82	7.03	7.88	9.49
DEC	1.60	2.28	2.24	2.23	2.19	2.49	3.36

PEAM	0.00	0.00	0.00	0.00	0.00	0.00	0.00
ETPIP	5.19	6.64	6.99	6.98	7.33	7.62	11.08
PIP	49.89	56.32	59.24	60.83	61.76	61.56	50.59
PRPIP	2.90	3.73	3.89	3.95	4.24	4.55	5.73
PYR	29.88	16.73	11.60	8.68	6.50	5.34	4.92
PEPIP	7.21	9.85	10.27	10.45	9.83	9.53	12.44
DPEAM	0.10	0.16	0.18	0.20	0.14	0.11	0.20
PNPIP	0.34	0.43	0.54	0.58	0.74	0.73	1.35
MNPIP	0.29	0.42	0.34	0.28	0.24	0.19	0.83
UN.	0.00	0.00	0.00	0.00	0.00	0.00	0.00

Denitrogenation %

4.20	5.71	6.94	8.04	9.22	10.37	12.85

RUN: P350

Feed: Pyridine

Temperature (K)	Pressure (atm)	Molar Ratio (g-mol H2/g-mol feed)
623.00	69.00	13.00

W/F (hr g-cat/g-mol feed)

	42.00	70.00	98.00	126.01	153.99	182.02	210.00
Organic Products, mole %							
PEN	5.54	8.75	10.68	12.00	13.66	14.47	16.00
DEC	2.39	2.67	2.70	2.97	3.42	3.91	5.35
PEAM	0.00	0.00	0.00	0.00	0.00	0.00	0.00
ETPIP	14.50	31.17	44.83	63.05	63.15	64.90	56.47
PIP	46.86	32.11	22.89	5.02	4.72	4.30	5.32
PRPIP	5.01	6.57	6.25	6.16	6.38	6.74	8.33
PYR	18.15	7.55	4.57	3.27	2.35	0.00	0.00
PEPIP	7.11	9.51	6.37	4.25	3.99	3.84	3.34
DPEAM	0.27	0.58	0.47	0.35	0.34	0.32	1.27
PNPIP	0.07	0.19	0.75	2.66	1.74	1.32	1.58
MNPIP	0.09	0.90	0.49	0.28	0.25	0.20	2.35
UN.	0.00	0.00	0.00	0.00	0.00	0.00	0.00
Denitrogenation %	7.93	11.42	13.38	14.97	17.08	18.38	21.35

RUN: P375

Feed: Pyridine

Temperature (K)	Pressure (atm)	Molar Ratio (g-mol H2/g-mol feed)
648.00	69.00	13.00

	W/F (hr g-cat/g-mol feed)						
	42.00	70.00	98.00	126.01	153.99	182.02	210.00
Organic Products, mole %							
PEN	16.14	22.40	24.71	28.09	29.51	30.82	36.15
DEC	5.82	7.61	8.14	7.95	8.50	8.92	8.78
PEAM	0.00	0.00	0.00	0.00	0.00	0.00	0.00
ETPIP	31.37	49.72	49.09	47.74	45.96	44.85	43.04
PIP	12.46	5.67	4.53	2.79	4.18	5.06	2.74
PRPIP	9.29	9.15	8.48	7.90	7.83	7.84	6.45
PYR	19.37	0.39	0.00	0.00	0.00	0.00	0.00
PEPIP	3.59	1.59	1.17	0.88	1.00	1.15	0.71
DPEAM	0.32	0.05	0.02	0.00	0.00	0.02	0.00
PNPIP	1.02	2.87	3.45	4.22	2.65	0.95	2.13
MNPIP	0.63	0.55	0.41	0.44	0.37	0.39	0.00
UN.	0.00	0.00	0.00	0.00	0.00	0.00	0.00

Denitrogenation %

21.97	30.01	32.85	36.04	38.01	39.74	44.93

RUN: P400

Feed: Pyridine

Temperature (K)	Pressure (atm)	Molar Ratio (g-mol H2/g-mol feed)
673.00	69.00	13.00

W/F (hr g-cat/g-mol feed)

	42.00	70.00	98.00	126.01	153.99	182.02	210.00
Organic Products, mole %							
PEN	20.31	29.79	31.80	34.08	36.09	36.87	42.33
DEC	7.72	9.04	9.60	10.47	10.70	11.03	9.12
PEAM	0.00	0.00	0.00	0.00	0.00	0.00	0.00
ETPIP	35.81	45.91	42.54	39.65	39.23	37.06	34.89
PIP	9.74	3.96	3.98	3.91	3.85	3.80	3.63

PRPIP	8.59	8.23	7.89	7.40	7.42	7.06	6.84
PYR	10.92	0.00	0.00	0.00	0.00	0.00	0.00
PEPIP	2.56	0.27	0.33	0.36	0.48	0.58	0.68
DPEAM	0.50	0.00	0.00	0.00	0.00	0.00	0.00
PNPIP	1.92	2.00	1.92	1.71	1.81	1.68	1.62
MNPIP	1.91	0.78	1.95	2.42	0.43	1.91	0.89
UN.	0.00	0.00	0.00	0.00	0.00	0.00	0.00

Denitrogenation %

28.03	38.83	41.40	44.54	46.79	47.90	51.45

RUN: PR13

Feed: Pyridine

Temperature (K)	Pressure (atm)	Space Time (hr g-cat/g-mol feed)
623.00	69.00	126.01

R (g-mol-H2/g-mol feed)

	7.00	10.00	13.00	16.00	19.00
Organic					

Products,

	mole %				
PEN	9.56	10.78	10.95	11.69	12.85
DEC	1.88	2.54	2.83	3.54	4.06
PEAM	0.00	1.77	1.73	1.43	1.31
ETPIP	56.39	52.94	54.04	51.92	47.27
PIP	7.15	8.20	8.67	6.20	8.10
PRPIP	4.96	5.57	4.76	4.73	4.64
PYR	2.84	1.55	1.15	1.10	1.36
PEPIP	2.93	3.50	3.57	3.20	4.16
DPEAM	0.18	0.35	0.49	0.49	0.36
PNPIP	1.15	1.50	2.42	3.21	3.11
MNPIP	1.27	1.04	0.32	0.90	1.43
UN.	11.70	10.25	9.08	11.58	11.35

Denitrogenation %

11.44	13.32	13.78	15.23	16.92

RUN: Q225

Feed: Quinoline

Temperature (K)	Pressure (atm)	Molar Ratio (g-mol H2/g-mol feed)
498.00	69.00	13.00

	W/F (hr g-cat/g-mol feed)						
	42.00	70.00	98.00	126.01	153.99	182.02	210.00
Organic Products, mole %							
MCH	0.00	0.00	0.00	0.00	0.00	0.00	0.00
ECH	0.00	0.00	0.00	0.00	0.00	0.00	0.00
PCH	0.00	0.00	0.00	0.00	0.00	0.00	0.00
PCHE	0.00	0.00	0.00	0.00	0.00	0.00	0.00
PCHAM	0.00	0.00	0.00	0.05	0.00	0.00	0.00
PB	0.00	0.00	0.00	0.00	0.00	0.00	0.00
MEB	0.01	0.02	0.04	0.06	0.08	0.12	0.23
IDAN	0.00	0.00	0.01	0.02	0.03	0.03	0.07
UN.	0.00	0.00	0.00	0.00	0.00	0.00	0.00
DHQ	0.00	0.00	0.00	0.00	0.00	0.30	0.34
EB	0.00	0.00	0.00	0.00	0.00	0.00	0.00
AN	0.00	0.05	0.16	0.20	0.08	0.06	0.00
BZTHQ	2.64	3.90	4.20	5.36	2.68	2.32	1.56
EAN	0.18	0.35	0.42	0.24	0.28	0.12	1.96
OPA	0.23	0.40	0.54	1.12	0.53	0.58	0.50
Q	34.94	26.21	23.59	21.93	20.03	19.61	19.22

PYTHQ	61.99	69.06	71.04	71.01	76.29	76.85	76.13

Denitrogenation %

	0.01	0.03	0.05	0.08	0.11	0.16	0.30

RUN: Q250

Feed: Quinoline

Temperature (K)	Pressure (atm)	Molar Ratio (g-mol H2/g-mol feed)
523.00	69.00	13.00

W/F (hr g-cat/g-mol feed)

42.00	70.00	98.00	126.01	153.99	182.02	210.00

Organic Products, mole %							
MCH	0.00	0.00	0.00	0.00	0.00	0.00	0.00
ECH	0.00	0.00	0.00	0.00	0.00	0.01	0.01
PCH	0.00	0.00	0.00	0.00	0.02	0.08	0.19
PCHE	0.00	0.00	0.00	0.00	0.03	0.04	0.06

PCHAM	0.00	0.00	0.00	0.07	0.07	0.05	0.08
PB	0.00	0.00	0.00	0.00	0.01	0.04	0.04
MEB	0.00	0.05	0.11	0.16	0.16	0.26	0.44
IDAN	0.00	0.00	0.00	0.03	0.04	0.05	0.07
UN.	0.00	0.00	0.00	0.00	0.00	0.00	0.00
DHQ	0.00	0.19	1.69	2.81	3.38	3.92	4.36
EB	0.00	0.00	0.00	0.00	0.00	0.00	0.00
AN	0.00	0.00	0.00	0.55	0.45	0.64	0.19
BZTHQ	1.63	2.36	7.94	9.92	10.61	11.32	10.95
EAN	0.00	0.29	0.26	0.98	1.03	1.39	0.29
OPA	0.00	0.56	2.14	1.47	1.42	1.32	0.81
Q	18.00	12.34	10.10	9.41	9.24	9.19	9.12
PYTHQ	80.37	84.21	77.76	74.60	73.54	71.67	73.37

Denitrogenation %

0.01	0.06	0.11	0.19	0.27	0.48	0.83

RUN: Q275

Feed: Quinoline

Temperature (K)	Pressure (atm)	Molar Ratio (g-mol H2/g-mol feed)
548.00	69.00	13.00

	W/F (hr g-cat/g-mol feed)						
	42.00	70.00	98.00	126.01	153.99	182.02	210.00
Organic Products, mole %							
MCH	0.00	0.00	0.00	0.00	0.00	0.00	0.00
ECH	0.00	0.00	0.00	0.00	0.00	0.01	0.02
PCH	0.00	0.00	0.00	0.08	0.25	0.31	0.67
PCHE	0.00	0.00	0.00	0.01	0.10	0.12	0.19
PCHAM	0.00	0.00	0.00	0.12	0.08	0.11	0.10
PB	0.00	0.00	0.00	0.06	0.04	0.08	0.12
MEB	0.05	0.12	0.31	0.29	0.38	0.52	0.77
IDAN	0.01	0.01	0.01	0.05	0.04	0.03	0.07
UN.	0.00	0.00	0.00	0.00	0.04	0.04	0.00
DHQ	0.00	2.13	3.94	4.99	5.65	6.18	7.65
EB	0.00	0.00	0.00	0.00	0.00	0.00	0.00
AN	0.00	0.08	0.11	0.39	0.48	0.20	0.22
BZTHQ	3.27	5.42	7.24	9.07	9.03	10.88	11.06
EAN	0.15	0.54	0.70	0.99	1.07	1.12	0.71
OPA	0.14	1.07	1.43	1.25	1.41	1.39	1.41
Q	13.55	9.41	8.63	7.92	7.85	7.28	7.52

PYTHQ	82.84	81.24	77.63	74.77	73.59	71.72	69.49

Denitrogenation %

	0.05	0.12	0.31	0.50	0.81	1.07	1.83

RUN: Q300

Feed: Quinoline

Temperature (K)	Pressure (atm)	Molar Ratio (g-mol H2/g-mol feed)
573.00	69.00	13.00

W/F (hr g-cat/g-mol feed)

	42.00	70.00	98.00	126.01	153.99	182.02	210.00
Organic Products, mole %							
MCH	0.00	0.00	0.00	0.00	0.00	0.00	0.00
ECH	0.00	0.00	0.00	0.00	0.00	0.01	0.01
PCH	0.00	0.00	0.03	0.05	0.70	1.01	1.89
PCHE	0.00	0.00	0.00	0.07	0.19	0.26	0.38

PCHAM	0.00	0.00	0.00	0.12	0.06	0.07	0.10
PB	0.00	0.00	0.07	0.17	0.19	0.21	0.23
MEB	0.06	0.30	0.49	0.53	0.59	0.73	0.92
IDAN	0.01	0.01	0.01	0.05	0.02	0.03	0.05
UN.	0.00	0.00	0.00	0.00	0.06	0.08	0.09
DHQ	1.09	2.97	4.21	7.30	8.14	8.78	7.93
EB	0.00	0.00	0.00	0.00	0.00	0.00	0.00
AN	0.13	0.13	0.22	0.16	0.18	0.14	0.19
BZTHQ	8.06	9.63	10.23	12.70	11.15	9.76	10.48
EAN	0.36	0.72	0.90	0.85	1.03	0.80	1.31
OPA	0.86	0.75	1.00	1.05	1.37	1.48	1.64
Q	13.07	9.43	8.06	8.15	7.88	7.59	7.34
PYTHQ	76.37	76.06	74.78	68.80	68.46	69.04	67.44

Denitrogenation %

0.07	0.31	0.60	0.87	1.68	2.25	3.48

RUN: Q325

Feed: Quinoline

Temperature	Pressure	Molar Ratio
(K)	(atm)	(g-mol H2/g-mol feed)
598.00	69.00	13.00

	W/F (hr g-cat/g-mol feed)						
	42.00	70.00	98.00	126.01	153.99	182.02	210.00
Organic Products, mole %							
MCH	0.00	0.00	0.00	0.00	0.00	0.00	0.00
ECH	0.00	0.00	0.00	0.00	0.00	0.02	0.07
PCH	0.03	0.21	0.91	0.76	2.04	2.73	5.76
PCHE	0.18	0.27	0.32	0.32	0.33	0.62	0.97
PCHAM	0.06	0.00	0.05	0.05	0.10	0.11	0.15
PB	0.00	0.00	0.15	0.46	0.46	0.55	0.84
MEB	0.34	0.60	0.71	0.89	0.93	0.91	1.28
IDAN	0.02	0.01	0.02	0.06	0.02	0.03	0.10
UN.	0.00	0.00	0.00	0.19	0.11	0.07	0.11
DHQ	2.09	5.35	7.23	13.64	11.91	13.74	10.75
EB	0.00	0.00	0.00	0.00	0.00	0.00	0.00
AN	0.81	0.49	0.33	0.42	0.33	0.16	0.44
BZTHQ	15.48	20.60	20.08	17.66	19.41	14.85	13.57
EAN	0.81	1.89	1.00	1.06	2.74	1.01	1.52
OPA	1.94	1.56	1.79	1.81	1.53	1.80	2.06
Q	12.68	8.88	7.79	7.55	6.98	6.97	6.54

PYTHQ	65.57	60.13	59.61	55.13	53.11	56.43	55.84
Denitrogenation %							
	0.57	1.09	2.11	2.48	3.78	4.86	9.01

RUN: Q350

Feed: Quinoline

Temperature (K)	Pressure (atm)	Molar Ratio (g-mol H2/g-mol feed)
623.00	69.00	13.00

	W/F (hr g-cat/g-mol feed)						
	42.00	70.00	98.00	126.01	153.99	182.02	210.00
Organic Products, mole %							
MCH	0.01	0.01	0.02	0.03	0.02	0.06	0.12
ECH	0.01	0.01	0.03	0.04	0.03	0.11	0.19
PCH	0.31	1.65	3.06	4.52	6.52	10.94	18.28
PCHE	0.12	0.45	0.79	0.91	0.96	1.29	1.50

PCHAM	0.05	0.04	0.08	0.08	0.02	0.12	0.22
PB	0.12	0.22	0.52	0.91	0.99	1.36	1.73
MEB	0.41	0.65	0.91	1.12	0.94	0.99	1.49
IDAN	0.03	0.01	0.02	0.02	0.03	0.05	0.04
UN.	0.04	0.15	0.24	0.45	0.71	0.67	0.63
DHQ	4.00	5.99	8.85	14.47	14.50	11.81	9.41
EB	0.04	0.00	0.01	0.00	0.04	0.06	0.00
AN	0.60	0.44	0.54	0.47	0.29	0.55	0.86
BZTHQ	23.99	28.86	30.52	27.70	27.84	26.14	22.55
EAN	0.38	0.47	0.56	0.26	1.33	1.32	1.80
OPA	1.89	3.17	3.27	3.18	4.26	4.05	3.06
Q	11.96	8.89	7.89	7.81	7.41	7.00	6.74
PYTHQ	56.05	48.99	42.67	38.03	34.10	33.50	31.37

Denitrogenation %

1.05	3.00	5.36	7.55	9.53	14.85	23.36

RUN: Q375

Feed: Quinoline

Temperature (K)	Pressure (atm)	Molar Ratio (g-mol H2/g-mol feed)
648.00	69.00	13.00

	W/F (hr g-cat/g-mol feed)						
	42.00	70.00	98.00	126.01	153.99	182.02	210.00
Organic Products, mole %							
MCH	0.05	0.10	0.11	0.13	0.17	0.18	0.16
ECH	0.04	0.07	0.07	0.09	0.11	0.19	0.22
PCH	1.00	2.55	4.85	7.60	12.69	18.74	25.32
PCHE	0.29	0.39	0.98	1.08	0.99	1.05	0.79
PCHAM	0.08	0.09	0.24	0.31	0.34	0.42	0.41
PB	0.31	0.47	0.80	1.34	1.50	1.64	1.66
MEB	0.42	0.49	0.95	1.02	0.80	0.97	1.16
IDAN	0.03	0.03	0.02	0.05	0.04	0.03	0.04
UN.	0.03	0.14	0.19	0.25	0.45	0.54	0.55
DHQ	6.02	8.46	9.49	11.65	12.84	9.96	7.92
EB	0.04	0.00	0.00	0.00	0.05	0.09	0.00
AN	0.77	0.78	0.68	0.62	0.58	0.53	0.39
BZTHQ	33.68	35.85	36.43	41.05	35.74	30.69	31.82
EAN	0.49	0.59	0.64	0.70	0.67	0.84	0.54
OPA	3.82	5.72	5.12	4.76	5.33	6.27	6.44
Q	9.25	6.56	5.89	5.83	5.83	5.50	5.13

PYTHQ	43.67	37.70	33.55	23.52	21.85	22.36	17.45
Denitrogenation %							
	2.18	4.09	7.78	11.31	16.35	22.88	29.35

RUN: Q375R

Feed: Quinoline

Temperature (K)	Pressure (atm)	Molar Ratio (g-mol H2/g-mol feed)
623.00	69.00	13.00

W/F (hr g-cat/g-mol feed)

	40.00	70.01	100.00	130.01	160.00	190.04	210.00
Organic Products, mole %							
MCH	0.01	0.02	0.03	0.05	0.12	0.12	0.18
ECH	0.01	0.02	0.04	0.05	0.09	0.09	0.12
PCH	0.48	1.25	4.57	7.86	11.88	11.59	16.33
PCHE	0.30	0.96	1.29	1.77	0.67	1.78	1.59

PCHAM	0.06	0.07	0.08	0.13	0.09	0.25	0.12
PB	0.27	0.60	0.61	0.96	0.85	1.25	1.18
MEB	0.64	0.99	0.84	1.48	0.63	0.95	1.11
IDAN	0.03	0.03	0.03	0.04	0.05	0.05	0.03
UN.	0.26	0.49	0.55	0.61	0.56	0.53	0.44
DHQ	5.28	8.06	10.18	15.17	11.96	11.47	9.92
EB	0.00	0.06	0.00	0.00	0.04	0.02	0.00
AN	0.91	0.73	0.94	1.07	0.90	1.55	0.97
BZTHQ	33.86	28.37	30.32	27.51	34.22	31.20	32.51
EAN	0.92	0.00	1.29	0.79	2.52	1.53	1.55
OPA	3.26	5.43	3.58	3.70	5.25	4.97	4.22
Q	5.52	5.76	5.09	5.59	4.48	5.37	5.56
PYTHQ	48.20	47.16	40.55	33.21	25.69	27.27	24.17

Denitrogenation %

1.73	3.93	7.42	12.22	14.33	15.86	20.55

RUN: Q400

Feed: Quinoline

Temperature (K)	Pressure (atm)	Molar Ratio (g-mol H2/g-mol feed)
673.00	69.00	13.00

	W/F (hr g-cat/g-mol feed)						
	42.00	70.00	98.00	126.01	153.99	182.02	210.00
Organic Products, mole %							
MCH	0.01	0.02	0.03	0.03	0.05	0.06	0.05
ECH	0.03	0.03	0.05	0.06	0.09	0.11	0.07
PCH	4.87	6.21	8.24	10.98	13.54	23.19	25.22
PCHE	1.24	1.47	1.71	1.79	2.12	2.00	1.92
PCHAM	0.15	0.26	0.26	0.13	0.16	0.16	0.15
PB	0.69	1.06	1.26	1.46	1.61	1.55	1.56
MEB	0.90	1.13	1.31	1.52	1.67	1.35	0.98
IDAN	0.03	0.05	0.05	0.05	0.09	0.10	0.12
UN.	0.27	0.56	0.59	0.62	0.71	0.49	0.69
DHQ	10.22	10.94	11.07	10.72	11.85	11.26	9.86
EB	0.05	0.06	0.07	0.06	0.08	0.10	0.12
AN	1.34	1.21	1.01	0.88	1.08	1.02	0.99
BZTHQ	48.34	48.52	48.80	47.03	38.38	29.85	28.50
EAN	0.64	0.53	0.45	0.45	0.77	1.09	2.06
OPA	9.46	8.02	6.92	6.77	8.50	10.03	10.23
Q	9.52	6.71	5.01	4.63	4.27	4.02	3.62

PYTHQ	12.24	13.19	13.17	12.83	15.05	13.64	13.85

Denitrogenation %

7.83	10.04	12.72	15.96	19.23	28.45	30.04

RUN: Q3505

Feed: Quinoline

Temperature (K)	Pressure (atm)	Molar Ratio (g-mol H2/g-mol feed)
623.00	34.50	13.00

W/F (hr g-cat/g-mol feed)

	42.00	70.00	98.00	126.01	153.99	182.02	210.00
Organic Products, mole %							
MCH	0.00	0.00	0.00	0.00	0.02	0.01	0.02
ECH	0.00	0.00	0.00	0.00	0.03	0.03	0.04
PCH	0.04	0.09	0.30	0.30	0.74	1.21	1.43
PCHE	0.00	0.00	0.11	0.12	0.25	0.58	0.72

PCHAM	0.00	0.00	0.00	0.00	0.07	0.17	0.25
PB	0.00	0.00	0.13	0.17	0.21	0.56	0.59
MEB	0.04	0.17	0.20	0.24	0.26	0.63	0.79
IDAN	0.00	0.00	0.00	0.00	0.03	0.12	0.16
UN.	0.00	0.00	0.00	0.00	0.00	0.00	0.00
DHQ	0.85	1.70	1.36	1.14	2.17	1.96	3.24
EB	0.00	0.00	0.00	0.00	0.00	0.00	0.00
AN	0.00	0.14	0.36	1.15	1.15	2.07	3.00
BZTHQ	16.50	18.68	24.96	47.31	45.80	49.40	65.07
EAN	0.00	0.18	0.17	1.56	1.52	0.61	1.25
OPA	1.20	1.03	1.35	2.56	2.63	2.23	2.48
Q	37.44	24.54	23.28	15.15	14.51	13.50	8.77
PYTHQ	43.94	53.48	47.77	30.29	30.62	26.93	12.20

Denitrogenation %

0.08	0.26	0.74	0.83	1.53	3.13	3.75

RUN: PQ225

Feed: Pyridine-Quinoline

Temperature (K)	Pressure (atm)	Molar Ratio (g-mol H2/g-mol feed)
498.00	69.00	13.00

	W/F (hr g-cat/g-mol feed)						
	42.00	70.00	98.00	126.01	153.99	182.02	210.00
Organic Products, mole %							
PEN	0.00	0.00	0.00	0.00	0.00	0.00	0.00
DEC	0.00	0.00	0.00	0.00	0.00	0.00	0.00
PEAM	0.00	0.00	0.00	0.00	0.00	0.00	0.00
ETPIP	0.00	0.00	0.00	0.00	0.00	0.00	0.00
PIP	0.15	0.05	0.16	0.09	0.18	0.29	0.54
PRPIP	0.00	0.00	0.00	0.00	0.00	0.00	0.00
PYR	48.23	48.43	47.33	45.79	44.28	43.53	42.12
PEPIP	0.00	0.05	0.08	0.04	0.04	0.04	0.11
DPEAM	0.00	0.00	0.00	0.00	0.00	0.00	0.00
PNPIP	0.00	0.00	0.00	0.00	0.00	0.00	0.00
MNPIP	0.00	0.00	0.00	0.00	0.00	0.00	0.00
UN.	0.00	0.00	0.00	0.00	0.00	0.00	0.00
MCH	0.00	0.00	0.00	0.00	0.00	0.00	0.00
ECH	0.00	0.00	0.00	0.00	0.00	0.00	0.00
PCH	0.00	0.09	0.16	0.23	0.28	0.37	0.47
PCHE	0.00	0.00	0.00	0.00	0.00	0.00	0.00
PCHAM	0.00	0.00	0.00	0.00	0.00	0.00	0.00

PB	0.00	0.00	0.00	0.00	0.00	0.00	0.00
MEB	0.00	0.00	0.00	0.00	0.00	0.00	0.00
IDAN	0.00	0.00	0.00	0.00	0.00	0.00	0.00
UN.	0.00	0.00	0.00	0.00	0.00	0.00	0.00
DHQ	0.00	0.00	0.00	0.00	0.00	0.00	0.00
EB	0.00	0.00	0.00	0.00	0.00	0.00	0.00
AN	0.00	0.00	0.00	0.00	0.00	0.00	0.00
BZTHQ	0.00	0.00	0.00	0.00	0.00	0.00	0.00
EAN	0.00	0.00	0.00	0.00	0.00	0.00	0.00
OPA	0.00	0.00	0.00	0.00	0.00	0.00	0.00
Q	13.68	8.84	7.39	5.89	6.33	5.87	4.46
PYTHQ	37.94	42.54	44.87	47.96	48.89	49.90	52.29

Denitrogenation %

0.00	0.09	0.16	0.23	0.28	0.37	0.47

RUN: PQ300

Feed: Pyridine-Quinoline

Temperature (K)	Pressure (atm)	Molar Ratio (g-mol H2/g-mol feed)
573.00	69.00	13.00

	W/F (hr g-cat/g-mol feed)						
	42.00	70.00	98.00	126.01	153.99	182.02	210.00
Organic Products, mole %							
PEN	0.00	0.00	0.00	0.00	0.00	0.00	0.00
DEC	0.00	0.00	0.00	0.00	0.00	0.00	0.00
PEAM	0.00	0.00	0.00	0.00	0.00	0.00	0.00
ETPIP	0.00	0.00	0.00	0.00	0.00	0.00	0.00
PIP	6.46	8.87	11.95	12.98	16.38	17.38	17.72
PRPIP	0.00	0.00	0.00	0.00	0.00	0.00	0.00
PYR	28.55	27.77	22.63	20.31	17.50	17.21	15.97
PEPIP	0.86	0.88	1.21	2.84	3.20	3.19	3.19
DPEAM	0.00	0.00	0.00	0.00	0.00	0.00	0.00
PNPIP	0.00	0.00	0.00	0.00	0.00	0.00	0.00
MNPIP	0.00	0.00	0.00	0.00	0.00	0.00	0.00
UN.	0.00	0.00	0.00	0.00	0.00	0.00	0.00
MCH	0.00	0.00	0.00	0.00	0.00	0.00	0.00
ECH	0.00	0.00	0.00	0.00	0.00	0.00	0.00
PCH	0.55	0.84	1.11	1.69	2.29	3.12	4.09
PCHE	0.00	0.00	0.00	0.00	0.00	0.00	0.00
PCHAM	0.00	0.00	0.00	0.00	0.00	0.00	0.00

PB	0.00	0.00	0.00	0.00	0.00	0.00	0.00
MEB	0.00	0.00	0.00	0.00	0.00	0.00	0.00
IDAN	0.00	0.00	0.00	0.00	0.00	0.00	0.00
UN.	0.00	0.00	0.00	0.00	0.00	0.00	0.00
DHQ	6.44	6.47	6.76	8.86	9.48	9.72	9.88
EB	0.00	0.00	0.00	0.00	0.00	0.00	0.00
AN	0.00	0.00	0.00	0.00	0.00	0.00	0.00
BZTHQ	0.47	0.58	0.61	0.72	0.00	0.55	0.00
EAN	0.00	0.00	0.00	0.00	0.00	0.00	0.00
OPA	0.00	0.00	0.00	0.00	0.00	0.00	0.00
Q	7.67	2.47	2.53	2.70	3.00	3.06	2.95
PYTHQ	48.99	52.13	53.21	49.89	48.14	45.76	46.20

Denitrogenation %

0.55	0.84	1.11	1.69	2.29	3.12	4.09

RUN: PQ350

Feed: Pyridine-Quinoline

Temperature (K)	Pressure (atm)	Molar Ratio (g-mol H2/g-mol feed)
623.00	69.00	13.00

	W/F (hr g-cat/g-mol feed)						
	42.00	70.00	98.00	126.01	153.99	182.02	210.00
Organic Products, mole %							
PEN	0.00	0.00	0.00	0.10	0.17	0.22	0.32
DEC	0.00	0.00	0.00	0.00	0.00	0.00	0.00
PEAM	0.00	0.00	0.00	0.00	0.00	0.00	0.00
ETPIP	0.29	0.00	0.31	0.60	0.75	1.29	1.48
PIP	0.42	0.16	0.67	0.76	0.85	1.81	1.97
PRPIP	2.59	0.17	0.51	2.08	0.82	1.08	1.26
PYR	8.02	5.85	3.85	2.44	1.20	1.29	0.77
PEPIP	2.95	3.15	3.38	3.30	2.80	2.02	1.52
DPEAM	0.00	0.00	0.00	0.00	0.00	0.00	0.00
PNPIP	0.00	0.00	0.00	0.00	0.00	0.00	0.00
MNPIP	0.00	0.00	0.00	0.00	0.00	0.00	0.00
UN.	0.00	0.00	0.00	0.00	0.00	0.00	0.00
MCH	0.00	0.00	0.00	0.00	0.00	0.19	0.57
ECH	0.00	0.00	0.00	0.00	0.00	0.24	0.66
PCH	1.16	2.44	3.92	6.56	14.60	23.72	25.88
PCHE	0.00	0.00	0.00	0.00	0.00	0.00	0.00
PCHAM	0.00	0.00	0.00	0.00	0.00	0.00	0.00

PB	0.00	0.00	0.00	0.00	0.00	0.00	0.00
MEB	0.00	0.00	0.00	0.00	0.00	0.00	0.00
IDAN	0.00	0.00	0.00	0.20	0.15	0.21	0.19
UN.	0.00	0.00	0.00	0.23	0.29	0.22	0.27
DHQ	22.35	23.00	26.26	33.62	36.18	39.14	39.08
EB	0.38	0.21	0.38	0.52	0.72	0.65	0.72
AN	0.00	0.00	0.00	0.00	0.90	1.76	1.05
BZTHQ	15.53	16.72	14.12	9.88	7.41	8.69	9.84
EAN	0.00	0.00	0.00	0.00	0.00	0.00	0.00
OPA	2.12	1.70	1.39	1.63	1.78	2.49	2.60
Q	8.56	5.93	4.27	3.60	2.17	0.00	0.00
PYTHQ	35.63	40.69	40.94	34.48	29.20	14.99	11.80

Denitrogenation %

1.54	2.64	4.30	7.38	15.65	25.22	28.34

RUN: PQ400

Feed: Pyridine-Quinoline

Temperature (K)	Pressure (atm)	Molar Ratio (g-mol H2/g-mol feed)
673.00	69.00	13.00

	W/F (hr g-cat/g-mol feed)						
	42.00	70.00	98.00	126.01	153.99	182.02	210.00
Organic Products, mole %							
PEN	0.29	0.33	0.42	0.68	0.56	0.62	1.00
DEC	0.00	0.00	0.00	0.00	0.10	0.17	0.34
PEAM	0.00	0.00	0.00	0.00	0.00	0.00	0.00
ETPIP	0.49	0.98	0.78	1.52	2.77	2.48	1.05
PIP	1.00	1.28	0.93	2.28	3.28	2.89	1.77
PRPIP	0.92	1.42	0.82	1.49	1.89	1.31	0.71
PYR	3.37	2.55	0.74	0.91	0.65	0.21	0.12
PEPIP	1.61	0.50	0.47	0.46	0.34	0.31	0.20
DPEAM	0.00	0.00	0.00	0.00	0.00	0.00	0.00
PNPIP	0.00	0.00	0.00	0.00	0.00	0.00	0.00
MNPIP	0.00	0.00	0.00	0.00	0.00	0.00	0.00
UN.	0.00	0.00	0.00	0.00	0.00	0.00	0.00
MCH	0.30	0.22	0.40	0.55	0.45	1.51	2.80
ECH	0.23	0.33	0.44	0.83	0.84	1.93	2.55
PCH	6.30	11.03	19.86	37.84	48.64	56.60	59.10
PCHE	0.00	0.00	0.00	0.00	0.00	0.00	0.00
PCHAM	0.00	0.00	0.00	0.00	0.00	0.00	0.00

PB	0.00	0.00	0.00	0.00	0.00	0.00	0.00
MEB	3.91	0.89	0.87	3.77	6.84	7.64	7.41
IDAN	0.48	0.10	0.38	0.11	0.00	0.00	0.00
UN.	0.38	0.85	1.38	0.62	0.60	0.00	0.00
DHQ	13.01	15.26	21.16	21.87	16.62	13.52	16.70
EB	0.73	1.38	0.89	2.10	3.98	1.61	1.14
AN	1.94	14.41	3.06	5.06	0.00	0.00	0.00
BZTHQ	33.55	30.82	28.43	12.44	8.16	5.97	3.04
EAN	0.00	0.00	0.00	0.00	0.00	0.00	0.00
OPA	3.84	4.34	6.00	5.78	4.29	3.22	2.11
Q	6.25	2.89	2.99	0.69	0.00	0.00	0.00
PYTHQ	21.39	10.42	9.98	0.97	0.00	0.00	0.00

Denitrogenation %							
	12.24	14.28	23.26	45.90	61.41	70.08	74.31

Appendix C

Mass Balance

The quantitative analysis was achieved by injecting the organic liquid product using a 1.0 μl syringe into the gas chromatograph. The detector of the GC was a flame ionization detector. The areas produced by the chromatograms were converted to g-moles by deviding the area of each peak by the corresponding response factor. Response factors were produced by injecting standard solutions of the expected products. The solvent used to prepare those solutions was n-hexadecane. The relation between the peak area and the concentration of each of the products was found to be linear in the region of interest.

The mass balance was checked by making use of the on-line analysis. Data from Run P350 at a space time of 126 hr g-cat/g-mol nitro-compound were used to demonstrate the mass balance. The conditions during that run where as follows

Π = Reactor pressure = 69 atm

F_{PYR_0} = Flow rate of pyridine = 0.03968 g-mol/hr

F_{H_2} = Flow rate of hydrogen = 0.51584 g-mol/hr

W/F = Space time = 126 hr g-cat/g-mol PYR

P_{PYR_0} = Initial partial pressure of pyridine

$= \frac{F_{PYR_0}}{F_{PYR_0}+F_{H_2}}\Pi = 4.929$ atm

T_{GSV} = Temperature of the gas sampling valve = 473 K

P_{GSV} = Pressure inside the gas sampling valve = 5 psig = 1.34 atm

V_{GSV} = Volume of gas sampling valve loop = 1.2 cc

Then the number of moles in the gas sampling valve loop is given by:

$$N_{GSV} = \frac{\left[\frac{F_{PYR_0}}{F_{PYR_0}+F_{H_2}}\right] P_{GSV} V_{GSV}}{R_g T_{GSV}} \tag{C.1}$$

where R_g is the gas constant, then

$$N_{GSV} = \frac{\left[\frac{0.03968}{0.03968+0.51584}\right](1.34)(1.2\times10^{-3})}{(0.08206)(473)} \tag{C.2}$$
$$= 3.71268\times10^{-6} g-mol$$

Carbon balance:

$$\text{moles of carbon IN} = 3.71268\times10^{-6}\times5 = 1.85634\times10^{-5}$$

Usind the data in Table C.1 and With the assumption that the unknown (UN.) nitrogen compounds have eight carbon atoms, then the moles of carbon in the product stream is

$$\begin{aligned}\text{moles of carbon OUT} = [&5(0.32+0.00+0.12+0.08) \\ &+10(0.08+0.11+0.01+0.07) \\ &+6(0.01)+7(1.67)+8(0.016+0.00)]\times10^{-6} \\ &= 1.828\times10^{-5}\ g-mol\end{aligned} \tag{C.3}$$

The error percent is given by

$$\text{error percent} = \frac{|1.828 - 1.856|}{1.856} = 1.51 \; percent$$

Table C.1: g-mol of HDN products; Run P350 at W/F=126 hr g-cat/g-mol (on-line analysis)

compound	g-mol of products $\times 10^{-6}$
PEN	0.32
DEC	0.08
PEAM	0.00
ETPIP	1.67
PIP	0.12
PRPIP	0.16
PYR	0.08
PEPIP	0.11
DPEAM	0.01
PNPIP	0.07
MNPIP	0.01
UN.	0.00

Appendix D

Fugacity Coefficients

The generalized form of the equation of state (EOS) is

$$P = \frac{R_g T}{v - b} - \frac{a}{v^2 + ubv + wb^2} \tag{D.1}$$

In most of the equations of state the parameter b is treated as temperature independent while the parameter a is treated as temperature dependent. The parameters u and w have constant values for the major equations of state. For van der Waals EOS, both u and w are are zeros, for Redlich-Kwong EOS $u = 1$ and $w = 0$ and for Peng-Robinsion EOS, $u = 2$ and $w = -1$.

In this study the Peng-Robinson EOS was considered for calculating the equilibrium properties. This equation has the follwoing form [101]:

$$P = \frac{RT}{v - b} - \frac{a}{v(v + b) + b(v - b)} \tag{D.2}$$

where:

$$a_i = 0.45724 R^2 T_c^2 / P_c \tag{D.3}$$

$$b_i = 0.07780 R T_c / P_c \tag{D.4}$$

where T_c and P_c are the critical temperature and critical pressure respectivelly. The values of T_c and P_c for some of the compounds were calculated using Lydersen's correlations [62].

$$T_c = \frac{T_b}{0.567 + \Sigma\Delta T - (\Sigma\Delta T)^2} \tag{D.5}$$

$$P_c = \frac{M}{(0.34 + \Sigma\Delta P)^2} \tag{D.6}$$

where:

T_b normal boiling point of copmound i

M molecular weight of copmound i

ΔT temperature group contibution

ΔP pressure group contibution

The values of Lydersen's critical-property increments (ΔT and ΔP) are given in Perry's Chemical Engineering Handbook [72].

Define the following terms

$$\alpha = \left[1 + (0.37464 + 1.54226\omega - 0.26992\omega^2)(1 - T_r^{0.5})\right]^2 \tag{D.7}$$

$$A = \frac{a\alpha P}{R^2T^2} = 0.45724\alpha P_r/T_r^2 \tag{D.8}$$

$$B = \frac{bP}{RT} = 0.07780P_r/T_r \tag{D.9}$$

The polynomial form of the above equation can be written in the following form

$$Z^3 - (1 - B)Z^2 + (A - 3B^2 - 2B)Z - (AB - B^2 - B^3) = 0 \tag{D.10}$$

For a mixture, the parameters a, b, A, and B are functions of composition:

$$a = \sum_{i=1}^{n}\sum_{j=1}^{n} y_i y_j (a\alpha)_{ij} \tag{D.11}$$

$$b = \sum_{i=1}^{n} y_i b_i \tag{D.12}$$

$$A = \sum_{i=1}^{n}\sum_{j=1}^{n} y_i y_j A_{ij} \tag{D.13}$$

$$B = \sum_{i=1}^{n} y_i B_i \tag{D.14}$$

where $(a\alpha)_{ij} = [(a\alpha)_i (a\alpha_j)]^{0.5}$, and $A_{ij} = (A_i A_j)^{0.5}$

The parameters for fluid i or j are constants for a particular substance but different for different substances. The fugacity coefficient for component i in a mixture can be calculated from the following equation

$$ln\hat{\phi}_i = \frac{B_i}{B}(Z-1) - ln(Z-B) - \frac{A}{2.828B} \left[\frac{\sum_{ij}^{n} y_j A_{ij}}{a} - \frac{B_i}{B}\right] ln\left(\frac{Z+2.214B}{Z-0.414B}\right) \tag{D.15}$$

Table D.1 includes the normal boiling point, the molecular weight, the estimated critical temperature and pressure, and the parameters a_i and b_i.

A sample of the computer output that performs the fugacity coefficients is presented in the here. The data are taken from Run PQ300 at a space time of 210 hr g-cat/g-mol feed. In this output, TC, PC, AC, MF, and FCOEF represent critical temperature, critical pressure, accentric factor, mole fraction, and fugacity coefficient respectively.

Table D.1: Data needed for fugacity coefficient calculations

Compound	T_b K	M g-mol	T_c K	P_c atm	a_i $l^2.atm.K^{1/2}.mol^{-2}$	b_i $l.mol^{-1}$
H_2	–	2.01	41.25	20.80	1.51	0.014
PEN	309.25	72.15	470.35	33.80	408.62	0.099
DEC	447.25	142.29	615.20	20.89	1293.54	0.209
PIP	379.15	85.15	585.04	46.72	510.08	0.089
PYR	388.25	79.10	617.15	60.00	453.95	0.073
ETPIP	403.95	113.20	601.26	31.89	800.16	0.134
PRPIP	424.35	127.23	617.97	28.55	957.17	0.154
PEPIP	471.35	155.29	660.19	23.60	1365.96	0.199
PEAM	377.55	87.17	554.54	35.36	589.52	0.111
DPEAM	475.15	157.30	638.09	20.72	1428.87	0.219
DHQ	478.15	139.24	696.32	31.51	1168.83	0.157
OPA	499.15	135.21	713.73	32.49	1202.69	0.156
AN	457.15	93.13	698.37	50.42	735.85	0.098
PCHAM	333.15	141.26	471.81	28.25	492.69	0.119
PCH	429.85	126.24	626.28	27.75	1018.21	0.160
ECH	404.95	112.22	604.12	30.89	835.93	0.139
PB	432.35	120.20	638.51	31.77	933.43	0.143
EB	409.35	106.17	615.66	35.97	752.65	0.122
Q	511.15	129.16	772.40	37.49	1273.12	0.146
PyTHQ	524.15	133.20	771.54	36.67	1297.97	0.149
BzTHQ	495.15	133.20	741.24	34.11	1262.39	0.154
PCHE	428.15	124.23	626.83	29.13	972.10	0.153

TEMPERATURE	PRESSURE				
573.15	69.00				
---	--	--	--	--	---
COMPONENT	TC	PC	AC	MF	FCOEF
---	--	--	--	--	---
PEN	470.350	33.800	0.251	0.000000	0.682727
DEC	615.200	20.890	0.490	0.000000	0.352032
PEAM	554.540	35.360	0.500	0.000000	0.549523
ETPIP	601.260	31.890	0.350	0.000000	0.453369
PIP	585.040	46.720	0.250	0.083446	0.559484
PRPIP	617.970	28.550	0.350	0.000000	0.408150
PYR	617.150	60.000	0.240	0.075224	0.572385
PEPIP	660.190	23.600	0.420	0.015030	0.316003
DPEAM	638.090	20.720	0.400	0.000000	0.323111
PNPIP	660.190	23.600	0.420	0.000000	0.316003
MNPIP	601.260	31.890	0.350	0.000000	0.453369
UN.	638.090	20.720	0.400	0.000000	0.323111
MCH	569.500	33.500	0.285	0.000000	0.511438
ECH	609.000	29.900	0.243	0.000000	0.432704
PCH	639.000	27.700	0.258	0.019259	0.379085
PCHE	626.830	29.130	0.255	0.000000	0.403940
PCHAM	471.810	28.250	0.250	0.000000	0.645848
PB	638.510	31.770	0.344	0.000000	0.401652
MEB	637.000	28.000	0.360	0.000000	0.378642

IDAN	654.000	34.600	0.500	0.000000	0.390373
UN.	696.320	31.510	0.430	0.000000	0.324794
DHQ	696.320	31.510	0.430	0.046541	0.324794
EB	617.100	35.600	0.301	0.000000	0.454883
AN	699.000	52.400	0.382	0.000000	0.430360
BzTHQ	741.240	34.110	0.512	0.000000	0.285334
EAN	687.000	35.800	0.250	0.000000	0.373398
OPA	713.730	32.490	0.450	0.000000	0.309901
Q	772.400	37.490	0.450	0.013911	0.278281
PyTHQ	771.540	36.670	0.450	0.217605	0.274979
H2	41.250	20.800	-0.220	0.528984	1.445377

Appendix E

Analytical Process

The analytical tool used to measure the concentrations of the reaction products was a *HP* 5730*A* gas chromatograph equiped with thermal conductivity detector and flame ionization detector. Chromatograms with retetion time, peak area, and area percent were produced by a reporting integrator *HP* 3380. In order to optimize the measurment procedure, different columns were used with differnt operating conditions before selecting the column and the conditions for the analytical process.

The expected products of the HDN reactions of pyridine and quinoline were either purchased or prepared in our laboratory. Standard solutions from these compounds were prepared and were analysed under the same conditions as the HDN products for calibration, comparison, and identification of the products. Some liquid products were analyzed by gas chromatography/mass spectroscopy for confirmation of the major products and identification of some of the minor products. The major products of the HDN reactions of pyridine and quinoline are listed in Table E.1. The retention times listed in this table resulted from the column and the conditions stated in Section 5.1.5. Samples of these compounds were used to identify products and for calibrating chromatographic peaks.

Table E.1: Major HDN products of pyridine and Quinoline

Compound	Manufacturer	Retention time min.	Purity
Pentane	BDH Inc.	1.34	99
Decane	Fisher Scientific	7.14	-
Pentylamine	Eastman	5.95	-
Ethylpiperidine	Aldrich	6.20	99
Piperidine	Fisher Scientific	6.70	99
Propylpiperidine	Prepared in Lab.	7.40	-
Pyridine	Fisher Scientific	9.95	99
Pentylpiperidine	Prepared in Lab.	11.60	-
Dipentylamine	Aldrich	12.40	99
Methylcyclohexane	Aldrich	3.26	99
Ethylcyclohexane	Aldrich	4.82	99
Propylcyclohexane	Aldrich	6.45	99
Propylcyclohexene	Aldrich	7.09	75
Propylcyclohexylamine	Aldrich	9.84	98
Propylbenzene	Eastman	10.36	-
Methylethylbenzene	Aldrich	11.36	99
Indan	Aldrich	13.59	97
Decahydroquinoline	Aldrich	15.58	97
Ethylbenzene	Fisher Scientific	18.53	-
Aniline	Fisher Scientific	20.03	100
Bz-Tetrahydroquinoline	Aldrich	21.42	
Ethylaniline	Aldrich	23.65	98
Propylaniline	Aldrich	26.35	97
Quinoline	Aldrich	28.80	96
Py-Tetrahydroquinoline	Aldrich	35.99	98

Appendix F

ESR Runs

This Appendix includes the steps of the runs made for the ESR studies. The spectra was taken after each step. The relative intesity of the Mo^{+5} peak is given in arbitray units. The number of spins/g of catalyst was calculated. The effect of sulfiding the Mo/Al_2O_3 or $Mo\text{-}M/Al_2O_3$ (where M = Ni, Co or W) catalysts by ESR is well described in literature [54,53,108]. When the catalyst was sulfided the major part of molybdenum is converted to MoS_2 and MS_2. Smaller amounts of oxysulfides, polymeric sulfur and different valencies of molybdenum or metals (Ni, Co, W) may be present.

When the catalyst was sulfided the intensity of of Mo^{+5} line increased significantly (compare Tables F.1 and F.2). The enhancement of Mo^{+5} ions could be due to the following mechanism.

$$H_2S \longrightarrow H^+ + SH^- \tag{F.1}$$

$$Mo^{+6} + H^+ \longrightarrow Mo^{+5} + \frac{1}{2}H_2 \tag{F.2}$$

From this it is believed that two sites were formed on sulfiding the $Mo\text{-}Ni/Al_2O_3$ catalyst. Type *I* Site is a sulfur vaccancy associated with molybdenum and is responsible for hydrogenation and hydrogenolysis reactions. Type *II* Site is Brönsted

acid site which is responsible for hydrogenolysis reactions. The existance of SH (sulfahydnyl group) may also be considered to act as a Brönsted acid. However, the electron affinity of a H^+ site should be stronger than that of a H atom in SH, therefore H^+ sites are more readily promote reactions involving a carbonium ion mechanism. Thus, according to Yang et al. [108], the hydrogenolysis reactions enhanced the quinoline HDN conversion.

The effects of hydrogen and pyridine on the Ni-Mo/Al_2O_3 catalysts by ESR study are given in Tables E.1 and E.2. From these observations it seems that Mo^{+5} takes part in main reaction.

$$Mo^{+6} + H \longrightarrow Mo^{+5} + H^+ \tag{F.3}$$

$$Mo^{+5} + R \longrightarrow Mo^{+6} + R^\bullet \tag{F.4}$$

$$R^\bullet + H^+ \longrightarrow Products \tag{F.5}$$

Where R any species, could be pyridine or products.

Table F.1: ESR results of unsulfided Ni-Mo/Al_2O_3 at different conditions, Run No.1

step	condition	relative intensity	spins/g $\times 10^{15}$
1	evacuate and heat at 400°C for 2 hr.	22	1.41
2	add hydrogen at room temperature	33	2.11
3	heat at 400°C for 2 hr.	160	10.20
4	evacuate at room temperature	138	8.58
5	add pyridine at room temperature	135	8.65
6	heat at 400°C for 2 hr.	57	3.65
7	add pyridine, condense using ice	47	3.04
8	heat at 400°C for 5 hr.	11	0.70
9	add hydrogen and heat for 15 hr.	167	10.70
10	evacuate at room temperature	176	11.30
11	evacuate at 400°C for 2 hr.	89	5.70
12	add hydrogen at room temperature	105	6.37

Table F.2: ESR results of sulfided Ni-Mo/Al_2O_3 at different conditions, Run No.2

step	condition	relative intensity	spins/g $\times 10^{15}$
1	evacuate and heat at 400°C for 2 hr.	91	3.83
2	add H_2S at room temperature	92	5.90
3	heat at 400°C for 2 hr.	108	6.92
4	evacuate at room temperature	149	9.55
5	add hydrogen at room temperature	91	5.83
6	heat at 400°C for 2 hr.	222	14.20
7	evacuate at room temperature	215	13.80
8	add pyridine at room temperature	189	12.10
9	heat at 400°C for 2 hr.	118	7.56
10	add pyridine, condense using ice	108	6.92
11	heat at 400°C for 5 hr.	27	1.73
12	add hydrogen and heat for 15 hr.	190	12.20
13	evacuate at room temperature	137	8.78
14	evacuate at 400°C for 2 hr.	18	1.15
15	add hydrogen at room temperature	21	1.35

Appendix G

Results of Regression

In this Appendix the results of the non-linear regression of the modelling are presented. Samples of plots of the model having the best fit for the pyridine system are also presented.

PA is the partial pressure of the reacting nitrogen compound, atm.

Ra is the actual rate, g-mol/s

Rp is the predicted rate, g-mol/s

pre is the percent relative error

Model 1 Pyridine

T=498

k1	k2		
0.1332E-05	0.1642E+01		
PA	Ra	Rp	pre
0.4742E+01	0.1250E-05	0.1251E-05	-0.06
0.4630E+01	0.1202E-05	0.1204E-05	-0.19

0.4514E+01	0.1191E-05	0.1157E-05	2.86
0.4423E+01	0.1130E-05	0.1121E-05	0.79
0.4358E+01	0.1044E-05	0.1096E-05	-4.91
0.4263E+01	0.1030E-05	0.1060E-05	-2.86
0.4142E+01	0.1056E-05	0.1015E-05	3.88

T=523

0.5400E-05	0.4562E-01		
0.4094E+01	0.5602E-05	0.5350E-05	4.50
0.3592E+01	0.5379E-05	0.5310E-05	1.29
0.3162E+01	0.5081E-05	0.5266E-05	-3.64
0.2710E+01	0.4963E-05	0.5205E-05	-4.89
0.2106E+01	0.5164E-05	0.5089E-05	1.47
0.1754E+01	0.4916E-05	0.4988E-05	-1.46
0.1288E+01	0.4886E-05	0.4783E-05	2.11

T=548

0.1115E-04	0.1285E+00		
0.3356E+01	0.1055E-04	0.1051E-04	0.40
0.2401E+01	0.1018E-04	0.9818E-05	3.51
0.1865E+01	0.8808E-05	0.9204E-05	-4.50
0.1316E+01	0.8078E-05	0.8241E-05	-2.01
0.9789E+00	0.7228E-05	0.7341E-05	-1.56
0.7023E+00	0.6543E-05	0.6286E-05	3.93
0.5973E+00	0.5812E-05	0.5770E-05	0.73

T=573

0.2937E-04	0.4151E+00		
0.2107E+01	0.1893E-04	0.1888E-04	0.27
0.1406E+01	0.1418E-04	0.1439E-04	-1.49
0.9962E+00	0.1131E-04	0.1113E-04	1.56
0.7851E+00	0.9266E-05	0.9205E-05	0.66
0.6250E+00	0.7876E-05	0.7613E-05	3.34
0.5678E+00	0.6751E-05	0.7013E-05	-3.87
0.4809E+00	0.5969E-05	0.6069E-05	-1.68
T=598			
0.3955E-04	0.2118E+00		
0.1266E+01	0.2457E-04	0.2453E-04	0.19
0.6809E+00	0.1710E-04	0.1704E-04	0.37
0.4689E+00	0.1282E-04	0.1312E-04	-2.31
0.3500E+00	0.1024E-04	0.1049E-04	-2.44
0.2625E+00	0.8539E-05	0.8301E-05	2.79
0.2154E+00	0.7297E-05	0.7020E-05	3.80
0.1901E+00	0.6359E-05	0.6299E-05	0.95
T=623			
0.9515E-04	0.6412E-01		
0.7361E+00	0.2813E-04	0.2801E-04	0.42
0.2834E+00	0.1870E-04	0.1893E-04	-1.23
0.1687E+00	0.1369E-04	0.1394E-04	-1.85
0.1154E+00	0.1076E-04	0.1072E-04	0.44
0.8357E-01	0.8866E-05	0.8377E-05	5.52

Model 2 Quinoline

T=498

k1	k2		
0.1696E-05	0.2412E+03		
PA	Ra	Rp	pre
0.1794E+01	0.2103E-04	0.2119E-04	-0.76
0.1355E+01	0.1439E-04	0.1367E-04	4.95
0.1217E+01	0.1067E-04	0.1089E-04	-2.08
0.1136E+01	0.8481E-05	0.8989E-05	-5.99
0.1033E+01	0.7129E-05	0.7265E-05	-1.91
0.1002E+01	0.6079E-05	0.6330E-05	-4.13
0.9861E+00	0.5291E-05	0.4590E-05	13.23

T=523

0.2135E-05	0.9474E+02		
0.9277E+00	0.2685E-04	0.2728E-04	-1.62
0.6370E+00	0.1728E-04	0.1657E-04	4.08
0.5118E+00	0.1270E-04	0.1233E-04	2.93
0.4535E+00	0.1001E-04	0.9854E-05	1.54
0.4415E+00	0.8211E-05	0.8827E-05	-7.50
0.4306E+00	0.6964E-05	0.7181E-05	-3.12
0.4282E+00	0.6039E-05	0.5855E-05	3.05

T=548

0.1584E-04	0.6794E+02		
0.7042E+00	0.2834E-04	0.2859E-04	-0.86
0.4642E+00	0.1797E-04	0.1716E-04	4.50
0.4078E+00	0.1300E-04	0.1345E-04	-3.49
0.3617E+00	0.1021E-04	0.1022E-04	-0.05
0.3515E+00	0.8376E-05	0.8705E-05	-3.92
0.3271E+00	0.7124E-05	0.7262E-05	-1.94
0.3253E+00	0.6177E-05	0.5630E-05	8.86
T=573			
0.1699E-04	0.3848E+02		
0.6673E+00	0.2859E-04	0.2877E-04	-0.61
0.4602E+00	0.1799E-04	0.1749E-04	2.77
0.3798E+00	0.1308E-04	0.1281E-04	2.08
0.3579E+00	0.1022E-04	0.1093E-04	-6.93
0.3375E+00	0.8402E-05	0.8591E-05	-2.25
0.3191E+00	0.7136E-05	0.7225E-05	-1.24
0.3156E+00	0.6190E-05	0.5705E-05	7.84
T=598			
0.6925E-04	0.1570E+02		
0.6275E+00	0.2886E-04	0.2911E-04	-0.88
0.4163E+00	0.1817E-04	0.1756E-04	3.34
0.3490E+00	0.1317E-04	0.1297E-04	1.53
0.2871E+00	0.1038E-04	0.1039E-04	-0.09
0.2795E+00	0.8508E-05	0.8970E-05	-5.43

0.2653E+00	0.7220E-05	0.7871E-05	-9.02
0.2621E+00	0.6262E-05	0.5646E-05	9.83

T=623

0.2855E-03	0.8443E+01		
0.5811E+00	0.2917E-04	0.2908E-04	0.30
0.4206E+00	0.1815E-04	0.1819E-04	-0.21
0.3464E+00	0.1318E-04	0.1298E-04	1.47
0.2982E+00	0.1036E-04	0.1048E-04	-1.20
0.2852E+00	0.8497E-05	0.9193E-05	-8.19
0.2815E+00	0.7195E-05	0.7248E-05	-0.74
0.2809E+00	0.6237E-05	0.5572E-05	10.66

T=648

0.5082E-03	0.8542E+01		
0.4379E+00	0.3013E-04	0.3037E-04	-0.79
0.2946E+00	0.1866E-04	0.1813E-04	2.81
0.2586E+00	0.1343E-04	0.1315E-04	2.04
0.2459E+00	0.1047E-04	0.1089E-04	-4.01
0.2350E+00	0.8588E-05	0.8988E-05	-4.66
0.2357E+00	0.7266E-05	0.7203E-05	0.86
0.2350E+00	0.6299E-05	0.5984E-05	4.99

T=673

0.1301E-02	0.6145E+01		
0.4164E+00	0.3028E-04	0.3015E-04	0.40
0.2881E+00	0.1868E-04	0.1901E-04	-1.74

0.2159E+00	0.1355E-04	0.1299E-04	4.12
0.2009E+00	0.1057E-04	0.1102E-04	-4.24
0.1751E+00	0.8699E-05	0.9022E-05	-3.71
0.1652E+00	0.7375E-05	0.7073E-05	4.09
0.1536E+00	0.6408E-05	0.6253E-05	2.41

Model 2 Pyridine-Quinoline

------- ----------

T=498

k1	k2		
0.8055E-05	0.1219E+03		
PA	Ra	Rp	pre
0.2984E+01	0.1305E-04	0.1309E-04	-0.33
0.2757E+01	0.8744E-05	0.8510E-05	2.67
0.2619E+01	0.6640E-05	0.6765E-05	-1.87
0.2453E+01	0.5537E-05	0.5499E-05	0.70
0.2385E+01	0.4655E-05	0.4909E-05	-5.47
0.2320E+01	0.4038E-05	0.4176E-05	-3.41
0.2174E+01	0.3697E-05	0.3392E-05	8.25

T=573

0.4472E-04	0.2271E+02		
0.1619E+01	0.2221E-04	0.2140E-04	3.63
0.1357E+01	0.1438E-04	0.1537E-04	-6.89

0.1116E+01	0.1096E-04	0.1137E-04	-3.69
0.1010E+01	0.8763E-05	0.9051E-05	-3.29
0.9002E+00	0.7372E-05	0.7093E-05	3.79
0.8932E+00	0.6247E-05	0.6144E-05	1.65
0.8305E+00	0.5499E-05	0.4982E-05	9.41

T=623

0.1311E-03	0.1971E+01		
0.6547E+00	0.2868E-04	0.2757E-04	3.86
0.4596E+00	0.1799E-04	0.1923E-04	-6.88
0.3146E+00	0.1327E-04	0.1347E-04	-1.49
0.2329E+00	0.1050E-04	0.1100E-04	-4.78
0.1303E+00	0.8781E-05	0.8829E-05	-0.54
0.5043E-01	0.7552E-05	0.7116E-05	5.78
0.3025E-01	0.6573E-05	0.6751E-05	-2.70

T=673

0.2421E-03	0.3309E+00		
0.3817E+00	0.3051E-04	0.3144E-04	-3.05
0.2246E+00	0.1894E-04	0.1745E-04	7.87
0.1474E+00	0.1375E-04	0.1382E-04	-0.53
0.6538E-01	0.1088E-04	0.1043E-04	4.13
0.2642E-01	0.8971E-05	0.8891E-05	0.89
0.8649E-02	0.7617E-05	0.7852E-05	-3.08
0.5034E-02	0.6607E-05	0.6490E-05	1.77

Figures G.1 to G.3 give an example of the statistical analysis for the pyridine modelling (Model 1). The first plot shows the actual data points and the model as a function of the response variable. The second plot shows the predicted versus the actual data. The third represents the residual plot.

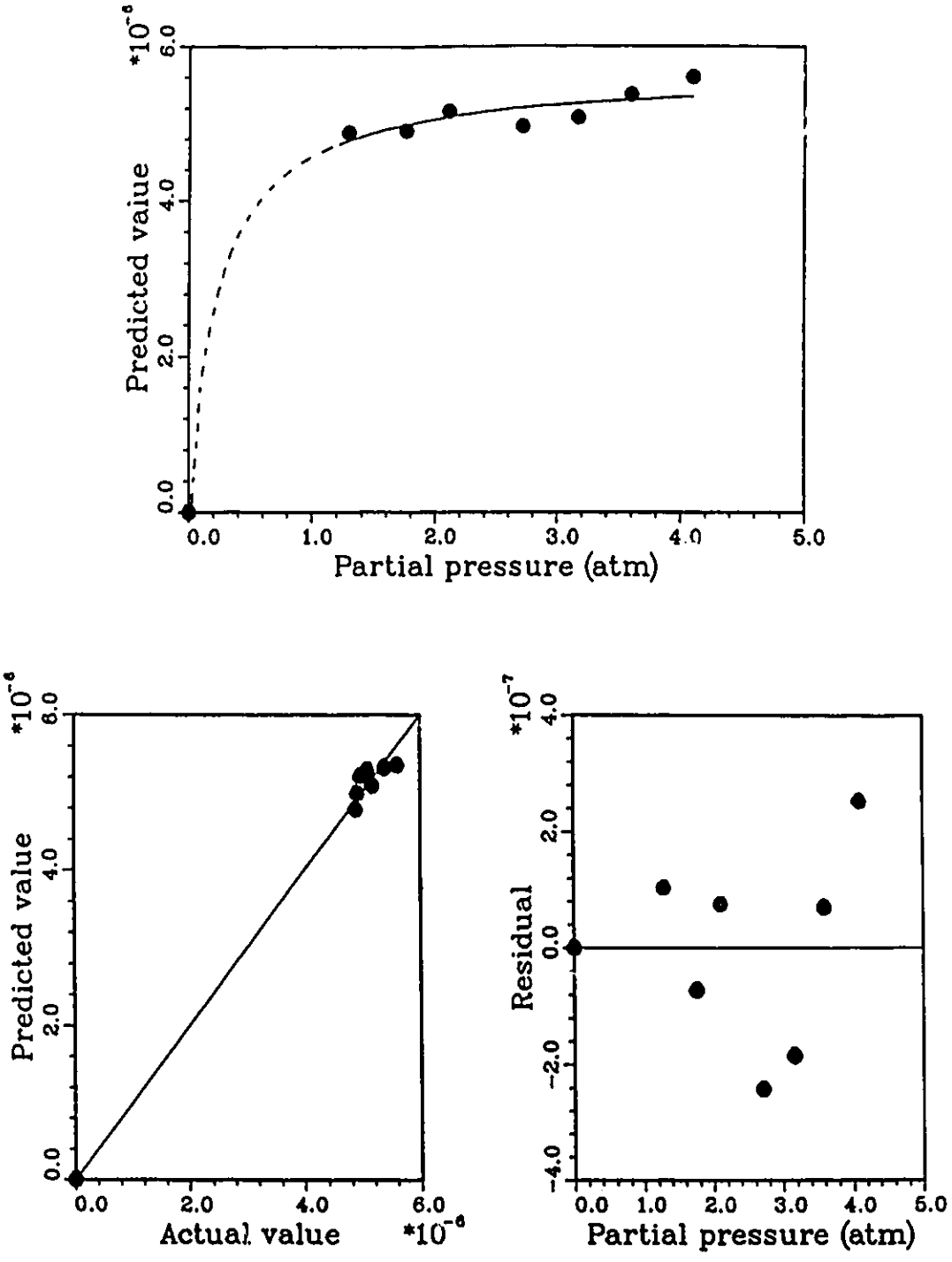

Figure G.1: Statistical analysis; Pyridine at 523 K

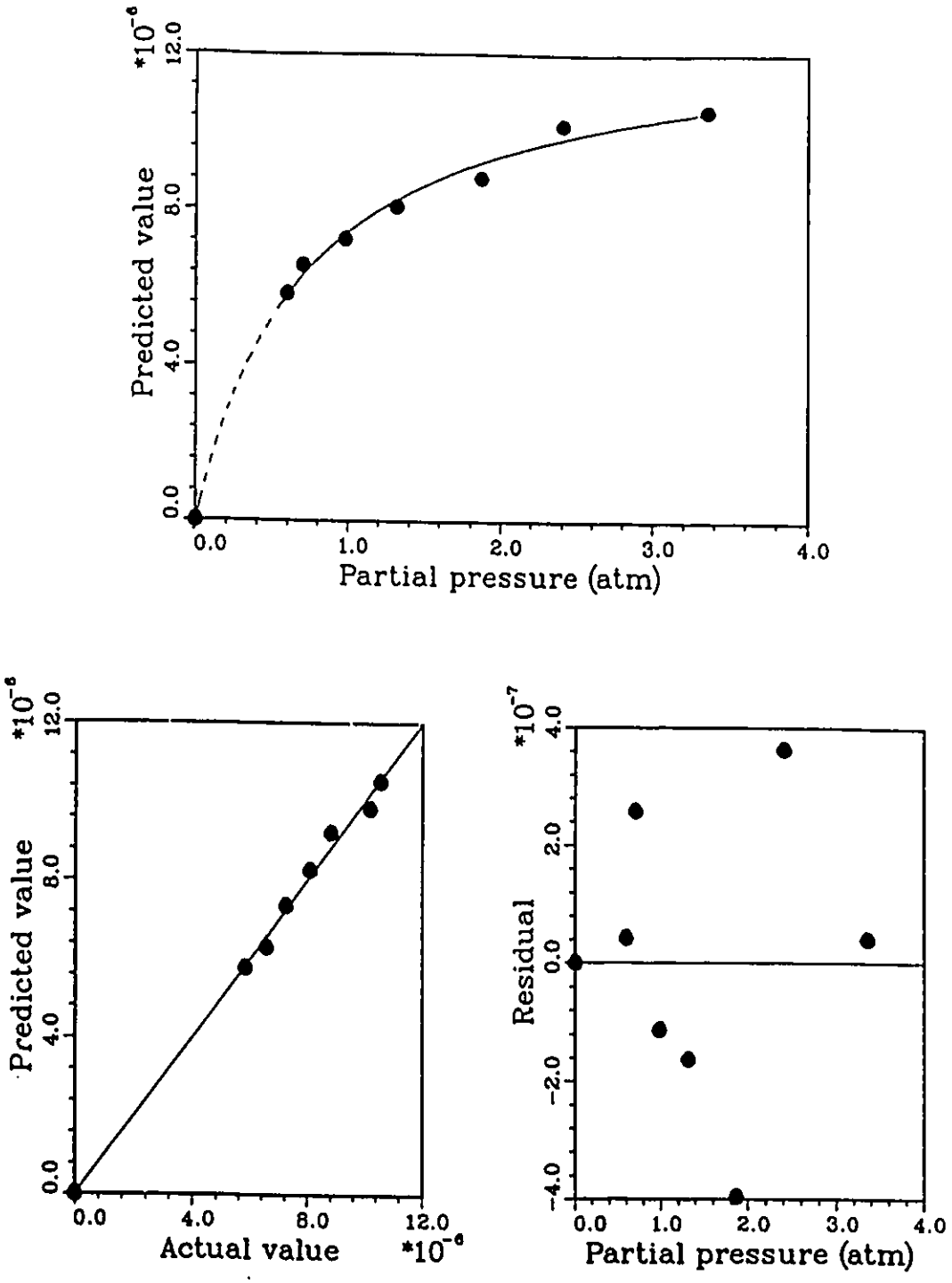

Figure G.2: Statistical analysis; Pyridine at 548 K

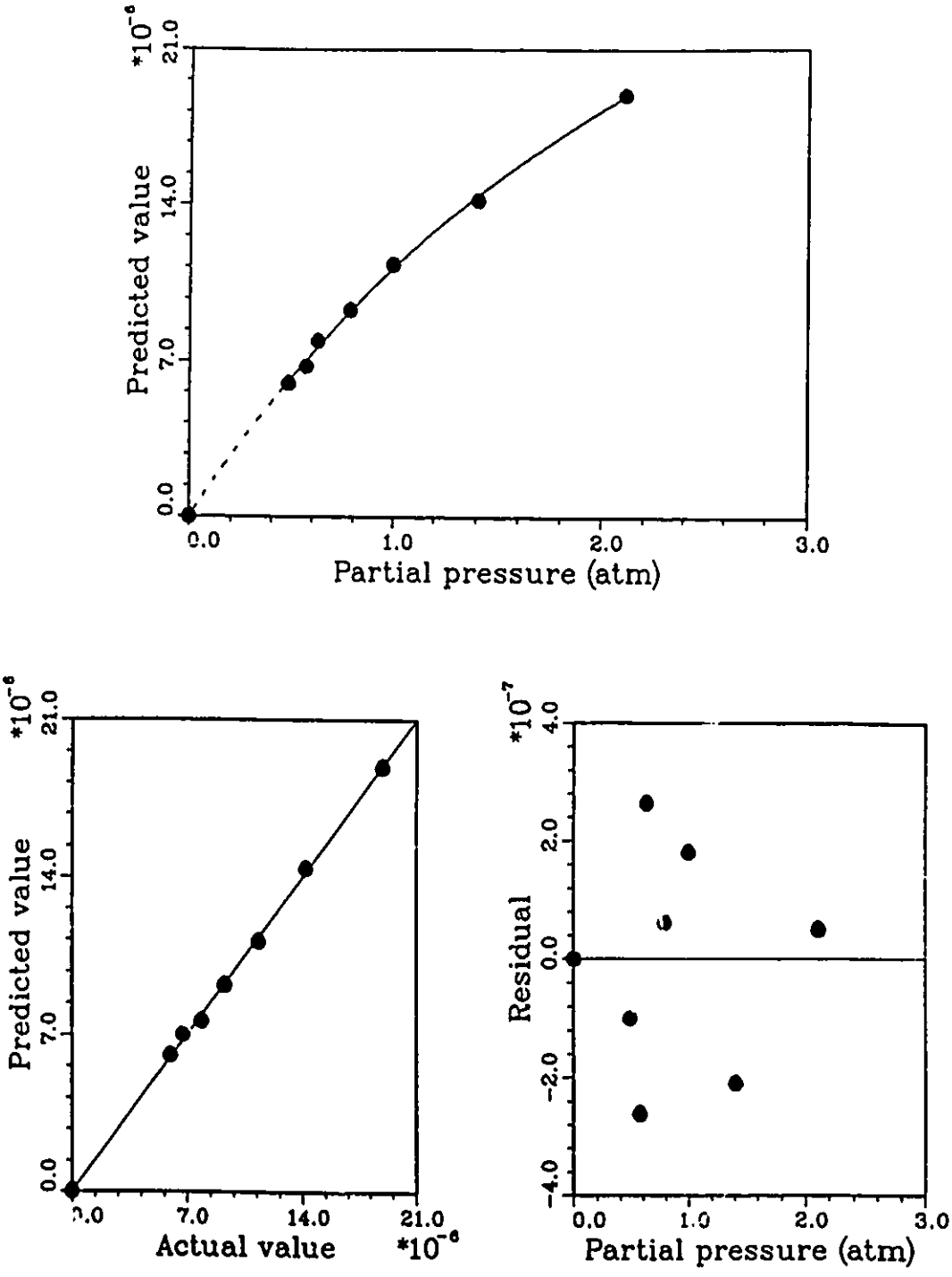

Figure G.3: Statistical analysis; Pyridine at 573 K

Appendix H

Computer Program

The copmuter program (EQNQUI FORTRAN) which includes the differential equations resulted from the mechanistic model of quinoline HDN is presented in this Appendix. This program contains also the derivatives of the equations with respect to the responses as well as the parameters.

```
      SUBROUTINE EQN(NE,X,Y,RPAR,YPRIME)
      IMPLICIT REAL*8(A-H,O-Z)
      DIMENSION Y(4),YPRIME(4),RPAR(4)
C   Y(1)=PYTHQ
C   Y(2)=DHQ
C   Y(3)=OPA
C   Y(4)=HC
C                Q <----> PYTHQ --2--> OPA --1--> HC + NH3
C                |          |
C              BZTHQ <----> DHQ --3--> HC + NH3
C-------------------------------------------------------------
```

```
      XD=(Y(1)+Y(2)+Y(3))+RPAR(4)*Y(4))
      X3=(RPAR(2)*Y(1)-RPAR(1)*Y(3))
      X4=(RPAR(1)*Y(3)+RPAR(3)*Y(2))
C-----------------------------------------------------------
      YPRIME(1) = -RPAR(2)*Y(1)/XD
      YPRIME(2) = -RPAR(3)*Y(2)/XD
      YPRIME(3) = X3/XD
      YPRIME(4) = X4/XD
      RETURN
      END
C***********************************************************
      SUBROUTINE JAC(NE,X,Y,RPAR,DYPDY)
      IMPLICIT REAL*8(A-H,O-Z)
      DIMENSION Y(4),DYPDY(4,4),RPAR(5)
C-----------------------------------------------------------
      XD=(Y(1)+Y(2)+Y(3))+RPAR(4)*Y(4))
      X3=(RPAR(2)*Y(1)-RPAR(1)*Y(3))
      X4=(RPAR(1)*Y(3)+RPAR(3)*Y(2))
C-----------------------------------------------------------
      DYPDY(1,1) = -RPAR(2)/XD + RPAR(2)*Y(1)/XD**2
      DYPDY(1,2) =  RPAR(2)*Y(1)/XD**2
      DYPDY(1,3) =  RPAR(2)*Y(1)/XD**2
      DYPDY(1,4) =  RPAR(2)*Y(1)*RPAR(4)/XD**2
C
```

```
      DYPDY(2,1) =  RPAR(3)*Y(2)/XD**2
      DYPDY(2,2) = -RPAR(3)/XD + RPAR(3)*Y(2)/XD**2
      DYPDY(2,3) =  RPAR(3)*Y(2)/XD**2
      DYPDY(2,4) =  RPAR(3)*Y(2)*RPAR(4)/XD**2
C
      DYPDY(3,1) =  RPAR(2)/XD - X3/XD**2
      DYPDY(3,2) = -X3/XD**2
      DYPDY(3,3) = -RPAR(1)/XD - X3/XD**2
      DYPDY(3,4) = -X3*RPAR(4)/XD**2
C
      DYPDY(4,1) = -X4/XD**2
      DYPDY(4,2) =  RPAR(3)/XD - X4/XD**2
      DYPDY(4,3) =  RPAR(1)/XD - X4/XD**2
      DYPDY(4,4) = -X4*RPAR(4)/XD**2
      RETURN
      END
C*************************************************************
      SUBROUTINE DPEQN(NE,NP,X,Y,RPAR,DFDP)
      IMPLICIT REAL*8(A-H,O-Z)
      DIMENSION Y(4),DFDP(4,5),RPAR(5)
C-------------------------------------------------------------
      XD=(Y(1)+Y(2)+Y(3))+RPAR(4)*Y(4))
      X3=(RPAR(2)*Y(1)-RPAR(1)*Y(3))
      X4=(RPAR(1)*Y(3)+RPAR(3)*Y(2))
```

```
C-------------------------------------------------------------
      DFDP(1,1) =  0.0
      DFDP(1,2) = -Y(1)/XD
      DFDP(1,3) =  0.0
      DFDP(1,4) =  RPAR(2)*Y(1)*Y(4)/XD**2
C
      DFDP(2,1) =  0.0
      DFDP(2,2) =  0.0
      DFDP(2,3) = -Y(2)/XD
      DFDP(1,4) =  RPAR(3)*Y(2)*Y(4)/XD**2
C
      DFDP(3,1) = -Y(3)/XD
      DFDP(3,2) =  Y(1)/XD
      DFDP(3,3) =  0.0
      DFDP(3,4) = -X3*Y(4)/XD**2
C
      DFDP(4,1) =  Y(3)/XD
      DFDP(4,2) =  0.0
      DFDP(4,3) =  Y(2)/XD
      DFDP(4,4) = -X4*Y(4)/XD**2
      RETURN
      END
```

Appendix I

Derivation of the Kinetic Equations

This Appendix includes the derivation of the equations of Model 3. In this model the overall HDN reaction is represented by the following lumped equation

$$A + H_2 = NC + HC$$

where A is the reacting nitrogen compound, NC is the product nitrogen compounds, and HC is the product hydrocarbons. This model is expressed in terms of the fugacities of the compounds instead of their partial pressures. Calculations of the fugacities are shown in Appendix D.

Assuming that hydrogen and nitrogen compounds are adsorbed on two different catalytic sites [31,110], then the surface reaction consists of four elementary steps:

(1) Adsorption of nitrogen compound, A, on u-type active sites;

(2) adsorption of hydrogen on v-type active sites;

(3) reaction between adsorbed A and adsorbed H_2; and

(4) desorption of products, NC and HC, from u-type active sites.

The mechanism of the above reaction can be pictured as follows

$$A + u \;=\; Au \qquad (I.1)$$

$$H_2 + 2v = 2Hv \tag{I.2}$$

$$Au + 2Hv + u = NCu + HCu + 2v \tag{I.3}$$

$$NCu = NC + u \tag{I.4}$$

$$HCu = HC + u \tag{I.5}$$

The rate expressions for the four steps is expressed in terms of partial pressure and fugacity coefficient, and are given by

$$-r_1 = k_A P_A P_u \hat{\phi}_A \hat{\phi}_u - k'_A P_{Au} \hat{\phi}_{Au} \tag{I.6}$$

$$-r_2 = k_H P_{H_2} P_v^2 \hat{\phi}_{H_2} \hat{\phi}_v^2 - k'_H P_{Hv}^2 \hat{\phi}_{Hv}^2 \tag{I.7}$$

$$-r_3 = k_{sr} P_{Au} P_{Hv}^2 P_u \hat{\phi}_{Au} \hat{\phi}_{Hv}^2 \hat{\phi}_u - k'_{sr} P_{NCu} P_{HCu} P_v^2 \hat{\phi}_{NCu} \hat{\phi}_{HCu} \hat{\phi}_v^2 \tag{I.8}$$

$$-r_4 = k_{NC} P_{NCu} \hat{\phi}_{NCu} - k'_{NC} P_{NC} P_u \hat{\phi}_{NC} \hat{\phi}_u \tag{I.9}$$

$$-r_5 = k_{HC} P_{HCu} \hat{\phi}_{HCu} - k'_{HC} P_{HC} P_u \hat{\phi}_{HC} \hat{\phi}_u \tag{I.10}$$

Define the adsorption equilibrium constants as

$$K_A = k_A / k'_A \tag{I.11}$$

$$K_{H_2} = k_H / k'_H \tag{I.12}$$

$$K_{sr} = k_{sr} / k'_{sr} \tag{I.13}$$

$$K_{NC} = k'_{NC} / k_{NC} \tag{I.14}$$

$$K_{HC} = k'_{HC} / k_{HC} \tag{I.15}$$

Substituting in the above rate equations gives

$$-r_1 = k_A (P_A P_u \hat{\phi}_A \hat{\phi}_u - P_{Au} \hat{\phi}_{Au} / K_A) \tag{I.16}$$

$$-r_2 = k_H (P_{H_2} P_v^2 \hat{\phi}_{H_2} \hat{\phi}_v^2 - P_{Hv}^2 \hat{\phi}_{Hv}^2 / K_{H_2}) \tag{I.17}$$

$$-r_3 = k_{sr} (P_{Au} P_{Hv}^2 P_u \hat{\phi}_{Au} \hat{\phi}_{Hv}^2 \hat{\phi}_u - P_{NCu} P_{HCu} P_v^2 \hat{\phi}_{NCu} \hat{\phi}_{HCu} \hat{\phi}_v^2 / K_{sr}) \tag{I.18}$$

$$-r_4 = k'_{NC}(P_{NCu}\hat{\phi}_{NCu}/K_{NC} - P_{NC}P_u\hat{\phi}_{NC}\hat{\phi}_u) \quad (I.19)$$

$$-r_5 = k'_{HC}(P_{HCu}\hat{\phi}_{HCu}/K_{HC} - P_{HC}P_u\hat{\phi}_{HC}\hat{\phi}_u) \quad (I.20)$$

Assuming that the surface reaction is the rate controlling step, then

$$k_A \longrightarrow \infty \quad (I.21)$$

$$k_H \longrightarrow \infty \quad (I.22)$$

$$k'_{NC} \longrightarrow \infty \quad (I.23)$$

$$k'_{HC} \longrightarrow \infty \quad (I.24)$$

But r_1, r_2, r_4, and r_5 must remain finite, then

$$P_{Au}\hat{\phi}_{Au} = K_A P_A P_u \hat{\phi}_A \hat{\phi}_u \quad (I.25)$$

$$P_{Hv}\hat{\phi}_{Hv} = \sqrt{K_{H_2}P_{H_2}\hat{\phi}_{H_2}}P_v\hat{\phi}_v \quad (I.26)$$

$$P_{NCu}\hat{\phi}_{NCu} = K_{NC}P_{NC}P_u\hat{\phi}_{NC}\hat{\phi}_u \quad (I.27)$$

$$P_{HCu}\hat{\phi}_{HCu} = K_{HC}P_{HC}P_u\hat{\phi}_{HC}\hat{\phi}_u \quad (I.28)$$

Let the total u-type active site pressure be

$$P_u^t = P_u\hat{\phi}_u + P_{Au}\hat{\phi}_{Au} + P_{NCu}\hat{\phi}_{NCu} + P_{HCu}\hat{\phi}_{HCu} \quad (I.29)$$

$$P_u^t = P_u\hat{\phi}_u(1 + K_A P_A\hat{\phi}_A + K_{NC}P_{NC}\hat{\phi}_{NC} + K_{HC}P_{HC}\hat{\phi}_{HC}) \quad (I.30)$$

Let the total v-type active site pressure be

$$P_v^t = P_v\hat{\phi}_v + P_{Hv}\hat{\phi}_{Hv} \quad (I.31)$$

$$P_v^t = P_v\hat{\phi}_v(1 + \sqrt{K_{H_2}P_{H_2}\hat{\phi}_{H_2}}) \quad (I.32)$$

The fugacity coefficients of solids or solid-like states are unity, and the fugacity of species i is $\hat{f}_i = P_i\hat{\phi}_i$, then the Langmuir isotherms for pressures P_u and P_v are

$$P_u = \frac{P_u^t}{1 + K_A\hat{f}_A + K_{NC}\hat{f}_{NC} + K_{HC}\hat{f}_{HC}} \quad (I.33)$$

$$P_v = \frac{P_v^t}{1+\sqrt{K_H \hat{f}_{H_2}}} \tag{I.34}$$

Substituting Equations I.25–I.28 in Equation I.18 would give

$$-r_3 = k_{sr} P_u^2 P_v^2 \left[K_A \hat{f}_A (K_{H_2} \hat{f}_{H_2}) - K_{NC} \hat{f}_{NC} K_{HC} \hat{f}_{HC} / K_{sr}\right] \tag{I.35}$$

$$-r_3 = k_{sr} P_u^2 P_v^2 K_A K_{H_2} \left[\hat{f}_A \hat{f}_{H_2} - \frac{K_{NC} K_{HC}}{K_A K_{H_2} K_{sr}} \hat{f}_{NC} \hat{f}_{HC}\right] \tag{I.36}$$

The relation between the thermodynamic reaction equilibrium constant (K_{eq}) and the surface reaction equilibrium constant (K_{sr}) is given by

$$K_{eq} = \frac{K_{sr} K_A K_{H_2}}{K_{NC} K_{HC}} \tag{I.37}$$

Substituting Equations I.33, I.34 and I.37 in Equation I.36 will give

$$-r_3 = \frac{k_{sr} (P_u^t)^2 (P_v^t)^2 K_A K_{H_2} \left[\hat{f}_A \hat{f}_{H_2} - \hat{f}_{NC} \hat{f}_{HC} / K_{eq}\right]}{\left[1 + K_A \hat{f}_A + K_{NC} \hat{f}_{NC} + K_{HC} \hat{f}_{HC}\right]^2 \left[1 + \sqrt{K_{H_2} \hat{f}_{H_2}}\right]^2} \tag{I.38}$$

Assuming that nitrogen containing compounds have comparable adsorption equilibrium constants [88], then

$$-r_3 = \frac{k_A K_A K_{H_2} \left[\hat{f}_A \hat{f}_{H_2} - \hat{f}_{NC} \hat{f}_{HC} / K_{eq}\right]}{\left[1 + K_A \hat{f}_{A_0} + K_{HC} \hat{f}_{HC}\right]^2 \left[1 + \sqrt{K_{H_2} \hat{f}_{H_2}}\right]^2} \tag{I.39}$$

where $k_A = k_{sr} (P_u^t)^2 (P_v^t)^2$

If hydrogen is in excess, as in this case, then the Equation I.39 can be written as

$$-r_3 = \frac{k \left[\hat{f}_A \hat{f}_{H_2} - \hat{f}_{NC} \hat{f}_{HC} / K_{eq}\right]}{\left[1 + K_A \hat{f}_{A_0} + K_{HC} \hat{f}_{HC}\right]^2 \left[1 + \sqrt{K_{H_2} \hat{f}_{H_2}}\right]^2} \tag{I.40}$$

Recalling that at partial pressure of nitrogen compound greater than 1 kPa, then $\sum_j \theta_j = 1$ and $\sum_j K_j P_j >> 1$ [92], hence Equation I.38 will be reduced to

$$-r_3 = \frac{k \left[\hat{f}_A \hat{f}_{H_2} - \hat{f}_{NC} \hat{f}_{HC} / K_{eq}\right]}{\left[\hat{f}_A + (K_{NC}/K_A) \hat{f}_{NC} + (K_{HC}/K_A) \hat{f}_{HC}\right]^2} \tag{I.41}$$

and Equation I.39 will be reduced to

$$-r_3 = \frac{k\left[\hat{f}_A - \hat{f}_{NC}\hat{f}_{HC}/K_{eq}\right]}{\left[\hat{f}_{A_0} + (K_{HC}/K_A)\hat{f}_{HC}\right]^2} \tag{I.42}$$

If the reaction is irreversible then

- The surface-controlled rate expression will be

$$-r_3 = \frac{k_A K_A K_{H_2} \hat{f}_A \hat{f}_{H_2}}{\left[(1 + K_{H_2}\hat{f}_{H_2})(1 + K_A\hat{f}_{A_0} + K_{HC}\hat{f}_{HC})\right]} \tag{I.43}$$

  and with the above mentioned assumptions the rate expression will be reduced to

$$-r_3 = \frac{k_s \hat{f}_A}{\hat{f}_{A_0} + (K_{HC}/K_A)\hat{f}_{HC}} \tag{I.44}$$

- The adsorption-controlled rate expression will be

$$-r_1 = \frac{k_a\left[\hat{f}_A\hat{f}_{H_2} - \hat{f}_{NC}\hat{f}_{HC}/K_{eq}\right]}{\hat{f}_{H_2}\left[1 + K_A\hat{f}_{A_0} + K_{HC}\hat{f}_{HC}\right]} \tag{I.45}$$

  or

$$-r_1 = \frac{k_{ad}\left[\hat{f}_A - \hat{f}_{NC}\hat{f}_{HC}/K_{eq}\right]}{\hat{f}_{A_0} + (K_{HC}/K_A)\hat{f}_{HC}} \tag{I.46}$$

- The desorption-controlled rate expression will be

$$-r_4 = \frac{k'_{nc}\left[K_{eq}\hat{f}_A\hat{f}_{H_2} - \hat{f}_{NC}\hat{f}_{HC}\right]}{\hat{f}_{HC}\left[1 + K_A\hat{f}_{A_0} + K_{HC}\hat{f}_{HC}\right]} \tag{I.47}$$

  or

$$-r_4 = \frac{k_{ds}\left[K_{eq}\hat{f}_A - \hat{f}_{NC}\hat{f}_{HC}\right]}{\hat{f}_{HC}\left[\hat{f}_{A_0} + (K_{HC}/K_A)\hat{f}_{HC}\right]} \tag{I.48}$$

$k_a = k_A P_u^t$

$k'_{nc} = k'_{NC} P_u^t$

Where:

P	partial pressure
P_u^t	total type-u active sites expressed in pressure
P_v^t	total type-v active sites expressed in pressure
K_i	adsorption equilibrium constant of species i
K_{sr}	surface reaction equilibrium constant
K_{eq}	thermodynamic reaction equilibrium constant
$\hat{f}_i$	fugacity of compound i
$\hat{\phi}_i$	fugacity coefficient of compound i
k_i	adsorption constant of compound i
k_i'	desorption constant of compound i

Subscripts:

A	reaction reactant
NC	nitrogen compound product
HC	pure hydrocarbon

Appendix J

Mass and Heat Transfer Effects

This Appendix includes the calculations for the partial pressure drop between the main stream and the catalyst surface. It also contains the calculations for the temperature drop from catalyst particle to ambient gas stream.

J.1 Mass Transfer Effects

This effect includes the diffusion between the catalyst surface and the bulk fluid in addition to the diffusion inside the pore itself.

J.1.1 External Diffusion

The estimation of the external diffusion is accomplished by applying the method of Yoshida et al. [109]. The data for this estimation are taken from run P350 at W/F=126. The conditions which apply for this run are as follows:

T =623 K

W/F =126 hr g-cat/g-mol

$\overline{R}$ =13 g-mol H_2/g-mol feed

ϕ =Shape factor (0.9 for irregular particles)

W =5.0000 g

A_m =1539300 cm^2/g

G_m =Molal mass velocity of gas feed (hydrogen and pyridine) based on the total cross-section of the catalyst bed, g-mol/hr-cm^2.

$=\frac{0.55552}{3.14159(1.076/2)^2} = 0.32867$ g-mol/hr-cm^2.

r_{mj} =Molal reaction rate of component j per unit mass of the catalyst.

r_{mA} $=\frac{(0.9766)(0.55552)}{5.00000}$=0.10850 g-mol/hr g-cat.

R_j =Dimensionless term of component j

R_A $=\frac{0.10850}{(1539300)(0.9)(0.32867)}= 2.383\times10^{-7}$

$(y_j)_{in}$ =Mole fraction of component j in feed

$(y_j)_{out}$ =Mole fraction of component j in product

y_j =Mole fraction of component j at the interface

y_A $=\frac{(0.0714)-(.0017)}{2}$=0.03485

$\frac{R_A}{y_A}$ $=\frac{2.383\times10^{-7}}{0.03485} = 6.83787 \times 10^{-6}$

The value of $\frac{\Delta P_A}{P_A}$ is obtained from $\frac{R_j}{y_j}$ versus $\frac{\Delta P_j}{P_j}$ correlation given in Figure 2 by Yoshida et al. [109]. This value is much lower than 0.0001, hence the external diffusion effects are neglected.

Note that A represents pyridine in the above calculations. Similar calculations were made for the other components, and all showed that $\frac{\Delta P_j}{P_j}$ is less than 0.0001.

J.1.2 Internal Diffusion

Internal diffusion is the extent of transport process in the interior of the catalyst. Internal diffusion can be either molecular or pore type of diffusion.

Molecular Diffusion

The molecular diffusion was verified by changing the feed velocity while keeping all the process variables constant (Table J.1). The variation of conversion is an indication of the extent of molecular diffusion. The variation in the conversion was in the limits of the experimental error and as such it was concluded that molecular diffusion was not controlling.

Table J.1: Variation of conversion with feed velocity

run number	temperature (K)	W/F	$\overline{R}$	feed rate g-mol/hr	conversion (%)
P2504	523	126.0	13	0.03968	45.02
P250M	523	126.0	13	0.05230	45.29

Pore Diffusion

The extent of pore diffusion was verified by measuring the conversion of the reaction at two runs of identical conditions except the particle size (Table J.2). Again it was concluded that the pore diffusion is not controlling since the reduction of the particle size did not result in enhancing the conversion.

Table J.2: Variation of conversion with catalyst size

run number	temperature (K)	W/F	R	catalyst size mesh/hr	conversion (%)
P2504	523	126.0	13	20/24	45.02
P250P	523	126.0	13	24/42	44.51

J.2 Heat Transfer Effects

Calculations for the temperature drop from catalyst particle to ambient gas stream was based on the method of Yoshida et al. [109]. The data of run P225 at W/F=126 hr g-cat/g-mol feed were used for these calculations.

The heat capacities, C_p, of the product organics were estimated making use of the group contribution for molar liquid heat capacities and the method described by the equation given by Sternling and Brown [72]

$$\frac{C_{pl} - C_p}{R} = (0.5 + 2.2\omega)[3.67 + 11.64(1 - T_r)^4 + 0.634(1 - T_r)^{-1}] \qquad (J.1)$$

Using this equation and data from Tables 3-183 and 3-336, the heat capacities for the organic products were estimated at 498 K. From the standard thermodynamics

$$C_p = \Sigma_{j=1}^{n} C_{p_j} y_j \qquad (J.2)$$

thus,

$$C_p = 0.0059 \times 42.00 + 0.0620 \times 27.98 + 0.0117 \times 50.30 \qquad (J.3)$$

$$+0.9147 \times 17.79 + 0.0031 \times 64.57 = 19.044\ cal/g - mol\ K$$

The products of the Run P225 are piperidine and alkyl-piperidines. The heat of formation of these compounds were estimated using the group contribution (Table

3-335 [72]).

$$\Delta H_f = \Delta H_{f_{PIP}} + \Delta H_{f_{ETPIP}} + \Delta H_{f_{PRPIP}} + \Delta H_{f_{PEPIP}} - \Delta H_{f_{PYR}} \qquad \text{(J.4)}$$

thus,

$$\Delta H_f = -(21.55 + 16.24 + 21.18 + 31.06) - (27.70) = -117.73\ kcal/g - mol$$

The conditions which apply for this run are as follows:

T =498 K

W/F =126 hr g-cat/g-mol

$\overline{R}$ =13 g-mol H_2/g-mol feed

ϕ =Shape factor (0.9 for irregular particles)

W =5.0000 g

A_m =1539300 cm^2/g

G_m =Molal mass velocity of gas feed (hydrogen and pyridine) based on the total cross-section of the catalyst bed, g-mol/hr-cm^2.

$=\frac{0.55552}{3.14159(1.076/2)^2} = 0.32867$ g-mol/hr-cm^2.

r_{mj} =Molal reaction rate of component j per unit mass of the catalyst.

r_{mA} $=\frac{(0.1025)(0.55552)}{5.00000}$=0.01139 g-mol/hr g-cat.

Making use of the above information, then

$$Q_A = -\frac{r_{m_A}\Delta H}{a_m \phi C_p G_m} \qquad \text{(J.5)}$$

$$Q_A = \frac{0.01139 \times 117730}{1539300 \times 0.9 \times 19.044 \times 0.32867} = 1.55 \times 10^{-4}$$

From Figure 4 in the paper of Yoshida et al. [109], the value of ΔT that corresponds to this value of Q_A is less than 0.01 K, hence the catalyst surface temperature effect can be neglected.